



**Investigation of the functions of sumo in
conserved biological processes in
Saccharomyces cerevisiae.**

Grace Cochrane

Thesis submitted for Doctor of Philosophy

Newcastle University

Faculty of Medical Sciences

Biosciences Institute

June 2021

Declaration

I certify that this thesis is my own work, except where acknowledged. Work in this thesis has not been previously submitted for another degree or qualification at this or any other university.

Abstract

The small ubiquitin-like modifier (sumo) is a conserved post-translational modification found throughout eukaryotes. Over the last 25 years a large range of studies have investigated the role of sumoylation, identifying hundreds of substrates and linking sumo to a diverse range of key cellular processes, including stress responses, the response to DNA damage and cell cycle progression. Although sumoylation has also been shown to be essential in a number of eukaryotes, including the model yeast *Saccharomyces cerevisiae*, the fundamental role(s) of sumoylation remains unclear. Sumo dysregulation is associated with a number of human diseases, including cancer, hence it is important to understand and characterise the role(s) of sumo pathways within these diseases. In an attempt to identify the important functions of sumoylation, a recent SGA screen carried out in our lab used a *S. cerevisiae* strain with reduced sumo (Smt3) function to identify a number of suppressor proteins which were able to suppress the growth defects of this *smt3* mutant. Excitingly, several novel cytoskeletal-related suppressors proteins were identified which rescued the *smt3* growth phenotype, including subunits of the CCT chaperonin complex, β -tubulin and branched F-actin. Hence, the aim of this thesis was to further characterise the phenotypes associated with the *smt3* mutant and to investigate the relationship of other proteins in the sumo conjugation/deconjugation pathways, the role of polysumoylation and the effect of different *S. cerevisiae* strain backgrounds within stress responses including exposure to cold temperature, responses to oxidative stress and cell cycle progression. In addition, another aspect of this study was to investigate the relationship of the *smt3* mutant with the novel suppressor proteins including subunits of the CCT complex, β -tubulin and F-actin.

Excitingly, this study has revealed novel and strain specific roles for sumoylation and polysumoylation within *S. cerevisiae* stress responses, cell cycle progression and chromosome dynamics, including a novel, strain specific role for sumoylation during S phase. In addition, data in this study also revealed that enzymes within the sumo conjugation and deconjugation pathways respond differently when presented with different stresses. Interestingly, our studies of the relationships between *smt3* and the novel cytoskeletal suppressor proteins

revealed that although these suppressors partially suppress the *smt3* growth defects, the *smt3* strain also suppresses several phenotypes associated with the cytoskeletal suppressors. Furthermore, our data suggests that β -tubulin is a substrate of sumoylation in *S. cerevisiae* cells. Thus, these results are consistent with a model in which sumoylation is functionally linked to the cytoskeleton by the interaction of sumo with microtubules and F-actin. Given that dysregulation of sumo, the CCT complex, F-actin and microtubules are common in many human diseases, this study provides novel insights into the relationship between the mutations in these complexes, potentially identifying new routes for the development of therapeutic treatments for human diseases.

Acknowledgements

Firstly, I would like to thank my supervisor, Brian Morgan, for his support, encouragement, enthusiasm and advice throughout the duration of my PhD. Secondly, I would like to thank Jan Quinn for co-supervising my PhD project and would also like to acknowledge the BBSRC for funding this project.

I would also like to thank all the members (past and present) of the yeast labs who have made the PhD experience so enjoyable and have provided me with suggestions and ideas throughout this project. Katie and Suki in particular have made lab work so much fun and full of endless cups of tea! Additionally, I would like to thank Peter Banks for providing a number of yeast strains used in this study and thanks also go to the Newcastle University Flow Cytometry Core Facility for enabling use of the FACS equipment.

Finally, I would like to thank my family and friends for their continued support during my PhD. A special mention goes to my parents, who have never lost faith in me- even through the dark times, and also thanks to the best siblings, Frankie and Joe.

Table of Contents

Chapter One: Introduction	1
1.1 Ubl Modifications and Conjugation	1
1.1.1 Ubls.....	1
1.1.2 The Small Ubiquitin-like Modifier Protein (sumo)	3
1.1.3 The Ubl Conjugation Cycle.....	5
1.1.3.1 Sumo Pre-processing	5
1.1.3.2 E1 Enzymes	8
1.1.3.3 E2 Enzymes.....	9
1.1.3.4 E3 Ligases.....	9
1.1.3.5 Deconjugases.....	11
1.2 Sumo Substrates.....	13
1.2.1 Sumo Consensus Sequences.....	13
1.2.2 Modes of Sumo Attachment	15
1.2.3 Sumo Substrates.....	17
1.2.3.1 Ran-GAP1.....	18
1.2.3.2 Septins	18
1.2.3.3 Sumo Proteomics.....	20
1.2.3.4 Early sumo Proteomics	20
1.2.3.5 Difficulties in Covalent Sumo Substrate Identification	21
1.2.3.6 Analysis of Sumo Datasets.....	25
1.3 Sumo Function.....	28
1.3.1 SIM domains	28
1.3.2 STUbLs	29
1.3.3 Crosstalk between different PTMs	31
1.3.4 Mitosis	33
1.3.5 Gene Expression	37

1.3.6 Sumo “cloud”	44
1.3.7 The Sumo Stress Response	44
1.3.7.1 Global Changes in Sumoylation	45
1.3.7.2 Heat Shock.....	45
1.3.7.3 Response to DNA Damage.....	47
1.3.7.4 The Spindle Assembly Checkpoint (SAC)	49
1.3.6.5 Oxidative Stress	52
1.3.7.6 Eukaryotic Cold Temperature Adaptation	56
1.4 smt3 SGA screen.....	58
1.4.1 Characterisation of the smt3 strain	59
1.4.2 Identification of Novel smt3 Suppressor Mutations.....	59
1.4.2.1 Tubulin.....	62
1.4.2.2 The CCT Complex.....	64
1.4.2.3 The Arp2/3 complex	72
1.5 Sumo and Disease.....	74
1.5.1 Cancer.....	74
1.5.2 Neurodegenerative Diseases.....	76
1.5.2.1 Parkinson’s Disease	76
1.5.2.1 Alzheimer’s Disease.....	76
1.5.3 Viral and Bacterial Infections.....	78
1.5.3.1 Ebola.....	78
1.5.4 smt3 Suppressors and Disease	79
1.5.4.1 Tubulin and Disease.....	80
1.5.4.2 The Arp2/3 Complex and Disease.....	81
1.5.4.3 The CCT Complex and Disease.....	83
1.6 Summary and Aims.....	85
Chapter Two: Materials and Methods.....	87
2.1 Yeast Techniques	87
2.1.1 Growth Conditions	88
2.1.2 Strain Construction.....	89

2.1.3 Yeast Recombination Cloning	90
2.1.3 Yeast Transformation	91
2.1.4 Growth Curves	91
2.1.5 Sensitivity Tests	91
2.1.6 Cold Temperature Shift	92
2.1.7 H ₂ O ₂ Treatment	92
2.1.8 Protein Lysis.....	92
2.1.9 Protein Extraction (TCA)	92
2.1.10 RNA Extraction.....	93
2.1.11 DNA Content Analysis (FACS)	94
2.2 Molecular Biology Techniques.....	94
2.2.1 Polymerase Chain Reaction (PCR)	94
2.2.1.1 Gene Deletions	94
2.2.1.2 PCR of <i>S. cerevisiae</i> Colonies	95
2.2.2 Agarose Gel Analyses, Gel Extraction and DNA Sequencing	96
2.2.3 Escherichia coli Transformation and Plasmid Extraction.....	96
2.2.4 Yeast Plasmid Extraction	96
2.2.5 Restriction Digests.....	97
2.3 Biochemical Techniques	98
2.3.1 Western Blotting	98
2.3.2 Immunoprecipitation.....	99
2.3.3 Quantitative Reverse Transcriptase-PCR (RT-qPCR).....	100
2.3.4 Chromosomal qPCR.....	101
2.4 Statistical Analysis	103
Chapter Three: The Functions and Regulation of Smt3 in Stress Responses	104
3.1 Introduction.....	104
3.2 Results and Discussion.....	105
3.2.1 <i>smt3</i> phenotypes are conserved in different strain backgrounds.....	105
3.2.2 Polysumoylation is important for the response to cold temperatures	107

3.2.3 Investigation of the sumo pathway enzymes involved in the response to cold temperatures.....	117
3.2.4 <i>ULP2</i> and <i>UBA2</i> gene expression are modified in the response to cold temperature	123
3.2.5 Smt3 and the response of cells to oxidative stress	128
3.2.6 Ubiquitination is induced in response to cold temperatures	136
3.3 Summary.....	141
Chapter Four: Investigation of the functions of sumoylation in cell cycle progression	146
4.1 Introduction.....	146
4.2 Results and Discussion.....	147
4.2.1 <i>smt3</i> cells display defects in G2/M phase progression.....	147
4.2.2 Duplication of specific chromosomes contribute to <i>smt3</i> aneuploidy.....	148
4.2.3 The chromosomal location of the top 100 <i>smt3</i> suppressor proteins does not appear to correlate with aneuploidy in the <i>smt3</i> mutant.....	154
4.2.4 Loss of Smt3 function causes cell cycle defects in different strain backgrounds	158
4.2.5 Polysumoylation mutants also show cell cycle defects	160
4.2.6 Suppression of <i>smt3</i> associated defects by mutations of the Arp2/3 complex and the CCT complex.....	166
4.2.6.1 Investigation of mutations of the Arp2/3 complex	167
4.2.6.2 Investigation of mutation of the CCT complex	175
4.3 Summary.....	183
Chapter Five: Characterisation of the relationship between Tub2 and Smt3	189
5.1 Introduction.....	189
5.2 Results and discussion	191
5.2.1 Suppression of <i>smt3</i> and <i>tub2</i> associated defects in the <i>tub2smt3</i> double mutant	191
5.2.1.1 <i>smt3</i> growth defects are restored in the <i>tub2smt3</i> double mutant	191
5.2.1.2 Cell cycle analysis of the <i>tub2</i> and <i>tub2smt3</i> double mutants	192
5.2.1.3 <i>smt3</i> cells are extremely resistant to microtubule depolymerising agents.....	197

5.2.1.4 <i>smt3</i> mutants express Tub2 at wild type levels.....	200
5.2.1.5 HMW sumo conjugates are rescued in <i>tub2smt3</i> cells	202
5.2.1.6 <i>tub2smt3</i> double mutants display specific aneuploidy	202
5.2.2 Investigation of Tub2 as a sumo substrate.....	205
5.2.3 Construction of a “plasmid shuffle” strain to enable studies of Tub2 mutations	208
5.2.4 Investigation of covalent and non-covalent interactions of sumo with Tub2	216
5.2.4.1 Investigation of non-covalent interactions of sumo with Tub2.....	217
5.2.4.2 Investigation of covalent interactions of sumo with Tub2	230
5.2.4.2.1 Analysis of the role of K324 in the function of Tub2	231
5.2.4.2.2 Analysis of the role of K320, K324, K332 and K336 in the function of Tub2 .	242
5.3 Summary.....	246
Chapter Six: Final Discussion	251
6.1 Highlights of this study	251
6.2 Sumo and Disease.....	253
6.3 Final Remarks	254
References.....	257

Abbreviations

5'FOA	5-Fluoroorotic Acid
<i>A. thaliana</i>	<i>Arabidopsis thaliana</i>
AA	Amino Acid
AP	Affinity purification
AP-MS	Affinity purification coupled with mass spectrometry
APC	Anaphase Promoting Complex
Arp	Actin Related Protein
BiFC	Bimolecular fluorescence complementation
BSA	Bovine Serum Albumin
CCT	Chaperone Containing TCP-1
Chr	Chromosome
CSP	Cold Shock Protein
<i>D. melanogaster</i>	<i>Drosophila melanogaster</i>
DAmP	Decreased Abundance by mRNA Perturbation
DDR	DNA Damage Response
DMSO	Dimethyl sulfoxide
DNA	Deoxyribonucleic Acid
<i>E. coli</i>	<i>Escherichia coli</i>
EDTA	Ethylenediaminetetraacetic acid
EV	Empty Vector
FACS	Fluorescence-activated Cell Sorting
H ₂ O ₂	Hydrogen Peroxide
HIV	Human Immunodeficiency Virus
HMW	High Molecular Weight
<i>H. sapiens</i>	<i>Homo sapiens</i>
HSP	Heat Shock Protein
HU	Hydroxy Urea
IP	Immunoprecipitation
kDa	Kilodalton

LCA	Leber congenital amaurosis
<i>M. musculus</i>	<i>Mus musculus</i>
MAP	Microtubule Associated Protein
mM	Millimolar
mRNA	Messenger Ribonucleic Acid
MS	Mass Spectrometry
N-WASP	Wiscott-Aldrich syndrome protein
Nat	Nourseothricin
NDSM	Negatively Charged Amino acid-dependent Sumoylation Motif
NEM	N-Ethylmaleimide
ns	Non specific
OD	Optical density
PBS	Phosphate Buffered Saline
PCNA	Proliferating Cell Nuclear Antigen
PCR	Polymerase Chain Reaction
PDSM	Phosphorylation-dependent Sumoylation Motif
PEG	Polyethylene glycol
PMSF	Phenylmethane sulfonyl fluoride
PRO	Promoter
PTM	Post Translational Modification
q-PCR	Quantitative Polymerase Chain Reaction
qRT-PCR	Quantitative Real-Time Polymerase Chain Reaction
RNA	Ribonucleic Acid
ROS	Reactive Oxygen Species
SAC	Spindle Assembly Checkpoint
<i>S. cerevisiae</i>	<i>Saccharomyces cerevisiae</i>
<i>S. pombe</i>	<i>Schizosaccharomyces pombe</i>
SD	Synthetic dextrose
SDS	Sodium dodecyl sulphate
SGA	Synthetic Genetic Array
SIM	SUMO Interactive Motif
SSR	SUMO Stress Response

STUbL	SUMO Targeted Ubiquitin Ligase
sumo	Small Ubiquitin-Like Modifier
TBS	Tris Buffered Saline
TBZ	Thiabendazole
TCA	Trichloroacetic Acid
TE	Tris EDTA
TER	Terminator
ts	Temperature Sensitive
Ub	Ubiquitin
UbIS	Ubiquitin-like Modifiers
UTR	Untranslated region
WaLP	wild-type α -lytic protease
WT	Wild Type
YFG	Your Favourite Gene
YPD	Yeast Extract Peptone Dextrose

List of Figures

Figure 1.1 Comparison of the human ubiquitin and Sumo-1 3D structure.....	4
Figure 1.2 The Smt3 conjugation/ deconjugation pathway in <i>S. cerevisiae</i> cells.....	6
Figure 1.3. Three different modes of sumoylation.	16
Figure 1.4. Proteolytic cleavage sites in human ubiquitin and SUMO-1 proteins.....	23
Figure 1.5 Different PTMs regulate the activity of Foxm1b.	40
Figure 1.6 Sumoylation and phosphorylation regulate the transcriptional activity of STAT-5.....	42
Figure 1.7 Redox regulation of the sumo conjugation/deconjugation enzymes.....	54
Figure 1.8 CCT1-8 form an octameric structure.	66
Figure 1.9 The Arp2/3 complex enables branching of F-actin.	70
Figure 2.1 Schematic diagram of gene deletion in <i>S. cerevisiae</i>	89
Figure 2.2 Schematic diagram of yeast recombination cloning.	90
Figure 3.1 Smt3 is required for the response of cells to cold temperature in different strain backgrounds.....	108
Figure 3.2 Global sumoylation is induced in in response to cold temperature.....	112
Figure 3.3 Polysumoylation is induced in the response of cells to cold temperatures.....	114
Figure 3.4 Siz1 and Ulp2 are important for cold-induced global sumoylation.....	124
Figure 3.5 <i>ULP2</i> gene expression is increased upon exposure of cells to cold temperature.....	127
Figure 3.6 Smt3 is important for the response of cells to oxidative stress.....	132
Figure 3.7 The sumo E3 ligases Siz1 and Siz2 are important for response to H ₂ O ₂	134
Figure 3.8 Ulp1 and Ulp2 have different functions in responses to H ₂ O ₂	135
Figure 3.9 HMW sumo conjugates in <i>siz2</i> Δ cells are greatly induced in oxidative stress.....	137
Figure 3.10 Global ubiquitination is induced by cold temperatures.....	139
Figure 3.11 Cold temperature and oxidative stress affect the sumo conjugation/ deconjugation pathway in distinct ways.....	142
Figure 4.1 <i>smt3</i> cells have cell cycle defects.....	149
Figure 4.2 Loss of Smt3 function causes specific multichromosome aneuploidy.....	153

Figure 4.3 Analysis of the chromosomal locations of the top 100 suppressor and enhancer mutations identified in the <i>smt3</i> SGA screen.....	155
Figure 4.4 <i>smt3</i> mutant cells display similar cell cycle defects in different strain backgrounds.....	156
Figure 4.5 <i>smt3</i> mutant cells display similar multichromosome aneuploidy in different strain backgrounds.....	157
Figure 4.6 <i>smt3</i> cell cycle phenotypes are conserved in the <i>smt3-allR</i> strain.....	164
Figure 4.7 Loss of polysumoylation causes specific multichromosome aneuploidy.....	165
Figure 4.8 <i>smt3</i> cell cycle phenotypes are rescued in the <i>arp2smt3</i> double mutant.....	168
Figure 4.9 <i>smt3</i> cell cycle phenotypes are rescued in the <i>arp3smt3</i> double mutant.....	169
Figure 4.10 The <i>arp2smt3</i> mutant displays specific aneuploidy.....	172
Figure 4.11 <i>SMT3</i> gene expression is not rescued in the <i>cct8smt3</i> double mutant.....	178
Figure 4.12 <i>smt3</i> cell cycle phenotypes are rescued in the <i>cct8smt3</i> double mutant.....	179
Figure 4.13 The <i>cct8</i> mutant and the <i>cct8smt3</i> double mutant display specific aneuploidy.....	180
Figure 5.1 The <i>tub2</i> allele suppresses cell cycle and aneuploidy phenotypes associated with the <i>smt3</i> allele.....	193
Figure 5.2 The <i>smt3</i> mutation suppresses the sensitivity of the <i>tub2</i> mutant to a microtubule depolymerising drug.....	195
Figure 5.3. The levels of sumo do not affect the levels of α - and β -tubulin.....	198
Figure 5.4. HMW sumo conjugates are rescued in <i>tub2smt3</i> double mutants.....	201
Figure 5.5 The <i>tub2</i> and <i>smt3</i> single mutants and the <i>tub2smt3</i> double mutant display specific aneuploidy.....	203
Figure 5.6 Tub2 is sumoylated in <i>S. cerevisiae</i>	206
Figure 5.7 Strategy to create the pRS316- <i>TUB2</i> plasmid.....	209
Figure 5.8 Verification of the Tub2 “Plasmid Shuffle Starting Strain”	210
Figure 5.9 Tub2 Plasmid Shuffle Strategy.....	211
Figure 5.10. GC136 cells express wild type Tub2 levels.....	214
Figure 5.11 Cell cycle analysis of the YCplac111- <i>TUB2</i> (GC136) strain.....	215
Figure 5.12 Identification of a putative Tub2 SIM domain.....	218
Figure 5.13 Construction of the YCplac111- <i>SIM</i> strain.....	219
Figure 5.14. Mutations of the Tub2 SIM domain are not lethal.....	220

Figure 5.15 Cell cycle analysis of the YCplac111- <i>SIM</i> (GC138) strain.....	223
Figure 5.16 <i>SIM</i> mutants are not sensitive to microtubule depolymerisation agents.....	224
Figure 5.17 Identification of covalent sumo binding site in Tub2.....	227
Figure 5.18 Construction of the YCplac111- <i>K324R</i> (GC137) strain.....	229
Figure 5.19. The Tub2 K324R mutation is not lethal.....	234
Figure 5.20 Cell cycle analysis of the YCplac111- <i>K324R</i> (GC137) strain.....	235
Figure 5.21 <i>K324R</i> mutants are not sensitive to microtubule depolymerisation agents.....	236
Figure 5.22 Construction of the YCplac111- <i>Quad</i> strain.....	238
Figure 5.23. The Tub2 quad mutation is not lethal.....	239
Figure 5.24 Cell cycle analysis of the YCplac111- <i>Quad</i> strain.....	240
Figure 5.25 <i>Quad</i> mutants are not sensitive to microtubule depolymerisation agents.....	243
Figure 6.1 Sumo is functionally linked to the cytoskeleton by interaction(s) with microtubules and F-actin.....	254

List of Tables

Table 1.1 <i>Saccharomyces cerevisiae</i> Ubls and sequence homology with ubiquitin.....	2
Table 1.2 Comparison of the sumo conjugation/ deconjugation enzymes in the indicated species.....	7
Table 1.3 Sumoylation of mammalian transcription factors can promote transcriptional activation and repression.	38
Table 1.4 Top suppressor proteins identified in the <i>smt3</i> SGA screen and their associated complexes.....	60
Table 1.5 Nomenclature of the <i>S. cerevisiae</i> and mammalian CCT genes.....	67
Table 1.6 Nomenclature of the <i>S. cerevisiae</i> and mammalian Arp2/3 genes.....	71
Table 2.1. <i>S. cerevisiae</i> strains used in this study.	88
Table 2.2 PCR primers used in this study.	97
Table 2.3 Antibodies used in this study.....	99
Table 2.4 RT-qPCR primers used in this study.....	101
Table 2.5 Chromosomal qPCR primers used in this study.....	102
Table 4.1 Analysis of the chromosomal profiles of the <i>smt3</i> mutants.	181
Table 5.1 Analysis of the chromosomal profiles of the <i>smt3</i> , <i>tub2</i> and <i>tub2smt3</i> mutants.....	204

Chapter One: Introduction

1.1 Ubl Modifications and Conjugation

1.1.1 Ubls

In order to regulate protein function and maintain cellular homeostasis, eukaryotic cells have developed a sophisticated system of posttranslational modifications. These modifications act as molecular switches by enabling the addition of a small protein moiety or functional group onto a substrate protein. Importantly, post-translational modifications enable a rapid, reversible change in protein function without any permanent damage to the protein itself. Examples of modifications include acetylation, phosphorylation, and the more recent addition of the Ubiquitin-like proteins (Ubls) (Lin and Carroll, 2018). Ubiquitin, as the name suggests, is a small protein found ubiquitously throughout eukaryotes and was the first Ubl to be identified. Covalent attachment of a ubiquitin moiety to a substrate occurs via an isopeptide bond between the lysine residue on the target protein and the ubiquitin C-terminus (Cappadocia and Lima, 2017, Zheng and Shabek, 2017). Although the classic function of ubiquitin was originally identified as targeting the substrate for degradation via the 26S proteasome, a number of different cellular roles, including signalling, have now been associated with ubiquitination (Nandi et al., 2006).

Several other Ubls have since been discovered within the last twenty years, including sumo, Urm and Nedd (Table 1.1). Although it must be noted that Ubls do not all share high sequence homology, the 3D structures are remarkably similar (Table 1.1). Importantly, the conservation of a characteristic β -grasp fold (consisting of an α -helix surrounded by a 5 stranded β -fold) appears to be crucial for Ubl function and identity (Hochstrasser, 2009).

Ubl	% Homology to Ubiquitin	B-grasp Fold	E1	E2
Ubiquitin	100	Yes	Uba1- Uba6	Many
Sumo	18	Yes	Aos1-Uba2	Ubc9
Urm	Undetectable	Yes	Uba4	Unknown
Rub1	55	Yes	Uba3-Ula1	Ubc12
Atg8	Undetectable	Yes	Atg7	Atg3

Table 1.1 *Saccharomyces cerevisiae* Ubls and sequence homology with ubiquitin.

(Hochstrasser, 2009, Pang et al., 2019, Herrmann et al., 2007)

1.1.2 The Small Ubiquitin-like Modifier Protein (sumo)

Following ubiquitin, arguably the most well characterised Ubl is the Small Ubiquitin-like Modifier (sumo) protein. Sumo was first identified in 1996 in a complex with Ran-GAP1 and has since been found to target >3500 proteins in human cells (Hendriks and Vertegaal, 2016, Mahajan et al., 1997). Sumo conjugation is dynamic, resulting in a very small fraction of cellular proteins being sumoylated at any one time, likely explaining why sumo remained elusive for such a long time. *Saccharomyces cerevisiae* cells express a single sumo protein, Smt3, which was originally identified in a genetic screen as a suppressor of a mutation in the centromeric binding protein Mif2 (Meluh and Koshland, 1995). Mammals express several sumo genes (Sumo1-4) whereas other yeast and invertebrates express just one (Table 1.2). As sumo is highly conserved throughout eukaryotes it is perhaps not surprising that it is essential for viability, with the notable exceptions of *Schizosaccharomyces pombe* and *Candida albicans*. However, it must be noted that *S. pombe* and *C. albicans* cells lacking sumo have problems progressing through G2 and M phases and are extremely slow growing, indicating that sumo is important for cell cycle progression (Leach et al., 2011). Conversely, *S. cerevisiae* cells lacking Smt3 are inviable and loss of sumo conjugation arrests cells in G2/M phase (Biggins and Murray, 2001, Matunis et al., 1996, Takahashi et al., 1999). Remarkably, human Sumo-1 can compensate for the loss of Smt3 in budding yeast, illustrating the significant degree of conservation of sumo function in eukaryotes (Newman et al., 2017). Indeed, further research in mammalian cells has also confirmed the essential nature of sumo. For example, mice expressing a Sumo-2 null allele die in early embryogenesis with embryos showing severe growth defects and reduced cell proliferation, illustrating the importance of Sumo-2 for both growth and viability in mammalian cells (Zhang et al., 2008a, Wang et al., 2014b).

Although sumo shares just 18% sequence homology to ubiquitin (Table 1.1), the 3D structures are exceptionally similar (Figure 1.1). However, one noticeable difference between the two 3D structures is the extended N-terminal extension of sumo, which ubiquitin lacks (Figure

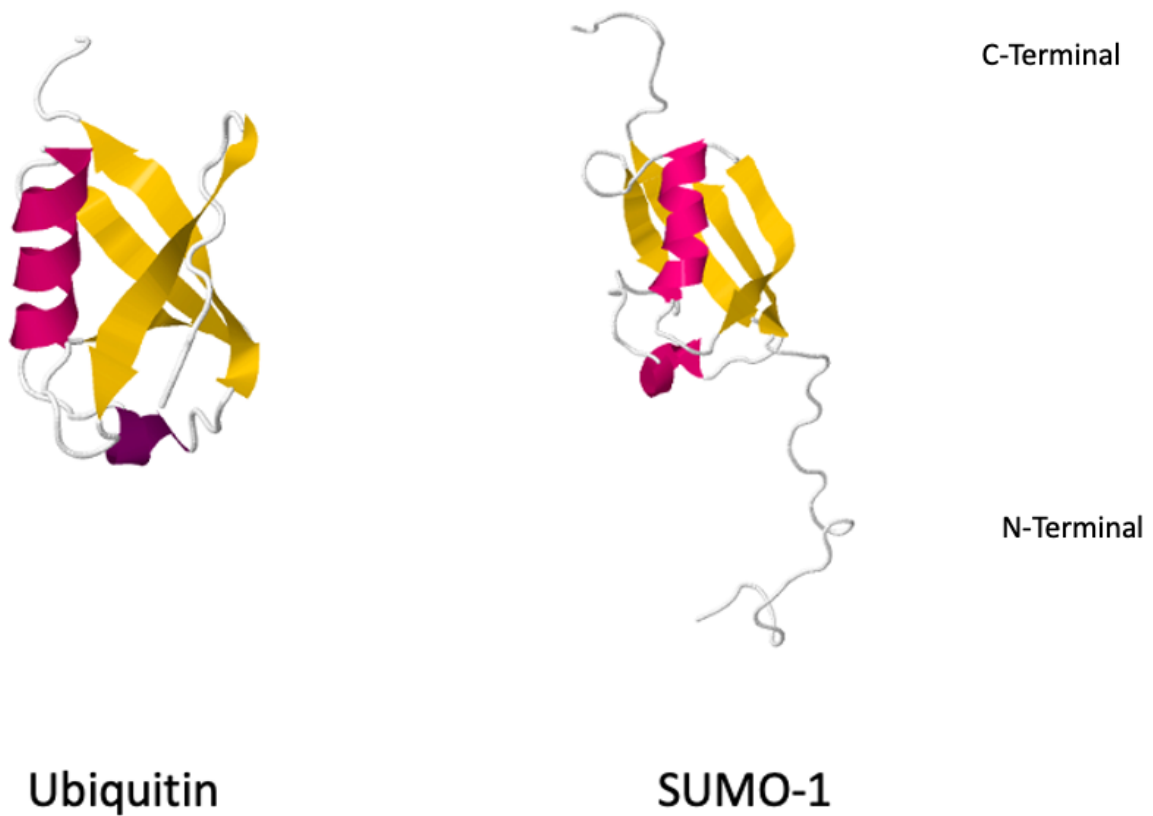


Figure 1.1 Comparison of the human ubiquitin and Sumo-1 3D structure. Human Ubiquitin (PBD 1UBQ) and SUMO-1 (PBD 1A5R) 3D structures were obtained from the online Protein Data Bank (<https://www.rcsb.org>). α - helices are represented in pink and β -sheets are represented in yellow.

1.1). This ~20 amino acid sumo "tail" harbours three key lysine residues which themselves can be sumoylated, generating a "polysumo tail" on substrates. However, interestingly these three lysine residues are only present within the N-terminal region of Smt3 in *S. cerevisiae* and SUMO-2/3 in human cells. Furthermore, truncation of the Smt3 N-terminal domain is not lethal, suggesting that polysumoylation with these three lysines is not an essential aspect of sumoylation function (Bylebyl et al., 2003).

1.1.3 The Ubl Conjugation Cycle

The conjugation pathway is another shared feature of the UbIs. Conjugation of the Ubl to the target substrate involves an E1 (activating), E2 (conjugating) and E3 (ligase) cascade of enzymes. However, the number of enzymes and their specificity can vary in the different Ubl conjugation pathways (Table 1.1). For example, there is a single E2 (Ubc9) in the sumo conjugation pathway, compared to >100 E2s within the ubiquitin pathway. Another similarity shared between the Ubl conjugation pathways is that (with the exception of urm) all UbIs are translated as immature precursor proteins which require C-terminal processing for activation. This processing is achieved by the action of one of the Ubl-specific deconjugases and reveals a Gly-Gly motif which enables the Ubl to then be conjugated to the catalytic cysteine of the E1 enzyme in an ATP-dependent manner. The Ubl is then passed onto the catalytic cysteine on the E2 and finally, with the aid of an E3 ligase, the Ubl is attached to the target protein (Fig. 1.2). The sumo conjugation cycle will now be described in more detail; for information regarding the specific conjugation of other UbIs, see reviews (Cappadocia and Lima, 2017, Streich and Lima, 2014).

1.1.3.1 Sumo Pre-processing

UbIs including sumo are translated in the cell as immature precursor proteins and require isopeptidase activity in order to produce a mature Ubl. Sumo activation requires cleavage of the C-terminal amino acids to reveal a di-glycine motif, which is achieved by a Ubl-specific protease. Smt3 maturation in *S. cerevisiae* arises through the hydrolysis action of the Ulp1 protease (Li and Hochstrasser, 1999b) (Table 1.2).

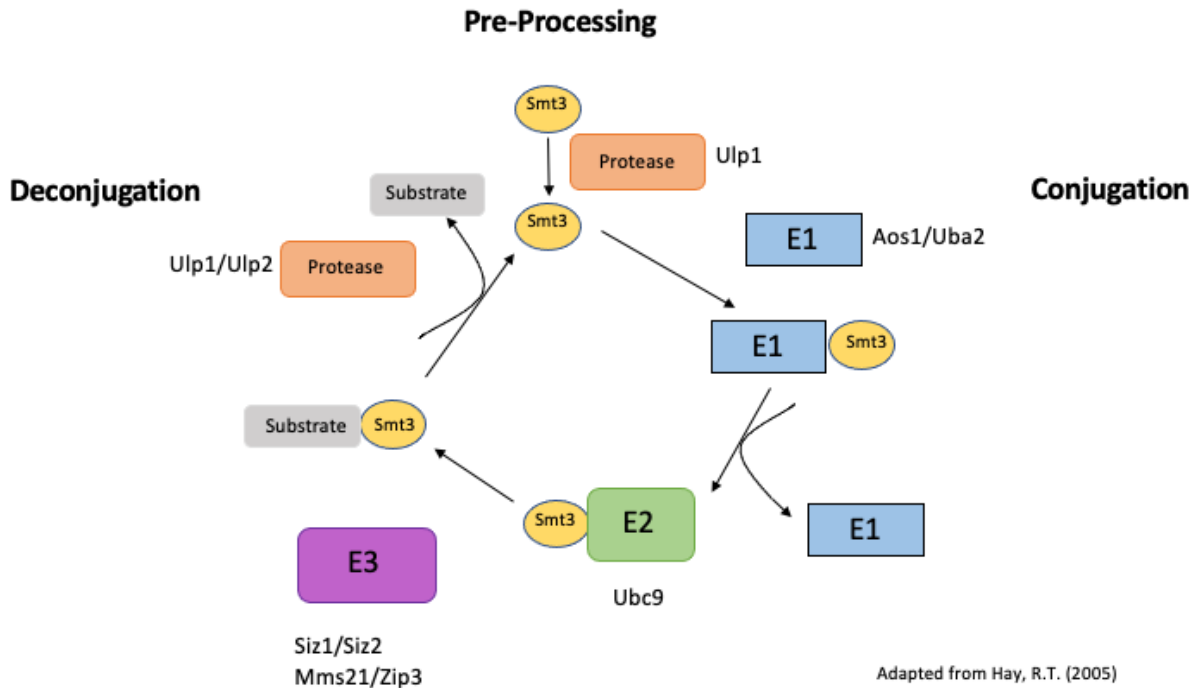


Figure 1.2 The Smt3 conjugation/ deconjugation pathway in *S. cerevisiae* cells. The Smt3 isopeptidase Ulp1 cleaves the Smt3 C-terminal domain to reveal a Gly-Gly motif, enabling Smt3 maturation. Activated Smt3 then enters the Smt3 conjugation cycle where it is adenylated by the E1 heterodimer AOs1/Uba2, forming a thioester bond between Smt3 and the Uba2 catalytic cysteine. Next, the E1-Smt3 complex facilitates the transfer of Smt3 onto the catalytic cysteine of the E2 enzyme, Ubc9. The four *S. cerevisiae* sumo E3 ligases aid substrate recognition, although this is not essential for Smt3 conjugation. The presence of the Smt3 deconjugases Ulp1 and Ulp2 remove Smt3 from substrates, enabling sumo to re-enter the conjugation cycle. Adapted from (Hay, 2005).

Sumo Conjugation Protein Homologues					
Organism	Sumo	E1	E2	E3	Desumoylases
<i>S. cerevisiae</i>	Smt3	Aos1	Ubc9	Siz1	Ulp1
		Uba2		Siz2	Ulp2
				Mms21	
				Zip3	
<i>S. pombe</i>	Pmt3	Uba4	Ubc9	Pli1	Ulp1
		Uba2		Pli2	Ulp2
<i>H. sapiens</i>	SUMO1	SAE1	UBC9	PIAS1	SEN1
	SUMO2	SAE2		PIAS2	SEN2
	SUMO3			PIAS3	SEN3
	SUMO4			PIAS4	SEN4
				RAN-BP2	SEN5
				MMS21	SEN6
				HDAC2	SEN7
				HDAC4	
<i>Arabidopsis thaliana</i>	SUM1	SAE1a	SCE1	SIZ1	At3g48480
	SUM2	SAE1b		MMS21	ULP1d
		SAE2		PIAL1	ULP1c
				PIAL2	

Table 1.2 Comparison of the sumo conjugation/ deconjugation enzymes in the indicated species. Adapted from (Novatchkova et al., 2012).

1.1.3.2 E1 Enzymes

All Ubl E1 enzymes contain a conserved Ubl domain which facilitates the transfer of the mature Ubl onto the E2 conjugating enzyme (Olsen et al., 2010). Firstly, E1 adenylation activates the Ubl, enabling formation of a thioester bond between the catalytic cysteine residue of the E1 and the Ubl. Subsequently, the Ubl is transferred to the catalytic cysteine residue of the E2 enzyme where it also forms a thioester bond. All Ubl E1s contain conserved adenylation domains, suggesting that they may have diverged from a primitive E1 enzyme. In addition, the crystal structures of both the ubiquitin E1 and the sumo E1 are remarkably similar, suggesting that the two enzymes have similar mechanisms (Lois and Lima, 2005). Interestingly, comparison of the activation step of the eukaryotic Ub1s with the bacterial Moad show that both pathways form adenylates as a precursor to substrate ligation, strongly suggesting that Ub1s originated from a common bacterial ancestor (Lake et al., 2001). Bacterial protein modifications will not be discussed in further detail, for more information please see the following reviews (Macek et al., 2019, Pisithkul et al., 2015).

Initial discovery of the *S. cerevisiae* sumo E1 (the essential heterodimer Aos1/Uba2) was facilitated by sequence analysis of the Ubiquitin E1 enzyme (Uba1), suggesting that all Ubl E1 enzymes share conserved domains (Johnson et al., 1997). Indeed, both Uba1 and Aos1/Uba2 have extremely similar crystal structures (Lois and Lima, 2005). Upon recognition of mature Smt3, Aos1/Uba2 adenylates the C-terminal Smt3 diglycine motif in an ATP-dependent manner. An intermediate Smt3-Uba2 complex is formed by the creation a thioester bond between the matured Smt3 diglycine motif and the catalytic cysteine residue (cys177) of Uba2. Finally, Smt3 is then transferred onto the catalytic cysteine residue (cys93) on the E2 conjugating enzyme Ubc9 (Olsen et al., 2010, Bylebyl et al., 2003). Interestingly, a temperature sensitive Uba2 mutant expressed in budding yeast prevents sumo conjugation at the non-permissive temperature, highlighting the importance of Uba2 and sumoylation for cell growth (Schwienhorst et al., 2000).

1.1.3.3 E2 Enzymes

Mammalian and budding yeast cells both express a single sumo E2 (Ubc9) which is essential for viability (Dieckhoff et al., 2004). This is in contrast to the Ubiquitin pathway in *S. cerevisiae* cells, of which only one E2 (Cdc34) out of 11 is essential (Schwob et al., 1994). Sumoylation is prevented in *S. cerevisiae* cells expressing a temperature sensitive mutant version of Ubc9 at the non-permissive temperature, highlighting the importance of Ubc9 within the sumo conjugation pathway. Studies investigating the sumo E2 enzyme in mammalian cells identified that Ubc9 knockout mice are embryonic lethal, although sumoylation in mice expressing a single Ubc9 allele is indistinguishable from wild type mice (Nacerddine et al., 2005). Interestingly, the loss of Ubc9 in mammalian cells leads to multiple mitotic defects, including chromosome mis-segregation (Nacerddine et al., 2005). Although there is only 56% sequence homology between all Ubc9 orthologues, structural analysis revealed that they all contain a conserved Ubc domain. This Ubc domain is ~150 amino acids in size and contains the critical cysteine residue required for catalysing Ubl conjugation, suggesting that all sumo E2 enzymes have conserved enzymatic activity (Olsen and Lima, 2013).

Remarkably, unlike the Ubiquitin E2s, Ubc9 is able to directly recognise sumoylation motifs and catalyse sumo conjugation without the aid of an E3 ligase (Bernier-Villamor et al., 2002). It has also been proposed that Ubc9 may be post-translationally modified to facilitate substrate identification. For example, sumoylation of the Ubc9 N-terminal domain has been shown to enhance the sumoylation of the transcriptional regulator Sp100 in mammalian cells (Knipscheer et al., 2008). Interestingly, sumoylated Ubc9 shows a five-fold affinity for Sp100 compared to unmodified Ubc9 suggesting that sumoylated Ubc9 promotes the recognition and sumo conjugation of Sp100.

1.1.3.4 E3 Ligases

The final stage in Ubl conjugation involves E3 ligases which provide substrate specificity and enable the transfer of the Ubl moiety onto the target protein. E3s facilitate the alignment of the target lysine with the Ubl-E2 complex, and in the case of sumo catalysing sumo-substrate conjugation.

S. cerevisiae express just four sumo E3 ligases; Siz1, Siz2, Zip3 and Mms21 in comparison to >100 E3s present within the ubiquitin pathway (Pichler et al., 2017). Interestingly, the *S. cerevisiae* sumo E3 ligases are not essential, with the exception of Mms21. However, expression of a null Mms21 ligase restores viability, suggesting that Mms21 may have an additional cellular role distinct from sumo conjugation (Reindle et al., 2006). Indeed, additional studies revealed that Mms21 null mutants show an increased sensitivity to the DNA damaging agents methyl methane sulphonate (MMS) and ultra violet (UV) light, suggesting that Mms21 plays a key role in the sumo-mediated response to DNA damage (Zhao and Blobel, 2005). Nevertheless, with just four sumo E3 ligases present in *S. cerevisiae* it is indicative that there is significant overlap in substrate specificity. Indeed, global sumoylation is dramatically reduced in *siz1*Δ cells, whilst >90% of sumoylation is abolished in *siz1*Δ*siz2*Δ cells, suggesting that Siz1 and Siz2 target the majority of substrates for sumoylation in *S. cerevisiae* cells and that no single group of substrates is essential (Reindle et al., 2006). However, it may also be the case that Ubc9 is able to sumoylate substrates in vivo without the requirement of an E3 ligase, as detailed above.

Although *siz1*Δ*siz2*Δ cells are viable, they display a G2/M delay and appear as large budded cells showing extreme sensitivity to cold temperatures (Johnson and Gupta, 2001a). There is also evidence for functional redundancy between the sumo E3 ligases in *S. cerevisiae*. For example, the rDNA silencer Net1 is subject to sumoylation by either Siz1, Siz2 or Mms21 in budding yeast cells, illustrating the significant overlap in substrate specificity between the sumo E3 ligases (Reindle et al., 2006).

All *S. cerevisiae* sumo E3 ligases belong to the Siz-PIAS-RING (SP-RING) family of sumo E3 ligases which interact with the sumo E2 enzyme to facilitate sumo conjugation. E2 recognition is achieved by the RING domain expressed by all sumo E3 ligases, in which the co-ordination of two zinc ions contained within the RING domain interact with the N-terminal region of the sumo E2 (Zheng et al., 2000). In addition to interacting with the sumo E2, all SP-RING ligases have been shown to contain a PIAS (protein inhibitor of activated STAT) domain which interacts with sumo via an SXS motif (Minty et al., 2000, Hochstrasser, 2001). Once sumo is bound to the E3 ligase, realignment of the sumo-E3 thioester bond is catalysed by the RING domain, facilitating the release of sumo onto target substrates. Interestingly, although this

mechanism was first identified in Ubiquitin E3 ligases, sumo-E3 re-alignment appears to be conserved throughout UbIs including Sumo and Nedd (Plechanovová et al., 2012). Recent studies have identified that Sumo E3 ligases also contain a characteristic N-terminal PINIT domain which is essential for ligase activity in addition to facilitating the E3-Smt3 interaction (Takahashi and Kikuchi, 2005). Furthermore, deletion of the PINIT domain prevents the E3 interaction with Smt3 *in vitro*, highlighting the importance of the E3 N-terminal domain (Takahashi and Kikuchi, 2005).

To date there are nine identified mammalian Sumo E3 ligases which fall into three main categories: SP-RING, RAN-BP2 and ZNF451. SP-RING ligases are the most common E3 in mammalian cells and are also referred to as PIAS ligases. The RAN-BP2 family of sumo E3 ligases show no homology to other known Ubl E3 ligases and only display ligase activity in higher eukaryotes. Interestingly, mammalian RAN-BP2 ligases include the E3 ligase RanBP2 which localises to the nuclear pore and is embryonic lethal in mice knockout models, illustrating that RanBP2 is essential in mammalian cells (Aslanukov et al., 2006). Interestingly, reduced RanBP2 expression results in both mitotic delays and aneuploidy, suggesting that RanBP2 has a key role in the regulation of mitosis (Dawlaty et al., 2008).

The most recently discovered class of sumo E3 ligases, the ZNF451 family, bind to the N-terminal region of Ubc9 using a cluster of internal repeats. Interestingly, ZNF451 E3 ligases are sumo2/3-specific and are exclusively expressed in mammalian cells. Structural analysis has revealed that two essential SIM domains—located in the ZNF451 E3 ligases facilitate catalysis of sumo from Ubc9 onto the substrate in a manner similar to RAN-BP2 (Reverter and Lima, 2005). ZNF451 ligases. Nevertheless, the role(s) of the ZNF451 family of sumo E3 ligases currently remains unclear, although ZNF451 substrates have been shown to be involved in transcriptional activation (Karvonen et al., 2008).

1.1.3.5 Deconjugases

Ubl modification of substrates is extremely dynamic and the removal of UbIs is catalysed by Ubl-specific deconjugases which allow the Ubl to be rapidly removed from the substrate and recycled. The majority of Ubl deconjugases are cysteine proteases, characterised by an active

site containing a conserved catalytic triad of His-Asp-Cys residues. Indeed, Ubl binding within the cysteine active site causes rearrangement of the catalytic core, facilitating the cleavage of the Ubl from the substrate (Ronau et al., 2016).

Ulp1 and Ulp2 are the only two sumo cysteine proteases expressed in *S. cerevisiae* cells. Ulp1, arguably the more important, is essential for growth whereas *ulp2* Δ cells are viable but show considerable growth defects (Li and Hochstrasser, 2000). Indeed, deletion of one chromosomal copy of *ULP1* in diploid cells results in large budded cells, whilst *ulp1^{ts}* mutants arrest in G2/M phase (Li and Hochstrasser, 1999b). Furthermore, Ulp1 also exhibits C terminal hydrolase activity, which is important for the cleavage of the Smt3 C terminal domain, enabling the maturation of Smt3. Hence, loss of Ulp1 prevents maturation of Smt3 and thus blocks sumoylation. Both Ulp1 and Ulp2 contain a conserved C terminal catalytic domain which contains two conserved cysteine residues and two conserved histidine residues (Li and Hochstrasser, 1999b). Mutation of either of these four catalytic residues results in loss of protease activity, suggesting that these residues form the catalytic core (Li and Hochstrasser, 1999b).

Ulp1 and Ulp2 display just 10% substrate overlap, suggesting that they act on specific substrates. Moreover, Ulp1 localises to the nuclear pore whilst Ulp2 is found within the nucleus, suggesting that the localisation of the two enzymes influences the recognition of target substrates. Indeed, deletion of the N-terminal domain of Ulp1 prevents Ulp1 localisation at the nuclear pore and leads to an accumulation of Smt3-conjugated substrates in the cell, suggesting that Ulp2 cannot compensate for the loss of Ulp1 in these cells (Li and Hochstrasser, 2003).

Mammalian cells express seven sumo deconjugases, SENP1-7 (Kunz et al., 2018). Mammalian SENP6 and SENP7 specifically cleave SUMO2/3 from sumo-substrate complexes indicating that sumo deconjugases show substrate specificity (Lima and Reverter, 2008). Structural analysis of the SENPs by X-Ray crystallography revealed that the active sites of SENP6/SENP7 both contain four conserved loops. Interestingly, removal of loop 1 dramatically reduces the cleavage activity of SENP6 and SENP7, whilst expression of SENP7^{V713E} abolishes cleavage of SUMO2/3 from substrates (Lima and Reverter, 2008). Thus these findings suggest that the

SEN6/7 active site may confer substrate specificity in mammalian cells (Lima and Reverter, 2008).

In contrast to the deconjugation of sumo in *S. cerevisiae*, many more ubiquitin deconjugases (DUBs) are present to remove ubiquitin from substrates. Unlike Ulp1, all *S. cerevisiae* DUBs are non-essential and this has led to the suggestion that there is a considerable substrate overlap in DUB function. Nevertheless, this does not seem to be true for the sumo deconjugation pathway. Ulp1 and Ulp2 show just 10% substrate overlap in budding yeast cells, suggesting that both Ulp1 and Ulp2 have distinct target substrates (Srikumar et al., 2013b).

1.2 Sumo Substrates

Although the characterisation of the sumo conjugation pathway described above revealed the similarities between the sumo and ubiquitin conjugation pathways, the nature of sumo substrate recognition remained uncharacterised in early studies investigating sumoylation. Hence, subsequent research has focussed on the characterisation of sumo consensus sequences and the identification of sumo substrates.

1.2.1 Sumo Consensus Sequences

Initial studies investigating substrate sumoylation suggested that sumo conjugation is facilitated by a conserved sequence motif which surrounds the target lysine residue within the substrate (Yunus and Lima, 2009a). Importantly, this motif provides a guide for the conjugation enzymes to ensure that the correct lysine(s) are modified. Interestingly, research over the last two decades has found that sumo can bind to substrates either covalently or non-covalently, with such non-covalent interactions have been suggested to act as a “scaffold” for the formation and stability of larger protein complexes (Raman et al., 2013, Matunis et al., 2006). Recognition of covalent sumo modification will now be discussed, with sumo non-covalent consensus motifs detailed later in section 1.3.1.

Early proteomic data revealed that sumo is covalently bound to lysine residues in target substrates using the conserved motif Ψ KXE (where Ψ is a hydrophobic amino acid, K is the

target lysine, X is any amino acid and E is glutamic acid) (Rodriguez et al., 2001). Mutation of either Ψ or E within the Ψ KXE motif was shown to inhibit sumoylation of target lysines, although the use of a range of amino acids at the X residue in mammalian p53 does not appear to affect sumoylation, suggesting flexibility of the amino acid located at position X (Stindt et al., 2011). However, not all lysines that are sumoylated in substrates adhere to the Ψ KXE motif (Impens et al., 2014). Indeed, strikingly, only ~50% of lysines that are sumoylated in substrates adhere to this motif in human cells (Impens et al., 2014). Moreover, Impens et al. (2014) suggested that ~11% of substrates express an inverted Ψ KXE motif, and that ~21% of substrates express motifs which do not show any homology to the classic Ψ KXE motif. Indeed, the range of potential sumo sites present in proteins has hindered the identification of substrates. Instead, sophisticated prediction software has been developed to identify potential sumo binding sites, although it is important to emphasise that these must be verified using other biochemical techniques (Beauclair et al., 2015, Zhao et al., 2014).

In addition to the Ψ KXE motif, proteomic analysis has suggested that two additional motifs (NDSM and PDSM) occur in several sumo substrates. The NDSM motif contains a group of negatively charged residues downstream from the Ψ KXE site (Yang et al., 2006). One early study characterising NDSM motifs revealed that the mammalian transcription factor Elk1 contains a NDSM motif downstream of the K249 sumoylation site. Elk1 K249 sumoylation promotes transcriptional repression by recruitment of the histone deacetylase HDAC-2 to target promoters. To investigate the importance of the Elk1 NDSM motif in mammalian cells, mutation of acidic residues located within the putative Elk1 NDSM (Elk1^{E255A,E256A,E258A}), promoted transcriptional activation in a similar manner to Elk1 K249R. These results emphasise the importance of both NDSMs and Ψ KXE motifs for modulating protein function, highlighting the importance of these negatively charged NDSM domains (Yang et al., 2006). Interestingly, this study also revealed that the expression of Elk1^{E255A,E256A,E258A} reduces the interaction between Elk1 and the sumo E2 Ubc9 interaction. Mutation of either the N-terminal Ubc9 basic motif or Elk1 NDSM motif reduces the Elk1-Ubc9 interaction but does not abolish substrate sumoylation, suggesting that the Elk1 NDSM may act to enhance the interaction with Ubc9 to promote sumoylation (Yang et al., 2006).

In contrast, the PDSM motif (Ψ KXEXXSP) comprises a serine phosphorylation site located \sim 3 residues downstream of the Ψ KXE motif, indicative that phosphorylation may influence the sumoylation status of these particular substrates (Hietakangas et al., 2006). Interestingly, this study revealed that 71% of sumo substrates containing PDSM motifs have a role in transcriptional regulation. To further characterise PDSM motifs, experiments carried out in mammalian cells revealed that inhibiting phosphorylation of the serine residue within the PDSM motif can prevent substrate sumoylation. For example, the heat shock protein HSF4, a target for SUMO-2 sumoylation in human cells, was found to contain a PDSM motif. Mutation of the serine residue within the HSF4 PDSM motif inhibits HSF4 sumoylation, proposing that HSF4 sumoylation is dependent on phosphorylation (Hietakangas et al., 2006).

1.2.2 Modes of Sumo Attachment

As illustrated in Figure 1.3, sumo can attach to target proteins in three distinct modes. The simplest sumo modification is monosumoylation, in which sumoylation occurs on a single lysine residue in the target protein. For example, the mitotic checkpoint protein BubR1 is monosumoylated in mammalian cells, with K250 being the sole BubR1 sumoylation site identified to date (Yang et al., 2012a). BubR1 K250 sumoylation is essential to facilitate the removal of BubR1 from kinetochores, thus mutation of BubR1 K250 results in mitotic delays and aneuploidy, arising from the sustained association of BubR1 with the kinetochore (Yang et al., 2012a). Hence this example illustrates how a single sumo moiety can affect the function of BubR1.

Multisumoylation occurs when a single sumo moiety is bound to multiple lysine residues in the same protein. For example, the mammalian DNA clamp Proliferating cell nuclear antigen (PCNA) has been identified as a multisumoylated protein in mammalian cells. Interestingly, it has been found that the sumoylation status of PCNA is influenced upon exposure of cells to different stress conditions (Gali et al., 2012). Another example of a multisumoylated substrate is the transcription factor, ETV4, which can be sumoylated on five different lysine residues to promote recruitment of the Ubiquitin E3 ligase RNF4 to facilitate ubiquitin-mediated ETV4 degradation in mammalian cells. Interestingly, reducing the number of sumo

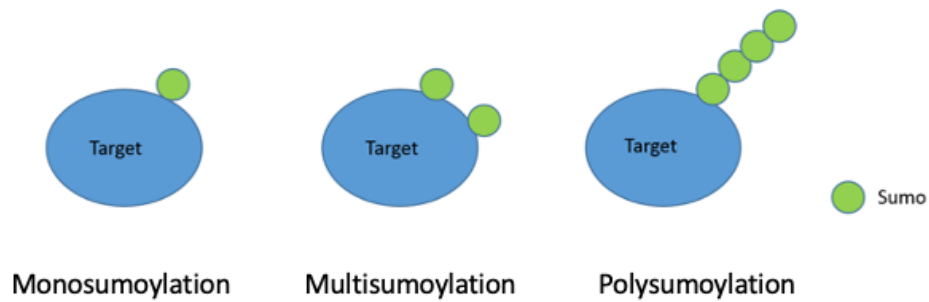


Figure 1.3. Three different modes of sumoylation. Target proteins can be subject to monosumoylation (the conjugation of a single sumo moiety to a single lysine residue), Multisumoylation (the conjugation of a single sumo moiety to multiple lysine residues) or polysumoylation (the conjugation of a sumo moiety onto an existing sumoylated lysine residue, creating a sumo “chain”) (Pichler et al., 2017). Examples of each type of sumoylation are described in more detail in section 1.2.3.

conjugation sites (by mutagenesis) in ETV4 reduces the efficiency of ETV4 degradation, suggesting that ETV4 recognition by RNF4 is dependent on multisumoylation of the transcription factor (Aguilar-Martinez et al., 2016). The third and final mode of sumo attachment is polysumoylation, in which the sumoylation of a sumo moiety already bound to a lysine residue on the target protein enables the generation of a polysumo “chain”. Unlike Ubiquitin, the extended N terminal sumo “tail” contains three crucial lysine residues which themselves are subject to sumoylation. In *S. cerevisiae* cells, Smt3 can be polysumoylated on lysine residues K9, K11 and K15. However, K15 is contained within a sumoylation site consensus motif and consequently polysumoylation primarily occurs upon K15 (Bylebyl et al., 2003). Interestingly, a mutant yeast strain expressing a version of Smt3 in which the three N-terminal lysines have been substituted with arginine to prevent polysumoylation (*smt3-allR*) is viable, indicating that polysumoylation is not an essential function of sumoylation (Bylebyl et al., 2003). Furthermore, truncation of the Smt3 N-terminal domain also retains viability, suggestive that mono and/or multisumoylation is sufficient for viability in *S. cerevisiae*. Nevertheless, *smt3-allR* mutant cells do show increased sensitivity to HU, display aberrant chromatin organisation and display a slight increase of aneuploidy compared to wild type cells, suggestive that polysumoylation may be important in mitosis (Srikumar et al., 2013a). Proteomic studies have also revealed that an abundance of polysumoylated substrates arises during several cellular stress responses, such as heat stress, suggestive that polysumo chains may function in responses to cellular stresses (Golebiowski et al., 2009).

Thus, as illustrated above, the type of covalent sumo modification may influence the change in a protein’s function. Importantly, the identification of a sumo consensus sequence enabled the identification of hundreds of putative sumo substrates using sequence analysis tools, which provided insights into the function of sumoylation. However, *in vivo* validation is always required to confirm sumo-substrate interactions. Although thousands of sumo substrates have been identified in the last two decades, the next section will focus on the identification of key sumo substrates and the proteomic methods applied during the identification of these proteins.

1.2.3 Sumo Substrates

Sumo was originally identified in 1997 as a modifier of the GTPase activating protein Ran-GAP1 in mammalian cells (Mahajan et al., 1997). Since the initial discovery of sumo, hundreds of new sumo substrates have since been identified in eukaryotic cells, ranging from transcription factors to mitotic kinases (Ban et al., 2011, Impens et al., 2014, Yu et al., 2018, Hendriks and Vertegaal, 2016). Nevertheless, the identification of sumo substrates has often proved difficult, with the rapid cycling of sumo on/off substrates often hindering substrate identification. Sumo conjugation affects protein function(s) in a variety of ways including cellular localisation, influencing protein complex formation and modulating transcription, thus it is clear why sumo targets a broad range of substrates.

1.2.3.1 Ran-GAP1

The first sumo substrate to be identified was Ran-GAP1, a GTPase activating protein expressed in mammalian cells. Studies investigating the localisation of the Ran-GAP1 at the nuclear pore revealed that an unknown modification of Ran-GAP1 facilitated localisation of Ran-GAP1 from the cytoplasm to the nuclear pore (Mahajan et al., 1997). Subsequent peptide sequencing of the modified Ran-GAP1 in mammalian cells identified a small ~10kDa protein which today is known as SUMO-1 (Mahajan et al., 1997). Interestingly, a large proportion of Ran-GAP1 remains in a sumoylated state in the cell and is targeted to the nuclear pore, suggesting a stable interaction between sumo and Ran-GAP1. In contrast to Ran-GAP1, only a small fraction of other identified sumo substrates are sumoylated in the cell at any one time, leading to the proposal of the “sumo enigma”. The “sumo enigma” suggests that only a small fraction of target substrates are required to be in a sumoylated state, indicating that sumoylation has a potent cellular effect on protein function and the downstream cellular processes (Hay, 2005). The majority of sumo substrates remain in an unsumoylated state at any one time, which is likely to be a major factor as to why sumo remained undiscovered for a considerable amount of time. Nevertheless, subsequent studies characterising Smt3 substrates in budding yeast have provided key insights into the important cellular roles of sumo.

1.2.3.2 Septins

Early studies investigating sumoylation in *S. cerevisiae* cells indicated that sumoylation was important for cell cycle progression. For example, Smt3 was found to localise to the bud neck during early G1, whilst the pattern of sumoylated conjugates changed throughout the cell cycle suggestive that different substrates are sumoylated at different times (Li and Hochstrasser, 1999a). Indeed, the first sumo substrates identified in *S. cerevisiae* were the septins (Johnson and Blobel, 1999). Septins are conserved GTP-binding proteins found throughout eukaryotes which interact together to form large complexes analogous to cellular scaffolds. In budding yeast cells, septins are essential for cell cycle progression, forming a ring structure at the bud neck during G1 which stays present throughout mitosis (Longtine et al., 1996). Three of the *S. cerevisiae* septins, Cdc3, Cdc11 and Shs1/Sep7, were identified as the first sumo substrates in budding yeast and remain one of the major sumo substrates in *S. cerevisiae* cells, suggestive of an important role for sumoylation during mitosis (Johnson and Blobel, 1999). Cdc3 contains three covalent sumoylation sites, whilst Cdc11 and Shs1/Sep7 contain one and two respectively. Surprisingly, mutation of the sumo consensus sequence to inhibit sumo binding within these three septins either separately or together was not lethal, suggesting that septin sumoylation is not an essential aspect of sumoylation (Johnson and Blobel, 1999). Nevertheless, the HMW sumo conjugates observed in *S. cerevisiae* cells arrested in G2/M were dramatically reduced in cells expressing the septin sumoylation mutants, indicating that the major sumo substrates during the cell cycle are indeed septins. Nevertheless, septin rings remain in place after cytokinesis in the septin sumoylation mutants, indicative that sumoylation may promote septin ring disassembly (Johnson and Blobel, 1999). Further work confirmed that Siz1 relocates to the bud neck during mitosis to facilitate sumoylation of the septins Cdc3 and Cdc11 (Johnson and Gupta, 2001b). Taken together, these studies suggest an important role for septin sumoylation during mitosis, possibly promoting disassembly of the septin ring to allow exit out of mitosis.

Although Ran-GAP1 in mammalian cells and the septins in budding yeast appear to be the major sumo substrates in the respective eukaryote, the identification and characterisation of other sumo substrates has often been met with many difficulties. Despite the large number of studies investigating sumoylation over the past two decades, the fundamental roles of sumoylation remain largely unknown. To date, the majority of sumo studies have utilised proteomics in order to identify pathways and proteins which are linked to sumo functions.

1.2.3.3 Sumo Proteomics

The development of sophisticated sumo proteomics over the last two decades has provided an extensive insight into the role of sumo in eukaryotes. Indeed, many studies have employed a “phishing” approach to identify substrates which has generated a huge amount of proteomic data linking sumo to key metabolic processes and stress responses. However, with such a large amount of data and a vast array of substrates, identifying which are the crucial substrates and understanding how cell processes and molecular mechanisms are influenced by sumoylation remain major areas of further investigation. Furthermore, the dynamic cycling of sumo on/off substrates coupled with the small fraction of substrates actually modified in the cell at any given time further impedes progress to understand the essential function(s) of sumoylation. The development of sumo proteomics will now be discussed in more detail, focussing on the generation and analysis of large datasets of sumo substrates.

1.2.3.4 Early sumo Proteomics

Early studies attempting to gain insight into the sumo proteome often coupled affinity purification with mass spectrometry (AP-MS). One of the first proteomic studies using this approach identified 271 new sumo substrates in *S. cerevisiae* cells (Wohlschlegel et al., 2004). However, the low abundance of purified substrates prevented the authors finding already known sumo substrates, highlighting the initial difficulties in sumo proteomics. Nevertheless, this study did observe that sumoylation is critical in several biological processes, including transcription and responses to stress, providing initial insights into the importance of sumoylation (Wohlschlegel et al., 2004). In agreement with this work, Panse et al. (2004) also found that many sumo substrates were linked to transcription and mRNA processing in *S. cerevisiae* cells (Panse et al., 2004). Importantly, Panse et al. established that the bulk of sumoylated substrates in yeast are located at the nuclear pore or within the nucleus, suggesting that sumoylated substrates have important nuclear functions (Panse et al., 2004).

Early proteomic studies aiming to identify sumoylated proteins in both yeast and mammalian cells rapidly identified that a large number of sumoylated substrates were associated with the

response to cellular stresses (Lewicki et al., 2015). For example, to gain insight into the sumo proteome in response to one such stress, replication stress, mammalian cells were treated with the DNA crosslinking agent mitomycin C (MMC), with treated cells subject to proteomic analysis. MMC activates the DNA damage response kinases ATM and ATR which phosphorylate DNA checkpoint proteins in response to double strand DNA breaks and single strand DNA accumulation (Meek et al., 2008). Strikingly, 702 unique sumo substrates were identified after MMC treatment compared to untreated cells, with the subsequent analysis revealing that the majority of these substrates were nucleolar (Munk et al., 2017). In addition, mammalian cells exposed to the DNA replication inhibitor Hydroxyurea (HU) showed significant crosstalk between sumoylation and phosphorylation, providing insights into the crosstalk between different PTMs. For example, 127 proteins were found to be subject to both modifications in HU-treated cells, suggesting a coordinated response between different posttranslational modifications in order to maintain genomic stability (Munk et al., 2017). Nevertheless, although recent proteomic studies have provided important insights into the cellular pathways affected by protein sumoylation, a number of early sumo proteomics were met with difficulties, as described below.

1.2.3.5 Difficulties in Covalent Sumo Substrate Identification

Identification of sumo substrates using mass spectrometry has proved challenging in native conditions for a variety of reasons. As sumoylation affects a small fraction of proteins in steady state conditions the majority of studies to date have incorporated AP-MS using epitope-tagged versions of sumo in order to enrich sumo-interacting proteins. However, these approaches could result in enhanced sumo overexpression or may modify the normal native sumo-substrate interactions. In addition, the conditions used in affinity purifications may disrupt weak sumo-substrate interactions, hindering identification of the substrate(s). Nevertheless, it is important to identify endogenous sumo substrates to ensure that substrates characterised by previous studies are not artefacts of a mutant sumo construct. Hence, other approaches to characterise endogenous sumo substrates involve immunoprecipitation using monoclonal SUMO-1 antibodies, although these approaches also have caveats, as detailed below (Becker et al., 2013).

Although AP-MS enables the identification of protein modifications, this technique does not provide any further insights regarding the location of these modification(s) within the substrate. Hence, the identification of site-specific modifications would enable further characterisation of these substrates, such as mutagenesis of the identified residues. Identification of site-specific lysine residues targeted for ubiquitination has been well characterised with the treatment of cellular extracts with use of the serine protease trypsin prior to MS analysis. Cellular extracts are treated with trypsin which cleaves ubiquitin at an arginine residue immediately preceding the diglycine motif. Trypsin digestion of ubiquitin results in a small KGG motif remaining on substrates, acting as a “marker” of ubiquitination. The development of an α -KGG antibody which recognises this KGG remnant left upon the ubiquitinated protein after trypsin digestion enables identification of these ubiquitinated substrates. Indeed, immuno-purification of extracts using this α -KGG antibody coupled with MS allows identification of site-specific ubiquitin modifications (Xu et al., 2010). However, initial studies attempting to identify site-specific sumo modifications using the same approach were met with difficulties. For example, trypsin digestion of SUMO-1-substrate complexes leaves a bulky adduct of 19 amino acids which is difficult to identify using mass spectrometry, as indicated by the green arrow on Figure 1.4.

Attempts to characterise site-specific sumo modifications have been aided by the generation of a 6HIS3-tagged SUMO2^{T90K} mutant which expresses a lysine residue instead of a threonine at the C-terminal domain (Tammsalu et al., 2014). Trypsin digestion of this 6HIS3-SUMO2^{T90K} mutant leaves a di-glycine remnant, which can subsequently be enriched in the same way as ubiquitin, as described above (Tammsalu et al., 2014). Trypsin treatment of immunopurified 6HIS3-SUMO2^{T90K} coupled with mass spectrometry identified 1002 novel sumoylation sites in 539 proteins, highlighting that many proteins are multi or poly-sumoylated and providing insights into the sumo proteome (Tammsalu et al., 2014). An alternative approach to identify site-specific sumo modifications within endogenous sumo substrates has utilised a novel threonine protease WaLP. WaLP cleaves after threonine residues and has been shown to

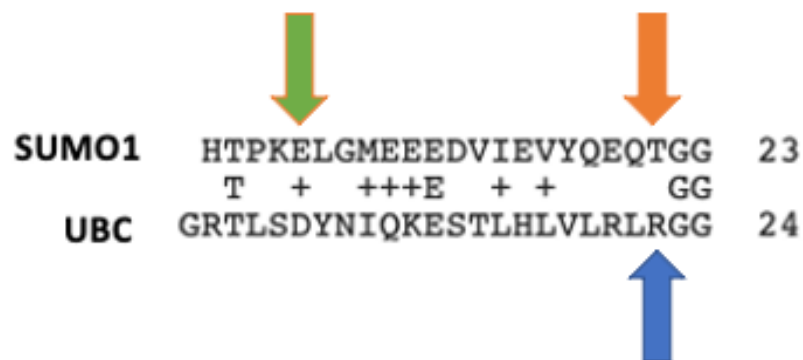


Figure 1.4. Proteolytic cleavage sites in human ubiquitin and SUMO-1 proteins. Alignment of the C terminal amino acid sequences of proteins encoded by the human *Sumo1* and human ubiquitin *UBC* genes. The trypsin digestion site at the C terminal Ubc arginine residue is indicated by the blue arrow, with the SUMO-1 trypsin digestion site indicated by the green arrow. The SUMO-1 WaLP digestion site at the C terminal threonine residue is indicated by the orange arrow.

cleave all mammalian SUMO proteins after the C-terminal TGG motif (Lumpkin et al., 2017). Remarkably, treatment of mammalian SUMO1 with WaLP leaves a KGG motif on substrates, similar to the effect of trypsin treatment of ubiquitinated substrates (Fig. 1.4). Moreover, Lumpkin et al (2017) used WaLP coupled with mass spectrometry to identify 1209 unique sumo binding sites on proteins in mammalian cells. This study also revealed that almost two thirds of the identified substrates contained more than one sumo binding site, suggesting the widespread importance of multisumoylation (Lumpkin et al., 2017).

Although traditional mass spectrometry methods have provided insights into the sumo proteome and the location of sumo modifications within these substrates, the identification of sumo substrates using the traditional MS methods does not provide information regarding the *in vivo* cellular location of the sumoylated protein(s) (although this may be inferred using other known data about the substrate). In an attempt to identify both the *in vivo* locations of sumoylated proteins and *in vivo* interactions between sumo and proteins, a bimolecular fluorescence complementation (BiFC) assay was developed in *S. cerevisiae* cells. (Sung et al., 2013). To characterise covalent sumo interactions in *S. cerevisiae* cells, genes tagged with the N-terminal domain of the Venus fluorescent protein (VFP) were crossed with a library of genes expressing VN C-terminal domain, producing a fluorescent signal when two proteins tagged with complimentary domains of the VFP interact. Importantly, *in vivo* assays allow the localisation of these interactions to be determined by microscopy. Remarkably, use of the BiFC assay revealed 367 covalent Smt3-protein interactions of which 224 of these 367 interactions were novel, suggesting that the stringent AP-MS techniques used in previous studies were ineffective at identifying weaker sumo-substrate interactions. Interestingly, 89% of sumo-substrate interactions were found to be nuclear and a significant number of sumoylated proteins were located at the spindle pole (Sung et al., 2013). Furthermore, the use of nocodazole to induce mitotic arrest in *S. cerevisiae* cells revealed that a number of cell-cycle related proteins, including the Cyclin-dependant kinase Cdc28 were subject to sumoylation. Taken together, the results from the BiFC assay suggest a significant role for sumo during the cell cycle, in agreement with Johnson and Blobel (1999).

The covalent conjugation of Smt3 to a target lysine residue involves the interaction of Smt3 with the sumo conjugation machinery, with the mature Smt3 diglycine residue enabling the

formation of a thioester bond with the E1. Therefore to investigate the non-covalent SIM interactions in *S. cerevisiae* cells, Sung et al. repeated the BiFC assay with a Smt3 mutant lacking the C terminal gly-gly residues (Smt3 Δ GG). Although the Smt3 Δ GG identified 87 non-covalent interactions, it is clear that a large number of proteins contain SIM domains, with this study providing an initial insight into the nature of SIM-containing substrates (Sung et al., 2013).

In conclusion, it appears that although the sumo proteome has been difficult to define, powerful mass spectrometry techniques have aided the identification of putative sumo substrates. Although hundreds of proteomic datasets now exist for sumoylated substrates, these datasets on their own do not show the full extent of the sumoylated landscape. Thus, analysis of sumo datasets has provided vast insights into the nature of sumoylation, with the ability to compare numerous sumo proteomic datasets facilitated by the increase of open access to raw mass spectrometry data.

1.2.3.6 Analysis of Sumo Datasets

In order to provide further insights into the sumo proteome in human cells, Hendriks and Vertegaal (2016) analysed 22 independent sets of sumo proteomic data in addition to any publicly available raw mass spectrometry data (Hendriks and Vertegaal, 2016). This study identified 7327 novel sumo sites located in 2355 different proteins, suggesting that sumoylation affects ~18% of the human proteome. Interestingly, analysis of the top 100 most reported sumo sites suggests that 79% of these sumo substrates are conjugated by sumo via the classic KXE motif. However, further analysis revealed that adherence of sumoylation to the KXE motif is dramatically reduced when cellular stress occurs suggesting that sumoylation motifs may be less strictly adhered to when a rapid increase in sumo conjugation is required (Hendriks and Vertegaal, 2016)

An overlap of covalent sumo conjugation sites with other PTMS (such as ubiquitination, acetylation or methylation) has also been identified in several studies. Indeed, Hendricks and

Vertegaal (2016) confirmed that 29% of sumo sites identified by mass spectrometry are shared with other PTMS, suggesting that sumoylation may compete with other modifications in order to finely tune the regulation of the activity or function of a protein. Interestingly, of the 5,032 sumoylation sites analysed in a study by Hendricks and Vertegaal (2016), ~26% of sumoylated lysine residues were also found to be subject to ubiquitination (Hendriks and Vertegaal, 2016).. Strikingly, further analysis of these shared ubiquitination and sumoylation lysine residues revealed that just 14% of sumoylated lysine residues within the classic KXE sumoylation consensus motif were also ubiquitinated. Hence, this observation strongly supports the hypothesis that the KXE motif provides specificity for sumoylation rather than ubiquitination of the lysine residue residing with the KXE motif (Hendriks and Vertegaal, 2016).

A more thorough understanding of global sumo interacting networks has been achieved by comparing both physical and genetic sumo interactions. Physical interactions have been identified through MS and use peptide sequences to enable substrate identification. On the other hand, genetic screens enable the identification of genetic interactions between different mutants. For example, Synthetic Genetic Array (SGA) screens performed in *S. cerevisiae* are a valuable genetic tool for identifying genetic interaction(s) linked with a mutation in a gene of interest (GOI). The SGA screen typically involves crossing a yeast strain containing a mutation in the GOI with a library of yeast mutant strains (Tong and Boone, 2006). Characterisation of the growth of the constructed double mutants, which all contain the mutant GOI together with individual gene mutations contained in the library, reveals mutations which improve the growth (suppressors) or reduce the growth (enhancers) associated with the mutant GOI. The analysis of novel enhancer interactions (which exaggerate the phenotype of the mutant gene of interest) and suppressor interactions (which alleviate the phenotype of the mutant gene of interest) can then be used to characterise the relationships between the two genes and potentially reveal genes that act in the same of different pathways.

In an initial attempt to characterise the genetic interaction network of sumo in *S. cerevisiae* cells, Makhnevych et al. (2009) conducted an SGA crossing a number of mutants from the sumo conjugation pathway with the yeast deletion (for essential genes) and temperature

sensitive (ts) library (for non-essential genes). Interestingly, the query strains used in this study included a ts allele of Smt3 (*smt3-331*) in addition to mutant alleles of the sumo E2, E3 and deconjugase enzymes. Strikingly, results from this SGA screen revealed that 20% of the genetic interactions with the *smt3-331* allele were lethal, leading the authors to suggest that 20% of sumo interactions may be non-covalent SIM interactions. Moreover, ~80% of genetic interactions were conserved between mutants of the sumo pathway, suggestive that the sumo conjugation pathway is highly co-ordinated (Makhnevych et al., 2009). Subsequent comparison of the SGA dataset (genetic) with AP-MS and yeast two hybrid (physical) data revealed that 93% of sumoylated proteins belong within 15 distinct biological processes, including DNA replication and chromosomal segregation (Makhnevych et al., 2009). Furthermore, both the physical and genetic datasets analysed in this study displayed significant overlap which is remarkable considering that physical and genetic pathways do not commonly show high levels of overlap (Kelley and Ideker, 2005) (Makhnevych et al., 2009). For example, 17% of identified substrates were found in both the Makhnevych et al. SGA and AP-MS datasets, indicative that sumoylated substrates may be sumoylated within the same molecular complexes within a given pathway. In conclusion, this study not only highlights the essentiality of sumoylation within a variety of cellular processes but also highlights the diversity of the genetic and physical interaction networks of sumoylated proteins.

It is clear that a remarkable number of studies have extensively analysed the sumo proteome in eukaryotes over the last two decades. Indeed, the development of sophisticated mass spectrometry techniques have led to the identification of thousands of sumo substrates, providing an insight into numerous sumo-regulated biological processes. However, it is also clear that further studies are needed to authenticate *bona fida* substrates and to validate putative sumo binding sites.

Proteomic studies have provided large datasets regarding the nature of covalent sumo conjugates, suggesting that sumoylation is important within a variety of cellular processes (Makhnevych et al., 2009). However, the essential nature of sumoylation remains uncharacterised. Nevertheless, the subsequent identification and characterisation of non-covalent sumo interactions have also provided key insights in the role of sumoylation, which will now be discussed in further detail.

1.3 Sumo Function

1.3.1 SIM domains

In addition to the covalent attachment of a sumo moiety onto a target lysine, protein function(s) can also be modified through the presence of Sumo Interacting Motif (SIM) domains. Sumo-SIM interactions are non-covalent and stabilise protein-protein interactions, suggesting that sumo may act as a platform on which larger complexes can assemble (Matunis et al., 2006). SIM domains are short sequences characterised by a hydrophobic core flanked by acidic residues. Importantly, these acidic residues create a β -grasp fold which interacts with a cleft on a sumo moiety, enabling direct contact with polysumoylated substrates (Hay, 2013).

Prior to the identification of SIM domains, studies in mammalian cells identified a Ubiquitin interaction motif which facilitated the non-covalent interaction between ubiquitin chains and the 26S proteasome (Young et al., 1998). Ubiquitin interaction motifs are typically ~30 amino acid in length with a hydrophobic core. Mutations removing the hydrophobic charges within the Ubiquitin interaction motif prevent Ubiquitin binding, suggesting that hydrophobic interactions are essential for Ubiquitin-substrate interactions (Young et al., 1998). In contrast to Ubiquitin consensus interaction motifs, SIM domains are short which has hindered their identification using sequence analysis (Seu and Chen, 2009). In addition, SIM domains show plasticity, not always adhering to a strict motif. For example, Jardin et al. (2015) analysed >100 SIM domains in budding yeast but were unable to find one common motif (Jardin et al., 2015). Nevertheless, additional techniques such as NMR have aided identification of putative SIM domains. SIM domains are short sequences, hence sequence alignments obtained from NMR structural data of has aided with the identification of short SIM sequences located at the sumo-substrate interface (Seu and Chen, 2009).

Initial studies investigating SIM domains in mammalian cells identified that the Ubiquitin E3 ligase RNF4 expresses 4 N-terminal SIM domains which are essential for the interaction with polysumoylated substrates (Tatham et al., 2008). Deletion of 3 of the 4 RNF4 SIM domains

prevented the binding of polysumo chains, although RNF4 mutants with a single SIM deletion only mildly reduced the binding of polysumo chains, suggesting that multiple SIM domains act in tandem to recruit polysumoylated substrates (Tatham et al., 2008). Interestingly, downregulation of RNF4 results in an accumulation of HMW sumo substrates, proposing that SIM domains may regulate the level of polysumo conjugates in the cell.

Nevertheless, since the identification of RNF4 SIM domains, hundreds of eukaryotic proteins have subsequently been predicted to contain multiple SIM domains. For example, two SIM domains in the mammalian transcriptional regulator ZMYZM2 have been shown to be crucial for the recruitment of ZMYZM2 to chromatin. (Aguilar-Martinez et al., 2015). Interestingly, the same study revealed that epitope-tagged versions of additional SIM-contacting proteins PTRF, BLM, and ZMYM2 were able to bind a GST-tagged 5xSUMO-2 construct, but not to a GST-tagged single copy of SUMO-2. This strongly suggests that SIM domains have a preference to bind to multiple sumo moieties, such as those found on poly-sumoylated substrates, rather than single sumo moieties, in agreement with Tatham et al., (2008). Furthermore, SIM interactions between substrates found within the same complex may act similar to a “molecular glue” in order improve the stability of large protein complexes (Matunis et al., 2006).

Although the initial studies investigating the role of sumo SIM domains suggested that non-covalent sumoylation enhanced the stability of large protein complexes, recent studies have revealed a more novel role for SIM domains. Crosstalk between the sumo and ubiquitin pathways has been found to be mediated by the presence of these SIM domains, with the identification of ubiquitin E3 ligases which express SIM domains providing a link between sumo and ubiquitin modifications.

1.3.2 STUbLs

Studies in *S. cerevisiae* identified that a family of Sumo targeted Ubiquitin E3 ligases (STUbLs) recognise and target polysumoylated substrates for proteasomal-mediated degradation (Parker and Ulrich, 2012). STUbLs contain multiple SIM domains, thus are able to interact

with polysumoylated proteins, providing crosstalk between the sumo and ubiquitin pathways. STUbLs also contain RING domains (section 1.1.3.4), characterised by the co-ordination of two zinc atoms by an octamer consisting of eight cysteine and histidine residues (Lorick et al., 1999). RING domains enhance interactions between the STUbL and ubiquitin conjugation pathway E2 enzymes (Uzunova et al, 2007). Mutations within the SIM domains expressed by STUbLs prevent the recruitment of polysumoylated substrates to the proteome, suggesting that STUbLs directly interact with polysumoylated proteins (Mullen and Brill, 2008). *S. cerevisiae* cells express three STUbLs; Uls1 (also referred to as Ris1), Rad 18 and the Slx5/Slx8 heterodimer. Slx5/8 is the principle STUbL in budding yeast cells and was originally identified in a genetic screen identifying proteins which caused lethality when crossed with a strain containing a deletion of the Sgs1 DNA helicase (Mullen and Brill, 2008). In agreement with the multiple SIM domains expressed by STUbLs, studies have identified that the Slx5/Slx8 STUbL has a preference for polysumoylated, rather than multiumoylated, substrates (Tan et al., 2013). *slx5Δslx8Δ* cells accumulate extremely high levels of HMW sumo conjugates suggesting that the removal of polysumoylated substrates via STUbLs is an essential component of the sumo conjugation cycle (Uzunova et al., 2007). Interestingly, the same HMW sumoylation associated the *slx5Δslx8Δ* strain is also observed in *ubc4Δubc5Δ* cells, suggesting that these two E2 enzymes are responsible for the ubiquitination of polysumoylated proteins upon STUbL recognition. In vivo, *S. cerevisiae* Slx5/8 localise to double strand breaks and are extremely sensitive to HU, indicative that Slx5/8 may be important for the DNA damage response (Nagai et al., 2008).

In comparison to Slx5/8, much less is known about the nonessential STUbL Uls1 in budding yeast. Uls1 has been shown to interact with both Ubiquitin E2 enzymes and sumoylated substrates, suggesting that it functions as a STUbL in *S. cerevisiae* cells. Although Uls1 contains 4 N-terminal SIM domains, ubiquitin E3 ligase activity of Uls1 remains elusive (Uzunova et al., 2007) (Tan et al., 2013). Nevertheless, *uls1Δslx5/8Δ* cells accumulate HMW sumo conjugates strikingly similar to *slx5Δslx8Δ* double mutants, indicative that Uls1 is important for the removal of sumo conjugates (Tan et al., 2013).

The fourth and final STUbL expressed in *S. cerevisiae* cells is Rad18. Initial characterisation of Rad18 revealed that Rad18 has a key role in ubiquitinating PCNA during the DNA damage

response, although additional studies have since revealed that Rad18 also targets polysumoylated substrates for ubiquitination (Parker and Ulrich, 2012). Mutation of a putative SIM domain in Rad18 significantly reduced Rad18 covalent sumoylation, suggesting that the Rad18 SIM domain may promote Ubc9 recruitment to Rad18 (Parker and Ulrich, 2012). Interestingly, Rad18 is also subject to both covalent and non-covalent sumoylation.

Similar to many enzymes found within the Sumo and Ubiquitin conjugation pathways, STUbLs are highly conserved throughout eukaryotes. RNF4 was identified as the homologue of Slx5/Slx8 in mammalian cells, although these two proteins do share significant sequence homology (Galanty et al., 2012). Similar to yeast STUbLs, RNF4 contains four SIM domains and a C-terminal RING domain which enables recognition and ubiquitination of polysumoylated substrates. Interestingly, expression of RNF4 in *S. cerevisiae slx5Δslx8Δ* cells rescues the lethality of the *slx5Δ/slx8Δ/srs2Δ* strain, highlighting the conservation between RNF4 and Slx5/Slx8 functions (Mullen et al., 2011). RNF4 has since been shown to be important for genomic integrity, with studies investigating the disease acute promyelocytic leukaemia (APL) identifying a key role for RNF4 in the treatment of the disease. APL is caused by a chromosomal translocation, resulting in the fusion of the promyelocytic leukaemia (PML) and retinoic acid receptor α (RAR α) proteins. Interestingly, treatment of APL with arsenic has been shown to be extremely effective, resulting in degradation of the PML-RAR α fusion protein. Tatham et al. (2008) identified that arsenic-induced PML-RAR α fusion polysumoylation facilitated the recruitment of RNF4 and the subsequent degradation of the PML-RAR α fusion protein (Tatham et al., 2008).

In conclusion, SIM domains appear to facilitate the crosstalk between sumo and ubiquitin, targeting sumoylated proteins for proteasomal degradation. However, this crosstalk between different PTMs is not unique, and will now be discussed in further detail.

1.3.3 Crosstalk between different PTMs

Crosstalk between different PTMs has been shown to be important within a number of cellular processes, including mammalian antiviral responses and the response to DNA damage (Hunter and Sun, 2008). As described above, one mechanism of crosstalk between the sumo and Ubiquitin pathways is mediated. In addition, the post-translational modification of a

substrate often acts to inhibit or stimulate the modification of another PTM, as highlighted in the examples below.

Phosphorylation affects thousands of cellular substrates and plays key roles in a number of cellular and metabolic processes. As described in section 1.2.1, phosphorylation of PDSM motifs located downstream of the sumoylation motif can influence substrate sumoylation. For example, phosphorylation of the mammalian transcription factor c-Jun inhibits c-JUN sumoylation, increasing the transcriptional activity of the c-JUN downstream target genes (Tomasi and Ramani, 2018).

To further characterise the crosstalk between sumoylation and phosphorylation, Hendriks et al (2017) analysed sumo proteomic data to identify sites which were subject to both sumoylation and phosphorylation (Hendriks et al., 2017). Strikingly, >800 of identified sumoylation sites were also found to be subject to phosphorylation, with these co-modifications occurring in a cell cycle dependant manner (Hendriks et al., 2017). Treatment of mammalian cells with CDK inhibitors reduced both phosphorylation and sumoylation, suggesting that phosphorylation-dependant sumoylation is critical for cell cycle progression (Hendriks et al., 2017). Taken together, these two examples illustrate how the regulation of sumo and phosphorylation targeting the same substrates can modify protein function.

In addition to phosphorylation, recent studies have also suggested that sumo may compete with acetylation to modulate transcription factor activity (Van Rechem et al., 2010). For example, the mammalian tumour suppressor protein p53 is subject to both sumoylation and acetylation (Wu and Chiang, 2009). Interestingly, both acetylation and sumoylation of p53 occur on the same residue (K386) and act antagonistically to modulate the transcriptional activity of p53. Indeed, K386 sumoylation of p53 in mammalian cells prevents the association of p53 with DNA binding elements in order to prevent gene expression. Conversely, the acetylation of p53 K386 promotes the interaction between p53 and the histone acetyltransferase p-300, stimulating transcriptional activity (Wu and Chiang, 2009).

Numerous other PTMs, including methylation, have also been shown to compete for sumo binding sites throughout eukaryotes. These will not be discussed in further detail here, but

please see the following reviews for more details (Vu et al., 2018, Wu et al., 2019). It is clear that cross talk between different PTMS influence cellular signalling pathways, hence the characterisation and identification of sumo substrates could further aid our understanding of the role of sumoylation within these pathways. In order to characterise the function(s) of sumoylation, much knowledge has been gained by the characterisation of sumo function.

As mentioned in section 1.2.3.4, numerous proteomic studies have identified thousands of sumo substrates throughout a range of eukaryotic organisms, linking sumoylation to a diverse range of cellular processes. However, although these studies have provided large datasets and revealed hundreds of putative sumo substrates, the effect of sumoylation on these pathways requires the characterisation of individual substrates. Therefore, to gain insight into the nature and function of sumoylation of individual proteins within these pathways, much research has focussed on the characterisation of sumo substrates which have appeared in multiple proteomic datasets. Thousands of sumo substrates have been identified linking sumoylation to a plethora of cellular processes, for reviews see (Zilio et al., 2017, Costanzo et al., 2010, Hay, 2005, Hay, 2013). For the purpose of this thesis, we will focus on four established functions of sumoylation; mitosis, gene expression, the sumo “cloud” and the sumo stress response, each of which are described in more detail below.

1.3.4 Mitosis

Many essential aspects of sumo feature in mitosis, but the exact role(s) of sumo in mitosis are not clear. Initial work in *S. cerevisiae* initially identified Smt3 as a genetic suppressor of a mutation in the centromeric binding protein *MIF2*, providing an early link between Smt3 and mitosis (Meluh and Koshland, 1995). Hence it is unsurprising that several Smt3 mutants have subsequently been shown to display phenotypes associated with a cell cycle delay. For example, depletion of either Smt3 or Ubc9 in *S. cerevisiae* cells results in a G2 arrest, characterised by large budded cells containing a single nucleus (Biggins and Murray, 2001, Dieckhoff et al., 2004). In addition, *S. cerevisiae* cells expressing a ts *smt3-331* allele showed a defect in sister chromatid separation in addition to a metaphase delay when placed at the non-permissive temperature, suggesting that sumo may be a key regulator of mitotic progression (Biggins and Murray, 2001).

Examples linking sumo function to mitosis in *S. cerevisiae* will now be discussed, focussing on the mitotic spindle and the metaphase to anaphase transition. For additional information regarding the role of sumo in mitosis, please see reviews (Mukhopadhyay and Dasso, 2017, Gutierrez and Ronai, 2006, Mukhopadhyay and Dasso, 2010). Examples linking sumo to mitotic regulation in other eukaryotes will also be discussed to highlight the conservation of these pathways throughout eukaryotes.

The anaphase promoting complex (APC/C) is an evolutionary conserved protein complex which facilitates the entry into anaphase and the subsequent separation of sister chromatids during mitosis. The APC/C has ubiquitin E3 ligase activity, enabling the targeting of mitotic proteins for degradation to facilitate cell cycle progression. Interestingly, a number of substrates targeted for proteolytic degradation by the APC/C also appear to be regulated by sumoylation. For example, the degradation of B-cyclins, a major target of the APC/C, is impaired in *S. cerevisiae* cells expressing ts alleles of Smt3 or Ubc9 at the non-permissive temperature, suggesting that sumoylation of the APC/C subunits are critical for the timely entry into anaphase (Dieckhoff et al., 2004).

In addition to studies in budding yeast, Sumo mutants expressed in other species of yeast also show cell cycle defects similar to those observed in *S. cerevisiae* sumo mutants. For example, although deletion of *pmt3*, the sumo homologue expressed in *S. pombe*, is not lethal, *pmt3Δ* cells display chromosomal segregation defects similar to those detected in *S. cerevisiae* cells expressing ts alleles of Smt3 or Ubc9 at the non-permissive temperature (Tanaka et al., 1999). Interestingly, when compared to wild type cells, *pmt3Δ* cells showed a 50-fold higher loss of a non-essential minichromosome, suggestive that Pmt3 is crucial for chromosomal segregation (Tanaka et al., 1999).

Additional studies in mammalian cells also confirmed an important role for sumo in mitosis. For example, mammalian cells expressing reduced levels of either SAE1 or SAE2 show a delayed entry into anaphase, with both mutants also showing significant delays in chromosomal alignment, suggestive of a defect during anaphase (Eifler et al., 2018). Subsequent identification of the APC/C as a sumo substrate in mammalian cells confirmed

the findings of Dieckhoff et al. in yeast cells, in which inhibition of sumoylation prevented degradation of APC/C substrates, suggesting that sumoylation may affect APC/C activity. Indeed, inhibiting sumoylation of the APC4 subunit of the APC/C in mammalian cells lead to a delayed entry into mitosis, indicating that APC/C activity is subject to sumo-dependant regulation (Eifler et al., 2018). Consistent with the hypothesis that sumo is a key regulator of mitosis, the highly conserved mitotic kinase Aurora B, which regulates the separation of sister chromatids in anaphase has also been shown to be a target of sumoylation in mammalian cells (Ban et al., 2011). Aurora B is specifically sumoylated by PIAS3 on K202 which resides within the catalytic region of Aurora B. Sumo modification of Aurora B occurs early in G1 phase, with K202 sumoylation stimulating the subsequent autophosphorylation of Aurora B at T323. Hence, co-operativity between sumoylation and phosphorylation promotes the activation of kinase activity (Ban et al., 2011). Importantly, this example illustrates the potency of sumoylation, as the sumo modification of just a single lysine residue in Aurora B can trigger progression through the cell cycle. Furthermore, Pelisch et al (2014) also found that sumo co-localised and modified the *Caenorhabditis elegans* homologue of Aurora B, Air2, on chromosomes during metaphase, suggesting that Aurora B sumoylation is conserved throughout eukaryotes (Pelisch et al., 2014).

Studies focussing on the sumo deconjugases have provided further evidence for the relationship between sumo and the regulation of mitosis. In particular, reduced expression of deconjugase SenP5 reduces the rate of cellular proliferation in mammalian cells, suggesting that desumoylation of substrates is important in the timely completion of mitosis (Di Bacco et al., 2006). Furthermore, mammalian cells expressing reduced levels of SenP5 appear larger than wild type cells with a significant proportion of these cells containing >1 nucleus per cell (Di Bacco et al., 2006). Taken together these examples suggest that desumoylation of mitotic proteins may be important for cytokinesis to ensure that each daughter cell receives the correct number of chromosomes. It is clear that depletion of the enzymes involved in both the sumo “on” and “off” pathways result in mitotic delays, indicating that both sumo conjugation and deconjugation are crucial for timely cell division.

In addition to the APC/C, several other mitotic complexes are subject to regulation by sumoylation. One such example is the kinetochore, which contains ~60 proteins in yeast cells

and provides a physical link between chromosomes and microtubules during mitosis (Santaguida and Musacchio, 2009). Interestingly, overexpression of the mammalian sumo deconjugase SenP5 prevents the association of microtubule motor proteins (MAPs) with the kinetochore, resulting in cells arresting in metaphase (Zhang et al., 2008b). Interestingly, Sumo-2/3 are unable to localise at kinetochores in cells overexpressing SenP5, suggestive that the loss of sumoylation at kinetochores promotes a cell cycle arrest (Zhang et al., 2008b).

In addition to studies in budding yeast and mammalian cells, research using the nematode worm *C. elegans* has also provided key insights into the role of sumoylation during mitosis. In agreement with the findings in *S. cerevisiae* sumo mutants, chromosomal misalignment is apparent in *C. elegans* cells expressing reduced levels of either sumo or Ubc9 (Pelisch et al., 2014). Indeed, the rate of chromosome segregation was found to be almost twice as slow in Ubc9 knockdown cells compared with wild type cells, highlighting that inhibition of sumoylation promotes a delayed entry into anaphase (Pelisch et al., 2014). Interestingly, sumo localises to the spindle midzone in early metaphase in *C. elegans* cells, migrating to the centrosome in late metaphase. However, sumo co-localisation with the centrosome decreases as entry into anaphase begins, suggesting that removal of sumoylated proteins from centrosomes may facilitate timely anaphase entry (Pelisch et al., 2014). Targeting substrates for polysumoylation is known to recruit STUBs to target proteins for degradation, thus it is possible that polysumoylation of mitotic proteins may facilitate their degradation to allow entry into anaphase. Interestingly, during meiosis in *S. cerevisiae* cells, the Slx5/8 heterodimer triggers chromosomal separation (Liu et al., 2020). Hence it is possible that Slx5/8 may also promote chromosomal segregation during mitosis. Indeed, DNA content analysis revealed significant aneuploidy in *S. cerevisiae slx5Δ/slx8Δ* cells, which may arise from inaccurate chromosomal segregation (van de Pasch et al., 2013).

As illustrated above, sumoylation appears to be a critical regulatory mechanism to ensure faithful chromosomal segregation during cell division. However, although a large number of mitotic proteins have been identified as sumo substrates, further work is required to characterise the importance of sumoylation upon the individual substrates and the global effect of these sumoylated substrates. Nevertheless, mitotic proteins represent only a fraction of sumo substrates identified in large scale sumo screens. Transcription factors represent one

of most frequently identified category of sumo substrates in early sumo studies, suggesting that sumoylation may regulate gene expression, which will now be described in further detail.

1.3.5 Gene Expression

One of the first identified roles of sumoylation was the modulation of gene expression, with early work in mammalian cells identifying that transcriptional activity of the tumour suppressor p53 was enhanced by sumoylation (Kahyo et al., 2001). Indeed, changes in both transcriptional repression and, to a lesser extent, transcriptional activation have been closely linked with the sumoylation status of transcription factors. To date, sumo proteomic data suggests that ~300 transcription factors are subject to sumo conjugation in mammalian cells, highlighting that sumoylation is a key regulator of gene expression (Hendricks et al, 2017). Sumoylation can affect gene expression in a variety of different ways, with a number of different mechanisms proposed to explain how sumoylation regulates gene expression. Several examples of the influence of sumoylation upon transcription factor activity in human cells are shown in Table 1.3.

Firstly, sumoylation of transcription factors may facilitate the recruitment of additional proteins which directly bind to DNA sequences to modulate gene expression. For example, sumoylation of the mammalian transcription factor Elk-1 has been shown to recruit the histone deacetylase HDAC2 to chromatin (Gill, 2005). Importantly, the co-repressor HDAC2 prevents gene transcription and thus sumoylation promotes gene repression. Indeed, mutation of Elk1 sumoylation sites prevents the recruitment of HDAC2 and gene expression is not reduced. These findings are consistent with the hypothesis that sumo regulates downstream gene expression by HDAC2 through modification of Elk1 (Gill, 2005).

Another example of sumo-dependant gene repression is the sumoylation of the mammalian transcription factor Sharp-1 in mammalian cells. During embryonic development, Sharp-1 is subject to SUMO-1 modifications, enabling the recruitment of the co-repressing histone methyltransferase G9a in order to prevent skeletal muscle differentiation (Wang et al., 2013). Mutation of the identified Sharp-1 sumoylation sites K240 and K255 prevents the Sharp-1-G9a interaction, thus promoting undesirable cellular differentiation in muscle cells. This

example highlights the importance of sumoylation during embryonic maturity, in which sumo-regulated gene expression governs the fate of developing cells (Wang et al., 2013).

Transcriptional Effect	Target protein	Lysine Residue	Reference
Activation	p53	K368	Rodriguez et al, 1999
	HSF-1	K298	Hong et al, 2001
	GR	K277 K293 K703	Tian et al, 2002
Repression	HDAC1	K444 K476	David et al, 2002
	p300	K1020 K1024	Girdwood et al, 2003
	Jun	K229	Muller et al, 2000

Table 1.3 Sumoylation of mammalian transcription factors can promote transcriptional activation and repression. Examples of transcription factors in mammalian cells which are subject to sumoylation. Target lysine residues and the effect of sumoylation are detailed in columns 1 and 2. A more detailed review by Rosonina et al. (2017) provides more examples of transcription factors modified by sumo (Rosonina et al., 2017).

Gene expression can also be influenced by the cellular location of transcription factors with protein localisation known to be one consequence of protein sumoylation. Location of transcription factors within the cell is important, as transcription factors located outside of the nucleus are no longer able to interact with DNA to regulate gene transcription, providing a method of preventing gene expression. There are many examples of the effects of sumoylation on the localisation of mammalian transcription factors, for reviews see (Garcia-Dominguez and Reyes, 2009) and (Rosonina et al., 2017).

One well characterised example of sumo-induced transcription factor localisation is the mammalian transcription factor Foxm1b which is required for mitotic progression. Interestingly, sumoylation of Foxm1b occurs in late mitosis, concurrent with the degradation of Foxm1b and the repression of gene expression in late mitosis (Zhang et al., 2015, Wang et al., 2014a). Furthermore, sumoylation of Foxm1b also promotes the localisation of Foxm1b to the cytosol in order to prevent gene expression (Zhang et al., 2015). Interestingly, the expression of a Foxm1b-6KR mutant lacking the 6 Foxm1b sumoylation sites was unable to relocate to the cytosol, suggesting that the sumo-dependent localisation of Foxm1b is critical for gene repression in late mitosis. Foxm1b degradation in late M phase coincides with polysumoylation of Foxm1b, enabling the subsequent recruitment of STUbLs to promote ubiquitin mediated Foxm1b degradation (Zhang et al., 2015). Taken together, these results propose a mechanism in which Foxm1b sumoylation promotes mitotic progression by the localisation Foxm1b to the cytosol where it is degraded by the APC/C.

In contrast to these inhibitory effects of sumoylation, phosphorylation of Foxm1b by the mitotic kinase Plk1 in early mitosis promotes transcriptional activation of genes required for cell cycle progression. Interestingly, phosphorylation of Foxm1b prevents the sumoylation of Foxm1b by promoting the retention of Foxm1b to the nucleus, where it activates gene expression whilst unable to undergo sumo modification. Only in late M phase, when the levels of Plk1 drop, is Foxm1b able to undergo sumo modifications (Pietilä et al., 2016). Different PTMs often compete for the same residues in target substrates, although it remains to be determined whether this is true for phosphorylation/sumoylation of Foxm1b.

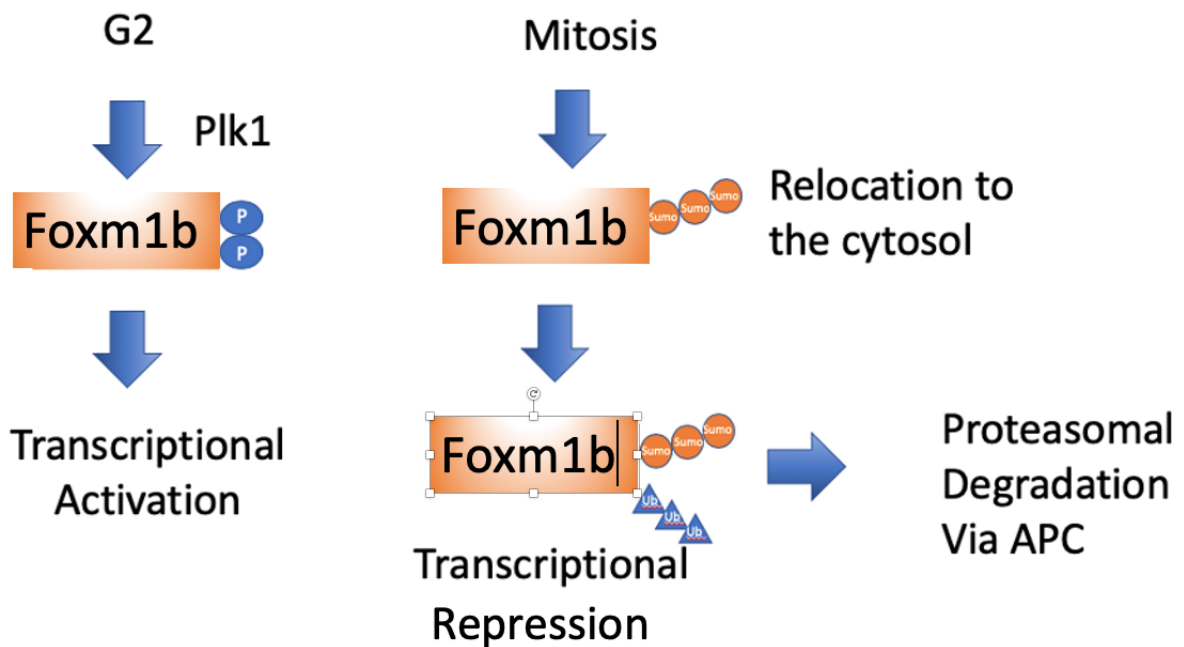


Figure 1.5 Different PTMs regulate the activity of Foxm1b. In late G2, phosphorylation of Foxm1b by Plk1 retains Foxm1b in the nucleus, promoting transcriptional activation. Towards late mitosis, the cellular levels of Plk1 drop, allowing Foxm1b sumoylation and the relocation of sumoylated Foxm1b to the cytosol, repressing transcription. Polysumoylation of Foxm1b enables the recruitment of STUBs, with the targeted degradation of Foxm1b by the APC/C, with cells now able to exit mitosis (Zhang et al., 2015).

Hence, Foxm1b regulation by Plk1 facilitates the progression of the cell through G2 phase and entry into mitosis. The levels of Plk1 activity and sumoylation of Foxm1b act antagonistically during the cell cycle, illustrating how different opposing modifications can influence the function of a protein (Fig. 1.5).

In addition to Foxm1b, other transcription factors have been shown to be regulated by sumoylation. For example, STAT5, an essential mammalian transcription factor crucial for lymphoid development, is sumoylated to promote transcriptional repression. In its inactive form, when transcription of lymphoid development genes are not required, STAT-5 remains in the cytosol, unable to access target DNA sequences to enable transcriptional activity (Levy and Darnell, 2002). However, activation of STAT-5, stimulated by cytokines, recruits the Jak3 protein kinase which induces STAT-5 Y694 phosphorylation. Importantly, phosphorylated STAT-5 dimers relocate to the nucleus, in order to modulate transcriptional activity, (Levy and Darnell, 2002). When transcriptional activity is no longer required, STAT-5 dephosphorylation promotes localisation to the cytosol, where STAT-5 remains inactive (Fig. 1.6) (Van Nguyen et al., 2012).

Although phosphorylation provides an on/off mechanism to modulate the transcriptional activity of STAT-5, recent evidence has also suggested that sumoylation may also affect the STAT-5 activity. For example, the nuclear accumulation of sumoylated STAT-5 is induced in mammalian cells depleted of SENP1, suggesting that sumoylated STAT-5 promotes transcriptional activity, with sumoylated STAT-5 retained in the nucleus (Van Nguyen et al., 2012). In order to determine the transcriptional effects of STAT-5 sumoylation, mutation of the STAT-5 sumoylation site K696 by expression of a STAT-5^{K696R} mutant revealed that STAT-5^{K696R} cells show reduced transcriptional activity. Although STAT-5^{K696R} mutants suggests that sumoylation of STAT-5 directly modulates gene expression, this mutation does not completely inhibit transcriptional activation, suggesting that other sumoylation sites or PTMs of STAT-5 are important (Van Nguyen et al., 2012).

Research has also revealed that the sumoylation inhibits the phosphorylation of STAT5 at Tyrosine 964, suggesting that sumoylation provides an “off” mechanism for STAT-5 activity.

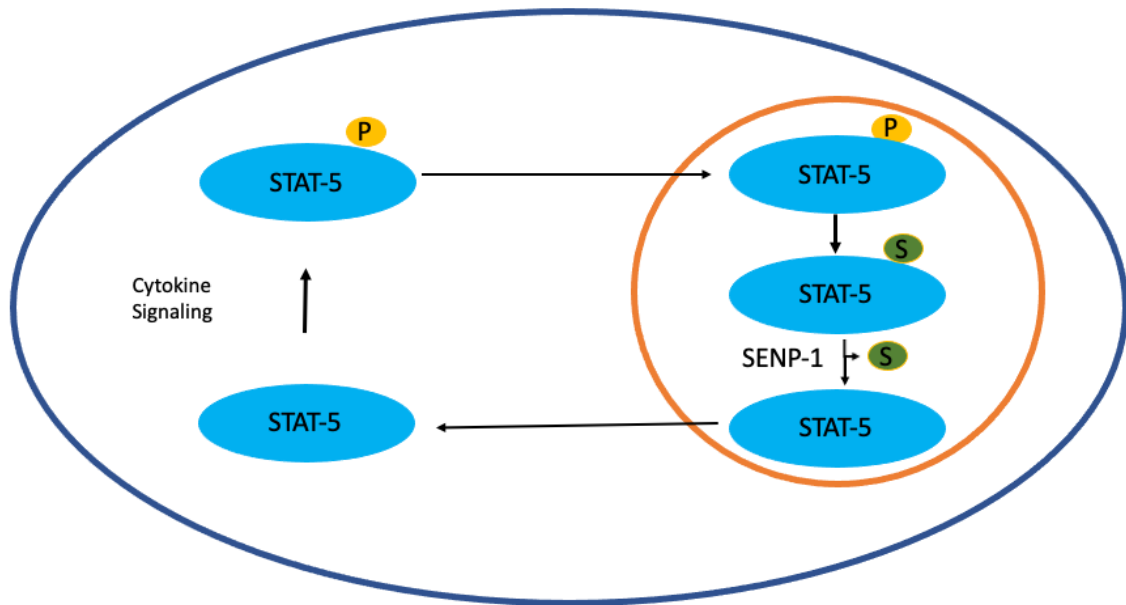


Figure 1.6 Sumoylation and phosphorylation regulate the transcriptional activity of STAT-5. Cytokine activity stimulates STAT-5 Y964 phosphorylation which promotes the nuclear localisation of STAT-5, activating transcription. When STAT-5 activity is no longer required, STAT-5 sumoylation promotes Y964 dephosphorylation. Nuclear SENP1 desumoylation of STAT-5 facilitates localisation of STAT-5 to the cytosol, where it remains in an inactive state. Modified from (Van Nguyen et al., 2012).

Interestingly, the expression of phosphomutant STAT-5^{Y694A} also inhibits STAT-5 sumoylation, suggesting that both phosphorylation and sumoylation are required for STAT5 regulation (Van Nguyen et al., 2012). Taken together, this example illustrates the importance of crosstalk between different PTMS in order to modulate gene expression using a single transcription factor. The phosphorylation of STAT-5 enables nuclear localisation and gene expression whilst STAT-5 sumoylation (by an unknown stimulus) promotes STAT-5 dephosphorylation. SENP1 desumoylates STAT-5 in the nucleus, facilitating cytoplasmic localisation and STAT-5 inactivation (Van Nguyen et al., 2012) (Figure 1.5). This example clearly highlights the levels of complex regulation governing the function of STAT-5. Similar regulatory mechanisms are also found in the regulation of other transcription factors, in which sumo affects transcription factor localisation in order to regulate gene expression.

Other examples suggesting that sumo has a key role in regulating gene expression include the discovery of that all four budding yeast histones were identified as sumo substrates in early sumo studies. Histones enable the condensation of DNA into chromatin, providing structural support whilst also modulating gene expression, with histone sumoylation acting to repress gene expression (Nathan et al., 2006). Indeed, expression of a constitutively sumoylated histone H2B significantly reduced transcriptional initiation, confirming that sumoylation has a negative effect on gene expression. Interestingly, reducing H2B sumoylation also promoted H2B acetylation in budding yeast (Nathan et al., 2006). Histone acetylation is generally associated with gene expression, thus the competition between sumoylation and acetylation sites may influence the transcriptional activity of yeast histones. Furthermore, adjacent sumoylation and acetylation sites were identified in budding yeast histones suggesting that competition between acetylation and sumoylation may regulate gene expression (Nathan et al., 2006).

It is clear that sumoylation has a potent effect on gene expression, with the sumoylation of transcription factors generally promoting transcriptional repression. Furthermore, the competitive interplay between sumo and other PTMs in order to affect transcription factor activity highlights the importance of the correct regulations of these modifications.

Nevertheless, although important for modulating transcriptional activity, sumo also plays a key role in many other cellular processes.

1.3.6 Sumo “cloud”

Sumoylation not only affects the regulation and function of the target protein but it can also influence the behaviour of other interacting proteins of the substrate. Indeed, many of these substrate interacting partners express SIM-domain(s), which allows recognition and binding to the sumoylated substrate. Sumo-SIM interactions can both stimulate and stabilise the formation of large protein complexes, which has led to the suggestion that a major function of sumo in cells is to act as a “molecular glue” to hold complexes together (Raman et al., 2013). For example, 7 subunits in the *S. pombe* TFIID complex have been found to be sumoylated suggesting that sumoylation is crucial for the stability of this large complex (Nie et al., 2015). The “sumo cloud” phenomena is observed in a number of large molecular complexes. Indeed, proteomic studies in *S. cerevisiae* have also confirmed that a number of sumoylated substrates reside with the same molecular complexes, with 12 putatively sumoylated proteins associated with the RNA Polymerase II complex (Panse et al., 2004).

Taken together, it appears that, in addition to modulating protein function, sumoylation can influence the stability of large protein complexes (Matunis et al., 2006). Thus, it can be concluded that sumoylation has diverse effects on a proteins function, although it is clear that further characterisation of sumo substrates is vital to understand the fundamental nature of sumoylation.

1.3.7 The Sumo Stress Response

The sumo stress response (SSR), has been well researched over the last twenty years, characterised by the rapid induction of HMW sumo conjugates in response to a variety of stress conditions. This conserved SSR is observed in many eukaryotes, although the exact mechanisms and pathways underlying many of these stress responses remain to be determined. The SSR is extremely important as the response of cells to external stresses must be tightly controlled in order to maintain homeostasis and ultimately maintain the survival of

the cell. Interestingly, the SSR is induced in response to a variety of cellular stresses, which will be described in more detail below.

1.3.7.1 Global Changes in Sumoylation

The most striking cellular response to a variety of stress conditions is the substantial increase in the levels of HMW sumo conjugates that is observed in eukaryotic cells. For example, Lewicki et al. (2015) subjected *S. cerevisiae* cells to a range of different stresses and found that although the characteristic accumulation of HMW sumo substrates was observed in response to different cellular stresses, the kinetics of the conjugation/deconjugation cycle differed between different stresses (Lewicki et al., 2015). Indeed, osmotic stress promoted maximum levels of HMW sumoylation in just two minutes whereas it took fifteen minutes before the majority of HMW sumo conjugates had accumulated in the response to ethanol. Moreover, HMW sumoylation is sustained in H₂O₂-treated cells for >sixty minutes in contrast to just ten minutes in sorbitol-treated cells (Lewicki et al., 2015). Hence, taken together, these results suggest that the SSR displays specific kinetics that are dependent on the nature of the stress condition.

1.3.7.2 Heat Shock

The cellular response to heat shock has been one of the most widely studied responses of the SSR. Saitoh and Hinchey (2000) initially demonstrated that HMW Sumo2/3 conjugates accumulate in mammalian cells within just 5 minutes of exposure to high temperatures (Saitoh and Hinchey, 2000). Interestingly, re-incubation of these heat-stressed cells at the lower permissive temperature results in an accumulation of free Sumo2/3. This led the authors to suggest that the SSR to heat is reversible and involves a dynamic turnover of free sumo. One explanation for the sustained increase in HMW sumo conjugates is the heat-sensitive nature of the SENPs (Pinto et al., 2012). Exposure of cells to high temperature renders the SENPs inactive, which the authors suggested is through inactivation of the catalytic cysteine of the SENPs. The importance of sumo for the response to high temperature is emphasised by the observation that human cells expressing reduced levels of Sumo2/3

display decreased survival rates compared to that of wild type cells when incubated at 42°C (Golebiowski et al., 2009). These results strongly indicate that sumoylation positively promotes cellular integrity at high temperatures.

Proteins are extremely prone to denaturation at high temperatures. Interestingly, the upregulation of Heat Shock Proteins (HSPs) is a characteristic response of cells to heat shock in order to prevent protein misfolding and to preserve protein function. For example, Hong et al. (2001) observed that sumoylation of HSF1, a key transcription factor that induces the expression of HSPs, facilitates HSF1 binding to HSP gene promoter regions to allow transcription of HSP genes during heat shock (Hong et al., 2001). Indeed, preventing sumoylation of HSF1, by expression of HSF1^{K298R} resulted in a reduction in the levels of both cellular HSF1 and HSF1-regulated gene expression. Hence, it appears that HSF K298 sumoylation is a crucial cellular response to high temperature (Hong et al., 2001).

Interestingly, Liebelt et al. (2019) demonstrated that inhibiting HSF1 expression in mammalian cells mimicked the SSR as there was a corresponding accumulation of Sumo2/3 conjugates (Liebelt et al., 2019). The same study also used mass spectrometry analysis to show that >450 proteins were subject to sumoylation upon heat shock. Interestingly, almost 50% of these sumo-conjugated proteins returned back to an unsumoylated state after incubation at the permissive temperature for 4 hours after heat stress (Liebelt et al., 2019). These observations clearly support the hypothesis that sumoylation is a rapid, dynamic response to heat stress. Furthermore, repeating the heat shock experiments with the addition of a proteasome inhibitor resulted in >80% of proteins remaining sumoylated 2 hours after heat stress, compared to just 50% when no proteasomal inhibitor is added (Liebelt et al., 2019). A corresponding increase in ubiquitin conjugates observed 2 hours after heat shock suggests that the majority of sumoylated proteins may be subject to degradation, which may explain the observed reduction in sumo conjugates after heat stress (Liebelt et al., 2019). Indeed, consistent with this hypothesis, Golebiowski et al (2009) showed that many proteins are subject to Sumo2/3 polysumoylation upon heat shock (Golebiowski et al., 2009). Thus, heat-stress induced polysumoylated substrates may be ubiquitinated by the recruitment STUbLs to facilitate the subsequent degradation of sumoylated proteins.

Collectively, these studies demonstrate that there is a co-ordinated substrate-specific sumo-induced response to heat stress which influences the expression of HSP genes and targets specific substrates for ubiquitin-mediated degradation (Barna et al., 2018).

Considering the importance of polysumoylation within the sumo-mediated response to high temperatures, it is surprising that this response has not been characterised using polysumoylation mutants. Indeed, *S. cerevisiae* cells expressing an *smt3-allR* mutant, which is unable to polysumoylate substrates, are not temperature sensitive, suggesting that polysumoylation is not essential in the response to high temperatures (Bylebyl et al., 2003). Conversely, the deletion of Ulp2, which primarily targets polysumoylated proteins for deconjugation, in *S. cerevisiae* cells, renders cells extremely sensitive to high temperatures. Interestingly, this *ulp2Δ* temperature sensitivity is reversed when crossed with the *smt3-allR* mutant suggesting that a build up of polysumoylated substrates is toxic for the cell (Bylebyl et al., 2003). The pattern of HMW sumo conjugates observed in *ulp2Δ smt3-allR* cells is strikingly similar to wildtype cells, suggesting that the accumulation of polysumoylated substrates may act as an important mechanism to both recognise and regulate high temperatures in budding yeast cells. Nevertheless, the importance of polysumoylation remains to be determined within the eukaryotic response to temperature stresses.

1.3.7.3 Response to DNA Damage

In addition to heat shock, proteomic data has also linked sumoylation to a variety of different cellular responses. One such example, the DNA damage response (DDR), is a sophisticated network of proteins activated upon identification of DNA damage. DDR pathways can be activated by a number of external stimuli, such as UV light, resulting in the activation of a variety of downstream cellular responses, including the activation of cell cycle checkpoints and the repair of DNA damage. Interestingly, a number of proteomic studies have identified proteins involved in the DDR as putative sumo substrates, whilst genetic screens also provide evidence of positive genetic interactions between sumo and components of the DDR (Hendriks and Vertegaal, 2015, Panse et al., 2004, Makhnevych et al., 2009).

Studies in *S. cerevisiae* identified that recovery from double strand DNA breaks is impaired in cells expressing a *ts ucb9-2* allele, indicating that sumoylation may be important for the timely response to DNA damage (Makhnevych et al., 2009). Indeed, deletion of the two major sumo E3 ligases Siz1 and Siz2 renders cells extremely sensitive to UV-induced DNA damage, indicating that sumoylation mediated by Siz1/2 is important during the DDR (Silver et al., 2011). UV light activates the Nuclear Excision Repair (NER) pathway which facilitates the removal of unwanted UV-induced adducts, such as thymine dimers, upon DNA strands and the subsequent repair of the damaged strand of DNA. Interestingly, the repair of pyrimidine dimers induced by UV treatment in *siz1Δsiz2Δ* cells was delayed compared to WT cells, suggesting that Siz1/2 directed sumoylation may be important for the NER pathway. Moreover, several NER proteins are known to be sumo substrates, illustrating that sumoylation is a key feature of the NER pathway (Silver et al., 2011).

Proliferating cellular nuclear antigen (PCNA), an essential DNA clamp, is found throughout eukaryotic cells and has been shown to facilitate the activation of the DDR upon recognition of DNA damage (Boehm et al., 2016). Although early studies in *S. cerevisiae* cells identified that PCNA is subject to cell-cycle regulated sumoylation to facilitate clamp loading, later studies in mammalian cells revealed that PCNA is sumoylated at stalled replication forks, suggestive that sumoylation of PCNA may be important for the DDR (Parker et al., 2008, Gali et al., 2012). Expression of PCNA^{K164R} in mammalian cells prevents PCNA sumoylation, leading to cells displaying an increased number of DNA double stranded breaks compared to cells expressing wild type PCNA (Gali et al., 2012). Recruitment of the DNA helicase Srs2 is a key feature of the DDR in budding yeast cells. Srs2 is recruited to sites requiring double strand repair and is important for the rescue of collapsed replication forks. Interestingly, Srs2 interacts with sumoylated PCNA via the Srs2 C-terminal SIM domain. A short stretch of hydrophobic residues within the Srs2 C-terminal form a β -sheet which interacts with the groove between α 1 and β 2 upon the sumo moiety enabling Sumo-SIM interactions between the two proteins (Armstrong et al., 2012). Interestingly, mutation of the Srs2 SIM domain abolishes the Srs2-PCNA interaction, highlighting the importance of sumo-SIM interactions.

Large scale proteomic studies have also identified important sumo substrates within the DDR. For example, mass spectrometry analysis of mammalian cells exposed to the DNA damaging

agent MMS led to the identification of 362 novel sumoylation sites (Hendriks and Vertegaal, 2015). One identified substrate, the histone demethylase JARID1B, is polysumoylated in response to MMS. Polysumoylated JARID1B subsequently promotes JARID1B degradation by recruitment of the STUbL RNF4. Interestingly, the sumo-mediated degradation of JARID1B during the DDR promotes transcription of DDR genes including JUN to initiate the DDR repair pathways (Hendricks et al, 2014). Thus, sumoylation not only affects the stability of proteins and protein complexes but also regulates gene expression to induce a co-ordinated response at sites of DNA damage.

It is apparent that sumoylation within the DDR is a carefully co-ordinated response to mediate DNA damage repair. To conclude, sumoylation of proteins involved in the DDR plays a key role in the recruitment of additional proteins to sites of DNA damage, enabling the stabilisation of large molecular complexes and the activation of DDR-specific genes. Nevertheless, sumoylation is also critical within a variety of other cellular checkpoints, including cell cycle checkpoints, with the progression through mitosis regarded as a key hallmark of sumoylation. The role of sumo in the transition to metaphase to anaphase will now be discussed in more detail.

1.3.7.4 The Spindle Assembly Checkpoint (SAC)

Phenotypes linking sumo mutants with defects during mitosis were evident in the initial studies characterising sumo and the sumo conjugation enzymes (section 1.3.4). Hence, it is not surprising that sumoylation appears to be an essential feature promoting the progression through mitosis. The regulation of a key mitotic checkpoint, the SAC, has been linked to sumoylation of mitotic proteins and will now be described in further detail.

Accuracy at the metaphase to anaphase transition during mitosis is critical for the fate of daughter chromatids, with inaccurate chromosome segregation resulting in genomic instabilities within the daughter cells. The SAC is a conserved mitotic checkpoint found throughout eukaryotes which prevents entry into anaphase until there is i) sufficient tension between kinetochores and microtubules and ii) all microtubules are attached in the correct biorientation to the kinetochore. Only when all sister chromatids are aligned and attached

correctly to opposite sides of the cell will the progression into anaphase occur (Lara-Gonzalez et al., 2012).

S. cerevisiae cells express a group of proteins known as the mitotic checkpoint complex (MCC) which accumulate when in the presence of incorrectly attached kinetochores, inhibiting activation of the APC/C (Lara-Gonzalez et al., 2012). Arguably the most important role of the SAC is to inhibit APC/C activity until all chromatids are positioned correctly. Thus, only when all microtubule-kinetochores interactions are sufficient, will the level of MCC proteins decrease, enabling the association of the APC/C with Cdc20, facilitating APC/C activation and consequently allowing the cell to progress into anaphase. Interestingly, studies have identified that the proteins located at the kinetochore are targeted for ubiquitination by the E3 ligase activity of the APC/C, resulting in proteolytic degradation of kinetochore proteins. One such protein targeted for ubiquitination by the APC/C is securin, which holds sister chromatids together, thus promoting the separation of the sister chromatids to opposite sides of the cell and the progression into anaphase (Lara-Gonzalez et al., 2012). For a more detailed review of other proteins associated with the SAC, please see reviews by (Lara-Gonzalez et al., 2012, Musacchio, 2015, Musacchio and Salmon, 2007).

Although the SAC is a crucial feature of the metaphase-anaphase transition during mitosis, the mitotic spindle, which facilitates the alignment of sister chromatids before entry into anaphase, is equally as important. The mitotic spindle is formed of microtubule polymers which are highly conserved polymeric structures formed by the polymerisation of α -tubulin and β -tubulin dimers. Microtubules have important cellular roles in addition to forming the mitotic spindle including providing structural support within the cytoskeleton and facilitating the movement of cellular cargo. Interestingly, both α - and β - tubulin are both highly conserved in eukaryotes, illustrating their fundamental roles in cellular functions (Goodson and Jonasson, 2018). One critical feature of the mitotic spindle is that the polymerisation and depolymerisation of microtubules is an extremely dynamic process which involves the addition or loss of tubulin subunits from the microtubule polymer, enabling rapid changes in microtubule length, known as dynamic instability. Arguably the most important function of microtubules is their role within mitosis. The mitotic spindle consists of hundreds of microtubule filaments with the dynamic instability of tubulin polymers enabling rapid changes

in spindle length to i) co-ordinate the correct alignment of sister chromatids during mitosis and ii) separate the two sister chromatids to opposite side of the cell during anaphase (Goodson and Jonasson, 2018). Microtubule associated proteins (MAPs) located at the mitotic spindle aid microtubule nucleation, facilitating the growth of microtubule polymers. MAPs will not be discussed further, but for additional reading please see the following review (Amin et al., 2019).

Considering the importance of microtubules within mitosis, it is not surprising that a number of sumoylated mitotic proteins are associated with the mitotic spindle. One such example, the mitotic kinase Bub-1, was initially identified in *S. cerevisiae*, as a highly conserved subunit of the MCC. In the presence of incorrectly attached kinetochores, Bub-1 recruits the Mad1-Mad2 complex, thereby activating the SAC and preventing mitotic progression (Kim and Gartner, 2021, London and Biggins, 2014). Furthermore, the association of Bub-1 with Cdc20 also prevents APC/C activation, hence it is not surprising that Bub-1 is subject to regulation by a variety of PTMS. Identification of Bub-1 as a sumo substrate in mammalian cells strongly indicates that this modification is conserved throughout eukaryotes. Indeed, sumoylation of mammalian Bub-1 in late mitosis promotes the removal of Bub-1 from kinetochores, thereby inactivating the SAC. The expression of a Bub-1^{K250R} mutant resulted in Bub-1^{K250R} associating with kinetochores, even after the SAC deactivation. Retention of Bub-1^{K250R} on kinetochores leading to a “delayed anaphase”, with (Yang et al., 2012b, Yang et al., 2012a). Thus, taken together, these results suggest that sumoylation of Bub-1 may be important for SAC inactivation and the timely entry into anaphase.

As mentioned earlier, MAPs aid the nucleation of microtubule filaments during metaphase to facilitate the attachment of the mitotic spindle to kinetochores. A number of MAPs have been identified as sumo substrates, suggesting that sumoylation of these proteins may modulate dynamics of the mitotic spindle. A few examples will now be discussed in further detail.

One example of an identified MAP is Kar9, which interacts with the mitotic spindle to promote the correct orientation of the mitotic spindle towards the bud neck during metaphase. Inhibiting sumoylation of Kar9 results in spindle misalignment in *S. cerevisiae* cells (Leisner et al., 2008). In WT cells, sumoylation of Kar9 facilitates the interaction of Kar9 with the mitotic

spindle, promoting the orientation of the spindle towards the bud neck. However, the association between Kar9 and the bud neck is lost when Kar9 cannot be sumoylated, suggesting that sumoylation is crucial for orientation of the mitotic spindle (Leisner et al., 2008). It is clear that the sumoylation of mitotic proteins is essential to regulate chromatid alignment in *S. cerevisiae*. The correct regulation of mitotic proteins is vital to maintain genomic integrity, as incorrectly orientated or attached sister chromatids could lead to unequal chromatid separation in anaphase. Studies in mammalian cells also suggest that sumoylation of mitotic proteins is required for the metaphase to anaphase transition (Lee et al., 2018). Upon correct sister chromatin alignment, activation of the APC/C promotes degradation of metaphase cyclins, facilitating the entry into anaphase. Interestingly, Apc4, one of the subunits of the APC/C, has been identified as a sumo substrate in mammalian cells (Lee et al., 2018). Expression of Apc4^{K772R/K798R} inhibits the sumoylation of Apc4, with Apc4^{K772R/K798R} cells showing a significant mitotic delay. Remarkably, Apc4^{K772R/K798R} mutants also display delayed degradation of APC/C substrates, suggesting that sumoylation of Apc4 likely promotes the timely activity of the APC/C (Lee et al., 2018).

Collectively, these data indicate the important roles of sumo in the correct orientation of sister chromatids in addition to promoting the timely transition from metaphase into anaphase, ensuring the equal distribution of chromatids to daughter cells. Errors occurring in either of these roles could result in the unequal segregation of sister chromatids, leading to the proposal that protein regulation by sumoylation acts to maintain genomic integrity. However, although it is clear that sumoylation is vital for mitotic progression, sumoylation is also a key response to external cellular stresses, as detailed below.

1.3.6.5 Oxidative Stress

Sumoylation appears to have a role in a variety of stress responses (section 1.3.6) hence it is not surprisingly that studies have also identified a key role for sumo in the response to oxidative stresses, including the response to reactive oxygen species (ROS). ROS are present in all cells and arise from both internal and external sources. Low levels of ROS have essential roles in cellular signalling, regulating a variety of cellular pathways in eukaryotic cells. For example, low levels of ROS are required for stem cell differentiation in mammalian cells

during embryogenesis (Juntilla et al., 2010). Whilst low levels of ROS are important for the cell, high levels of ROS can overwhelm cellular antioxidants and cause oxidative stress, causing damage to DNA, lipids and proteins in the cell (Veal et al., 2007). The presence of ROS mediates redox signalling in cells, enabling reversible or irreversible modification of target proteins, which is achieved by the oxidation of target cysteine residues. For example, in the presence of H₂O₂, sulphur-containing cysteine residues are readily oxidised to sulphenic acid (SOH). Sulphenics are reversible modifications, hence reduction of the cysteine by antioxidants can return the protein to its unmodified form. However, in the presence of high levels of ROS, further oxidation of sulphenics can occur, leading to the formation of irreversible sulphinic (SO₂H) or sulphonic (SO₃H) modifications upon the target cysteine (Fra et al., 2017). Cysteine oxidation has been shown to regulate a variety of cellular pathways, with redox signalling providing a mechanism of ROS sensing within the cell. (Veal et al., 2007) (Forman et al., 2014). Interestingly, many of the enzymes present within the sumo and ubiquitin conjugase/deconjugase pathways possess catalytic cysteine residues, suggestive that ROS-induced oxidation of these enzymes might be important for ROS sensing and the downstream cellular responses.

Initial studies investigating the regulation of the sumo conjugation/deconjugation pathway in mammalian cells identified that sumoylation conjugation pathway is subject to regulation by ROS (Bossis and Melchior, 2006). For example, treatment of mammalian cells with low levels (<1mM) of H₂O₂ results in a rapid decrease in global sumoylation whilst higher (>1mM) concentrations of H₂O₂ do not result in a loss of sumo conjugates. The presence of H₂O₂ induces the formation of a reversible intermolecular disulphide bond between the catalytic cysteine residues in Uba2 (C173) and Ubc9 (C93), inhibiting the activity of the sumo E1 and E2 enzymes (Fig. 1.7). E1-E2 inhibition prevents substrate sumoylation, rendering the sumo “on” conjugation pathway inactive. However, the sumo deconjugases are still active at low H₂O₂ concentrations, thus sumoylated substrates can still be desumoylated, resulting in a rapid decrease in global sumo conjugates (Bossis and Melchior, 2006). However, at higher concentrations (>1mM) of H₂O₂ the activity of the sumo deconjugases is also inhibited, essentially fixing in place any sumo conjugation that had occurred prior to H₂O₂ treatment. For example, studies in mammalian cells identified that high concentration of H₂O₂ (4mM)

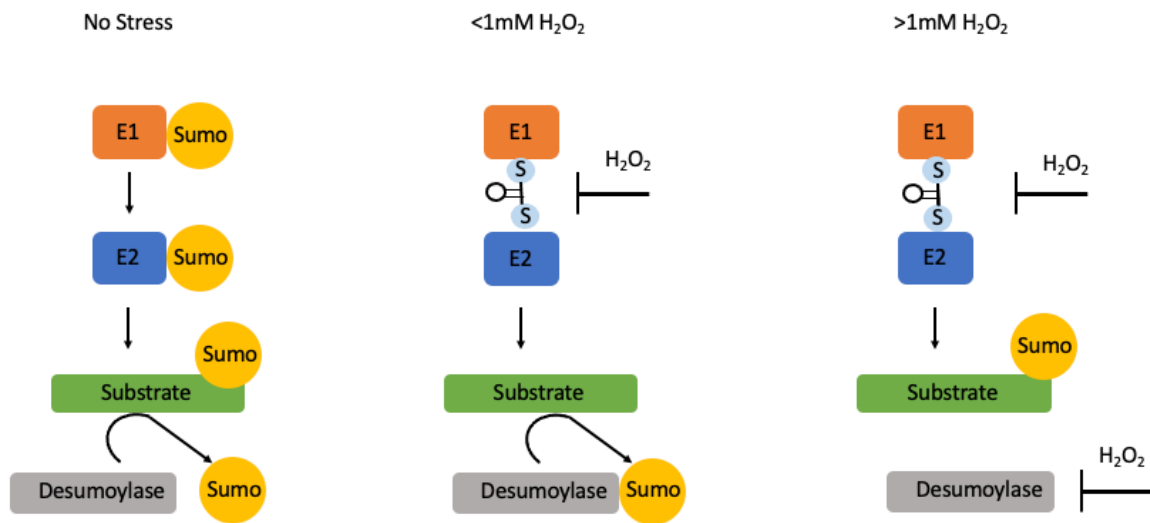


Figure 1.7 Redox regulation of the sumo conjugation/deconjugation enzymes. In low (<1mM) H₂O₂ concentrations, disulphide formation between the sumo E1 and E2 inhibits sumo conjugation. Desumoylases remain active, removing sumo from substrates, leading to a reduction in global sumoylation levels. In high levels of H₂O₂ (>1mM), disulphide bond formation within the desumoylases inhibits the desumoylation of sumoylated proteins. Sumo conjugation is also inhibited by the formation of a disulphide between the sumo E1 and E2, leading to a build up of residually sumoylated substrates in the cell. Adapted from (Bossis and Melchior, 2006).

induced the formation of a disulphide bond between the catalytic cysteines C603 and C613 in SENP1 (Xu et al., 2008). Dependant on the concentration of H₂O₂ treatment, the disulphide bond formation in SENP1 can be either reversible or irreversible, providing a mechanism for sensing ROS or limiting cellular damage at high H₂O₂ concentrations. Furthermore, high H₂O₂ concentrations also induce the formation of disulphide bonds in *S. cerevisiae* Ulp1, suggesting that inhibition of sumo deconjugases in oxidative stress is a conserved eukaryotic response (Xu et al., 2008). However, it must be noted that the characterisation of Ulp1 inhibition was studied *in vitro*, thus it remains to be determined as to whether ROS-mediated inhibition of Ulp1 is also true *in vivo* (Xu et al., 2008).

Studies have also identified that the ubiquitin conjugation pathway is subject to regulation by ROS. For example, work from our lab identified that disulphide bond formation between the ubiquitin E2 Cdc34 and the ubiquitin E1 Uba1 in response H₂O₂ results in a cell cycle arrest in *S. cerevisiae* cells (Doris et al., 2012). Under normal conditions, the CDK Sic1 is ubiquitinated and targeted for degradation by Cdc34, promoting entry into S phase. However, in response to ROS, the formation of a disulphide bond between Cdc34-Uba1 inhibits Cdc34, thus preventing Sic1 ubiquitination and inhibiting the entry into S Phase (Doris et al., 2012). Taken together these studies suggest that the E1 and E2 enzymes required for either sumo or ubiquitin conjugation are subject to redox regulation, suggesting that oxidation of Ubl conjugating enzymes is a conserved mechanism for sensing ROS.

Similar to ROS-induced inactivation of SENP1/Ulp1, the activity of DUBs have also been shown be regulated by ROS (Cotto-Rios et al., 2012). For example, low levels (1mM) of H₂O₂ promote oxidation of the catalytic cysteine within USP1, inactivating this DUB in mammalian cells (Cotto-Rios et al., 2012). Interestingly, the inactivation of USP1 has been linked with the response to DNA damage. During DNA replication, the recognition of stalled replication forks promotes the ubiquitination of PCNA, promoting the association of PCNA with enzymes in the DDR pathway to repair DNA lesions (Hoegge et al., 2002). However, in the presence of H₂O₂, the oxidation of USP1 prevents degradation of ubiquitinated PCNA, promoting activation of the DDR to facilitate the repair of damaged DNA (Cotto-Rios et al., 2012). This example suggests that low levels of ROS induce the activation of DNA repair pathways in an attempt to prevent damage caused by ROS to prevent extensive cellular damage.

Studies in budding yeast have also identified an important role for sumo-mediated activation of the DDR in response to ROS. For example, *S. cerevisiae* cells expressing a Ubc9^{D100A} mutant inhibit the formation of intermolecular disulphide bonds between Ubc9 and Aox2 during oxidative stress (Xu et al., 2008). Ubc9^{D100A} cells are unable to activate the DDR, suggesting that a key function of sumo inhibition in oxidative stress is the activation of the DDR pathway (Xu et al., 2008). Taken together, these examples of Ubc9 and USP1 suggest that a major role of ROS-induced inhibition of Ubl conjugating enzymes may be to regulate the DDR.

In conclusion, oxidation of the catalytic cysteine residues of the Ubl conjugation/deconjugation enzymes in response to ROS appears to be a conserved mechanism found throughout eukaryotes. ROS-mediated enzyme inhibition provides the cell with a sophisticated mechanism for sensing the levels of cellular ROS, ensuring that proteins and DNA are not damaged by free radicals. However, it is clear that further research is required to characterise the pathways affected by ROS-induced inhibition of Ubls.

The SSR has been studied extensively over the last two decades, with the sumo-mediated responses to stresses such as heat shock characterised in considerable detail. However, unlike the responses to heat or oxidative stress, the sumo-mediated cellular response to colder than normal temperatures is poorly understood in eukaryotes.

1.3.7.6 Eukaryotic Cold Temperature Adaptation

Key insights into the role of PTMs in the response of cells to cold temperature has come from research in plants. Plants are unable to move from their physical location, thus they must coordinate a rapid response to any climate or temperature changes to avoid cell death. Similar to other stress responses, it was found that exposing seedlings to freezing temperatures results in a massive increase in global sumo conjugates (Morrell and Sadanandom, 2019). Moreover, gene expression data from *Arabidopsis thaliana* suggests that sumoylation of the *ICE1* transcription factor in response to exposure of plants to low temperatures upregulates critical genes involved in cold temperature responses (Roy and Sadanandom, 2021, Miura et al., 2007). Additional studies by Miura et al. (2007) revealed that plants lacking a functional *SIZ1* gene, the homologue of the gene encoding the Siz1 sumo

E3 enzyme in *S. cerevisiae*, displayed extreme sensitivity to cold temperature, suggesting that Siz1-induced sumoylation may be important in conferring resistance to low temperatures. Sumoylation of ICE1 occurs on K393, which lies within a common sumo consensus motif, with ICE1 sumoylation mediated by Siz1 (Miura et al., 2007). Interestingly, inhibition of ICE1 sumoylation by the expression of an ICE1^{K393R} mutant inhibits the expression of downstream target genes when exposed to cold temperatures, rendering cells less tolerant to freezing conditions (Miura et al., 2007). Hence, it appears that sumo-mediated transcriptional activity is a key feature in the response to cold temperatures in plants. Nevertheless, research in mammalian cells has also provided key insights into the role of sumoylation at low temperatures.

Some studies of cold temperature responses and the links with sumoylation have been performed in animals. For example, studies investigating hibernation in squirrels revealed that sumo conjugation is massively induced upon torpor (Lee et al., 2007). A prolonged decrease in temperature and reduction in both metabolic rate and oxygen consumption enables squirrels to sustain long periods of hibernation without any organ damage. Lee et al. (2007) demonstrated that the levels of Sumo2/3 conjugated proteins are massively upregulated upon entering torpor, suggesting that hibernation-induced sumoylation may be cryoprotective (Lee et al., 2007). Furthermore, the same study also found that reducing the cellular levels of Ubc9 in mammalian cells leads to a significant increase in cell death upon oxygen deprivation. These results also highlight the importance of sumoylation for cell survival in a hypoxic environment. Importantly, the link between increased sumoylation and cryoprotection in hibernating mammals may be extremely important in improving clinical approaches to safely reduce metabolic rate in patients waiting for life saving surgery, such as heart transplants.

To date, relatively little research has focused on the response of *S. cerevisiae* cells to cold temperature stress compared to the abundance of studies that have investigated the responses of yeast cells to heat shock (for reviews see (Craig, 1985, Verghese et al., 2012)). However, prolonged exposure of *S. cerevisiae* cells to cold temperature results in changes to the cell membrane composition which is thought to induce the cold shock response (Aguilera

et al., 2007). These suggestions have led to the proposal of a currently uncharacterised signalling pathway which is thought to upregulate the expression of several cold shock proteins (CSPs) which subsequently act to induce the expression of downstream genes. Interestingly, the expression of genes including *INO1* and *OPI3* (which encode proteins involved in phospholipid synthesis) are upregulated budding yeast cells exposed to cold temperatures. Sumoylation is often associated with regulation of gene expression (section 1.3.5), with many transcription factors identified as sumo substrates, hence it is possible that sumoylation may be a key feature in the response to cold temperatures in *S. cerevisiae*. Although the pathways facilitating these cold-induced responses remain unknown, it is evident that further research is needed to determine the mechanisms which underlie the response to cold temperatures in yeast and other eukaryotes (Aguilera et al., 2007).

In conclusion, the global increase in the level of sumo-conjugated substrates appears to be a hallmark of the eukaryotic response which is conserved throughout a variety of cellular stresses. Taken together, studies mentioned in this section strongly suggest that sumoylation is a vital stress response mechanism in order to protect the cell from damaging agents. However, as the pathways and downstream sumo substrates in these stress responses often remain uncharacterised, it is clear that further research into these responses would enhance our understandings of the fundamental nature of sumoylation. Therefore, in order to investigate the essential function(s) of sumoylation, our lab has been investigating the novel role(s) of sumoylation in *S. cerevisiae*, as detailed below.

1.4 *smt3* SGA screen

As described in section 1.2.3.6, the budding yeast *S. cerevisiae* is a powerful eukaryotic model organism which can be used to investigate genetic interactions. To date, genetic interaction studies have linked sumo to a variety of different cellular processes (section 1.3). However, these studies have focussed on the sumo genetic enhancers, thus the sumo suppressor proteins remain to be characterised. Consequently, our lab carried out an SGA to characterise putative sumo suppressors, as detailed below.

1.4.1 Characterisation of the *smt3* strain

In order to investigate the essential functions of Smt3 in *S. cerevisiae*, previous work in our lab utilised a *smt3* mutant strain obtained from the commercially available DAmP strain collection (Breslow et al., 2008). The *smt3::DAmP* allele (from here named *smt3*) was constructed by insertion of an antibiotic cassette within the 3' untranslated region (UTR) of the *SMT3* gene. The insertion of this cassette acts to reduce mRNA levels from the *SMT3* gene, which leads to the subsequent decrease in cellular Smt3 protein levels. Indeed, our results reveal that Smt3 is expressed at just 10% of wild type levels within *smt3* cells (Lewis, 2016). Interestingly, *smt3* cells display several phenotypes including morphological defects, slow growth and are extremely sensitive to cold temperature (Lewis, 2016). Hence, an SGA screen was performed to attempt to identify gene mutations that suppress or enhance the poor growth phenotype of the *smt3* strain. The SGA screen was performed by crossing the *smt3* strain with the *S. cerevisiae* DAmP and gene deletion libraries which contain 842 DAmP mutations of the essential genes and 4291 deletions of the non-essential genes, respectively (Breslow et al., 2008) (Tong and Boone, 2006). Previous screens have identified enhancers of loss of function mutations of the *SMT3* gene but to date no suppressors have been reported (Makhnevych et al., 2009). Hence, we were particularly interested in the identification of any new suppressors of phenotypes associated with loss of Smt3 function. Several suppressor mutations were indeed found and were chosen for further analyses.

1.4.2 Identification of Novel *smt3* Suppressor Mutations

Strikingly, the *smt3* SGA screen revealed several novel genetic interactions not previously reported which dramatically improved the poor growth phenotype associated with the *smt3* allele (Lewis, 2016). Notably, several of the top new suppressor mutations were in genes encoding cytoskeletal-related proteins. Furthermore, several of the highest scoring suppressors encode proteins which belong to two major cytoskeletal complexes (see Table 1.4).

Gene	<i>smt3</i> SGA Suppressor Number	Subunit of complex
<i>TUB2</i>	4	Tubulin
<i>ARP2</i>	7	Arp2/3
<i>ARP3</i>	8	Arp2/3
<i>CCT8</i>	15	CCT
<i>CCT3</i>	20	CCT
<i>ARC35</i>	25	Arp2/3

Table 1.4 Top suppressor proteins identified in the *smt3* SGA screen and their associated complexes. Analysis of DAmP alleles identified in the *smt3* SGA screen as suppressors of the *smt3* growth defect, ordered from the highest to lowest suppressor (Lewis, 2016).

The top cytoskeletal suppressor was a *tub2::DAmP* allele. The *TUB2* gene encodes the only copy of β -tubulin in *S. cerevisiae* and is an essential component of microtubules (see section 1.3.7.4). Three of the top suppressors *arp2::DAmP*, *arp3::DAmP* and *arc35::DAmP* encode three of the essential components of the Arp2/3 complex, an evolutionary conserved seven protein complex which facilitates the branching of actin filaments. Finally, two of the top suppressors *cct3::DAmP* and *cct8::DAmP* encode components of the CCT complex, a conserved chaperonin complex which facilitates cytoplasmic protein folding. Notably, the two main substrates of the CCT complex are actin and tubulin, two major cytoskeletal filaments.

Gene ontology (GO) analysis is a powerful analytical tool which enables the mapping of biological processes with a gene of interest. GO analysis of *smt3* genetic interaction datasets from the SGA screen carried out in our lab identified that *smt3* genetic enhancers are strongly linked to DNA replication, chromosome segregation and response to heat (Lewis, 2016). Interestingly, the role of sumo within all of these cellular processes has been well characterised, highlighting why previous *smt3* genetic studies may have chosen to focus on the characterisation of *smt3* enhancers, as many were already known sumo substrates. In contrast, GO analysis of *smt3* suppressors from the *smt3* SGA screen revealed that the cellular processes associated with genetic suppression of *smt3* are largely involved in RNA processing and ribosomal biogenesis (Lewis, 2016). The understanding of sumo and its roles within these pathways are less clear, suggesting why previous studies may not have investigated putative *smt3* suppressor proteins.

Intriguingly, although 5 of the top suppressor proteins were subunits of either the Arp2/3 or CCT complex, Dr. Lewis identified that each of these complexes also contained *smt3* enhancers (Lewis, 2016). For example the SGA screen revealed that *cct4*, a subunit of the CCT complex the 39th strongest *smt3* enhancer in the *smt3* SGA screen. Additionally, *arc15*, a member of the Arp2/3 complex, was the 51st strongest *smt3* enhancer (Lewis, 2016). Nevertheless, it remains unclear as to why these complexes have subunits which are both strong *smt3* enhancers and suppressors.

To conclude, the *smt3* SGA screen revealed novel suppressors of the growth phenotypes associated with loss of sumo function. Moreover, the identity of these suppressors strongly suggested that at least some of the essential functions of sumo could be linked to the cytoskeleton. However, the nature of these interactions between sumo and the cytoskeleton remains to be determined. The three cytoskeletal complexes will now be described in more detail below.

1.4.2.1 Tubulin

The *tub2::DAmP* allele was the fourth highest suppressor identified in the SGA screen and encodes the protein β -tubulin. Tubulin is an essential cytoskeletal dimeric protein that consists of α - and β -tubulin subunits, as previously described in section 1.3.7.4.

S. cerevisiae cells express a single, essential gene, *TUB2*, that encodes β -tubulin and two genes, *TUB1* and *TUB3*, that encode α -tubulin (Schatz et al., 1986). The two *S. cerevisiae* α -tubulin genes are thought to have arisen from a gene duplication as although *TUB3* is a non-essential gene, there is extremely high sequence homology shared between the proteins encoded by the *TUB1* and *TUB3* genes (Little and Seehaus, 1988). Interestingly, *TUB1* accounts for the majority of α -tubulin that is expressed in *S. cerevisiae* cells (Luchniak et al., 2013). Indeed, *tub1* Δ cells are inviable whereas *tub3* Δ cells are viable (Leisner et al., 2008). Consistent with this observation, overexpression of *TUB3* can rescue the lethality of a *tub1* Δ mutant in *S. cerevisiae* cells. Interestingly, it has been shown that both α - and β -tubulin are subject to several different PTMs including phosphorylation and glycosylation, however the roles of tubulin modifications remain unclear (Magiera and Janke, 2014) (MacRae, 1997). It is also interesting to note that mammalian cells express many more α - and β -tubulin isoforms compared to *S. cerevisiae*. Furthermore, studies have revealed that different tubulin isoforms are expressed during different stages of development, suggesting that individual isoforms may have distinct cellular roles (Lopez-Fanarraga et al., 2001).

Considering how critical the function of tubulin is to a variety of cellular processes, relatively few studies have investigated the regulation of tubulin monomers. Studies of tubulin have been hindered by many problems as the overexpression and purification of tubulin from

bacteria is not possible due to the absence of chaperones required for tubulin folding, preventing the correct structural assembly of tubulin subunits (Johnson et al., 2011). In addition, it is difficult to purify large amounts of native tubulin subunits from eukaryotic cells for further analysis since the cellular levels of tubulin are tightly regulated and overexpression of tubulin monomers is lethal (Johnson et al., 2011). Hence, at present, the majority of *in vitro* studies studying tubulin have used α - and β -tubulin heterodimers derived from animal brain cells. Tubulin is abundant in animal brains, providing a large pool of α - β -tubulin heterodimers which can be purified for further study. However, despite these problems, Richards et al (2000) used site-directed mutagenesis of *TUB1* expressed in *S. cerevisiae* cells to reveal several phenotypes associated with tubulin function (Richards et al., 2000). Interestingly, a number of *tub1* point mutants showed phenotypes including increased sensitivity to both cold temperature and the microtubule depolymerising agent benomyl (Richards et al., 2000).

Identification of the *tub2::DAmP* allele as an excellent suppressor of the growth phenotypes associated with the *smt3* mutant suggests a strong genetic association between sumoylation and tubulin function. Interestingly, several large-scale proteomics studies have suggested that both α - and β -tubulin may be sumo substrates. For example, analysis of sumo conjugates in *S. cerevisiae* cells in studies by Panse et al. (2004) revealed that microtubules account for ~5% of sumoylated proteins in budding yeast (Panse et al., 2004). However, despite mass spectrometry data suggesting a link between sumo and β -tubulin in multiple studies, to date only a single study has identified a potential interaction between Smt3 and Tub2 in *S. cerevisiae* (Greenlee et al., 2018). Using yeast two hybrid analysis, Greenlee et al. (2018) suggested that a non-covalent interaction occurs between Smt3 and Tub2 in budding yeast cells (Greenlee et al., 2018). However, further analysis to validate and determine the nature of these interactions, such as immunoprecipitations and mutation of sumoylation sites, was not performed in this study, thus this interaction requires further characterisation.

Additional studies in the parasite *Giardia lamblia* have also provided evidence of tubulin modification by sumo. For example, α -tubulin immunoprecipitated with sumo in *G. lamblia* cells, suggesting that α -tubulin protein is indeed sumoylated (Di Genova et al., 2017). It is interesting to note that the mass spectrometry data in this same study revealed that

fragments of β -tubulin were also present in the sumo pull down, although the authors did not pursue this observation further (Di Genova et al., 2017). Additionally, siRNA knockdown of sumo in *G. lamblia* cells leads to a G1/S Phase arrest, with these cells showing a reduced rate of proliferation. Interestingly, both of these phenotypes are associated with phenotypes displayed by the *smt3* strain (Di Genova et al., 2017, Lewis, 2016). Furthermore, the depletion of sumo in *G. lamblia* cells results in cells displaying cytoskeletal abnormalities, with cells having a rounded structure rather than the characteristic oval cell membrane associated with WT *G. lamblia*. Nevertheless, the authors concluded that these cytoskeletal defects were not due to changes in tubulin localisation or polymerisation, suggesting that inhibiting sumoylation does not affect tubulin dynamics in *G. lamblia* (Di Genova et al., 2017).

Although the sumoylation of β -tubulin is yet to be confirmed, it is clear that a number of studies strongly suggest that β -tubulin is indeed targeted for sumoylation. These studies mentioned above in conjunction with the results from our lab suggesting that *tub2* is an extremely good suppressor of the *smt3* growth defect, provides strongly suggests that β -tubulin could be a *bona fida* sumo substrate. It must also be noted that although *tub1* was absent from the SGA screen, *tub3* Δ was identified as a mild suppressor (scoring 150/4999). However, as previous studies had identified Tub3 as a sumo substrate, coupled with *tub2* scoring extremely highly as a suppressor of *smt3*, work in this thesis will focus on the characterisation of the relationship between Tub2 and Smt3. Nevertheless, *tub2* was only one of five cytoskeletal *smt3* suppressor proteins, hence the remaining *smt3* suppressors will now be described in more detail.

1.4.2.2 The CCT Complex

Two of the top suppressors in the SGA screen were alleles of two genes, *cct3::DAmP* and *cct8::DAmP*, which encode components of the conserved chaperonin the CCT complex. In eukaryotic cells the recruitment of chaperonin complexes ensures the correct folding of large, newly translated proteins (Grantham, 2020). Chaperonin complexes are critical to prevent cell damage as mistakes in protein folding can lead to a build-up of unwanted protein aggregates in the cytosol, which are associated with a number of mammalian diseases (Grantham, 2020). The resolved 3D structure of the CCT complex revealed that eight protein subunits, CCT1-8,

are arranged in a double octameric ring with 1:1 stoichiometry (Fig. 1.8) (Leitner et al., 2012). Substrate folding by the CCT complex is an ATP-dependent process with each of the eight subunits containing an individual ATP-binding domain, leading to the proposal that each individual CCT subunit has a different function (Amit et al., 2010). Consistent with this hypothesis, overexpression of one CCT subunit cannot rescue the phenotypes associated with a mutation in another subunit, suggesting that each subunit has distinct properties (Stoldt et al., 1996).

Given that other top suppressors of the *smt3* mutation influence the functions of actin and tubulin it is remarkable that the two main substrates of the CCT complex have been found to be actin and tubulin (Llorca et al., 2001). Indeed, Arava et al. (2003) suggested that actin occupies >50% of CCT complexes in the cell at any one time, illustrating the importance of the CCT complex for correct actin folding (Arava et al., 2003). In addition, Brackley and Grantham (2009) proposed that the binding of substrates to CCT1-8 subunits is subunit specific, with different substrates binding to different CCT1-8 subunits (Brackley and Grantham, 2009). Interestingly, the nature of sequence-specific substrate binding to CCT1-8 complexes in eukaryotes is in contrast to the bacterial chaperonin complex GroEL, suggestive that eukaryotic substrate-chaperonin recognition is different to that of bacterial chaperonins (Llorca et al., 1999). For example, β -actin has been shown to specifically bind to the CCT δ , CCT β and CCT ϵ subunits within the CCT complex in mammalian cells (Llorca et al., 1999). 3D structural analysis of actin monomers identified that actin comprises a small and large domain, each of which bind to distinct CCT subunits (Llorca et al., 1999). Interestingly, point mutations of G146P and G150P located in the hinge region between the large and small domains in mammalian β -actin prevent CCT-mediated actin folding, suggesting that actin flexibility is crucial for the interaction with the CCT complex (McCormack et al., 2001).

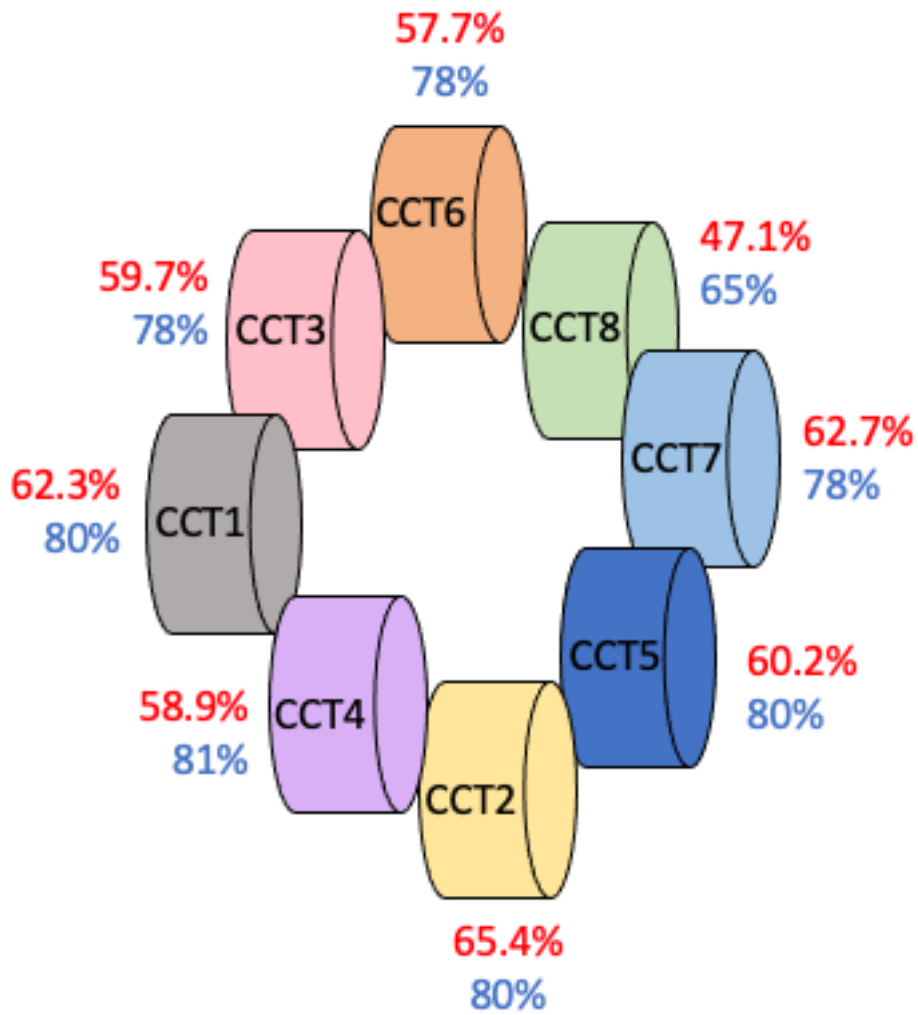


Figure 1.8 CCT1-8 form an octameric structure. Arrangement of the CCT1-8 subunits in *S. cerevisiae* cells as identified by (Leitner et al., 2012). The % identity and % homology of each of the *S. cerevisiae* CCT1-8 subunits compared to the mammalian homologues are detailed next to each subunit (Neef et al., 2014).

<i>S. cerevisiae</i> CCT Genes	Mammalian CCT Genes
<i>CCT1</i>	<i>CCTα/TCP-1</i>
<i>CCT2</i>	<i>CCTβ/TCP-2</i>
<i>CCT3</i>	<i>CCTχ/TCP-3</i>
<i>CCT4</i>	<i>CCTδ/TCP-4</i>
<i>CCT5</i>	<i>CCTϵ/TCP-5</i>
<i>CCT6</i>	<i>CCTζ-1/TCP-6</i>
	<i>CCTζ-2</i>
<i>CCT7</i>	<i>CCTη/TCP-7</i>
<i>CCT8</i>	<i>CCTθ/TCP-8</i>

Table 1.5 Nomenclature of the *S. cerevisiae* and mammalian CCT genes. Adapted from (Brackley and Grantham, 2009).

In contrast, to actin, eight CCT binding sites have been characterised in mammalian tubulin (Llorca et al., 1999). Studies investigating the interactions between tubulin and the CCT complex in mammalian cells identified that β -tubulin contains three N-terminal charged regions which facilitate interactions with CCT1 and CCT4 in addition to five β -tubulin C-terminal charged regions which interact with multiple CCT subunits (Gómez-Puertas et al., 2004). Thus, although CCT binding sites are located throughout β -tubulin, it has been proposed that the C-terminal amino acids within the region S277-V288 show increased affinity for CCT subunits compared to other CCT binding sites (Dobrzynski et al., 1996). Hence it is clear from these examples that both actin and tubulin bind to CCT in an orchestrated, specific CCT subunit-dependant manner. The ability of different CCT subunits to recognise different substrates may provide an explanation as to why different proteins found within the CCT complex were found to be both enhancers and suppressors of *smt3*. However, this proposal is purely speculative and would require further biochemical characterisation, which will not be investigated any further within this study. Disruptions in the folding of actin and tubulin by the CCT can be detrimental to the cell, highlighting the importance for specific CCT-substrate interactions, as detailed below.

Since actin and tubulin comprise the two major substrates of the CCT complex, it is perhaps unsurprising that the CCT complex has been linked to normal cell cycle progression (Grantham et al., 2006). For example, depletion of the CCT complex in mammalian cells results in a cell cycle arrest, with cells blocked at the G1/S boundary (Grantham et al., 2006). Interestingly, depletion of the CCT complex also reduces the level of tubulin in the cell, suggesting that unfolded or misfolded tubulin may be degraded. It has been well characterised that tubulin subunits having a key role throughout mitosis, forming the mitotic spindle (section 1.3.4), hence a reduction of tubulin may prevent the formation of mitotic spindles, hindering cell cycle progression. Other mitotic proteins have also been shown to be subject to regulation by the CCT complex. For example, Cdc20, which binds to and activates the Anaphase Promoting Complex (APC) (see section 1.3.4) in order to allow cells to progress through mitosis, has also been shown to be a substrate of the CCT complex (Lee et al., 2018). Studies in budding yeast carried out by Camasses et al. (2003) revealed that Cdc20 is bound to the CCT complex prior to interacting with the APC (Camasses et al., 2003). Upon entry into mitosis, Cdc20 is released from the CCT complex, enabling the interaction between Cdc20 and the

APC, promoting progression into anaphase (Camasses et al., 2003). This example also highlights additional roles for the CCT complex, distinct from its chaperonin properties. Another key mitotic regulator, polo kinase (see reviews of (Archambault and Glover, 2009)), has also been linked to the CCT complex. In particular, Liu et al. (2005) demonstrated that the CCT complex is critical for the correct folding of the Plk1 polo kinase in human cells (Liu et al., 2005). Plk1 activity is required in late G2 phase, with a depletion of Plk1 resulting in cells arresting in G2 (Liu et al., 2005). Interestingly, depletion of the CCT complex in mammalian cells is correlated with a depletion of Plk1 levels and Plk1 activity, resulting in a G2 arrest. Collectively, these results indicate that the CCT complex is crucial for timely progression through the cell cycle, whilst highlighting the importance of protein folding to ensure accurate protein function.

In addition, regulation of the cell cycle, the CCT complex has also been linked to eukaryotic cellular stress responses. For example, Somer et al. (2002) observed that the levels of mRNA from all the genes encoding each of the individual subunits of the CCT complex increase upon exposure of *S. cerevisiae* cells to cold temperatures (Somer et al., 2002a). In addition, investigations into the cold hardiness of the maggot *Delia antiqua* found that the transcript levels of *CCT1-8* increased in cold temperatures (Kayukawa and Ishikawa, 2009). Interestingly, this study also identified that upregulation of the CCT complex prevents actin depolymerisation, which was found to be important for preventing cell membrane damage, suggestive that upregulated CCT levels facilitate the cold hardiness of *D. antiqua* (Kayukawa and Ishikawa, 2009). Indeed, maggots that were not cold hardy expressed lower mRNA levels of the CCT subunits in cold conditions and were unable to prevent actin depolymerisation and maintain the structure of cell membranes. Hence, these results demonstrate a clear connection between the CCT complex and the response of cells to cold temperature.

To date, limited data has connected sumo with the CCT complex. Indeed, a study investigating the effect of nicotine in rat brains is currently the only published evidence linking sumo to the CCT complex (Kane et al., 2004). Microarray data highlighted that prolonged exposure of rats to nicotine led to an increase in *CCT* gene expression, with the expression of *TCP-3* and *TCP-8*

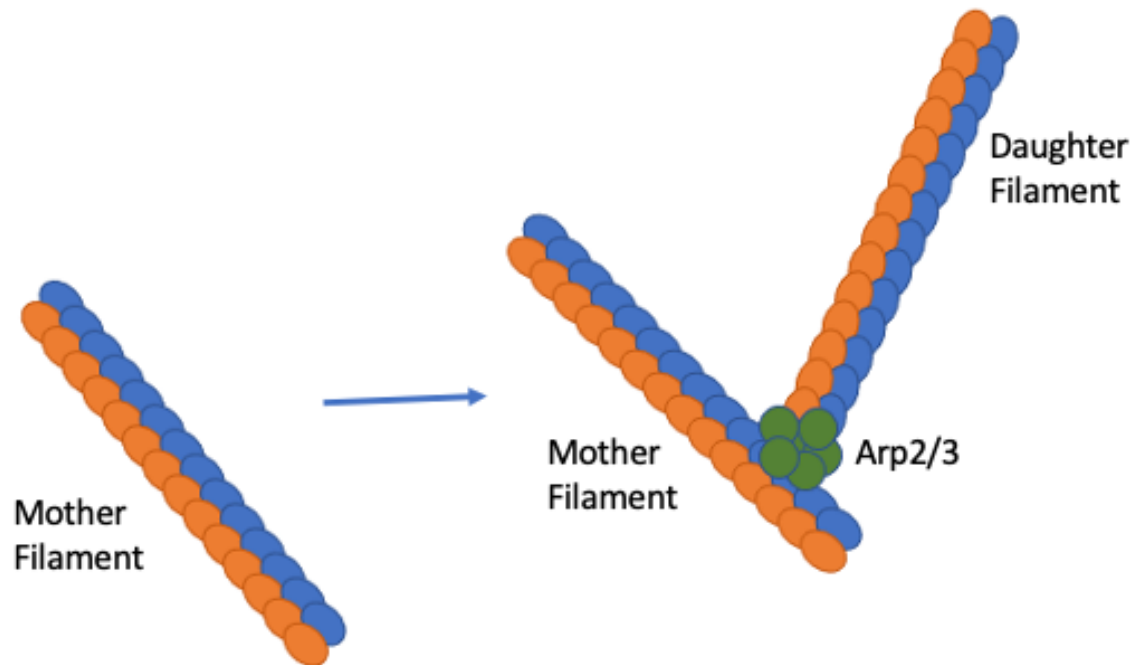


Figure 1.9 The Arp2/3 complex enables branching of F-actin. Association of the Arp2/3 complex and NPF proteins with F-actin facilitates actin branching by the formation of daughter filaments at 70 degree angles to the mother filament. Adapted from (Goley and Welch, 2006).

<i>S. cerevisiae</i> Arp2/3 Gene	Mammalian Arp2/3 Gene
<i>ARP2</i>	<i>ARP2</i>
<i>ARP3</i>	<i>ARP3</i>
<i>ARC40</i>	<i>ARPC1</i>
<i>ARC35</i>	<i>ARPC2</i>
<i>ARC18</i>	<i>ARPC3</i>
<i>ARC19</i>	<i>ARPC4</i>
<i>ARC15</i>	<i>ARPC5</i>

Table 1.6 Nomenclature of the *S. cerevisiae* and mammalian Arp2/3 genes. Adapted from (Pizarro-Cerdá et al., 2017)

greatly upregulated whilst gene expression of *TCP-4* was mildly reduced. Interestingly, the expression of *SUMO-1* *SUMO-2* were also significantly increased, by 79% and 37% respectively, when rats were exposed to high concentrations of nicotine (Kane et al., 2004). These results are particularly significant in relation to the *smt3* SGA screen carried out by our lab (section 1.4) as both *cct3::DAmp* and *cct8::DAmp* were very good suppressors of the growth defects associated with the *smt3* allele, whilst *cct4::DAmp* was a strong enhancer of the *smt3* growth defects. Nevertheless, it is intriguing that several CCT mutants appear to have similar phenotypes to the *smt3* strain, including cold sensitivity and a G2 arrest (Liu et al., 2005, Lewis, 2016, Somer et al., 2002b). The final set of cytoskeletal *smt3* suppressor proteins, found within the Arp2/3 complex, will now be described in more detail.

1.4.2.3 The Arp2/3 complex

Three of the top suppressors in the *smt3* SGA screen, *arp2::DAmp*, *arp3::DAmp* and *arc35::DAmp*, encode components of the essential, conserved Arp2/3 complex. Actin filaments are crucial for several cellular functions including cell mobility and cell structure (for reviews, see (Svitkina, 2018)).

In order to form actin filaments, monomeric G-actin requires ATP-dependant polymerisation to enable the formation of F-actin filaments. However, to facilitate actin branching, additional factors are recruited to actin polymers. The Arp2/3 complex is one such factor which enables actin branching to occur at a 70 degrees angle to the main actin filament (Fig. 1.9) (Goley and Welch, 2006). Actin branching is important in a plethora of actin structures (Pizarro-Cerdá et al., 2017). Initially identified as a binding partner to calmodulin, the *S. cerevisiae* Arp2/3 complex consists of seven individual subunits, Arp2, Arp3 and five different Arc proteins (see table 1.8 for mammalian Arp2/3 homologues) (Moreau et al., 1996, Mullins et al., 1997, Pizarro-Cerda et al., 2017). As described above (see section 1.5.2), mutant *DAmp* alleles encoding three of these subunits, Arp2, Arp3 and Arc35, were identified as very good suppressors of the growth defects associated with the *smt3* allele in the SGA screen. Importantly, all seven subunits are essential in eukaryotic cells, with the notable exception of

A. thaliana, where deletion of the genes encoding Arp2 and Arp3 does not result in loss of viability (Le et al., 2003). It has been suggested that the Arp2/3 complex mimics an actin dimer which enables binding to the growing end of the actin polymer (Goley and Welch, 2006). Interestingly, the Arp2/3 complex does not possess biochemical activity, but instead requires the interaction of nucleation promoting factors (NPFs) to facilitate ATP-dependant branching (Padrick et al., 2011). Interestingly, two NPFs were identified in the *smt3* SGA screen. The first, *abp1*, was a weak enhancer placing 3211/4999 whilst the second, *pan1*, was a mild suppressor, placing 517/4999. However, as neither of these alleles were significant suppressors or enhancers of the *smt3* growth defect, these were not considered for further analysis by Dr. Lewis (Lewis, 2016).

Considering that actin is a vital structure within the cytoskeleton, it is unsurprising that actin structures are important within a variety of cellular processes. For example, lamellipodia, structures vital for cell migration, are composed of actin (see review (Schaks et al., 2019)). Interestingly, Arp2/3 complexes have also been shown to localise to lamellipodia, suggesting that actin branching is crucial for cell migration. Actin polymerisation is also critical in phagocytosis to facilitate the engulfment of foreign bodies and the Arp2/3 complex is required to enable actin polymerisation to facilitate this process (May, 2001). Interestingly, the addition of the Arp2/3 inhibitor CK-666 to mammalian oocytes results displaying meiotic defects, with cells dividing asymmetrically (Sun et al., 2011). Hence, this data indicates multiple roles for the Arp2/3 complex, including an important role in cell cycle progression.

Studies investigating the role of the Arp2/3 complex in *S. cerevisiae* identified that expression of a temperature sensitive *arc35-1* allele resulted in large budded cells, which arrested in metaphase at the non-permissive temperature (Schaerer-Brodbeck and Riezman, 2003). Interestingly, the organisation of tubulin was deregulated within *arc35-1* cells, preventing formation of the mitotic spindle (Schaerer-Brodbeck and Riezman, 2003). Taken together, these examples suggest that the Arp2/3 may have a key role in regulation of the cell cycle in budding yeast.

Although several of the subunits of the Arp2/3 complex have been shown to be phosphorylated to date no studies have been published verifying sumo modification of Arp2

or Arp3. However, interestingly, this phosphorylation of the Arp2/3 complex is vital for cell motility in mammalian cells (Vadlamudi et al., 2004). Hence, it is possible that other modifications, such as sumoylation or ubiquitination, may also regulate the activity of the Arp2/3 complex. Indeed, Panse et al (2004) observed that both Arc35 and Arc40 were covalent sumo targets in *S. cerevisiae* using AP-MS techniques (Panse et al., 2004). However, further analysis is required to verify whether the Arc35, Arc40 or other subunits of the Arp2/3 complex are indeed sumo substrates.

In conclusion, it is clear that very few studies have currently been published which suggest that the top suppressor proteins identified in the *smt3* SGA screen are *in vivo* targets for sumoylation. Although several large-scale studies have previously identified putative sumo substrates within the CCT complex and Arp2/3, the essentiality and difficulties associated with studying the sumoylation of these substrates has hindered further studies. *smt3* suppressors have been overlooked in previous studies, thus the *smt3* SGA screen provides a novel insight into the uncharacterised role of sumoylation of the cytoskeleton. Hence, further studies elucidating and verifying putative *smt3* suppressors could allow important insights to be gained about the fundamental role(s) of sumoylation, including the role of sumo in mammalian diseases.

1.5 Sumo and Disease

Sumoylation is important for the regulation of a multitude of cellular processes, including cell division and apoptosis, hence it is not unexpected that dysregulation of the sumo pathway is closely linked to a number of human diseases. Sumoylation affects a wide variety of cellular substrates, including many transcription factors, thus changes in the pattern of sumoylation may give rise to genomic stabilities, promoting the onset of mammalian diseases. Below are some examples of human diseases associated with dysregulation of the sumo conjugation/deconjugation pathway.

1.5.1 Cancer

Cancer is characterised by uncontrolled cell growth and is currently one of the most prevalent global diseases, affecting >14 million people worldwide in 2015 (Torre et al., 2016). The

pathways underlying cancerous cell phenotypes are often poorly understood, although recent studies have identified a link between cancerous cells and dysregulated sumoylation. For example, a number of studies have identified that global sumoylation is elevated in cancerous cells, suggesting a link between increased sumoylation and cancer (Han et al., 2018). Moreover, Seeler et al. (2017) revealed that elevated levels of Ubc9 in breast cancer cells may contribute to the increase in sumoylation displayed in cancerous cells (Seeler and Dejean, 2017). Additional studies identified that cancer stem cells also showed elevated levels of sumoylation compared to wild type cells, which was found to be mediated by increased gene expression of *AOS1*, *UBA2* and *UBC9* (Du et al., 2016). Interestingly, depletion of Sae2 in cancer stem cells reduced the rate of cellular proliferation by 90% compared to untreated cancer stem cells, suggesting that *SAE1* overexpression is crucial for maintaining the phenotypes associated with cancer stem cells (Du et al., 2016). Taken together, these studies strongly suggest that upregulation of sumo conjugation enzymes may result in excess cellular proliferation, attributing to the phenotypes of cancerous cells.

A key function of sumoylation is the control of gene expression, with the activity of many transcription factors altered by sumoylation (section 1.3.5). Interestingly, the dysregulation of transcription factor activity is often attributed to the phenotypes of cancerous cells. For example, studies have revealed that the loss of transcriptional activity associated with the tumour suppressor protein p53 is linked to >50% of human cancers. p53 is a well characterised sumo substrate in mammalian cells with studies suggesting that p53 K386 sumoylation associated with repression of p53 transcriptional activity (Wu and Chiang, 2009). Furthermore, the upregulation of SUMO-1 in colon cancer is correlated with an increase levels of sumoylated p53, suggestive that aberrant sumoylation of p53 may prevent p53 transcriptional activity, promoting cancerous phenotypes (Zhang et al., 2013).

It is clear that overexpression of sumo and/or the sumo conjugation enzymes is linked to the phenotypes associates with cancerous cells. The above examples represent hundreds of studies which have published data suggesting links between sumo dysregulation and the onset of cancer. For more information linking sumo dysregulation to the onset of cancer please also see reviews of (Kroonen and Vertegaal, 2020, Eifler and Vertegaal, 2015). Although cancer is a prevalent disease linked to aberrant sumoylation, a number of

neurodegenerative disorders have also been associated with the dysregulation of the sumo pathway.

1.5.2 Neurodegenerative Diseases

In addition to cancer, aberrant sumoylation is associated with a number of other mammalian neurodegenerative diseases. For example, the onset of both Parkinson's Disease and Alzheimer's disease have both been associated with the dysregulation of sumo pathways, as described in more detail below. Please see the following reviews for information regarding additional neurodegenerative diseases linked to sumoylation (Princz and Tavernarakis, 2020, Dorval and Fraser, 2007).

1.5.2.1 Parkinson's Disease

Neurodegenerative diseases are characterised by a loss of neuronal cells in the brain and are tightly linked with the accumulation of unwanted protein aggregates. Synucleopathies are a family of neurodegenerative diseases characterised by the accumulation of α -synuclein aggregates, resulting in both motor and cognitive degradation (Xilouri et al., 2016). One example of such a disease is Parkinson's Disease, with the early onset of Parkinson's Disease linked to a loss of function of DJ-1. DJ-1 is a protein essential for the maintenance of dopamine neurone function and has been shown to be subject to sumo-mediated degradation in Parkinson's Disease patients (Shinbo et al., 2006). Interestingly, the expression of a mutated DJ-1 protein, DJ-1^{L166P}, is expressed in a number of Parkinson's Disease patients. Furthermore, this DJ-1^{L166P} point mutation promotes the polysumoylation and subsequent degradation of DJ-1 (Shinbo et al., 2006), suggesting that undesirable sumo-mediated DJ-1 degradation correlates with neuronal instability and subsequent onset of Parkinson's Disease. Thus, taken together, this example highlights illustrating that abnormal patterns of sumoylation can promote undesirable neuronal degeneration facilitated by the degradation of DJ-1.

1.5.2.1 Alzheimer's Disease

In addition to Parkinson's Disease, another common neurodegenerative disorder, Alzheimer's Disease, has also been linked to sumo dysregulation. Alzheimer's Disease is characterised by a build-up of Tau plaques in the brain, with Tau accumulation resulting in reduced memory function and cognitive abnormalities (Naseri et al., 2019). At present, there are no therapeutic treatments which can prevent the onset or deterioration of Alzheimer's Disease (Naseri et al., 2019). Hence, research investigating the prevention of Tau accumulation may provide key insights into future therapeutic treatments for Alzheimer's Disease.

Sumoylation of Tau has been identified in mammalian cells, with sumoylated Tau thought to induce a conformational change which stimulates the subsequent phosphorylation of Tau (Luo et al., 2014). Interestingly, Tau hyperphosphorylation is a hallmark of Alzheimer's Disease. For example, studies investigating PTMs present in the brain cells from patients suffering from Alzheimer's Disease identified that these cells expressed a hyperphosphorylated form of the Tau protein, which co-localises with SUMO-1 (Luo et al., 2014). Hence, it appears that Tau sumoylation may be associated with the onset of Alzheimer's Disease. Tau is also subject to other modifications, including ubiquitination, and it has been proposed that sumo and ubiquitin both compete for Tau K340 (Luo et al., 2014). For example, Tau ubiquitination in WT cells targets Tau for proteasomal-mediated degradation, acting as a feedback mechanism to regulate the levels of Tau in the cell. On the contrary, sumoylated Tau is no longer targeted for degradation and as a consequence accumulates in the cytoplasm, where it is hyperphosphorylated, leading to the formation of unwanted plaques and the onset of Alzheimer's Disease (Luo et al., 2014). Thus, this example highlights the importance of regulated Tau sumoylation in order to prevent Alzheimer's Disease, but also highlights the crosstalk between different PTMs in order to modulate the function of Tau.

Although it is apparent that PTMS, including sumoylation, appear to have important roles in promoting the onset of both Alzheimer's Disease and Parkinson's Disease, it is clear that the links between sumoylation and neurodegenerative diseases require further characterisation in order to develop therapeutic treatments. Sumoylation has also been associated with several viral and bacterial infections, as described in more detail below.

1.5.3 Viral and Bacterial Infections

Recent studies characterising viral and bacterial infections suggest that a number of viruses and bacteria have evolved to take advantage of the sumo pathway. Modulation of the sumo pathway within viral and bacterial infections promotes pathogenic survival whilst preventing detection by the host organism. Examples of viral and bacterial infections are detailed below, for further reviews, please see (El Motiam et al., 2020).

1.5.3.1 Ebola

With an average mortality rate of 50%, the Ebola virus is an extremely virulent pathogen. Infection with the Ebola virus results in a severe viral fever and is associated with downregulation of the interferon pathway in cells to facilitate Ebola entry into the cell (Baseler et al., 2017). Sumoylation has been linked to the infectivity of this virus. In particular, the Ebola virus expresses a matrix protein, VP24, which has recently been identified as a sumo substrate (Vidal et al., 2019). Moreover, mutations that inhibit the sumoylation of VP24 result in reduced VP24 stability, suggesting that sumoylation of VP24 is strongly associated with Ebola virality. Interestingly, the VP24 protein also expresses a SIM domain which, when mutated, can no longer disrupt the interferon pathway resulting in dramatically reduced Ebola infection rates (Vidal et al., 2019). Taken together, these results suggesting the importance of both covalent and non-covalent sumoylation for the virulent nature of Ebola. To conclude, it is clear that the Ebola virus takes advantage of sumo conjugation to facilitate entry into host cells and inhibit the mammalian interferon pathway, although the exact mechanisms remain to be determined (Vidal et al., 2019).

1.5.3.2 *Listeria monocytogenes*

In addition to viruses, bacteria have also been shown to enhance pathogenicity using the sumo pathway. For example, the pathogenic bacteria *Listeria monocytogenes* has been shown to disrupt the host cell sumo pathway in mammalian cells. However, in contrast to Ebola, *L. monocytogenes* achieves pathogenicity by reducing the levels of global sumoylation. *L. monocytogenes* cells express a pore-forming protein, LLO, which has been shown to target Ubc9 for proteasome-mediated degradation (Ribet et al., 2010). Importantly, as only one

sumo E2 is expressed in eukaryotes, the degradation of Ubc9 completely inhibits any further sumo conjugation in host cells. Interestingly, incubation of mammalian cells with a strain of *L. monocytogenes* expressing a mutant LLO protein does not result in a reduction in sumo conjugates, suggesting that the LLO protein is responsible for modulating the sumo pathway (Hamon et al., 2012). Furthermore, these LLO deficient cells also show a reduced rate of infection compared to cells incubated with wild type *L. monocytogenes* (Ribet et al, 2010).

The examples above illustrate that both the sumoylation of pathogenic proteins and the modulation of the sumoylation pathway caused by pathogens facilitate entry into the host cell. One possible explanation as to why pathogens target the sumo conjugation pathway could be that the sumo conjugation pathway contains relatively few enzymes in comparison to ubiquitin. This is particularly significant in the case of *L. monocytogenes*, in which the degradation of a single enzyme (Ubc9) within the sumo conjugation pathway results in the global inhibition of sumoylation (Hamon et al., 2012). Interestingly, both *L. monocytogenes* and Ebola appear to target the sumo pathway to facilitate entry to target cells, which involves interactions with the cytoskeleton of the host cell. This is extremely interesting considering that a number of the top *smt3* suppressors were related to the cytoskeleton, suggesting a link between sumo dysregulation, the cytoskeleton and mammalian diseases, although this is purely speculative. Hence, diseases associated with the novel *smt3* suppressors will now be discussed in more detail.

1.5.4 *smt3* Suppressors and Disease

As previously described in section 1.5, a number of the top suppressor proteins identified from the *smt3* SGA screen are closely linked to the regulation of the cytoskeleton. Importantly, numerous studies have indicated that dysregulation of essential cytoskeletal proteins is tightly linked to common human diseases including pathogenic and viral infections, neurological disorders and a variety of cancers. For reviews and further reading, please see (Hall, 2009, Lai and Wong, 2020).

Interestingly, a number of cytoskeletal-related diseases are also linked to sumo dysregulation, including Alzheimer's Disease, *L. monocytogenes* infection and numerous cancers. Thus, it is

tempting to speculate that sumo/cytoskeleton-related defects may attribute to the characteristics of these diseases.

1.5.4.1 Tubulin and Disease

A growing number of neurodegenerative disorders, such as Parkinson's Disease and Huntington's Disease are associated with the deregulation of tubulin and tubulin interacting proteins (Magiera et al., 2018). For example, mutations in the MAP Tau have been shown to be associated with neurone degeneration (Naseri et al., 2019). Furthermore, studies involving the genotyping of Parkinson's Disease patients revealed that the E3 ubiquitin ligase Parkin, which ubiquitinates α - and β -tubulin subunits to maintain microtubule stability, is subject to a variety of over 100 mutations (Ren et al., 2003). A variety of point mutations in Parkin render microtubules unstable, leading to neurone degeneration and the subsequent onset of Parkinson's Disease (Ren et al., 2015). Additionally, tubulin has also been linked to Leber congenital amaurosis (LCA), an incurable neurodegenerative disease characterised by early onset retinal and hearing loss. In particular, genotyping of LCA patients demonstrated that cells expressed a single amino acid mutation in the β -tubulin encoding gene *TUB4b* (Luscan et al., 2017). Studies identified that β -tubulin R391 interacts with the neighbouring K392 residue to form a binding site which facilitates the homodimerization of α - and β -tubulin in wild type cells (Luscan et al., 2017). Mutation of *TUB4b* R391 reduces the binding affinity of α - and β -tubulin, resulting in impaired microtubule stability, which has been proposed to attribute to neurodegeneration associated with LCA (Luscan et al., 2017). Taken together the examples described above illustrate the importance of microtubule stability for the maintenance of neurone function.

Tubulin function is also linked to other aspects of human health. For example, several pathogens exploit tubulin in order to enhance infection of the host cell. One such example, the opportunistic pathogen *L. monocytogenes*, has been shown to modulate tubulin function to facilitate cell motility (Costa et al., 2019). *L. monocytogenes* have characteristic actin-rich comet tails which facilitate the mobility of *L. monocytogenes* by the polymerisation of actin filaments (Lambrechts et al., 2008). Remarkably, microtubules forming atypical structures have been identified within these actin-rich comet tails (Costa et al., 2019). Furthermore,

inhibition of the tubulin recruiting protein stamin in *L. monocytogenes* infected cells reduces the motility of *L. monocytogenes* within these cells (Costa et al, 2019). Thus, these studies suggest that *L. monocytogenes* dependant microtubule recruitment through activation of stamin is vital for *L. monocytogenes* pathogenicity. Interestingly, as previously described in section 1.5.3.2, *L. monocytogenes* infection also inhibits the sumo conjugation pathway. Hence, modulation of both tubulin and sumoylation appear to be crucial for the pathogenicity of *L. monocytogenes*, which is extremely intriguing considering that *tub2*, an essential microtubule subunit, was the highest *smt3* cytoskeletal suppressor.

1.5.4.2 The Arp2/3 Complex and Disease

Dysregulation of the Arp2/3 complex has been associated with a number of human diseases, including viral and bacterial infections (Zhao et al., 2020, Welch et al., 1997). For example, *L. monocytogenes* exploits the Arp2/3 complex to facilitate actin remodelling and the subsequent invasion of the host cell (May et al., 1999). Interestingly, the ActA protein expressed by *L. monocytogenes* has an actin binding domain which has been shown to recruit the Arp2/3 complex (Skoble et al., 2001). Mutation of the actin binding region of ActA results in a reduction of Arp2/3 complexes located at the plasma membrane upon *L. monocytogenes* infection, suggesting that ActA facilitates mobilisation of the Arp2/3 complex to the cell membrane (Skoble et al., 2001, Lauer et al., 2001). However, it must be noted that these mutations of ActA do not prevent invasion of the host cell (Lauer et al., 2001). Further research by Frazelizi et al. (2001) also demonstrated that ActA coated beads directly bound to the Arp2/3 complex, suggesting that extracellular pathogens express specific proteins which directly bind to the Arp2/3 complex to allow entry into cells (Fradelizi et al., 2001). Similar to the LLO protein expressed by *L. monocytogenes*, the bacteria *Rickettsia conorii* expresses a surface protein, RickA, which has been shown to interact with the Arp2/3 complex (Gouin et al., 2004). Indeed, in a similar manner to ActA, RickA facilitates actin remodelling of the *R. conorii* actin tail, targeting the Arp2/3 complex for activation (Gouin et al., 2004). Indeed, Arp2/3 recruitment mediated by RickA induces polymerisation of the *R. conorii* actin-rich comet tail to promote *R. conorii* motility and the formation of filopodia (Gouin et al., 2004). Taken together, it appears that both *L. monocytogenes* and *R. conorii* recruit the

Arp2/3 complex to promote actin polymerisation within the actin tail of the respective pathogen to promote bacterial migration in the host cell.

The Arp2/3 complex has also been linked to viral infection. For example, the RNA retrovirus Human Immunodeficiency Virus (HIV) is able to enter human cells undetected by the immune response system and it has been suggested that the Arp2/3 complex facilitates entry of HIV into target cells through modulation of the cytoskeleton (Komano et al., 2004). Indeed, incubation of mammalian cells with the synthetic Arp2/3 inhibitor GFPVCA reduces HIV entry into cells to just 34.4% compared to that of untreated cells (Komano et al., 2004). This evidence strongly suggests that the Arp2/3 complex plays a key role to enable HIV entry into cells, although whether this function is direct or indirect is currently unknown. However, Arp2/3 binding sites have not been identified in HIV-encoded proteins, suggesting that activation of Arp2/3 in HIV-infected cells may be through the recruitment of Arp2/3 nucleating factors, rather than the direct interaction with the Arp2/3 complex (Spear et al., 2014).

Cell migration is clearly an important aspect attributing to the pathology of different cancers. Hence, since the Arp2/3 complex is tightly linked to actin regulation, which is important for cell migration, it is not surprising that dysregulation of the Arp2/3 complex is displayed in several different cancers. For example, increased *ARP2* gene expression has been detected in breast cancer, whilst Arp3 overexpression has been linked to colorectal cancer (Iwaya et al., 2007, Otsubo et al., 2004). Furthermore, increased expression of proteins found in the Arp2/3 complex has been tightly linked to increased cell motility in breast cancer cells (Wang et al., 2002). Interestingly, the Arp2/3 inhibitor Arpin, which inhibits cell motility through the binding of Arp3, has been shown to be downregulated in many cancers (Lomakina et al., 2016). Thus, these studies strongly indicate that dysregulation of the Arp2/3 complex can also lead to cancerous phenotypes through undesirable Arp2/3 activity.

To conclude, it is evident that the functions of the Arp2/3 complex to facilitate actin reorganisation is linked to different aspects of disease. However, despite these links, little is known about the regulation of the Arp2/3 complex and thus insight into these mechanisms may be beneficial for efforts to improve human health.

1.5.4.3 The CCT Complex and Disease

It has been estimated that the CCT complex is responsible for folding ~10% of cytosolic proteins. Hence, it is not surprising with such a large number of substrates, that dysregulation of the CCT complex would be predicted to lead to the onset of several diseases due to incorrect protein folding. Indeed, the CCT complex has been linked to many human diseases, including cancer. For example, the CCT complex is crucial for the correct folding of the p53 tumour suppressor protein to maintain its tumour suppressing properties (Trinidad et al., 2013). Mutations in p53 are extremely common in cancerous cells and >50% of all cancers are estimated to express a mutated version of p53. Interestingly, mutations within the N-terminal domain of p53 abolish interaction with the CCT complex leading to p53 inactivity, suggesting a pathway in which the incorrect functioning of the CCT complex could result in genomic instabilities (Trinidad et al., 2013). Consistent with these results, siRNA targeting of specific CCT subunits in mammalian cells resulted in an increase in misfolded cytosolic p53, (Trinidad et al., 2013). Moreover, these cells show an increased rate of cell invasion which is a defining feature of cancer cells, highlighting the importance of accurate folding for p53 function. Interestingly, knockdown of both the CCT subunits and p53 in cancer cell lines reduced cellular invasion, suggesting that the relationship of the CCT complex with p53 plays a key role in maintaining genomic stability by preventing unwanted cell invasion and proliferation.

Loss of function of the tumour suppressor protein von Hippel-Lindau (VHL) also results in a variety of cancerous phenotypes (Kim and Kaelin, 2004). Interestingly, the CCT complex has also been shown to be critical for the folding of the tumour suppressor VHL in mammalian cells (Melville et al., 2003). In wild type cells, the interaction between VHL and the CCT complex is mediated by a pair of hydrophobic β -strands in VHL, enabling the correct folding of VHL by the CCT complex (Feldman et al., 2003). Interestingly, mutations in VHL are associated with several mammalian cancers, with these mutations located in the VHL β -strands in VHL. Thus, similar to p53, this example highlights the importance of correct folding for the function of VHL (Feldman et al., 2003).

The CCT complex has also been linked to other human diseases. For example, Alzheimer's Disease is characterised by undesirable cellular aggregates of the Tau protein which accumulate to form plaques (Ballard et al., 2011). Interestingly, gene expression analysis of brain cells isolated from Alzheimer's patients show reduced CCT mRNA levels, raising the possibility that protein aggregates may accumulate due to reduced CCT activity and the associated increase in misfolded proteins (Brehme et al., 2014). Furthermore, reduced expression of either the CCT2, CCT5 or CCT7 gene in mammalian cells results in a significant number of cells containing unnecessary protein aggregates (Brehme et al., 2014). Further research investigating the functions of the CCT complex in mammalian cells revealed that siRNA targeting of CCT2/5/7 inhibits phagosomal degradation (Pavel et al., 2016). From these results, the authors suggested that phagosome inhibition is caused by actin misfolding which leads to a rise in protein aggregates. Actin is one of the main CCT complex substrates and hence it is unsurprising that a reduction in CCT activity may lead to actin misfolding. Nevertheless, the CCT complex has also been linked to other neurodegenerative diseases. For example, Huntington's Disease is a genetic disorder characterised by the accumulation of plaques containing the Huntington protein (htt) which leads to the neurodegeneration of the central nervous system (Bates et al., 2015). Tam et al. (2006) demonstrated that the N terminal domain of htt is crucial for CCT binding. Moreover, truncation of the N terminal domain of htt inhibits CCT binding, which promotes htt aggregates in the cytosol. Interestingly, the inherited mutations which give rise to Huntington's Disease are often always due to the presence of several glutamine repeats at the N terminus of htt (Schulte and Littleton, 2011). This raises the possibility that these repeats interfere with the interaction between htt and the CCT complex, resulting in inefficient htt folding. Collectively, it can be concluded that reduced CCT activity is often associated with the pathology of several neurodegenerative diseases, due to the misfolding of proteins in the cytosol.

Taken together, the studies presented above have clearly demonstrated that correct regulation of the cytoskeleton is crucial to prevent a multitude of different human diseases. However, there is still much to learn about the regulation of the cytoskeleton and how this regulation is linked to human diseases. Hence, research to characterise these regulatory pathways are essential to facilitate the development of new treatments and drug targets for

these diseases. Moreover, a number of cytoskeletal-related diseases are also associated with dysregulation of the sumo conjugation pathway, therefore identification and characterisation of the novel *smt3* cytoskeletal proteins may provide further insights into the underlying molecular mechanisms of these diseases.

1.6 Summary and Aims

Although many studies have identified important roles for sumo within a number of biological processes, the fundamental functions of sumo to facilitate cell growth and division remains elusive. Building on the data obtained from the *smt3* SGA screen carried out by Dr. Lewis, the aim of this study was gain further insight into the functions and regulation of sumoylation in the model organism *S. cerevisiae*.

Specific objectives were:

1. To characterise the sumo-mediated stress response to cold temperature and oxidative stress in *S. cerevisiae*
2. To identify and characterise cell cycle defects associated with a variety of *smt3* mutant strains
3. To investigate the putative interactions of Smt3 with Tub2 and characterise potential Tub2 covalent and non-covalent sumoylation sites

Chapter Two: Materials and Methods

2.1 Yeast Techniques

All yeast strains used in this study can be found in Table 2.1.

Name	Genotype	Source
GC1	MATa <i>his3Δ1 leu2Δ0 ura3Δ0 met15Δ0</i>	Lab Stock BY4741
GC4	MATa <i>leu2-3,112 trp1-1 ura3-1 ade2-1 his3-11,15 can1-100</i>	Lab Stock W303
GC10	MATa <i>arp2-DAmP::KanMX his3Δ1 leu2Δ0 ura3Δ0 met15Δ0</i>	(Breslow et al., 2008)
GC11	MATa <i>arp3-DAmP::KanMX his3Δ1 leu2Δ0 ura3Δ0 met15Δ0</i>	(Breslow et al., 2008)
GC13	MATa <i>arc35-DAmP::KanMX his3Δ1 leu2Δ0 ura3Δ0 met15Δ0</i>	(Breslow et al., 2008)
GC16	MATa <i>smt3-DAmP::NatMX his3Δ1 leu2Δ0 ura3Δ0 met15Δ0</i>	(Breslow et al., 2008)
GC17	MATa <i>smt3-DAmP::NatMX arp2-DAmP::KanMX lyp1::HPH::LEU2 can1Δ::STE2pr-Sp_his5 his3Δ1 leu2Δ0 ura3Δ0 met15Δ0</i>	Gift from C. Lewis
GC18	MATa <i>smt3-DAmP::NatMX arc35-DAmP::KanMX lyp1::HPH::LEU2 can1Δ::STE2pr-Sp_his5 his3Δ1 leu2Δ0 ura3Δ0 met15Δ0</i>	Gift from C. Lewis
GC19	MATa <i>smt3-DAmP::NatMX arp3-DAmP::KanMX lyp1::HPH::LEU2 can1Δ::STE2pr-Sp_his5 his3Δ1 leu2Δ0 ura3Δ0 met15Δ0</i>	Gift from C. Lewis
GC28	MATa <i>siz1Δ::KanMX his3Δ1 leu2Δ0 ura3Δ0 met15Δ0</i>	Gift from C. Lewis
GC29	MATa <i>siz2Δ::KanMX his3Δ1 leu2Δ0 ura3Δ0 met15Δ0</i>	Gift from C. Lewis
GC30	MATa <i>ulp1-DAmP::KanMX his3Δ1 leu2Δ0 ura3Δ0 met15Δ0</i>	(Breslow et al., 2008)
GC31	MATa <i>ulp2-DAmP::KanMX his3Δ1 leu2Δ0 ura3Δ0 met15Δ0</i>	(Breslow et al., 2008)
GC44	MATa <i>tub2-DAmP::KanMX his3Δ1 leu2Δ0 ura3Δ0 met15Δ0</i>	(Breslow et al., 2008)
GC49	MATa <i>smt3-DAmP::NatMX tub2-DAmP::KanMX lyp1::HPH::LEU2 can1Δ::STE2pr-Sp_his5 his3Δ1 leu2Δ0 ura3Δ0 met15Δ0</i>	(Breslow et al., 2008)
GC50	MAT?? <i>smt3-DAmP::NatMX leu2-3,112 trp1-1 ura3-1 ade2-1 his3-11,15 can1-100</i>	This study
GC51	MATa <i>his3-DAmP::KanMX his3Δ1 leu2Δ0 ura3Δ0 met15Δ0</i>	(Breslow et al., 2008)
GC55	MATa <i>can1Δ::STE2pr-URA3 lyp1Δ ura3Δ0 leu2Δ0 his3Δ1</i>	(Srikumar et al., 2013a)
GC57	MATa <i>smt3::smt3allR::NatMX can1Δ::STE2pr-URA3 lyp1Δ ura3Δ0 leu2Δ0 his3Δ1</i>	(Srikumar et al., 2013)
GC96	MATa <i>cct3-DAmP::KanMX his3Δ1 leu2Δ0 ura3Δ0 met15Δ0</i>	(Breslow et al., 2008)
GC97	MATa <i>cct8-DAmP::KanMX his3Δ1 leu2Δ0 ura3Δ0 met15Δ0</i>	(Breslow et al., 2008)
GC98	MATa <i>smt3-DAmP::NatMX cct3-DAmP::KanMX lyp1::HPH::LEU2 can1Δ::STE2pr-Sp_his5 his3Δ1 leu2Δ0 ura3Δ0 met15Δ0</i>	Gift from C. Lewis

GC99	MATa <i>smt3-DAmP::NatMX cct8-DAmP::KanMX lyp1::HPH::LEU2 can1Δ::STE2pr-Sp_his5 his3Δ1 leu2Δ0 ura3Δ0 met15Δ0</i>	Gift from C. Lewis
GC117	MATa <i>lys2-801 leu2-3,112 ura3-52 his3-Δ200 trp1-1[am] ubi1-Δ1::TRP1 ubi2-Δ2::ura3 ubi3-Δub-2 ubi4-Δ2::LEU2 [pUB39 Ub, LYS2][pUB100, HIS3]</i>	(Finley et al., 1994)
GC119	MATa <i>lys2-801 leu2-3,112 ura3-52 his3-Δ200 trp1-1[am] ubi1-Δ1::TRP1 ubi2-Δ2::ura3 ubi3-Δub-2 ubi4-Δ2::LEU2 [pUB39 Ub K63R, LYS2][pUB100, HIS3]</i>	(Spence et al., 1995)
GC134	MATa <i>tub2Δ::HIS3 can1Δ::STE2pr-URA3 lyp1Δ ura3Δ0 leu2Δ0 his3Δ1 [pRS316-TUB2, URA3]</i>	This study
GC136	MATa <i>tub2Δ::HIS3 can1Δ::STE2pr-URA3 lyp1Δ ura3Δ0 leu2Δ0 his3Δ1 [YCplac111-TUB2, LEU2]</i>	This study
GC137	MATa <i>tub2Δ::HIS3 can1Δ::STE2pr-URA3 lyp1Δ ura3Δ0 leu2Δ0 his3Δ1 [YCplac11-K324R, LEU2]</i>	This study
GC138	MATa <i>tub2Δ::HIS3 can1Δ::STE2pr-URA3 lyp1Δ ura3Δ0 leu2Δ0 his3Δ1 [YCplac111-SIM, LEU2]</i>	This study
GC139	MATa <i>tub2Δ::HIS3 can1Δ::STE2pr-URA3 lyp1Δ ura3Δ0 leu2Δ0 his3Δ1 [YCplac111-Quad, LEU2]</i>	This study

Table 2.1. *S. cerevisiae* strains used in this study.

2.1.1 Growth Conditions

Strains were grown at 30°C unless otherwise stated in YPD media (2% w/v Bactopeptone, 1% w/v Bacto-yeast extract, 2% w/v glucose with 2% w/v agar added for plates). To allow for selection, strains were grown in SD with the appropriate supplements (0.67% w/v Bacto-yeast nitrogen base, 2% w/v glucose, 20mg/L adenine sulphate, 10mg/L L-leucine, 10mg/L L-methionine, 10mg/L L-histidine hydrochloride, 30mg/L L-lysine hydromonochloride, 8mg/L uracil). When required, YPD was supplemented with 100mg/ml clonNAT (WERNER BioAgents) to allow for NAT selection or 1mg/ml 5'FOA (Zymo Research) for URA3 negative selection (section 5.3.6).

2.1.2 Strain Construction

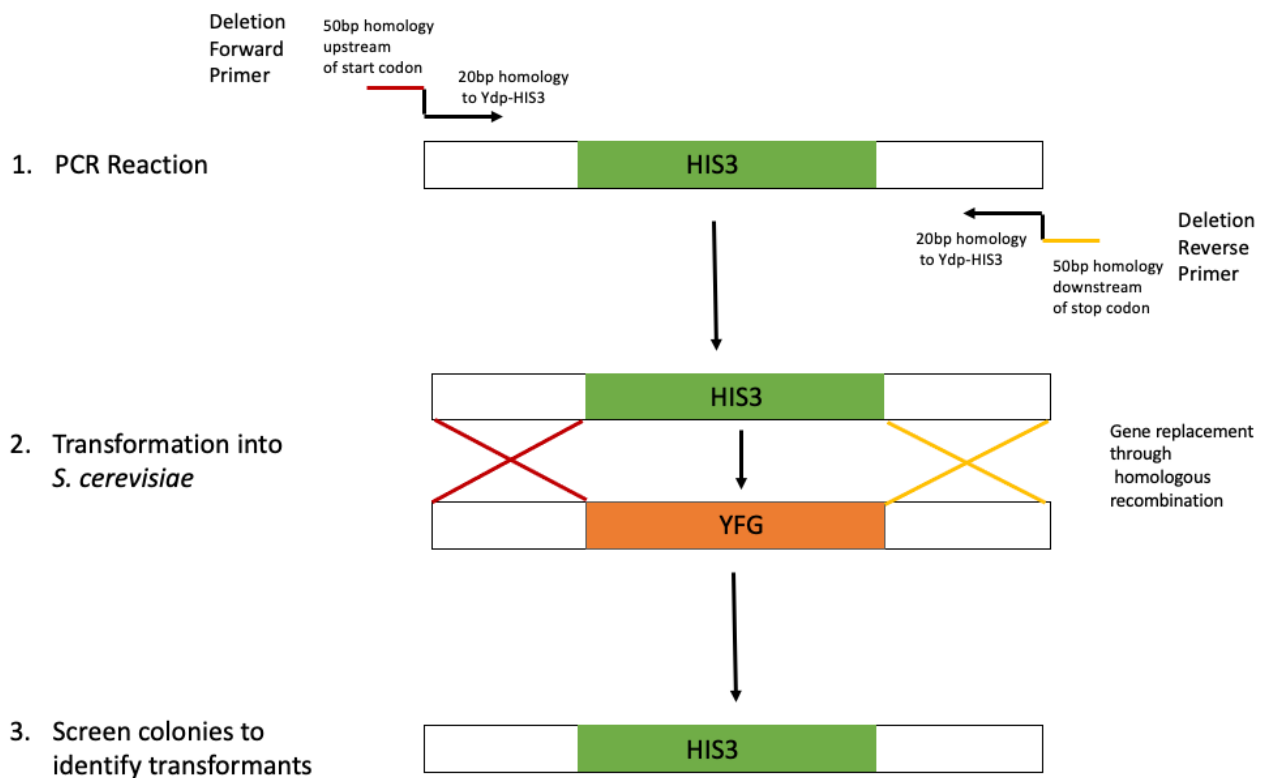


Figure 2.1 Schematic diagram of gene deletion in *S. cerevisiae*. YFG (your favourite gene, the gene of interest) is replaced by the *HIS3* selective marker gene from the YDpH plasmid (Berben et al., 1991). The forward primer has 50bp homology with the sequence located immediately upstream of the start codon of YFG and 20bp homology of the 5' start of the *HIS3* selective marker on the YDpHIS3 plasmid. The reverse primer has 50 bp homology with the sequence located immediately downstream of the stop codon of YFG and a further 20bp homology to the 3' end of the *HIS3* selective marker on the YDpHIS3 plasmid. A PCR reaction (see section 2.2.1) containing both the forward and reverse primers (see table 2.2) along with the YDpHIS3 plasmid as a template was performed to generate a deletion cassette containing the selective marker along with 50bp homology upstream and downstream of YFG. Deletion cassettes were subsequently transformed into *S. cerevisiae* cells (see section 2.1.3), plated onto selective media and successful transformants confirmed by PCR (see section 2.2.2).

2.1.3 Yeast Recombination Cloning

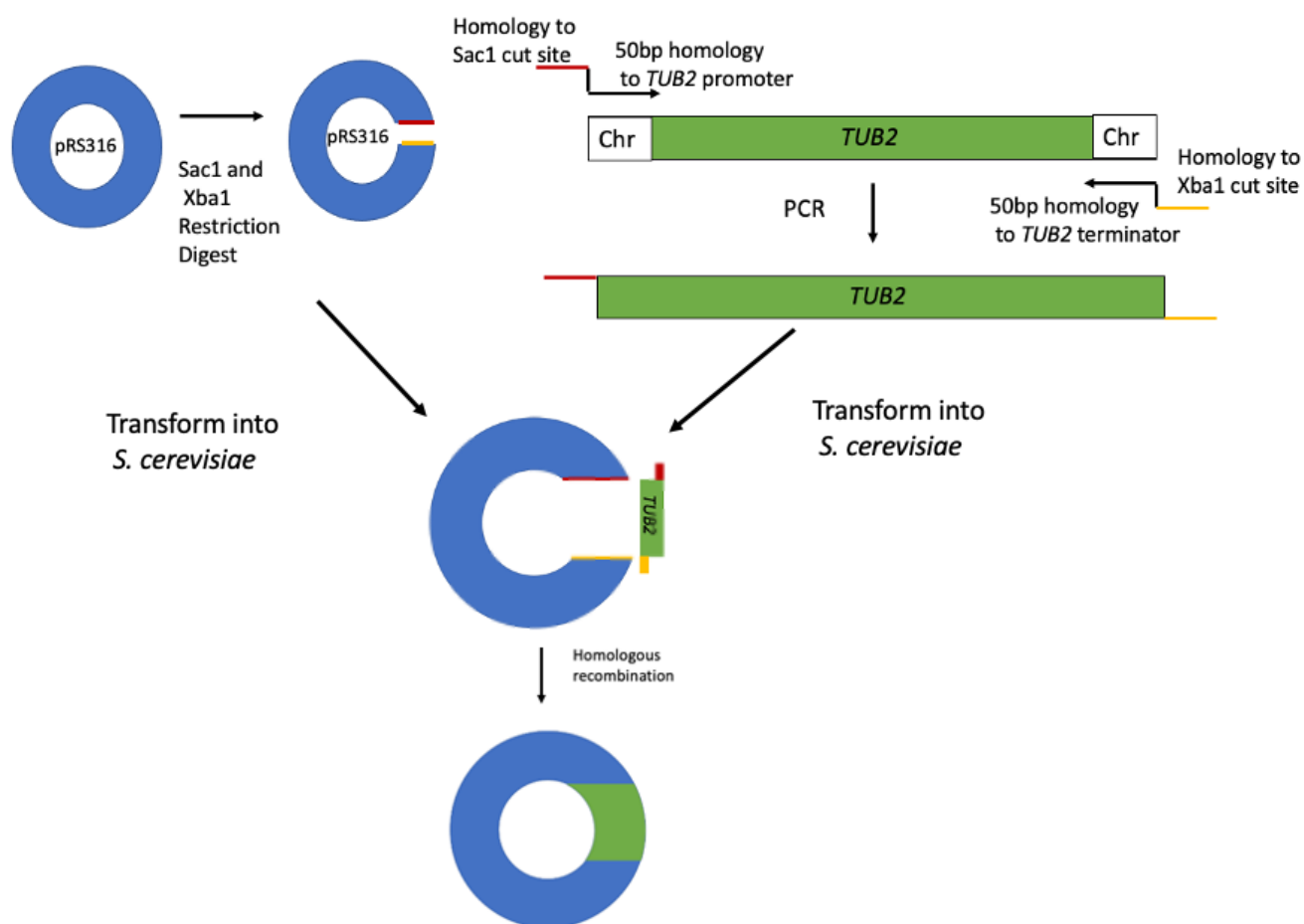


Figure 2.2 Schematic diagram of yeast recombination cloning. Schematic diagram of the pRS316-*TUB2* plasmid construction in *S. cerevisiae*. Forward primers were designed with 20bp homology to the pRS316 Sac1 cut site and the first 50bp of the *TUB2* promoter (Sikorski and Hieter, 1989). Reverse primers were designed with 50bp homology to the last 20bp of the *TUB2* terminator and 20bp homology to the pRS316 Xba1 cut site. A PCR reaction (see section 2.2.1) containing both the forward and reverse primers along with *S. cerevisiae* genomic DNA (taken from a plated colony) as template was performed to generate a cassette containing the *TUB2* gene including the promoter and terminator regions and with 20bp homology upstream and downstream to the Xba1 and Sac1 restriction enzyme cut sites respectively in pRS316. The *TUB2* cassette was run on a 1% agarose gel (see 2.2.2) to confirm the fragment size, transformed into *S. cerevisiae* and plated onto selective plates lacking

uracil. Transformants were screened by PCR using the M13 primers to confirm the presence of the *TUB2* insert (see section 2.2.1). Successful transformants were subsequently grown in SD-URA media overnight, plasmids were extracted and transformed into *E. coli* (see section 2.2.4).

2.1.3 Yeast Transformation

S. cerevisiae cells were grown to mid-log phase in the appropriate media and transformed using the LiAc method (Gietz and Schiestl, 2007). Briefly, 50ml of cells were pelleted 3000rpm 2 minutes, washed in 50ml dH₂O and pelleted at 3000rpm. The cell pellet was subsequently resuspended in 1ml LiAc/TE (0.1M LiAc, 1mM EDTA pH[8.0], 10mM Tris-HCl pH[7.4]). 50µg salmon sperm along with the transforming DNA (typically 5µl of the PCR cassette) were added to 200µl aliquots of cells. 1ml LiAc/TE/PEG (40% [w/v] PEG-4000, 0.1M LiAc, 1mM EDTA pH[8.0], 10mM Tris-HCl pH[7.4]) was added to the cells, gently mixed and incubated at 30°C for 30 minutes. After 15-minutes heat shock at 45°C, cells were pelleted at 7000rpm for 30 seconds and resuspended in 150µl dH₂O. Cells were plated on the appropriate selective media and left to grow at 30°C until colonies formed. Colonies were checked by PCR (see 2.2.1) and successful transformants confirmed by DNA sequencing.

2.1.4 Growth Curves

Cells were grown to mid-log phase in the appropriate media and diluted back overnight to reach an OD₆₆₀ of ~0.1 for the next morning. 1ml aliquots of cultures were taken at the indicated timepoints and measured on a spectrometer at OD₆₆₀. Graphs were plotted in Microsoft Excel and growth rates calculated using the following equation:

$$\text{Doubling time} = \frac{\text{Natural logarithm of 2}}{\text{Exponent of growth}}$$

2.1.5 Sensitivity Tests

Cells were grown to mid-log phase in the appropriate media. Cells were diluted back to an equal OD₆₆₀ with 5-fold serial dilutions of equal OD were spotted onto plates using a 48-pin tool (Sigma). H₂O₂ (Sigma Aldrich) or benomyl (Sigma Aldrich) were added to plates at the

indicated concentrations when required. Plates were then incubated at the indicated temperature and imaged after two days unless stated otherwise.

2.1.6 Cold Temperature Shift

50ml cultures of mid-log phase cells growing at 30°C were rapidly cooled to 20°C in an ice/water bucket with the flasks immediately transferred to a 20°C incubator. 7ml samples of culture were added to 7ml of ice cold 20% (w/v) TCA at the indicated time points and snap frozen. Proteins were extracted using the TCA method (see 2.1.7) and subsequently analysed by western blotting (see 2.3.1).

2.1.7 H₂O₂ Treatment

Mid-log phase cultures were treated with 5mM H₂O₂ (unless otherwise indicated) and incubated at 30°C. 5ml samples of culture were added to 5ml of ice cold 20% (w/v) TCA at the indicated time points and snap frozen. Proteins were extracted using the TCA method (see 2.1.7) and subsequently analysed by western blotting (see 2.3.1).

2.1.8 Protein Lysis

50ml of mid-log phase cells were washed in 1ml PBS, pelleted and snap frozen. Thawed pellets were resuspended in 100µl lysis buffer (25mM Tris-HCl pH[7.5], 1mM EDTA, 0.45mg/ml PMSF, 0.1 TIU/ml Aprotinin, 2µg/ml Leupeptin, 2µg/ml Pepstatin A, 20mM NEM) and 500 µl of chilled glass beads were added. After 6x30 seconds pulse in a beadbeater samples were pelleted for 10 minutes at 13000rpm until the supernatant became clear. Protein concentration was measured using the Bradford Protein Assay (Thermo Scientific).

2.1.9 Protein Extraction (TCA)

7ml of mid-log phase cultures were added to 7ml ice cold 20% (w/v) TCA and snap frozen. Pellets were thawed on ice, resuspended in 200µl 10% (w/v) TCA and placed into a ribolyser tube. 0.5ml ice cold glass beads were added and cells were homogenised with 6x15 second pulses in a bead beater with 15 seconds on ice in between pulses. An additional 500µl 10% TCA were added, ribolyser tubes pierced with a needle and the supernatant spun through into an Eppendorf tube. Proteins were pelleted at 13000rpm, 15 minutes, 4°C and washed twice

in ice cold acetone. Pellets were left to air dry, then resuspended in 40ml TCA buffer (1mM EDTA [pH 8.0], 100mM Tris-HCl [pH7.4], 1% [w/v] SDS, 0.5mg/ml PMSF, 12.5mM NEM). Samples were incubated at 25°C for 30 minutes then 42°C for 5 minutes and final protein concentrations were measured using a BCA assay (Pierce).

2.1.10 RNA Extraction

50ml of mid-log phase cells were pelleted at 3000rpm for 2 minutes, washed in 1ml dH₂O, transferred to a ribolyser tube and re-pelleted at 3000rpm for 2 minutes. Pellets were snap frozen. Pellets were thawed on ice and resuspended in 750µl TES buffer (0.1M Tris-HCl [pH7], 0.5% [w/v] SDS, 100mM EDTA) and 750ml acidic phenol-chloroform (Sigma). Samples were immediately vortexed, placed in a 65°C water bath and vortexed for 10 seconds at 10 minute intervals for 1 hour. Samples were placed on ice for 1 minute, vortexed for 20 seconds and then placed in a centrifuge at 4°C at 6000rpm for 15 minutes. 700µl of the aqueous phase was added to 700µl of pre-cooled acidic phenol-chloroform and then placed in a centrifuge at 4°C at 13,000rpm for 5 minutes. This step was repeated, and 500µl of the aqueous phase was then transferred to a 2ml Eppendorf tube containing 1.5ml 100% EtOH and 50µl 3M sodium acetate [pH5.2] and left at -80°C for 1 hour. RNA was pelleted at 13000rpm for 10 minutes, washed in 70% EtOH and left to dry at room temperature. The resulting RNA pellet was resuspended in 100µl dH₂O. RNA concentration was measured using a NanoDrop spectrometer (Labtech) and 5µl samples were analysed on a 1% agarose gel (section 2.2.2) to check RNA quality.

5µg RNA were treated with 1ml DNase (Primer Design) according to the manufacturer's instructions and samples were stored at -80°C until needed.

For RNA from cells exposed to cold temperature, 50ml mid-log phase cultures were grown at 30°C, cooled and immediately transferred to a 20°C incubator for the indicated times. For these experiments, 10ml samples of cultures were taken for subsequent RNA extraction. 5µg RNA were subsequently treated with DNase.

2.1.11 DNA Content Analysis (FACS)

5x10⁶ cells from mid-log phase cultures were pelleted, washed in 1ml dH₂O and resuspended in 400µl dH₂O. Cells were briefly sonicated, resuspended in 950µl 70% EtOH and kept at 4°C until required. On the day before FACS analysis, cells were pelleted at 7000rpm and washed once in 800µl 50mM sodium citrate [pH 7.2] and resuspended in 500µl RNase A solution (50mM sodium citrate [pH7.2], 0.25mg/ml RNase A). Samples were incubated at 30°C overnight without agitation. The following morning, Proteinase K was added to a final concentration of 20mg/ml (Ambion) and samples were incubated at 50°C for 1 hour before incubation with 500µl Sytox Green solution (50mM sodium citrate [pH 7.2], 4mM Sytox Green (Life Technologies)) for 1 hour at room temperature in the dark. A FACS Canto II flow cytometer (BD Life Sciences) was used to perform FACS analysis and data was analysed using FCS Express software (DeNovo).

To determine the number of minutes spent in each stage of the cell cycle, gating analyses were performed on FACS histograms using FCS Express software (DeNovo). The percentage of cells in each stage obtained from this gating analysis was multiplied by the doubling time of the respective strain (see section 2.1.4).

2.2 Molecular Biology Techniques

2.2.1 Polymerase Chain Reaction (PCR)

A thermocycler was used to carry out all PCR reactions using either Phusion High Fidelity Polymerase (Thermo Scientific) or DreamTaq Polymerase (Thermo Scientific) following manufacturer's instructions. The PCR primers used are listed in Table 2.2.

2.2.1.1 Gene Deletions

PCR reactions for gene deletion and epitope tagging cassettes were carried out using Phusion High Fidelity Polymerase under the following conditions:

1. 98°C for 2 minutes
2. 98°C for 30 seconds
3. X °C for 30 seconds

4. 72°C for 30 seconds/kb*
5. 72°C for 10 minutes

*Steps 3 and 4 were cycled 35 times

X denotes the annealing temperature of the primers, which was pre-determined using the online NEB TM calculator tool when designing the primers.

Each reaction typically consisted of 0.5ml Phusion, 0.1ng template DNA, 10µM forward and reverse primers, 10mM dNTP mix, 1.5mM MgCl₂, 10µl 5xPhusion buffer and dH₂O up to 50µl.

To confirm the size of the PCR product and for purification of PCR products the PCR material was analysed on a 1% agarose gel (2.2.2).

2.2.1.2 PCR of *S. cerevisiae* Colonies

PCR analyses of transformed *S. cerevisiae* colonies growing on plates was carried out using DreamTaq Polymerase under the following conditions:

1. 94°C for 2 minutes
2. 94°C for 30 seconds
3. X°C for 30 seconds
4. 72°C for 30 seconds/kb*
5. 72°C for 10 minutes

*Steps 3 and 4 were cycled 35 times

X denotes the annealing temperature of the primers, which was pre-determined using the online NEB TM calculator tool when designing the primers.

Each reaction consisted of 0.2U DreamTaq, 0.1ng template DNA, 10µM forward and reverse primers, 10mM dNTP mix, 5µl 10x DreamTaq buffer and dH₂O up to 50µl. To confirm the size of the PCR product, 5µl of PCR material were analysed on a 1% agarose gel (2.2.2).

2.2.2 Agarose Gel Analyses, Gel Extraction and DNA Sequencing

DNA and RNA products were analysed on a 1% agarose gel (w/v) and nucleic acids stained using Ethidium Bromide (0.5 µl/ml). Gels were run in TAE buffer (40mM Tris Acetate, 1mM EDTA [pH8]) for ~45-60 minutes at ~40V with DNA/RNA bands visualised using a GelDoc (BioRad). DNA bands to be extracted were excised from the agarose gel under UV light. DNA was subsequently extracted from the agarose using a QIAquick gel extraction kit (QIAGEN) according to the manufacturer's instructions. DNA concentration was measured using a Nanodrop spectrometer (Labtech) and DNA samples were sequenced by Eurofins.

2.2.3 *Escherichia coli* Transformation and Plasmid Extraction

Plasmids were transformed using a standard CaCl₂ method (Wood, 1983) into Subcloning Efficiency DH5α Competent *E. coli* cells (Invitrogen) and plated onto LB+Amp plates at 37°C overnight to select for ampicillin resistance (2% [w/v] bacto-tryptone, 1% [w/v] Bacto-yeast extract, 1% [w/v] NaCl [pH7.2], 0.1mg/ml ampicillin, 2% [w/v] agar). A single colony was picked and grown overnight at 37°C in LB+Amp liquid media (2% [w/v] bacto-tryptone, 1% [w/v] Bacto-yeast extract, 1% [w/v] NaCl [pH7.2], 0.1mg/ml ampicillin). Plasmids were then extracted using the GenElute Plasmid miniprep kit (Sigma) following the manufacturer's instructions. Plasmids were stored at -20°C until needed.

2.2.4 Yeast Plasmid Extraction

Mid-log phase cultures of *S. cerevisiae*, grown in SD media overnight, were pelleted at 3,000rpm for 5 minutes. Cell pellets were immediately resuspended in 200µl resuspension buffer (GenElute Plasmid miniprep kit) and 500ml ice-cold glass beads were added. Pellets were subjected to 5x15 seconds bead beating with 15 seconds on ice in between each step. Ribolyser tubes were pierced with a needle, the supernatant was spun through into an Eppendorf tube and 400µl Neutralisation solution (GenElute Plasmid miniprep kit) were added. Samples were then placed in a centrifuge at top 13000rpm for 10 minutes and the plasmid isolated according to the GenElute Plasmid miniprep kit instructions. Plasmids were eluted in 10µl nH₂O. 5µl of eluted plasmids were then immediately transformed in DH5α cells (2.2.3).

2.2.5 Restriction Digests

Plasmids were digested with the indicated restriction enzyme according to the manufacturer's instructions (Fermentas). To confirm that plasmids had been digested 1ml samples of the digests were analysed on a 1% agarose gel (2.2.2).

Primer Name	Sequence 5'-3'	Description
TUB2 Del Forward	ACATAGCAGCTACTACAACACTACAAAAGCAAATCTCCA CAAAGTAATATAGAATCCCCGGGGATCCGGTG	<i>TUB2</i> chromosomal deletion
TUB2 Del Reverse	TCAAAATTCTCAGTGATTGGTTCATCTTGGTTTTGTGGA GCACCAAATCAAGCTAGCTTGGCTGCAGGT	<i>TUB2</i> chromosomal deletion
TUB2 F Check	GAAAAAGGAAAAAACAGAA	<i>TUB2</i> deletion check
TUB2 R Check	TTTGATTTTTGTTTATTTTGCTC	<i>TUB2</i> deletion check
TUB2 YCPLAC111 F	TGCATGCCTGCAGGTGCAGCTTATTAGTGCTTTTCTTGTT TTATTTATTTT	YCplac111 <i>WT-TUB2</i>
TUB2 YCPLAC111 R	ACGGCCAGTGAATTCGAGCTATTTTAAAGATATTTAAT TAGTTTTTTTTGATTTTTG	YCplac111 <i>WT-TUB2</i>
TUB2 PRS316 F	ACGGCCAGTGAATTCGAGCTATTTTAAAGATATTTAAT TAGTTTTTTTTGATTTTTG	pRS316 <i>WT-TUB2</i>
TUB2 PRS316 R	GCCCGGGGGATCCACTAGTTATTTTAAAGATATTTAAT TAGTTTTTTTTGATTTTTG	pRS316 <i>WT-TUB2</i>
TUB2 K324R F	TTAGAGGTAAAGTTTCCGTTAGAGAGGTGGAAGATGA AATGCA	YCplac111 <i>TUB2-K324R</i>
TUB2 K324R R	TGCATTTTCATCTTCCACCTCTCTAACGGAACTTTACCT CTAA	YCplac111 <i>TUB2-K324R</i>
TUB2 SIM F	AAAGTAATATAATGAGAGAAGCTGCTGCTGCTTCGACA GGTCAGTGTGGTAA	YCplac111 <i>TUB2-SIM</i>
TUB2 SIM R	TTACCACACTGACCTGTGCAAGCAGCAGCAGCTTCTCT CATTATATTACTTT	YCplac111 <i>TUB2-SIM</i>
TUB2 QUAD F	TTGCAGCCTTCTTTAGAGGTAGAGTTTCCGTTAGAGAG GTGGAAGATGAAATGCATAGAGTGCAATCTAGAACT CAGACTATTTTCGTGGA	YCplac111 <i>TUB2-quad</i>
TUB2 QUAD R	TCCACGAAATAGTCTGAGTTTCTAGATTGCACTCTATGC ATTTTCATCTTCCACCTCTCTAACGGAACTCTACCTCTA AAGAAGGCTGCAA	YCplac111 <i>TUB2-quad</i>
HIS CHECK F	GTAAAGCGTATTACAAATGA	To check for presence of HIS deletion cassette
HIS CHECK R	GAAAGTGCCTCATCCAAAG	To check for presence of HIS deletion cassette
M13 F	GTAAAACGACGGCCAGTG	To screen plasmids for inserts

M13R	CAGGAAACAGCTATGACC	To screen plasmids for inserts
-------------	--------------------	--------------------------------

Table 2.2 PCR primers used in this study. All primers were produced by Sigma Aldrich.

2.3 Biochemical Techniques

2.3.1 Western Blotting

An equal volume of 4x loading dye (10% [w/v] SDS, 625mM Tris-HCl [pH6.8], 50% [v/v] glycerol, 0.1% [w/v] bromophenol blue) was added to protein samples after the protein concentration had been measured. Samples were prepared for electrophoresis by denaturation at 100°C for 5 minutes and 15µg samples (unless otherwise stated) were loaded onto an 8% or 13% SDS-PAGE gel (13% gels were used to analyse HMW sumo conjugates, with the stacking gel left on during the transfer). An additional lane was loaded with 5µl PageRule Pre-stained Ladder (ThermoFisher) as a marker of molecular weight. 13% gels were run at 200mV for ~1 hour until the 10kDa marker had run to the bottom of the gel; 8% gels were typically run for ~45 minutes until the 35kDa marker had run to the bottom of the gel. The gel was then transferred onto a Nitrocellulose membrane (Amersham) at 100mV for ~2 hours. Membranes were blocked with 10% (w/v) BSA, 1xTBST (1mM Tris-HCl [pH8], 15mM NaCl, 0.01% [v/v] Tween-20) for 30 minutes at room temperature and then incubated in primary antibody at 4°C overnight with agitation. The following day the membrane was washed 5x5 minutes in 1xTBST, incubated with secondary antibody (1:2000 in 5% (w/v) BSA, 1xTBST) for 1 hour and washed again 5x5 minutes in 1xTBST, all at room temperature. Blots were developed using ECL (GE Healthcare) and visualised either on X-Ray film or using a Typhoon FLA 9500 (GE Healthcare).

Membranes were re-probed with a different primary antibody as a loading control. First, membranes were stripped of antibodies by incubation in stripping buffer (100mM β-mercaptoethanol, 2% [w/v] SDS, 625mM Tris-HCl [pH 6.7]) at 50°C for 30 minutes. Membranes were washed 5x5 minutes in 1xTBST and incubated with the loading control primary antibody overnight at 4°C. The following day the membrane was washed, incubated with secondary antibody and visualised as described above.

All antibodies used in western blotting are listed in Table 2.3.

Antibody	Source	Dilution	Raised in
α-Smt3	Abcam	1:1000	Rabbit
α-Ub	Santa Cruz Biotechnology	1:1000	Mouse
α-Tub2	Abcam	1:1000	Rabbit
α-Ub K63	ThermoFisher	1:1000	Mouse
α-Skn7	Morgan et al. 1997	1:1000	Rabbit
α-Cdc28	Santa Cruz Biotechnology	1:1000	Mouse
α-a-Tubulin	Cancer Research	1:200	Mouse
α-Mouse HRP	Sigma Aldrich	1:2000	-
α-Rabbit HRP	Sigma Aldrich	1:2000	-

Table 2.3 Antibodies used in this study.

2.3.2 Immunoprecipitation

Protein samples were prepared as described above (2.1.6). For immunoprecipitation 200µl samples (200µg protein in lysis buffer) were made and 2µl were taken for a 1% input sample (stored at -20°C for later use). A 1:100 dilution of antibody (2µl) was added and left to rotate at 4°C overnight. Next, 20µl Protein A/G PLUS-Agarose beads (Santa Cruz Biotechnology) were added and left to rotate for 2 hours. Beads were pelleted at 1500rpm, 5 minutes at 4°C and the supernatant was removed. Beads were then washed twice in 500µl wash buffer (25mM Tris-HCl [pH7.5], 150mM NaCl) with a final wash in wash buffer + NP40 (25mM Tris-HCl [pH7.5], 150mM NaCl, 0.2% [v/v] NP40). The supernatant was removed and the beads were boiled in 12µl non-reducing loading dye (10% [w/v] SDS, 625mM Tris-HCl [pH6.8], 0.5% [w/v] bromophenol blue, 50% [w/v] glycerol) for 10 minutes. Samples were spun 13000rpm for 5 minutes and the supernatant transferred to a fresh Eppendorf tube. 1µl β-mercaptoethanol was added, samples were boiled for 5 minutes and the entire contents of the Eppendorf tube were analysed by SDS-PAGE gel/western blotting (2.3.1).

2.3.3 Quantitative Reverse Transcriptase-PCR (RT-qPCR)

One Step qPCR Mastermix with SYBR Green (Primer Design) was used to perform RT-qPCR.

The following cycles were used:

	Step	Conditions
1.	Reverse transcriptase	10 minutes 55°C
2.	Enzyme activation	2 minutes 95°C
3.	Denaturation	95°C 30 seconds *
4.	Data collection	60°C 60 seconds *

*Steps 3 and 4 were cycled 50 times.

RT-qPCR data collection was performed on a Rotor-Gene 6000 real-time PCR Cycler (Corbett). SYBR green detection was recorded and melt curves collected to ensure specificity of the primers used.

The qPCR primers used in this study are listed in Table 2.4.

qPCR Primer Name	Sequence 5'-3'
AOS1 FORWARD	AAGATGTTGGCCAATGGAAG
AOS1 REVERSE	TGCATTTCTGTAGCCACGAC
CCT8 FORWARD	GTCCGCTTGACATAGCCAAT
CCT8 REVERSE	CAATTCACCAACACCAGCAC
SIZ1 FORWARD	GCCTTCACCACGAAGGAATA
SIZ1 REVERSE	TCAAGCCCATTTCTTCATCC
SIZ2 FORWARD	GAATCGGAAGGATCCAGTGA
SIZ2 REVERSE	TGTTGTCGGTGTGTCATTT
SMT3 FORWARD	GGTGTCCGATGGATCTTCAG
SMT3 REVERSE	TCCAAATCTTCAGGGGTCTG
UBA2 FORWARD	CTGCTGCGAACATAAGGTCA
UBA2 REVERSE	CTGCTGCGAACATAAGGTCA

UBC9 FORWARD	TGGTATCCCAGGCAAAGAAG
UBC9 REVERSE	GATCCTGAACCCCAAGAACA
ULP1 FORWARD	TTGAACAATCCCTCCGAGTC
ULP1 REVERSE	CAAATTGCGAGGTTGTTTT
ULP2 FORWARD	GACGAGGGCTAAGCAGTTTG
ULP2 REVERSE	TTGGGACTAGATTGGCGTTC

Table 2.4 RT-qPCR primers used in this study. Primers were produced by Sigma Aldrich.

2.3.4 Chromosomal qPCR

DNA was extracted from mid-log phase cultures of *S. cerevisiae* cells using an alkaline lysis method amended from Pavelka et al. (2010). 1ml samples of mid-log phase cultures were washed twice with 500µl 1xPBS and resuspended in 100µl of 0.02M NaOH. Cells were incubated for 10 minutes at 100°C, pelleted at 13000rpm for 5 minutes and the supernatant collected. Supernatant concentrations were measured using a Nanodrop spectrometer (Labtech) and samples were stored at -20°C.

qPCR reactions were set up using PerfeCTa SYBR Green FastMix (Quantabio) following the manufacturer's instructions. 25ng DNA and 300µM primers were used per 20ml reaction. qPCR was performed using the following cycles:

	Step	Conditions
1.	Enzyme activation	2 minutes 95°C
2.	Denaturation	95°C 10 seconds *
3.	Data collection	60°C 60 seconds *

* Steps 2 and 3 were cycled 40 times.

qPCR data collection was performed on a Rotor-Gene 6000 real-time PCR Cycler (Corbett). SYBR green detection was recorded and melt curves collected to ensure specificity of the primers used.

Chromosomal qPCR primers used were identical to those described by Pavelka et al. (2010) and are listed in Table 2.5.

Chromosomal qPCR Primer Name	Sequence 5'-3'
Chr1F	ACAGCTTCTAAACGTTCCGTGTGC
Chr1R	GCGGTGTGTGGATGATGGTTTCAT
Chr2F	TTTCAGGATCACGAGCGCCATCTA
Chr2R	CGGCAAGTGTCTCACTGTTGCA
Chr3F	TTGTTTCTGTCCTTGCCACAGCTC
Chr3R	AGCGCCTTTACCTCAACCTACCAT
Chr4F	AGCCCTAGTTGCAGATCATCGTGT
Chr4R	AGAATATACGGCAACAGTGCCCGA
Chr5F	TCCGCCGGCAACTGTAAGTGTAAA
Chr5R	ATAGTAACCAACGAGAGCGCGCAA
Chr6F	TTAACCTTGGCGTTTCAGCATCCG
Chr6R	TGA TCTCCGCCGA TTGGTGTTC
Chr7F	TGTGCGTCTTCCCTAAAGCAGCTA
Chr7R	GCATTGGATGCGATGAGATGGCAA
Chr8F	TTGTGCGTCTAGCCGAAAGGTGTT
Chr8R	AGTTCTGCGGCAGTAATGTAGGGT
Chr9F	AAAGTTGGCGCTGGGTACTTTGAG
Chr9R	AGAACTGATGGCATTGATGGCCG
Chr10F	ATTTACCGTTAGTGTCAGCGCCA
Chr10R	CGACAGAGTAGTTTATGCCGAGGGTT
Chr11F	AGCTGGTGATGAGCCAAATGTCGT
Chr11R	TTTAGAGCAAGCGCCTTTGTGAGC
Chr12F	TGGAGATGAAGGGTTGTCGTTGGT
Chr12R	ACGTGTAGCGTTTCTGCTGGTCTT
Chr13F	AACCGTCTTTCGAGCAGTTGAAGG
Chr13R	ACAACAGCGGGAACCTAAGTGCAGA
Chr14F	GGGATTAACAATACGGTAAAGGGACG

Chr14R	CAACCACTGTCAGCACAAACTCCT
Chr15F	ATTTAGGCTGCACGGCTCAGTTCT
Chr15R	CTAGGTTCAGTCTTTGGCACACA
Chr16F	AAGAGCCTTGAAGTTCTCGGGTGA
Chr16R	TGA TGTTCTCTCGTTTGGCACTC

Table 2.5 Chromosomal qPCR primers used in this study (Pavelka et al., 2010).

2.4 Statistical Analysis

All statistical tests were performed using GraphPad Prism software (GraphPad Software). P values were derived from an unpaired Students T-test. (*) indicates $p < 0.05$, (**) indicates $p < 0.01$ and (***) indicates $p < 0.001$.

To determine the statistical significance of the Chromosomal qPCR assays, An unpaired Students T-test was performed using the dCt values of the respective samples. (*) indicates $p < 0.05$, (**) indicates $p < 0.01$ and (***) indicates $p < 0.001$. Samples that were not statistically significant (ns) are not labelled on the corresponding Chromosomal qPCR graphs.

Chapter Three: The Functions and Regulation of Smt3 in Stress Responses

3.1 Introduction

It has been well established that the dynamic nature of PTMs enable a rapid response to a variety of different cellular stresses in eukaryotes. Indeed, numerous studies have shown that sumoylation is an important hallmark of cellular stress, with responses to stresses including heat, oxidative or osmotic stress resulting in a rapid accumulation of HMW sumo conjugates (Lewicki et al., 2015, Golebiowski et al., 2009, Miura et al., 2007, Zhou et al., 2004). The extensive and wide-ranging stress-induced pattern of sumoylation has therefore led to multiple hypotheses which propose that protein sumoylation acts as a “guardian of the genome” (Zilio et al., 2017). However, although a number of sumo-induced stress responses have been studied in detail, the molecular pathways underlying many of these stress responses, including responses to oxidative stress, remains poorly understood. Furthermore, few studies have been performed to investigate the roles of the different types of sumo modification in stress responses. For example, Golebiowski et al. (2006) suggest that substrate polysumoylation is responsible for the accumulation of HMW sumo substrates in the response to heat shock in mammalian cells, (Golebiowski et al., 2009). Additional studies in *S. cerevisiae* have also identified that polysumoylation is important for the response to high temperatures. For example, deletion of the sumo deconjugase Ulp2 results in cells exhibiting extreme sensitivity to high temperatures (Bylebyl et al., 2003). Interestingly, *ulp2*Δ temperature sensitivity is significantly reduced when *ulp2*Δ is crossed with a strain unable to form polysumo chains upon substrates, suggesting that a build-up of polysumoylated substrates is toxic for the cell whilst identifying that polysumoylation is not essential for the response to heat shock (Bylebyl et al., 2003). Nevertheless, the role and importance of polysumoylation within other eukaryotic stress responses remains uncharacterised.

Previous work has shown that sumoylation is induced in response to oxidative stress in *S. cerevisiae* (Lewicki et al., 2015, Zhou et al., 2004). Work in our lab has our extended these observations to demonstrate that, similar to exposure of cells to high temperatures, exposing

S. cerevisiae cells to cold temperatures resulted in a dramatic and rapid increase in HMW sumoylated substrates (Lewis, 2016). However, the mechanism underlying this response of cells to cold temperatures was not investigated and the cold-induced sumo substrates remain unknown. Interestingly, it has been shown that hibernating mammals entering a torpor state, characterised by a sustained lowering of core body temperature, display sustained levels of elevated sumoylation (Lee et al., 2007). Hence, taken together, these data suggests that protein sumoylation may be important for cryogenic protection.

Hence the main aim of this results chapter is to build on this previous work to explore the roles and regulation of sumoylation in cellular responses to cold temperature and oxidative stress.

3.2 Results and Discussion

3.2.1 *smt3* phenotypes are conserved in different strain backgrounds

To investigate important functions of sumoylation in *S. cerevisiae*, previous studies in our lab utilised a mutant *smt3* strain, obtained from the commercially available DAmP mutant strain collection of essential *S. cerevisiae* genes (Breslow et al., 2008). This *smt3* strain harbours an antibiotic cassette within the 3' UTR of the *SMT3* gene which, as a result of the insertion, disrupts mRNA levels from the *SMT3* gene resulting in much reduced expression of the Smt3 protein (~10% of normal Smt3 levels) (Lewis, 2016). As predicted, the *smt3* mutant strain grows poorly and Dr. Lewis identified several morphological and stress response defects associated with *smt3* cells (Lewis, 2016). For example, *smt3* cells were found to be larger than wild type cells and have cell cycle delays (Lewis, 2016). In addition, cells containing the *smt3* allele displayed increased sensitivity to colder than normal growth temperatures (Lewis, 2016). However, these phenotypes associated with the *smt3* strain were not examined in depth.

Previous studies have shown that different strains of *S. cerevisiae* respond differently to environmental stresses (Petrezselyova et al., 2010, Veal et al., 2003). Hence, in an attempt to further characterise the functions of Smt3 in the response of *S. cerevisiae* cells to cold

temperatures, it was first important to determine whether the increased sensitivity of *smt3* cells to cold temperature is conserved in different strain backgrounds. The original studies by Dr. Lewis were performed with the *smt3::DAmP* allele expressed in the BY4741 strain background. Interestingly, previous work by our lab and others found that the BY4741 and W303 wild type strains respond differently to oxidative stress (Veal et al., 2003). For example, cells in the W303 strain background are much more sensitive to oxidative stress compared to cells of the BY4741 strain background (Veal et al., 2003). Hence, the first step in this study of Smt3 was to determine whether the *smt3* phenotypes observed in the BY4741 strain background were also conserved in the W303 strain background. In order to achieve this, the *smt3:NatMX* cassette was amplified by PCR using the *smt3* strain GC16 as a template. This cassette was then transformed into the W303 diploid strain, as depicted in Fig. 3.1A. The generation of the PCR cassette and subsequent transformation were performed by Dr. Lewis prior to the start of this project (Fig. 3.1A). Next, cells of the W303 diploid containing the *smt3:NatMX* cassette were sporulated, dissected and plated onto YPD+clonNAT plates to select for the presence of the NatMX cassette (Fig. 3.1A). This sporulation was successful and clonNAT resistant spores were obtained (Fig. 3.1B). Spores that were clonNAT resistant were subsequently checked by PCR to confirm the presence of the NatMX cassette and one of the positive spores expressing the *smt3:DAmP* allele was designated for further studies (named strain GC50).

Now that the haploid *W303smt3* mutant strain (GC50) had been created and verified, the next step was to determine whether any of the phenotypes observed in the original *smt3* mutant in the BY4741 strain background were conserved in the W303 strain background. Consistent with the original BY4741 *smt3* mutant (GC16), *W303smt3* mutant cells (GC50) grow poorly at the permissive temperature (30°C) and display similar morphological defects with the BY4741 *smt3* mutant (Figure 3.1D, data not shown). Furthermore, in a similar manner to BY4741 *smt3*, the sensitivity of *W303smt3* cells to cold temperatures was increased compared to W303 wild type cells. However, it must be noted that *W303smt3* mutant cells are perhaps not quite as sensitive to cold temperature as the original *smt3* mutant in the BY4741 strain background (Fig. 3.1C). Taken together, these results suggest that Smt3 functions are similar in both the BY4741 and W303 strain backgrounds, although the strain background does appear to influence these functions (Figure 3.1C). Interestingly,

W303smt3 cells (GC50) display increased sensitivity to high temperatures (37°C) which is not observed in *smt3* cells in the BY4741 background (GC16) (Fig. 3.1C). Furthermore, the placement of the 37°C plate back to the permissive temperature of 30°C for one day did not allow restoration of growth of the *W303smt3* mutant, suggesting that 37°C is a lethal temperature for *W303smt3* cells. In contrast, *smt3* cells in the BY4741 strain background could grow to some extent at 37°C and, in contrast to *W303smt3* mutant cells, recovered good growth when the 37°C plate was placed at 30°C. Hence, these results confirm that although Smt3 is involved in similar functions in different strain backgrounds, there are some strain specific differences.

3.2.2 Polysumoylation is important for the response to cold temperatures

As shown above, the loss of Smt3 function in different strain backgrounds affects the response of *S. cerevisiae* cells to low temperature (Fig 3.1C). Previous studies in our lab revealed that exposing wild type BY4741 (GC1) *S. cerevisiae* cells to the sub optimal temperature of 20°C resulted in a substantial increase in HMW sumo conjugates (Lewis, 2016) (Fig. 3.2A). This accumulation of HMW sumoylated proteins following exposure of cells to cold temperature is analogous to the induction of sumoylation that occurs in response to a number of cellular stresses, such as osmotic stress, suggesting that this is a conserved stress response (Lewicki et al., 2015). Next, to examine whether cold temperature also induces sumoylation in cells expressing the *smt3* allele in the BY4741 strain background, wild type (GC1) and *smt3* (GC16) cells were exposed to 20°C, with protein extracts analysed by western blotting (Fig. 3.2B). As can be seen in Fig. 3.2B, HMW sumo conjugates were induced rapidly in wild type cells, but not in *smt3* cells exposed to 20°C, with increased sumoylation detected in samples from the wild type cells within 5-10 minutes of the temperature shift (Fig. 3.2A). However, it is important to note that the sumo-induced cold response is extremely rapid and, although HMW conjugates remain in the cell after 60 minutes, the majority of sumo-substrate conjugation appears to take place within the first 5 minutes. Next, to identify whether cold temperature also induces sumoylation in different strain backgrounds expressing the *smt3* allele, wild type W303 (GC2) and *W303smt3* (GC50) cells were exposed to 20°C, with protein extracts analysed by western blotting (Fig. 3.2A). Importantly, wild type W303 cells rapidly

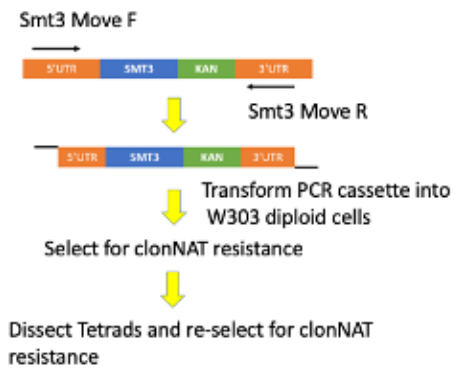
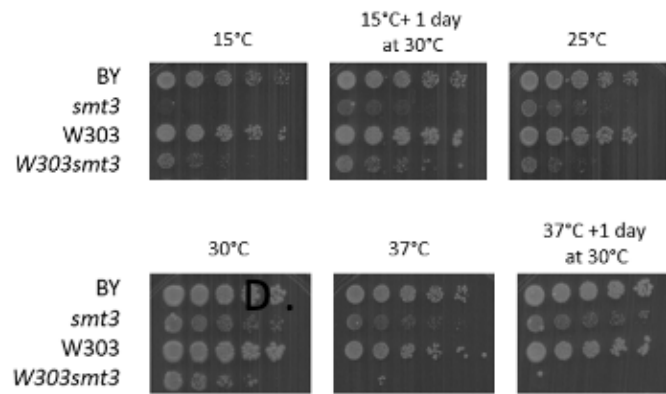
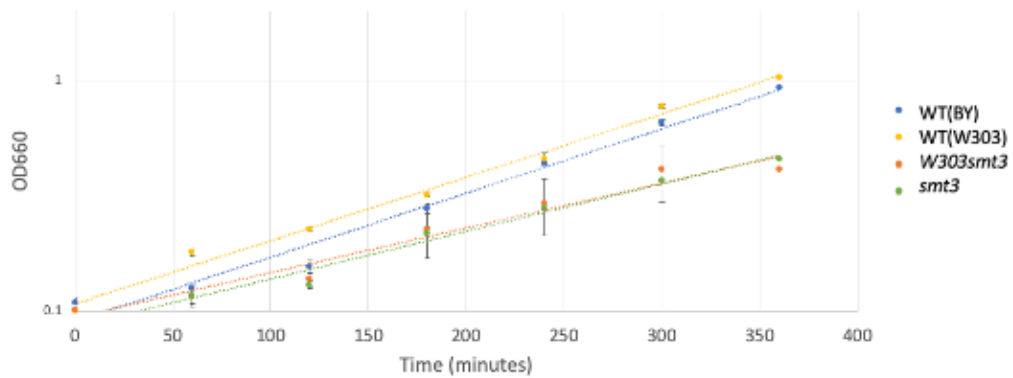
A.**B.****C.****D.**

Figure 3.1 Smt3 is required for the response of cells to cold temperature in different strain backgrounds. (A) To create the W303*smt3* strain, *smt3::DAmP* cassettes were amplified from *smt3* cells (GC16) using the Smt3 move Forward and Smt3 move Reverse primers as indicated on the diagram. PCR cassettes were transformed into the W303 diploid strain and plated onto YPD+clonNAT plates to select for clonNat resistance. Diploids were dissected and spores were plated onto YPD+clonNAT plates. These steps were performed by Dr. Lewis prior to the start of this project. The presence of the *smt3::DAmP* cassette in spores was subsequently confirmed by PCR using the Smt3 move primers as shown in the diagram. (B) Representative spores confirmed by PCR to either lack or contain the *smt3::DAmP* cassette were grown on YPD+clonNat media at 30°C. (C) Five-fold serial dilutions of mid-log growing cultures GC1, GC16, GC2 and GC50 cells were spotted onto YPD plates using a 48-pin tool and then incubated at the indicated temperatures for 3 days, apart from 15°C plates which were left for 5 days. (D) Mid-log growing cultures GC1, GC16, GC2 and GC50 were set back to an OD₆₆₀ 0.1 and samples taken every 60 minutes. Error bars represent the SD based on three biological repeats.

accumulate HMW conjugates analogous to the BY wild type strain (Fig. 3.2A/B). Furthermore, the western blots confirm that the *W303smt3* cells express much reduced levels of Smt3 and consequently lower levels of sumoylated proteins (Fig. 3.2A). These results are in contrast to wild type *W303* cells but remarkably similar to *smt3* cells in the BY4741 strain background, with *W303smt3* cells are unable to accumulate HMW sumo conjugates even after a 60 minute incubation at 20°C (Fig. 3.2A/B). Importantly, sumoylation in both the *smt3* (GC16) and *W303smt3* (GC50) strains is not induced by cold temperatures, suggesting that this response is conserved between different *S. cerevisiae* strain backgrounds (Fig. 3.2A/B). Indeed, quantification of free Smt3 levels in both *smt3* and *W303smt3* cells indicates that the free Smt3 levels in both of these two strains are just ~10% of the level of the respective wildtype suggesting that the lack of sumo function promotes sensitivity to cold temperatures (Fig. 3.2C). These results support the hypothesis that sumoylation has an important role in the response of different *S. cerevisiae* strains to cold temperatures. Thus, in conclusion, neither of the two *smt3* mutant strains are able to induce global sumoylation in response to cold temperature.

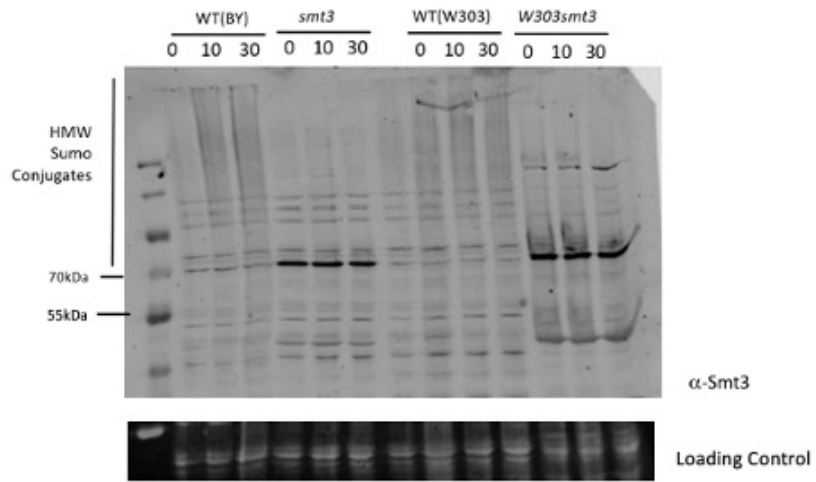
The data presented in Fig. 3.2A indicates that the increase in sumoylation following exposure of wild type cells to 20°C is largely detected in HMW bands. As polysumoylation has been shown to be important for the response to heat shock (Golebiowski et al., 2009), Fig. 3.2A suggested that polysumoylation may also be induced by exposure of cells to low temperature. Interestingly, the lack of detectable increases in HMW sumoylation in *smt3* mutant cells exposed to 20°C (Fig. 3.2A/B) suggests that inhibition of polysumoylation may infer increased sensitivity to cold temperature. Indeed, previous studies have suggested that many proteins are polysumoylated in *S. cerevisiae* in response to heat shock which may target them for degradation via STUbLs (Golebiowski et al., 2009). Thus, it was important to determine whether polysumoylation is also important for the response of cells to cold temperature.

The Smt3 protein in *S. cerevisiae* contains three lysine residues within the N-terminal domain which themselves can be subject to further sumoylation, leading to the generation of a poly sumo chain on the substrate (Fig. 3.3A) (Bylebyl et al., 2003). Hence, in order to investigate the importance of polysumoylation in the response of cells to cold temperature, a strain

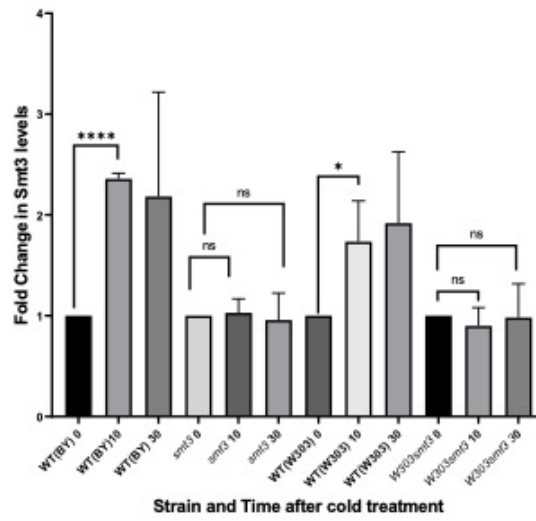
related to the BY4741/BY4742 strain background was obtained that is unable to form poly sumo chains (kindly provided by B. Raught) (Srikumar et al., 2013a). The *smt3-allR* strain (GC57) expresses a Smt3 protein in which all of the lysine residues of Smt3 have been substituted with arginine residues (Fig. 3.2A). Importantly, target proteins in the *smt3-allR* strain are still able to be mono- or multi-sumoylated but can no longer be polysumoylated. Hence, to investigate whether polysumoylation is important for the response of cells to cold temperature the next step was to examine growth of the *smt3-allR* strain and the isogenic control strain (GC55) (kindly provided by B. Raught) at a range of temperatures (Fig. 3.3B). Interestingly, *smt3-allR* cells display increased sensitivity to cold temperatures compared to wild type GC55 and GC1 cells (Figure 3.3B). However, this increased sensitivity of *smt3-allR* cells to cold temperatures is not as great as that observed in the *smt3* mutant strain in the BY4741 strain background (GC16) (Fig. 3.3B). Interestingly, the data also suggested that inhibition of polysumoylation has little effect on the ability of cells to grow at higher temperature, suggesting that polysumoylation may not be as important in the response to heat shock compared to the response to cold temperatures (Fig. 3.3B). Hence, these results strongly suggest that polysumoylation is important for the response of cells to low temperature. However, the observation that *smt3* mutant cells are more sensitive than *smt3-allR* cells to low temperature suggest that other forms of sumoylation also contribute to cellular responses to these conditions. As described above (Fig. 3.2A) the accumulation of sumoylated HMW conjugates is rapidly induced when cells are exposed to low temperature. It must also be noted that the wild type equivalent of the *smt3-allR* strain is derived from the BY4742 genetic background (GC55), thus is extremely similar to GC1 (BY4741 genetic background). Western blot analysis performed on protein extracts from GC55 cells incubated at 20°C identified an identical pattern of HMW sumoylation compared to the GC1 strain (data not shown). Hence, in agreement with Fig. 3.2A/C, HMW sumoylation is observed after cold treatment in three different *S. cerevisiae* strain backgrounds.

Next, to examine if these HMW conjugates involve polysumoylation, western blot analysis was performed on extracts from cells of the *smt3-allR* strain incubated at 20°C (Fig. 3.3C). As expected, an increased formation of HMW sumo conjugates was detected in wild type cells (GC1) exposed to 20°C with the formation of these HMW sumo conjugates were inhibited in the *smt3* mutant strain in the BY4741 genetic background (Fig. 3.3C). Interestingly, the

A.



B.



C.

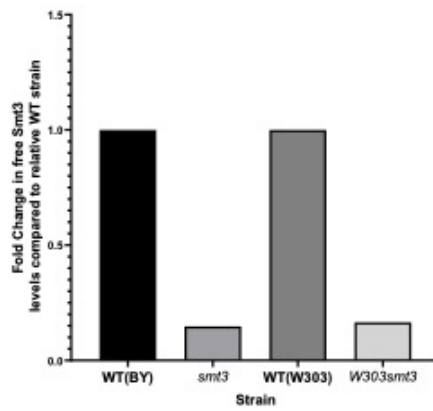


Figure 3.2 Global sumoylation is induced in response to cold temperature. (A) Proteins were TCA extracted from mid-log phase growing WT (GC1) *smt3* (GC16), WT (GC2) and W303*smt3* (GC50) cells, incubated at 20°C for the indicated timepoints and analysed by western blotting using an α -Smt3 antibody. Western blots are representative of three biological repeats. (B) Blots were stripped, re-probed with α -Skn7 as a loading control and quantified using Empiria Studio software (LI-COR, Inc.). Quantification of HMW Smt3 conjugates is based on proteins >70kDa in size recognised by the α -Smt3 antibody. Bars represent HMW sumo conjugates normalised to the 0 timepoint of the respective strain. P values were derived from an unpaired T-test, (*) indicates $p > 0.05$. Error bars represent SD from three biological repeats. (C) Quantification of free Smt3 levels in mid-log phase growing WT (GC1) *smt3* (GC16), WT (GC2) and W303*smt3* (GC50) cells, based on one repeat.

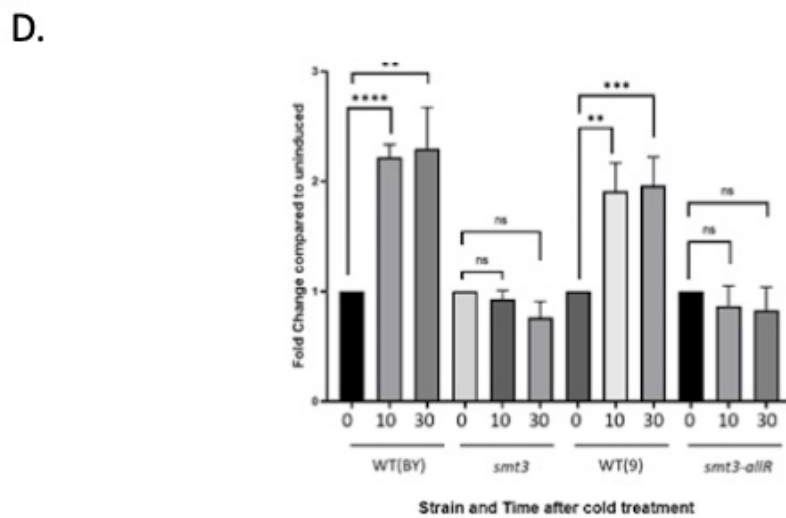
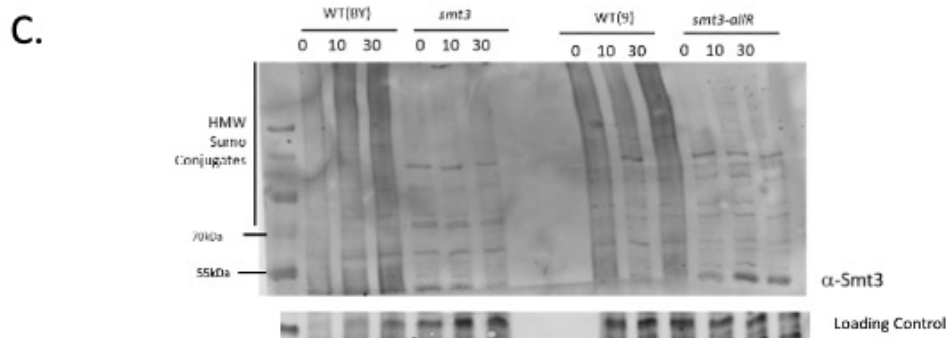
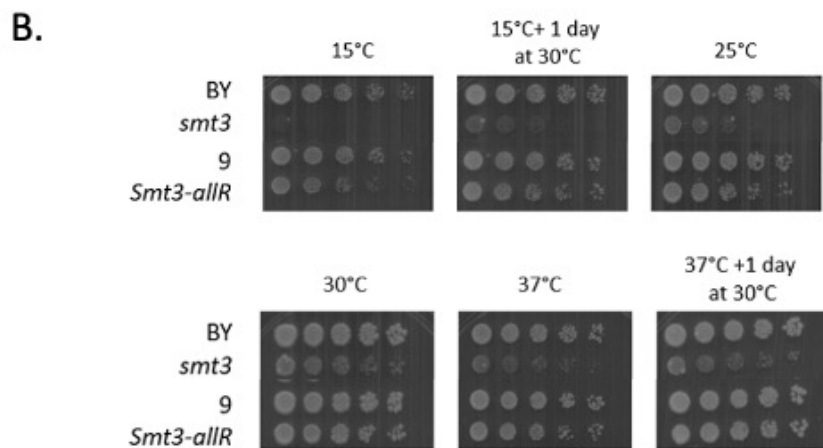
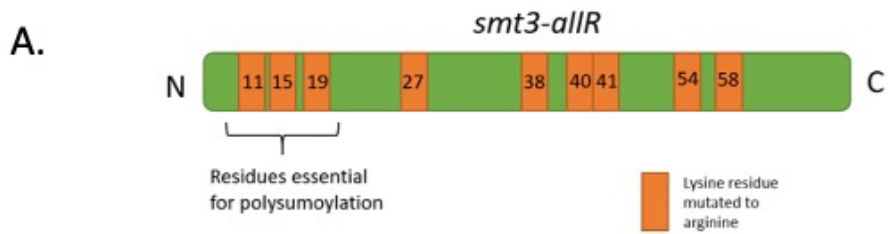


Figure 3.3 Polysumoylation is induced in the response of cells to cold temperatures. (A) Schematic representation of the mutant Smt3 protein expressed in the *smt3-allR* strain where all nine lysine residues in Smt3 have been substituted with arginine residues. (B) Five-fold serial dilutions of mid-log growing cultures GC1, GC16, GC57 and GC55 cells were spotted onto YPD plates using a 48-pin tool and incubated at the indicated temperatures. (C) Mid-log phase cultures of GC1, GC16 and GC57 cells were grown at 30°C and rapidly cooled and incubated at 20°C. Proteins were TCA extracted at the indicated timepoints after incubation at 20°C and analysed by western blotting using an α -Smt3 antibody. Western blots are representative of three biological repeats. A representative blot is shown. (D) Blots were quantified using Empiria Studio software (LI-COR, Inc.) using the Total Protein Stain as a loading control. Quantification of HMW Smt3 conjugates is based on proteins >70kDa in size recognised by the α -Smt3 antibody. Bars represent HMW sumo conjugates normalised to the 0 timepoint in the respective strain. Error bars represent SD from three biological repeats, P values were derived from an unpaired T-test.

formation of HMW sumo conjugates is severely inhibited in *smt3-allR* cells incubated at 20°C, closely mimicking the effect of lower Smt3 levels on the formation of cold-induced HMW sumo conjugates (Fig. 3.3C). Thus, Fig.3.3C highlights that the inability of *smt3-allR* cells to accumulate HMW sumo conjugates following exposure to 20°C is not due to the reduction in cellular Smt3 levels observed in *smt3* cells. It is also important to note that previous work has confirmed that the levels of the *smt3-allR* protein expressed in the *smt3-allR* strain are equivalent to wild type (GC55) levels of Smt3 (Srikumar et al., 2013a). Srikumar et al. (2013) also identified that the *smt3-allR* protein is not recognised as efficiently by an anti-Smt3 antibody compared to wild type (GC55) cells, suggesting why the uninduced *smt3-allR* sample (Fig. 3.3C, lane 7) appears to have lower *smt3-allR* protein levels (Srikumar et al., 2013a). To account for the discrepancy between *smt3-allR* expression and *smt3-allR* recognition by the α -Smt3 antibody, blots were quantified relative to the 0 timepoint of the respective strains (Fig. 3.D). Indeed, the data from the western blot analysis (Fig. 3.3C) are supported by quantification of the levels of HMW sumo conjugates (Fig. 3.3D). Taken together these results suggest that the formation of the majority of HMW sumo conjugates detected in response to exposure of cells to cold temperatures are polysumoylated substrates.

Collectively, these results indicate that the majority of HMW sumo conjugates that are induced in response to cold temperature involve polysumoylation, suggesting that polysumoylation is indeed important for the cellular response to cold. Indeed, consistent with this hypothesis, cells that cannot undergo polysumoylation display increased sensitivity to low temperatures. However, the data also suggests that other forms of sumoylation such as multi- and/or monosumoylation function in the response to cold temperature as cells which contain lower levels of general sumoylation are more sensitive to cold temperature than cells where only polysumoylation is prevented. Interestingly, it has been characterised that polysumoylated proteins are targeted for proteasomal degradation by the recruitment of STUbLs (Sriramachandran and Dohmen, 2014). Hence it would be interesting to identify whether polysumoylated proteins are targeted for degradation and, if so, the identification of the substrates targeted for degradation.

3.2.3 Investigation of the sumo pathway enzymes involved in the response to cold temperatures

Although few studies have comprehensively characterised the molecular response of mammalian cells to cold temperatures, several studies have been performed in plants. Cold-adaptation research in plants has focussed the characterisation of freeze-tolerance pathways in order to improve crop yields (Vyse et al., 2019). Interestingly, several enzymes in the sumo conjugation pathway of *Arabidopsis thaliana* have been shown to play a critical role in freeze tolerance (Miura et al., 2007). In particular, *A. thaliana* cells expressing a null mutation of the gene encoding the sumo E3 ligase Siz1 are extremely sensitive to cold temperature, suggesting that sumo-substrate conjugation mediated by Siz1 is vital for the appropriate cellular responses to prevent cellular damage from freezing (Miura et al., 2007). As described above, Fig. 3.2 and 3.3 indicate that sumo is important for the response of *S. cerevisiae* cells to cold temperatures. Hence, based on the observations in *A. thaliana*, it was possible that the *S. cerevisiae* homologue of Siz1 in *A. thaliana*, also named Siz1, is important for the cellular response to cold temperature. In agreement with Fig. 3.2 and 3.3, Miura et al. (2007) also suggest that the sumo conjugation pathway is important for the response of cells to cold temperature. However, it is also possible that regulation of sumo deconjugation pathways may be important for these cold temperature responses, although this has not yet been characterised in *A. thaliana*. Hence, it is important to determine if either of the two sumo deconjugation enzymes, Ulp1 and Ulp2, are involved in the response of *S. cerevisiae* cells to cold temperature.

Therefore the next step was to explore the role of the main sumo E3 enzymes in *S. cerevisiae* in responses to cold temperature. Although *S. cerevisiae* contains four sumo E3s the majority of sumoylation appears to be determined by the two E3 enzymes Siz1 and Siz2 (Johnson and Gupta, 2001b). Since neither Siz1 nor Siz2 are essential for viability the single *siz1* Δ and *siz2* Δ deletion mutants were obtained from the gene deletion collection (kindly provided by P. Banks). First, the sensitivity of the single *siz1* Δ and *siz2* Δ deletion mutants to a range of temperatures was examined. In contrast to the *smt3* mutant strain in the BY4741 genetic background (GC16), neither the *siz1* Δ (GC28) or the *siz2* Δ (GC29) mutant displayed temperature sensitivity when incubated at either 15°C or 37°C (Fig. 3.4A). However, there is

some redundancy between the Siz1 and Siz2 E3 ligases with studies suggesting an ~25% substrate overlap, thus it is possible that the lack of either Siz1 or Siz2 could be compensated by the remaining Siz (Makhnevych et al., 2009). Interestingly, *siz1Δsiz2Δ* double mutants are extremely cold sensitive when placed at 20°C, indicative that one or both of these enzymes are important for sumo conjugation during cold temperatures (Johnson and Gupta, 2001b).

Therefore, to further investigate any potential connections between Siz1 and the response of *S. cerevisiae* cells to cold temperatures, global sumoylation was examined by western blot analysis of protein extracts from *siz1Δ* cells exposed to 20°C (Fig. 3.4B). In contrast to wild type cells, there was almost no detectable induction of HMW sumo conjugates in *siz1Δ* cells at the initial time points after exposure of cells to 20°C (Fig. 3.4B). Strikingly, this lack of induction of sumoylation in protein extracts from *siz1Δ* cells appeared very similar to the sumoylation pattern observed in *smt3* cells following exposure to cold temperature (Fig. 3.4B). Almost no accumulation of HMW sumo conjugates was detected in protein extracts from *siz1Δ* cells even after 30 minutes at 20°C (Fig. 3.4B). Hence, this observation strongly suggests that Siz1 is the major E3 ligase responsible for the accumulation of HMW sumo conjugates when *S. cerevisiae* cells are exposed to cold temperature. Furthermore, these results also indicate that the presence of Siz2 in *siz1Δ* cells cannot fully compensate for the loss of induction of HMW sumo conjugates when these cells were exposed to low temperature, suggesting that there is little overlap in substrate specificity. However, unlike the *smt3* mutant, the *siz1Δ* and *siz2Δ* single mutants do not display an obvious increase in sensitivity to cold temperature (Fig. 3.4A). Hence, it is possible that Siz2 may be able to sumoylate a small number of key Siz1-dependent substrates in response to cold temperature, which is sufficient to retain viability. However, it must be noted that the data in Fig. 3.3A cannot be directly compared to Fig. 3.3B. For example, the growth analysis in Fig. 3.3A represents the growth and adaption at 20°C over several days whereas the induction HMW of sumoylation observed in Fig 3.3B is an acute response, occurring over a matter of minutes. It must also be noted that Ubc9 can directly sumoylate substrates without the need for an E3 ligase, thus it may be the case that Ubc9 directly sumoylates important substrates in *siz1Δ* cells when exposed to cold temperatures (Yunus and Lima, 2009b). As mentioned above, *siz1Δ siz2Δ* mutants appear as large budded cells showing extreme sensitivity when incubated at cold temperatures (Johnson and Gupta, 2001a). These findings suggest that Siz2 may

compensate for the loss of Siz1 in *siz1*Δ cells, whilst *siz1*Δ*siz2*Δ double mutants may not be able to accumulate HMW sumo conjugates in cold temperatures. Attempts were made to create the *siz1*Δ*siz2*Δ double mutants but were unsuccessful, hence it would be interesting to further analyse the phenotypes and HMW sumo conjugates associated with the *siz1*Δ*siz2*Δ strain when placed at 20°C. The cold sensitivity of the *siz1*Δ*siz2*Δ strain suggested that Siz2 may also have an important role in the response to cold temperatures. However, western blot analysis of *siz2*Δ cells incubated at 20°C identified that although the basal levels of HMW sumo conjugates are slightly higher in *siz2*Δ cells compared to *siz1*Δ cells, accumulation of HMW sumo conjugates could be detected in protein extracts from *siz2*Δ cells after 30 minutes at 20°C (Fig 3.4C). Thus, collectively, these data suggest that Siz1 is the main sumo E3 ligase important for the accumulation of HMW sumo conjugates in the response to cold temperatures.

These findings with respect to the role of Siz1 in cold temperature responses in *S. cerevisiae* are strikingly similar to the results from *A. thaliana* which demonstrated that loss of Siz1 function prevented global sumoylation in response to cold temperatures (Miura et al., 2007). Taken together, these data highlight the importance of Siz1 in the response to cold temperature in *S. cerevisiae* and suggests that conserved pathways are important for cold temperature responses in eukaryotic cells. Siz1 is a member of the SP-RING family of proteins, with homologues found throughout eukaryotes, including *S. cerevisiae*, *Oryza sativa* and *Mus musculus*. The high level of conservation between Siz1 homologues is suggestive that Siz1-mediated sumoylation during cold treatment may be a conserved pathway to facilitate the increase in HMW sumo conjugates to induce the downstream stress response pathways (Liu et al., 2015).

Nevertheless, the results presented above indicate that HMW sumo conjugates accumulate in response to exposure of *S. cerevisiae* cells to cold temperature and, moreover, that Siz1 plays a significant role in this accumulation. However, despite these results it was possible that the mechanism underlying the cold temperature-induced accumulation of these HMW sumo conjugates also involves inhibition of one or more of the desumoylases rather than involving activation of the sumo conjugation pathway. If this hypothesis is correct then the role of Siz1 would be to mainly provide constant sumoylation of substrates and then the

degree of sumoylation would be controlled by the relative activity of the desumoylases. Hence, the next step was to investigate whether the regulation of either of the two *S. cerevisiae* desumoylases, Ulp1 and Ulp2, is linked to the cold temperature-induced accumulation of HMW sumo conjugates. Previous work revealed that Ulp1 is essential for viability whilst *ulp2* Δ cells display severe growth defects and show extreme sensitivity to high temperatures (Bylebyl et al., 2003). To investigate the role of Ulp1/Ulp2 in response to cold temperatures, strains expressing DAmP alleles of *ulp1::DAmP* and *ulp2::DAmP* were obtained from the DAmP gene insertion library (Breslow et al., 2008)(kindly provided by P. Banks). The growth of these two mutant strains is relatively unaffected by the DAmP allele and so it was hoped that these partially functioning mutants would allow some insight into the potential roles of these desumoylases in responses to cold temperature. Firstly, the sensitivity of the single *ulp1::DAmP* (*ulp1*) and *ulp2::DAmP* (*ulp2*) mutants to a range of temperatures was examined (Fig. 3.4A). Neither *ulp1* nor *ulp2* exhibited any major growth defects at the permissive temperature of 30°C, suggesting that the effects of the DAmP insertion in each gene were relatively minor (Fig. 3.4A). Interestingly, the growth of the *ulp1* mutant, but not the *ulp2* mutant, was inhibited compared to wild type cells at 15°C (Fig. 3.4A). However, this inhibition of growth was not as great as the growth inhibition of the *smt3* mutant incubated at 15°C (Fig. 3.4A). This result is consistent with the exclusive role of Ulp1 in processing immature sumo to reveal the diglycine motif required for sumo conjugation (Dohmen, 2004). Thus, a reduction of Ulp1 activity in the *ulp1* strain would be expected to reduce the processing of immature Smt3, resulting in reduced levels of mature sumo available for substrate modification in *ulp1* cells. Hence, a reduction in the levels of mature sumo available in the cell will subsequently impact on the sumoylation of substrates, potentially leading to phenotypes similar to that associated with the *smt3* mutant strain. Moreover, in agreement with the relatively mild nature of the *ulp1* mutant allele, the growth of the *ulp1* mutant is not as sensitive to 37°C as the *smt3* mutant (Fig. 3.4A). Taken together, these results support a hypothesis in which reduced levels of sumoylation contribute to growth inhibition at low temperatures.

In contrast to the *ulp1* mutant, the *ulp2* mutant does not display any inhibition of growth at 15°C (Fig. 3.4A). However, the growth of the *ulp2* mutant was severely inhibited at 37°C (Fig. 3.4A). Importantly, this growth inhibition at high temperature is consistent with a previous

study of an *ulp2* Δ mutant (Bylebyl et al., 2003). Hence, these data suggest that the *ulp2::DAmP* allele reduces Ulp2 activity and, furthermore, suggests that Ulp2 has different roles in the response to high and low temperatures. Nevertheless, it must be noted that future qPCR analysis will need to be carried out in both *ulp1* and *ulp2* strains to determine the level of *ULP1* and *ULP2* expression in the respective strains .

Next, to further investigate potential connections between Ulp1 and Ulp2 and the response of *S. cerevisiae* cells to cold temperatures, global sumoylation was examined by western blot analysis of protein extracts from *ulp1* and *ulp2* cells exposed to 20°C (Fig. 3.4B). Strikingly, *ulp2* cells showed increased HMW sumo levels at the permissive temperature, with the basal level of HMW sumoylation in *ulp2* cells almost 50% more than that observed in wild type cells (Fig. 3.4C). Furthermore, there is only a slight increase in sumoylation observed in the *ulp1* strain upon exposure to 20°C (Figure 3.4.C). This data strongly suggests that inhibition of Ulp2 in the response to cold may help to sustain the high level of HWM sumo conjugates to allow the subsequent stress response. Indeed, studies have shown that Ulp2 is the major deconjugase involved in the removal of polysumo chains (Bylebyl et al., 2003). As described above (Fig. 3.2B/C/D) polysumoylation appears to be important for the response of cells to cold temperature, thus inhibition of Ulp2 may enable sustained sumo levels, with Ulp2 identified as the main *S. cerevisiae* desumoylase found to target polysumoylated substrates (Keiten-Schmitz et al., 2019). The purpose of this polysumoylation is unclear but one possibility is that cold temperature promotes polysumoylated substrates to be targeted for degradation.

Bossis and Melchior (2006) found that high levels of H₂O₂ inhibits desumoylation to maintain high levels of global sumoylation. Hence, it may also be the case that other cellular stresses, including cold temperature, influence desumoylation (Bossis and Melchior, 2006). For example, it is possible that sumo deconjugation enzymes may be inactivated rapidly in response to exposure of cells to cold temperature to maintain the elevated substrate sumoylation. Based on the finding of the present work, future studies are required to investigate the mechanism underlying regulation of Ulp2. For example, is the cellular localisation of Ulp2 influenced by cold temperature or is the activity of Ulp2 regulated by a cold temperature-induced post translational modification? Ulp2 is normally localised within

the nucleus, therefore cold temperature-induced localisation of Ulp2 to the cytoplasm may prevent desumoylation of HMW sumo substrates located in the nucleus (Srikumar et al., 2013a). Another possibility is that cold temperature may induce conformational changes of Ulp2 which render the protein inactive. Nevertheless, the mechanism of Ulp2 inactivation remains unclear and requires further characterisation.

Similar to *ulp2*, *ulp1* cells appear to have an increased basal level of HMW sumoylation compared to WT cells, indicative that Ulp1 inhibition may also be important in the response to cold (Fig. 3.4C). Interestingly, there is no increase in HMW sumo conjugates after *ulp1* cells have been exposed to 20°C. As mentioned previously, it is likely that there are lower levels of mature Smt3 within the *ulp1* strain compared to WT, thus the *ulp1* mutant could be predicted to have a pattern of cold-induced sumoylation similar to the *smt3* mutant. Nevertheless, even by 60 minutes there is not a significant accumulation of HMW sumo conjugates in the *ulp1* strain, suggesting that blocking the Ulp1 deconjugation pathway prevents the WT response to cold.

Moreover, the inability of *ulp1* to induce sumoylation coupled with its slight cold sensitivity supports the idea that *smt3* strain grows so poorly in cold temperatures due to its inability to active the SSR. Hence, taken together, these data suggest that although sumo conjugation is not induced in *ulp1* mutants, the basal levels of sumoylation are extremely high. Thus, it could be proposed that inhibition of both Ulp1 and Ulp2 contribute to the accumulation of HMW sumo conjugates observed in the response to cold temperatures. However, it must be noted that the quantification in Fig. 3.4C is based on a single experiment, hence these results are preliminary and will need to be repeated to accurately quantify the HMW sumo conjugates present in the *siz1Δ*, *siz2Δ*, *ulp1* and *ulp2* mutants.

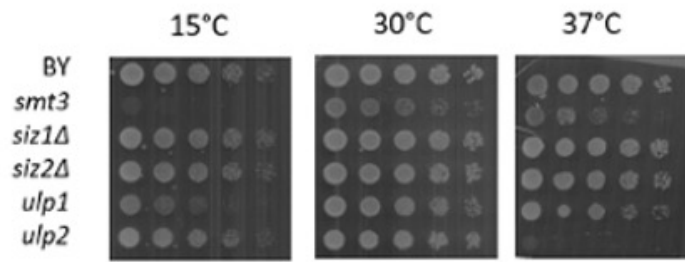
In conclusion, the data from Fig 3.4 suggests a model in which substrate sumoylation during exposure to cold temperatures is targeted by both Siz1 and Siz2, whilst the inhibition of Ulp1 and Ulp2 maintain the high level of global sumo conjugates. Sumoylation is not induced in cells lacking either Siz1 or Siz2 (Fig 3.4C), whereas *ulp2* cells do not appear to significantly induce sumoylation (Fig 3.4C). Hence these data suggest that the sumo “on” pathway has a more important role than the “off” mechanism in the response to cold temperatures.

Nevertheless, the pathways promoting Siz1/2 activation in response to cold remain unknown. One possibility is that cold-induced localisation of Siz1/ Siz2 may enable the sumoylation of specific substrate in cold temperatures. Siz1 has been shown to be a target of sumoylation, hence it is possible that sumoylation of Siz1 enhances its ligase activity during cold conditions, although this is not the case during heat stress (Westerbeck et al., 2014, Rytz et al., 2018). However, it is clear that further research is required to characterise the regulation and activation of the sumo “on” pathway in the response to sub-optimal growth temperatures.

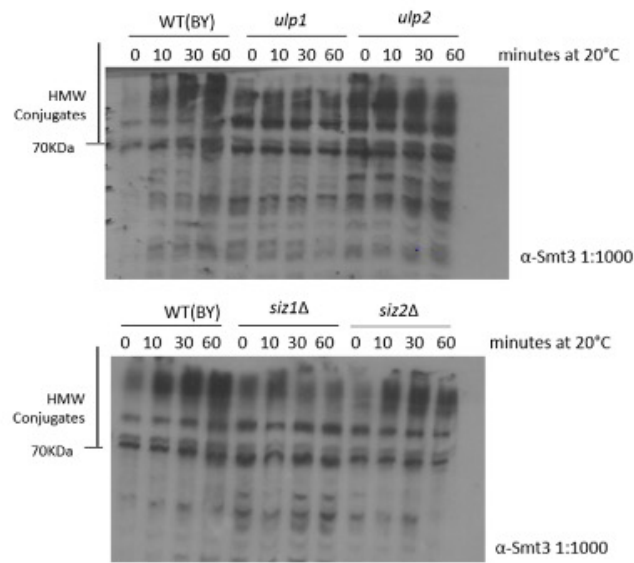
3.2.4 *ULP2* and *UBA2* gene expression are modified in the response to cold temperature

Siz1 targeted sumoylation of the transcription factor *ICE1* during cold temperatures leads to the increased expression of the freeze tolerance genes in plants (Miura et al., 2007). Consequently, in plants, at least one major role of cold temperature-induced sumoylation is to upregulate genes important for cold temperature acclimation. However, it was unknown whether the expression of genes encoding the sumo conjugation and deconjugation enzymes was changed in response to cold temperature. Hence, it was possible that the cold temperature-induced accumulation of HMW sumo conjugates observed in *S. cerevisiae* cells was in some way linked with alterations in the expression of genes encoding the sumo conjugation and deconjugation machinery. To examine this possibility, the expression of genes encoding the sumo conjugation and deconjugation machinery was examined by RT-qPCR performed on RNA isolated from wild type (GC1) cells exposed to 20°C for 0 or 10 minutes. The time point of 10 minutes was chosen as there was almost maximal accumulation of HMW sumo conjugates in wild type cells at this time point (Fig. 3.2A). Interestingly, the expression of genes encoding the sumo conjugation E1, E2 or E3 enzymes, *AOS1* (E1), *UBC9* (E2) *SIZ1* (E3) or *SIZ2* (E3), was unchanged 10 minutes after exposure of cells to 20°C (Fig. 3.5). Hence, these data suggest that the cold-induced accumulation of HMW sumo conjugates is not linked to increased expression of these genes associated with the sumo “on” pathway. However, expression of the sumo E1 *UBA2* was significantly reduced by ~50% after 10 minutes of cold treatment compared to untreated cells (Fig 3.5, $p=0.0007$). As sumoylation is almost

A.



B.



C.

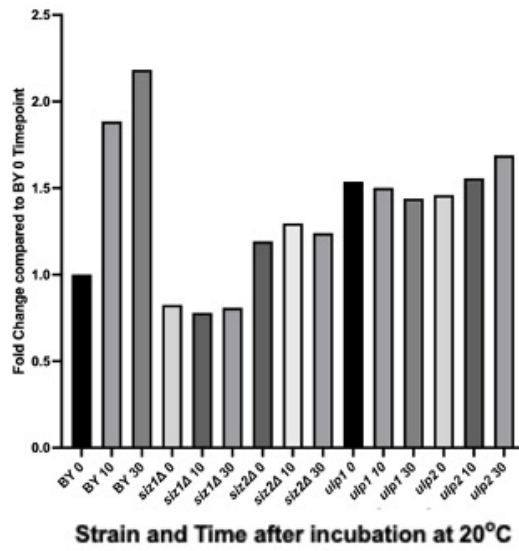


Figure 3.4 Siz1 and Ulp2 are important for cold-induced global sumoylation. (A) Five-fold serial dilutions of mid-log growing cultures GC1, GC16, GC28, GC29, GC 30 and GC31 cells were spotted onto YPD plates using a 48-pin tool and incubated at the indicated temperatures. (B) Mid-log phase cultures of GC1, GC16, GC28, GC29, GC 30 and GC31 cells were grown at 30°C and rapidly cooled and incubated at 20°C. Proteins were TCA extracted at the indicated timepoints after incubation at 20°C and analysed by western blotting using an α -Smt3 antibody. Western blots are representative of three biological repeats. A representative blot is shown. (C) Blots were stripped, re-probed with α -Skn7 as a loading control and quantified using ImageQuant (GE Healthcare). Quantification of HMW Smt3 conjugates is based on proteins >70kDa in size recognised by the α -Smt3 antibody. Bars represent HMW sumo conjugates normalised to the BY (GC1) 0 timepoint. Quantification is based on one repeat.

maximal at ~10 minutes, it is possible that inhibition of the “on” pathway by inhibiting the expression of *UBA2* prevents further sumoylation after this point. It must also be noted that although *UBA2* expression is repressed ~10 minutes after cold treatment, this will not be an immediate effect as there will be residual levels of Uba2 present in the cell. As observed in Fig 3.4B, inhibition of the Ulp1 and Ulp2 deconjugases maintains a high level of global sumo conjugates. Hence a feedback mechanism induced by the temperature shift may promote repression of *UBA2* to prevent toxic accumulation of HMW sumo complexes. One identified function of sumoylation is the regulation of gene expression (see section 1.3.5). Thus, transcription factors may be targeted for sumoylation to repress *UBA2* expression in cold temperatures. Furthermore, two transcription factors, *XBP1* and *YAP1*, which both have an identified role in the response to heat shock have been identified as regulators of *UBA2* in *S. cerevisiae* (Venters et al., 2011). Hence it would be interesting to investigate either of these transcription factors promote *UBA2* repression in cold temperature.

Western blot analysis in Fig. 3.4B suggested that inhibition of the desumoylases Ulp1 and Ulp2 is linked to the cold temperature-induced accumulation of HMW sumo conjugates (Fig 3.4B). Hence, it was possible that the inhibition of Ulp2 could be linked with inhibition of the expression of the *ULP2* and *ULP1* genes following exposure of cells to low temperature. However, the expression of the *ULP1* gene was unchanged 10 minutes after exposure of cells to 20°C (Fig. 3.5). Furthermore, the expression of *ULP2* appeared to be significantly activated 10 minutes after exposure of cells to 20°C compared to the 0 minute timepoint (Fig. 3.5). However, these results appear to contradict a model where inhibition of Ulp2 activity is important for the cold temperature-induced accumulation of HMW sumo conjugates. However, it is possible that any cold temperature-induced inactivation of Ulp2 is irreversible and thus in this scenario a pool of “new” inactivated Ulp2 would be important to replace inactivated Ulp2 and potentially restore normal sumoylation patterns after adaption to cold temperature has occurred or after restoration of normal growth temperatures. Although the mechanism underlying this upregulation of *ULP2* upon exposure of cells to cold temperature is unclear it is interesting to note that the transcription factor, Yap6, which is involved in stress responses in *S. cerevisiae* has been previously linked to regulation of *ULP2* (Venters et al., 2011). Hence, it will be interesting in future studies to investigate the mechanisms underlying the regulation of *ULP2* gene expression by cold temperature.

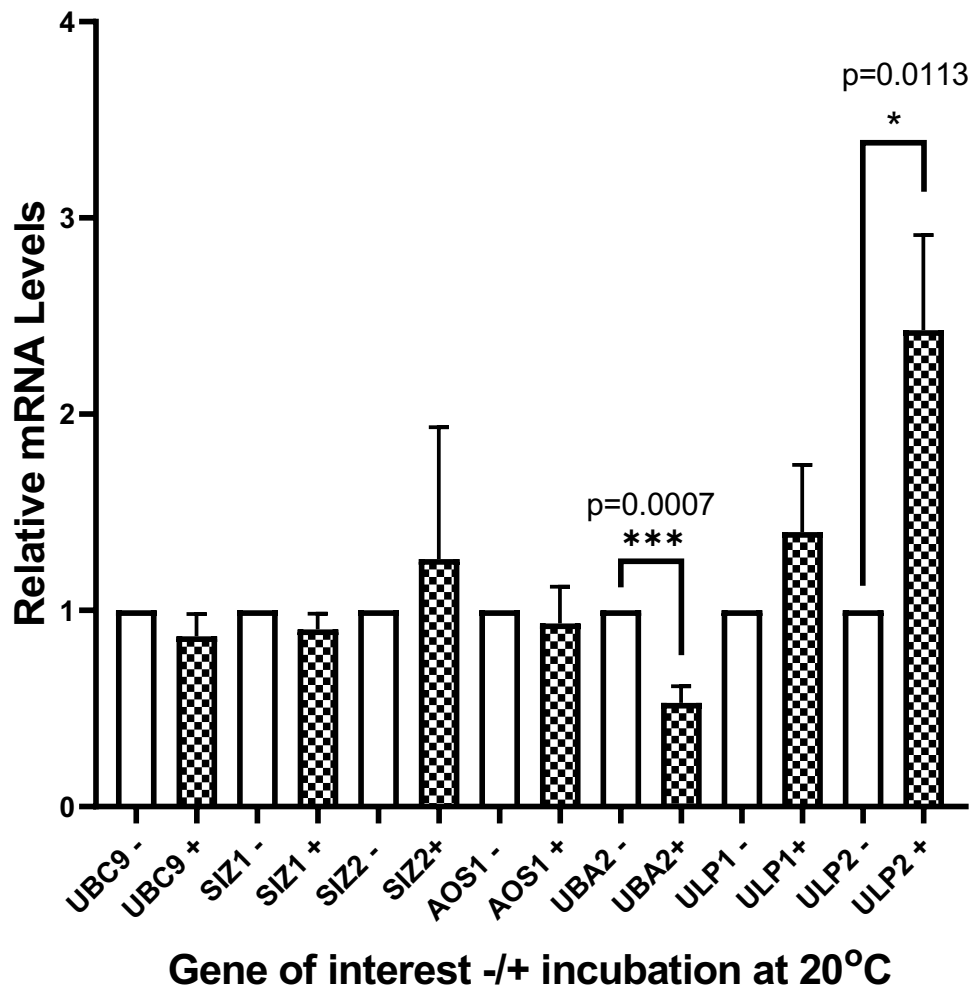


Figure 3.5 *ULP2* gene expression is increased upon exposure of cells to cold temperature.

The expression of genes encoding Smt3 conjugation/deconjugation enzymes was analysed at 0 and 10 minutes after shifting mid-log phase growing WT (GC1) cells from 30°C to 20°C. RNA was extracted from each time point and RT-qPCR analyses performed using primers specific for each of the indicated genes and normalised to the RNA levels of the *ALG9* gene. Error bars represent SD based on three biological repeats. P values were derived from an unpaired T-test.

Taken together, the data in Fig. 3.2 and Fig. 3.4 together propose a model in which cold temperature rapidly induces HMW sumoylation. Siz1 and Siz2 appear to be important for targeting specific substrates whilst inhibition of the desumoylases maintains the high level of global sumoylation, which is sustained >60 minutes after the initial exposure to 20°C. Furthermore, Fig 3.5 suggests that *UBA2* expression is rapidly decreased after exposure to 20°C whilst *ULP2* expression is induced, suggesting that a feedback mechanism prevents excess sumo conjugation after the initial exposure to 20°C to prevent cellular damage. However, it must be noted that the analysis of gene expression (Fig 3.5) is representative of one time point. Hence it would be interesting to analyse the gene expression of *UBA2* and *ULP2* at later timepoints.

3.2.5 Smt3 and the response of cells to oxidative stress

As described above, our studies of the phenotypes associated with the *smt3::DAmP* allele has provided a novel insight into the response of *S. cerevisiae* cells to cold temperature. Furthermore, the work presented here has revealed that polysumoylation plays an important role in these cold temperature responses (Fig. 3.3). Therefore, we next investigated whether analyses of these strains could provide insight into the role of sumo in other stress responses. As described in Chapter 1, section 1.3.6.5, oxidative stress is known to induce global sumoylation (Lewicki et al., 2015, Zhou et al., 2004). Furthermore, previous work has shown that the BY4741 and W303 strains of *S. cerevisiae* regulate responses to oxidative stress by different pathways (Veal et al., 2007, Veal et al., 2003). Hence, sensitivity of the two *smt3* mutant strains (GC16 and GC50) was examined in the BY4741 and W303 genetic backgrounds to a variety of H₂O₂ concentrations. Interestingly, both of the *smt3* mutants, in either the BY4741 or W303 genetic background, are more sensitive H₂O₂ than their respective wild type strains (Fig. 3.6A). Moreover, W303*smt3* (GC50) is much more sensitive to H₂O₂ than the original *smt3* mutant (GC16) in the BY4741 genetic background (Fig. 3.6A). The basis for this difference in sensitivity to H₂O₂ is unclear but could be linked to the increased sensitivity of the W303 wild type strain to H₂O₂ compared with the BY4741 wild type strain (Fig. 3.6A). Now that it had been determined that Smt3 is required for resistance of cells to H₂O₂ the next step was to examine the role of polysumoylation in H₂O₂ resistance. Interestingly, the *smt3-allR*

strain displayed a similar sensitivity to H₂O₂ compared to the original *smt3* mutant in the BY4741 genetic background, the most similar of the two *smt3* mutants with the *smt3-allR* strain background (Fig. 3.6A). However, at 4mM H₂O₂ the *smt3-allR* does appear to grow slightly less well than the *smt3* strain (Fig. 3.6A). Hence, these results suggest that polysumoylation is perhaps the most important of the types of sumoylation that can occur in cells for the response of cells to H₂O₂, although roles for the other forms of sumoylation such as mono- and/or multisumoylation in resistance to oxidative stress cannot be excluded.

Having established that sumo is required for the resistance of *S. cerevisiae* cells to H₂O₂ the next step was to characterise the global sumoylation in the wild type BY4741 strain (GC1) and the *smt3* mutant in the BY4741 strain background (GC16) in the response to H₂O₂. Midlog GC1 and GC16 cells were exposed to 5mM H₂O₂ for 5 minutes, with western blot analysis revealing that HMW sumo conjugates are increased ~2.5 fold in WT cells after H₂O₂ treatment (Fig. 3.6B). Conversely, HMW sumo conjugates appear to be only very slightly induced in the *smt3* strain following H₂O₂ treatment (Fig. 3.6B). Interestingly, this induction observed in the *smt3* strain is extremely similar to the response to cold temperature in *smt3* cells (Fig 3.2B). Hence, Fig3.6B reveals that sumoylation is induced rapidly following exposure of cells to H₂O₂ and is consistent with the H₂O₂ sensitivity of the various sumo mutant strains which indicated that polysumoylation is important for the resistance of cells to H₂O₂. Nevertheless, it must be noted that there is an air bubble in the WT(BY) uninduced lane on the western blot. Hence, although this blot demonstrates that HMW sumoylation appears to be markedly induced upon H₂O treatment, it is clear that further repeats will be necessary to confirm these results and to accurately quantify the induction of HMW sumoylation in the WT(BY) strain.

The results presented above suggest that polysumoylation is important for the response of *S. cerevisiae* cells to H₂O₂ (Fig. 3.6A/B). Furthermore, it was also found that the sumo E3 Siz1 contributes to the formation of many of the HMW sumo conjugates that accumulate after cells are exposed to low temperatures (Fig.3.4). Hence, next the potential roles of Siz1 and Siz2 in responses to H₂O₂ were investigated by testing the sensitivity of the single *siz1*Δ and *siz2*Δ mutants to a range of H₂O₂ concentrations. Interestingly, in contrast to the lack of increased sensitivity of the mutants to cold temperature, both *siz1*Δ and *siz2*Δ single mutants displayed increased sensitivity to H₂O₂ (Fig. 3.7A) suggesting that both of these E3s are

required for responses to H₂O₂. To further characterise the roles of Siz1 and Siz2 in responses to H₂O₂ the effects of the mutations on the viability of cells to a high concentration of H₂O₂ (3mM) was examined. Strikingly, this analysis revealed that both *siz1*Δ and *siz2*Δ cells display reduced survival after 60 minutes treatment with 3mM H₂O₂ compared to the wild type control cells (Fig. 3.7B). Indeed, both *siz1*Δ and *siz2*Δ showed significant (p=>0.005) sensitivity to 10 minutes 3mM H₂O₂ treatment compared to wildtype cells (Fig. 3.7B). Taken together, these results propose that both Siz1 and Siz2 are important for the sumo-mediated cellular response to H₂O₂.

Exposing mammalian cells to high levels of H₂O₂ promotes inhibition of sumo deconjugases, enabling the accumulation of HMW sumo conjugates in the cell (Bossis and Melchior, 2006). Hence, the next step was to investigate the potential roles of the *S. cerevisiae* desumoylases in the responses to H₂O₂. The sensitivity of the single *ulp1* and *ulp2* mutants (GC30 and GC31) were examined in a range of H₂O₂ concentrations (Fig. 3.8A). Surprisingly, the *ulp1* mutant, unlike the *smt3* mutant, displayed increased resistance to H₂O₂ (Fig. 3.8A). Furthermore, the *ulp1* mutant showed significantly increased viability when exposed to a high concentration of H₂O₂ (5mM) for 50 minutes compared to wild type cells (Fig. 3.8B).

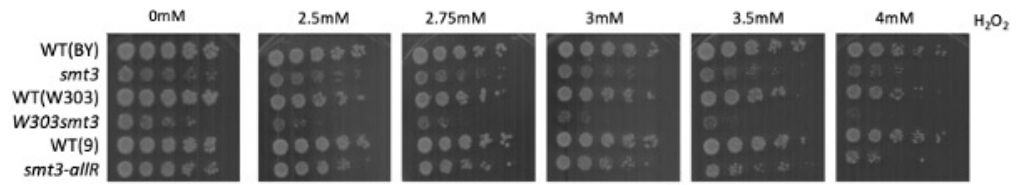
Considering that a major role of Ulp1 is to pre-process and mature Smt3, these results suggest that the increased resistance of *ulp1* mutant cells may instead be linked to loss of Ulp1 deconjugase activity rather than the pre-processing activity. However, in complete contrast to the *ulp1* results, the *ulp2* mutant displayed increased sensitivity to H₂O₂ compared to wild type cells (Fig. 3.8A). Hence, this result suggests that deconjugation of specific Ulp2 specific substrates is essential to provide resistance to H₂O₂. Collectively, these results indicate that Ulp1 and Ulp2 function in different aspects of cell responses to H₂O₂. Indeed, Ulp1 and Ulp2 show just 10% overlap in substrate specificity (Li and Hochstrasser, 2003). Hence the inhibition of Ulp1 during oxidative stress may promote the sumoylation of Ulp1 substrates which would usually be targeted for desumoylation. Interestingly, Lewicki et al (2015) identified that a large number of sumoylated substrates were linked to transcriptional control during the response to osmotic stress (Lewicki et al., 2015). Hence, it would be interesting to identify the sumoylated substrates after H₂O₂ treatment which would both identify similarities between different SSRs whilst characterising important pathways involved in the

response to H₂O₂ treatment. Nevertheless, the H₂O₂ induced sumo substrates currently remain uncharacterised, although it is possible that sumoylation of Ulp1 substrates are important for the response to oxidative stress.

Next, to further investigate the potential connections between Siz1, Siz2, Ulp1 and Ulp2 and the response of *S. cerevisiae* cells to H₂O₂, global sumoylation was examined. Western blot analysis of protein extracts from *siz1Δ*, *siz2Δ*, *ulp1* and *ulp2* cells exposed to 5mM H₂O₂ for five minutes confirmed that HMW conjugates accumulate rapidly in wild type (GC1) cells (Fig. 3.9A/B). In contrast to wild type (GC1) cells, there was only a marginal increase in HMW sumo conjugates in *siz1Δ* cells after 5mM H₂O₂ treatment (Fig. 3.9B). In contrast, an increase in HMW sumo conjugates could clearly be observed in the *siz2Δ* strain. Importantly, the HMW sumoylation induced in *siz2Δ* cells was ~twice the level observed in untreated cells (Fig. 3.9B). Hence, the degree of *siz2Δ* sumoylation induced by 5mM H₂O₂ is remarkably similar to the induction observed in WT cells, although the basal levels of sumoylation were higher than wild type (GC1) in *siz1Δ* and *siz2Δ* untreated cells (Fig 3.9B). Taken together, these western analyses propose that Siz1 may be the main E3 ligase responsible for sumoylation in response to H₂O₂.

Strikingly, the basal levels of sumoylation observed in the *ulp1* and *ulp2* strains were increased compared to the basal levels of sumoylation displayed in WT (GC1) cells. Nevertheless, there was almost no detectable induction of HMW sumo conjugates in *ulp1* cells after H₂O₂ treatment suggestive that inhibition of Ulp1 prevents any further sumoylation. Furthermore, the pattern of sumoylation observed in *ulp2* cells is remarkably similar to that of *ulp1* cells, suggestive that Ulp2 activity is also inhibited during oxidative stress (Fig. 3.9). Thus, it could be proposed that inhibition of both Ulp1 and Ulp2 contribute to the accumulation of HMW sumo conjugates observed in the response to H₂O₂ treatment in WT cells. Indeed, Xu et al. (2007) identified that after 4mM H₂O₂ treatment, the formation of an irreversible intermolecular disulphide bond involving the catalytic cysteine residue within Ulp1 *in vitro* prevents the irreversible oxidation of the catalytic cysteine by H₂O₂ whilst rendering Ulp1 inactive (Xu et al., 2008). Hence, this disulphide bond inhibits the sumo “off” pathway inactive whilst protecting the Ulp1 catalytic cysteine residue from irreversible oxidation by

A.



B.

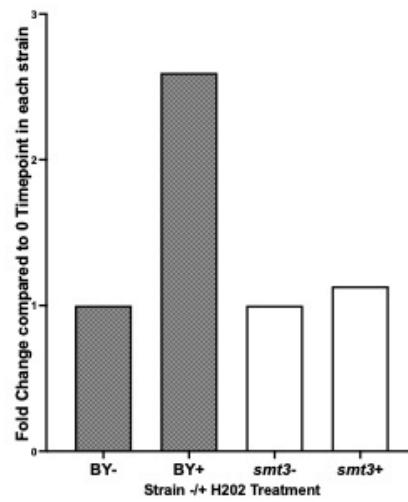
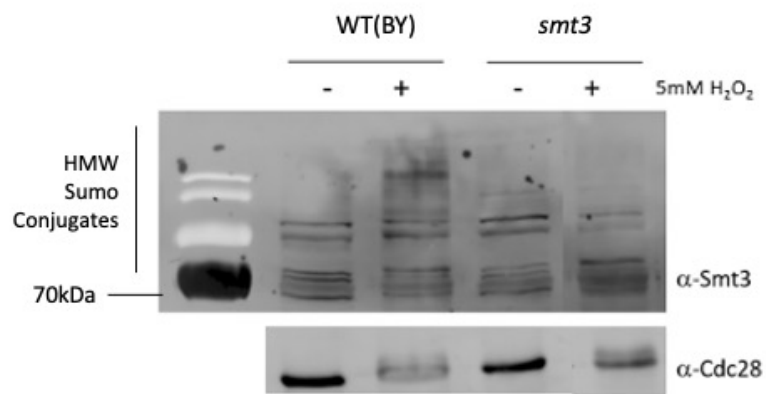
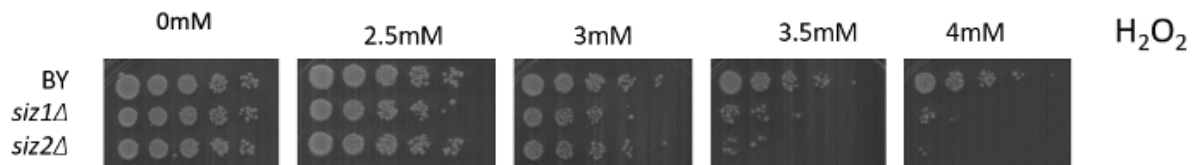


Figure 3.6 Smt3 is important for the response of cells to oxidative stress. (A) Five-fold serial dilutions of mid-log growing cultures GC1, GC16, G2, GC50, GC57 and GC55 cells were spotted onto YPD plates containing the indicated concentrations of H₂O₂ using a 48-pin tool and incubated at the indicated temperatures. (B) GC1 and GC16 cells were grown to midlog phase and treated with 5mM H₂O₂ for 5 minutes. Proteins were TCA extracted before and after 5mM H₂O₂ treatment and analysed by western blotting using an α -Smt3 antibody. Blots were stripped and re-probed with α -cdc28 as a loading control. Blots were quantified using ImageQuant (GE Healthcare). Quantification of HMW Smt3 conjugates is based on proteins >70kDa in size recognised by the α -Smt3 antibody. Bars represent HMW sumo conjugates normalised to the 0 timepoint of the respective strain. Quantification is based on one repeat. Western blots are representative of three biological repeats.

A.



B.

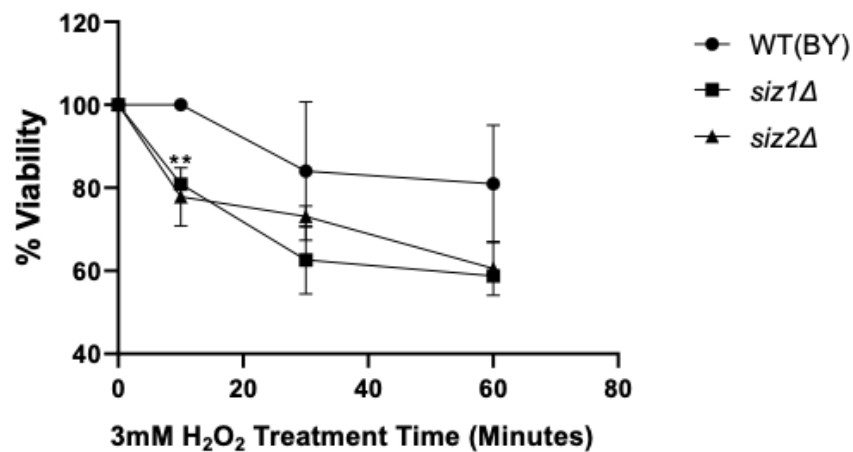
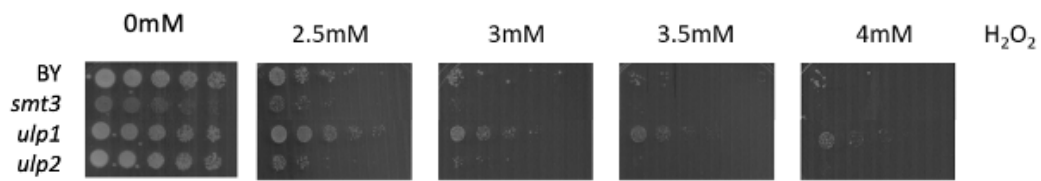


Figure 3.7 The sumo E3 ligases Siz1 and Siz2 are important for response to H₂O₂ (A) Five-fold serial dilutions of mid-log growing cultures GC1, GC28 and GC29 cells were spotted onto YPD plates containing the indicated concentrations of H₂O₂ using a 48-pin tool and incubated at the indicated temperatures. (B) Mid-log phase growing GC1, GC28 and GC29 cells were treated with treated with 3mM H₂O₂. Equal numbers of cells were plated onto YPD plates at the indicated time points after addition of H₂O₂. Surviving colonies which grew at 30°C were counted and % survival was calculated based on the 0 time point for each strain. Survival curves and spot tests are representative of three biological repeats, error bars represent SD, P values were derived from an unpaired T-test.

A.



B.

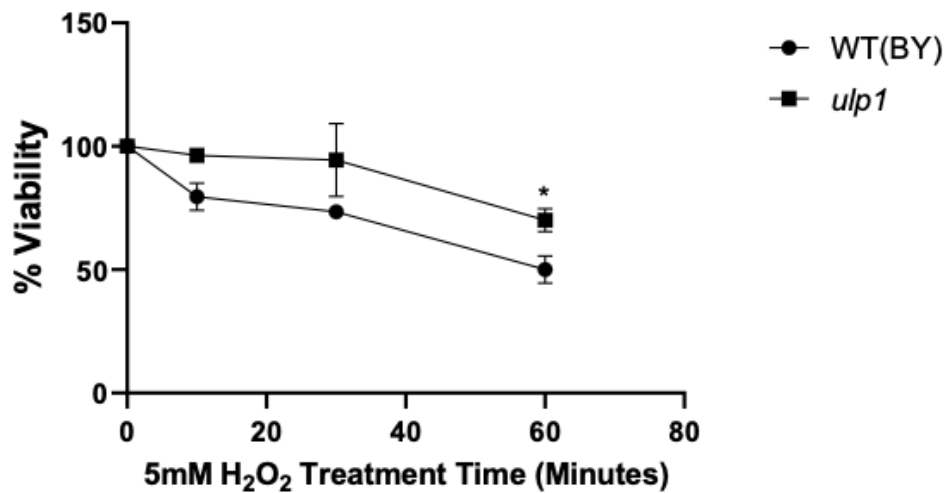


Figure 3.8 Ulp1 and Ulp2 have different functions in responses to H₂O₂. (A) Five-fold serial dilutions of mid-log growing cultures GC1, GC30 and GC31 cells were spotted onto YPD plates containing the indicated concentrations of H₂O₂ using a 48-pin tool and incubated at the indicated temperatures. (B) Mid-log phase growing GC1, GC30 and GC31 cells were treated with treated with 5mM H₂O₂. Equal numbers of cells were plated onto YPD plates at the indicated time points after addition of H₂O₂. Surviving colonies which grew at 30°C were counted and % survival was calculated based on the 0 time point for each strain. Survival curves and spot tests are representative of three biological repeats, error bars represent SD.

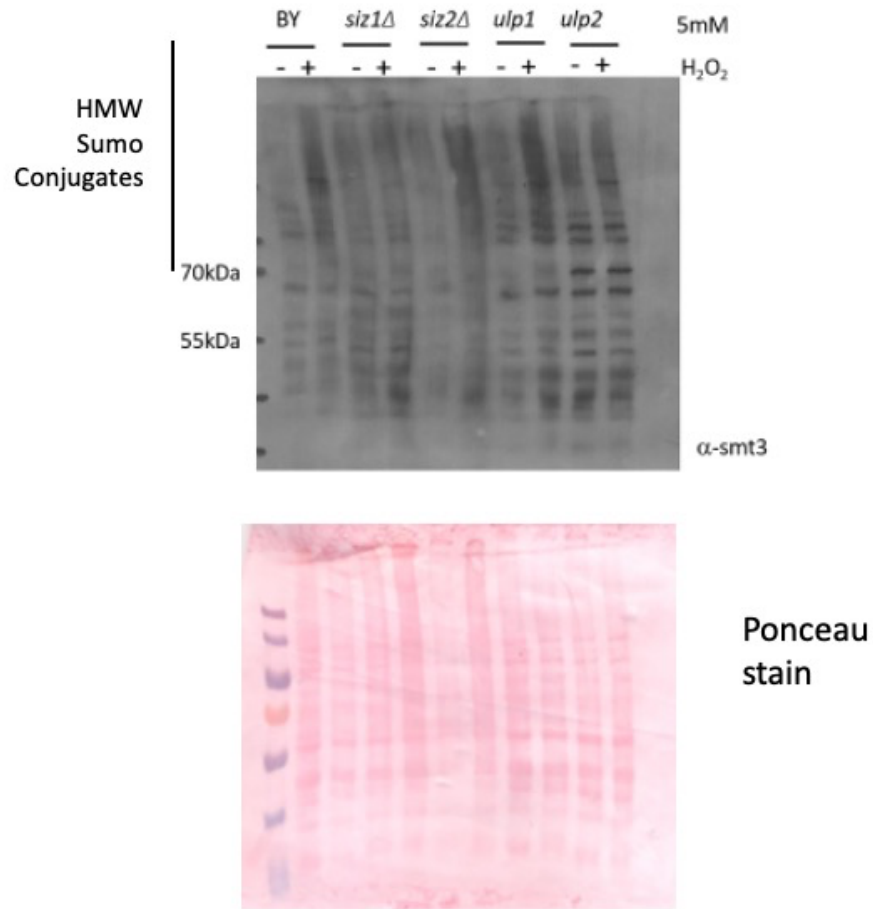
H₂O₂ (Xu et al., 2008). This study proposes that H₂O₂ treatment may promote inhibition of both the Ulp1 and Ulp2 sumo proteases *in vivo* (Fig 3.9). One hypothesis is that the formation of intramolecular disulphide bonds involving the catalytic cysteine in Ulp1 (and possibly also in Ulp2) may be induced in the response to 5mM H₂O₂ treatment *in vivo* to inhibit desumoylase activity whilst preventing against irreversible oxidation. However, further *in vivo* analysis is required to determine the nature of Ulp1/Ulp2 inhibition during oxidative stress.

To conclude, it appears that Siz1 is important for the “on” pathway to enable substrate sumoylation in the *S. cerevisiae* response to H₂O₂ treatment (Fig 3.9AB). This finding is in contrast to Fig 3.4, in which both Siz1 and Siz2 are important for mediating the response to cold temperature, highlighting that the SSR is different upon treatment with different stresses. Interestingly, these findings are in agreement with Lewicki et al. (2015) in which the kinetics of the enzymes involved in the *S. cerevisiae* SSR differ within the treatment of different cellular stresses (Lewicki et al., 2015). Additionally, after treatment with 5mM H₂O₂, the inhibition of Ulp1 and Ulp2 prevents global desumoylation, maintaining the high levels of sumo conjugates observed in Fig. 3.9. Importantly, although the western blot quantification was only performed once, the basal levels of sumoylation observed in the *siz2*Δ, *ulp1* and *ulp2* strains are extremely similar to Fig 3.4, although further repeats of Fig. 3.9B are vital to confirm the roles of Siz1, Ulp1 and Ulp2 in the response to oxidative stress.

3.2.6 Ubiquitination is induced in response to cold temperatures

The discovery of the STUbL family of ubiquitin E3 ligases revealed how polysumoylated substrates are subsequently targeted for ubiquitination (see Chapter 1, section 1.3.2). STUbLs contain conserved SIM domains which facilitate the recognition of polysumo chains on target proteins (Sriramachandran and Dohmen, 2014), which leads to ubiquitination of the polysumoylated substrate which targets it for degradation via the 26S proteasome (see section 1.3.2). The data presented in this chapter revealed that polysumoylation, detected as HMW sumo conjugates, is induced in *S. cerevisiae* following exposure of cells to cold temperature (for example see Fig. 3.2A). Furthermore, data in this study suggests that polysumoylation is important for the response of cells to cold temperature (Fig. 3.3B). Hence,

A.



B.

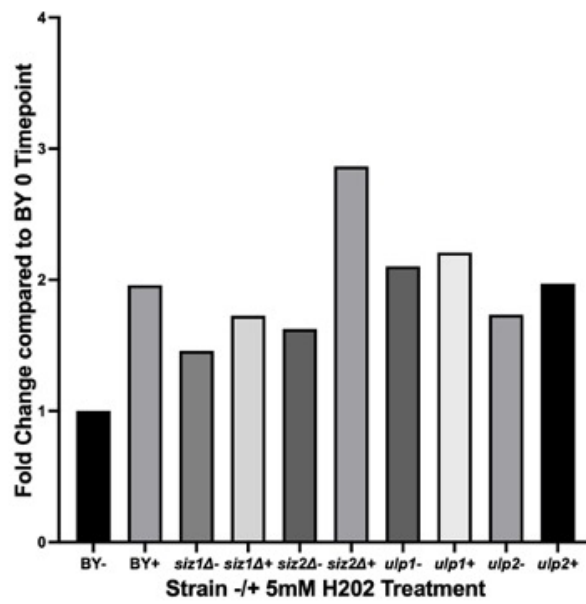


Figure 3.9 HMW sumo conjugates in *siz2*Δ cells are greatly induced in oxidative stress. (A) GC1, GC28, GC29, GC30 and GC31 cells were grown to midlog phase and treated with 5mM H₂O₂ for 5 minutes. Proteins were TCA extracted before and after 5mM H₂O₂ treatment and analysed by western blotting using an α-Smt3 antibody. Blots were stripped and stained with Ponceau as a loading control. (B) Blots were quantified using ImageQuant (GE Healthcare). Quantification of HMW Smt3 conjugates is based on proteins >70kDa in size recognised by the α-Smt3 antibody. Bars represent HMW sumo conjugates normalised to the BY (GC1) 0 timepoint. Quantification is based on one repeat and western blots are representative of two biological repeats.

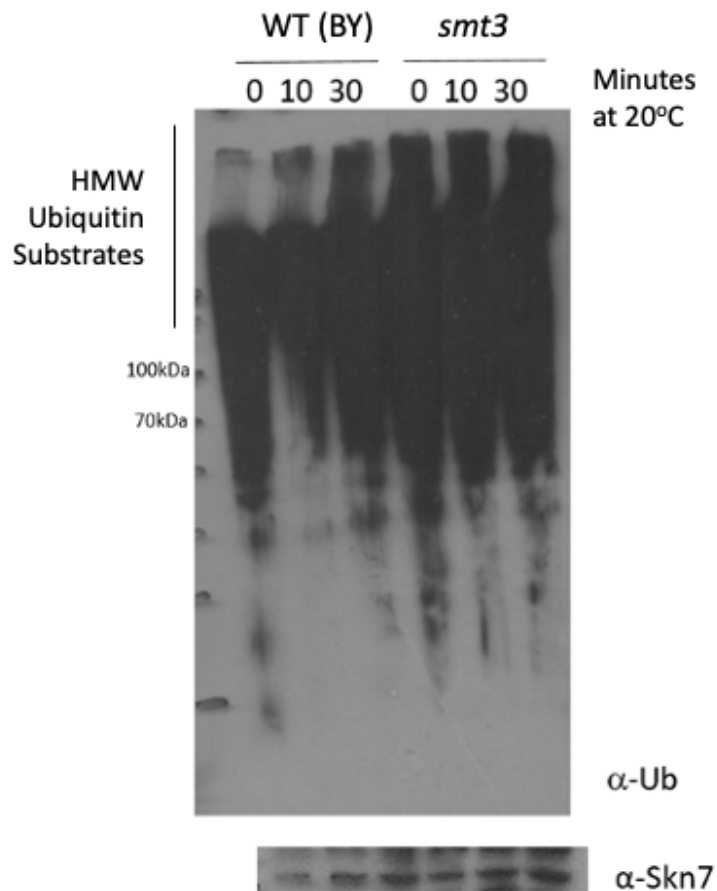


Figure 3.10 Global ubiquitination is induced by cold temperatures. GC1 and GC16 cells were grown at 30°C and rapidly cooled and incubated at 20°C. Proteins were TCA extracted at the indicated timepoints after incubation at 20°C and analysed by western blotting using an α -Ub antibody. Blots were stripped and re-probed with α -Skn7 as a loading control. Western blots are representative of two biological repeats. A representative blot is shown.

given the role of polysumoylation in facilitating STUbL-mediated ubiquitination, it was possible that one role of polysumoylation in responses to cold temperature could be involved with targeting specific proteins for ubiquitination. Thus, in order to gain insight into the potential relationships between sumoylation and ubiquitination during cold temperatures, global ubiquitination was examined by western blot analysis of protein extracts from wild type (GC1) and *smt3* (GC16) cells exposed to 20°C (Fig. 3.10). Consistent with our hypothesis that the accumulation of HMW polysumoylated leads to STUbL-mediated ubiquitination of substrates following exposure of cells to low temperature, HMW global ubiquitination is induced in wild type cells ~30 minutes after incubation of cells at 20°C (Fig. 3.10). Interestingly, the detected accumulation of ubiquitin conjugates occurs after the accumulation of HMW sumo conjugates has occurred (compare Fig. 3.2A with Fig. 3.10). After exposure of wild type cells to 20°C, HMW sumoylation appears to peak at ~10 minutes whereas an increase in HMW ubiquitination peaks at ~30 minutes (compare Fig. 3.2A with Fig. 3.10). Interestingly, ubiquitination of substrates <70kDa appears to reduce after 10 minutes incubation at cold temperature in WT cells, although the reason for this reduction is unclear (Fig. 3.10, lane 2). Hence, taken together, these data support the hypothesis that one role of cold temperature-induced polysumoylation is to stimulate the ubiquitination of certain (as yet unknown) proteins. Strikingly, western blot analysis of the *smt3* (GC16) strain revealed that the basal levels of HMW global ubiquitination are much higher than in WT (GC1) cells even before the shift to low temperature (Fig 3.10). However, this high basal level of ubiquitination in *smt3* cells obscured visualising any further increases in global ubiquitination following the shift to 20°C (Fig. 3.10). Additionally, it must be noted that the Skn7 loading control suggests that the WT(BY) uninduced sample may be under loaded, suggestive that that HMW ubiquitination may not be as pronounced as observed in the upper panel of Fig. 3.10 in lanes 1 and 2. Hence, further repeats and quantification are required to determine the degree of cold-induced ubiquitination

In addition, it is important to note that this analysis of ubiquitination in the wild type and *smt3* strains utilises an antibody that cannot distinguish between the different types of ubiquitin modifications. For example, K63 polyubiquitin chains have been linked to cellular signalling compared to K48 ubiquitination which is associated with proteasomal degradation. Although other analysis in the lab suggests that K63 linkages are not involved in responses of cells to

cold temperature (data not shown) further work is required to analyse the precise polyubiquitination linkages that are affected by cold temperature in the WT strain and in the *smt3* mutant growing at normal temperature. Nevertheless, it is clear that ubiquitination is important in the response to cold temperatures.

3.3 Summary

This chapter has identified that the cold sensitive phenotype associated with the original *smt3* mutant is conserved in different *S. cerevisiae* strain backgrounds. Indeed, neither the *smt3* nor *W303smt3* mutants were able to induce the HMW sumoylation in response to cold temperatures which was observed in WT cells, highlighting the importance of global sumoylation in the response to cold temperatures (Fig 3.2B/C). The reduction of cold-induced HMW sumo conjugates observed in *siz1Δ* cells (Figure 3.4) is remarkably similar to that observed in plants by Miura et al. (2007), proposing that Siz1 may recognise the bulk of sumo substrates in cold temperatures. Indeed, Fig 3.4 also suggests that Siz1 may also be the major E3 ligase required for sumoylation in response to cold temperatures in *S. cerevisiae*, as *siz2Δ* cells are still able to induce sumoylation upon exposure to cold. Sumoylation of the transcription factor Ice1 in *A. thaliana* during cold treatment is required to upregulate genes required for cold acclimation (Miura et al., 2007). BLAST sequence comparisons between the *A. thaliana* Ice1 sequence and the *S. cerevisiae* genome did not reveal a *S. cerevisiae* homologue, although it is possible that other transcription factors may be responsible for potentially upregulating *S. cerevisiae* survival genes. For example, the expression of several genes related to metabolic pathways are upregulated in budding yeast during the response to cold temperatures including *TIP1* and *ERG10*, although the transcription factors mediating this change in gene expression remain unknown (Rodriguez-Vargas et al., 2002). Interestingly, overexpression of *ERG10* promotes freeze tolerance in *S. cerevisiae* cells, hence it would be interesting to investigate the sumoylation status of upstream transcription factors which regulate *ERG10* activity during cold temperatures. Nevertheless, the substrates of cold-induced sumoylation remain elusive. Affinity purification coupled with mass spectrometry using cultures before and after cold treatment could identify putative sumo substrates and would allow an insight into whether any transcription factors are sumoylated.

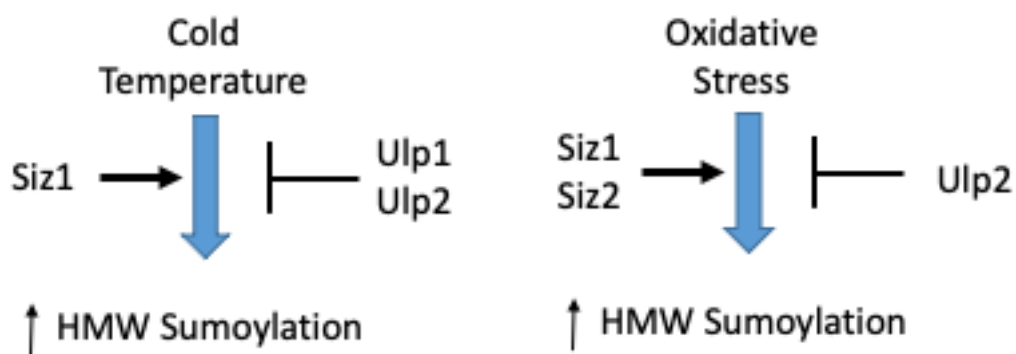


Figure 3.11 Cold temperature and oxidative stress affect the sumo conjugation/deconjugation pathway in distinct ways. Cold temperature induces HMW sumoylation, mediated by the E3 ligases Siz1 and Siz2. Inhibition of both sumo deconjugases, Ulp1 and Ulp2, prevent substrate desumoylation, sustaining the elevated HMW sumo levels in *S. cerevisiae* cells. Oxidative stress also induces HMW sumoylation, again mediated by the E3 ligases Siz1 and Siz2. However, in contrast to cold temperatures, only inhibition of Ulp2 appears to be important in the response to H₂O₂ treatment.

In addition to the importance of the “on” pathway in facilitating the sumo-mediated response to cold, Fig. 3.4 suggests that inhibition of the two *S. cerevisiae* desumoylases, Ulp1 and Ulp2, is also important to maintain high levels of global sumoylation during cold treatment. Hence, the current model in this study proposes that cold temperature induces sumoylation mediated by Siz1, whilst inhibition of Ulp1 and Ulp2 prevent substrate desumoylation. This model is further demonstrated by the identification that cold treatment significantly reduced *UBA2* expression whilst increasing *ULP2* expression (Fig 3.5). Extremely high levels of polysumoylated conjugates can be toxic for the cell (Bylebyl et al., 2003), hence a feedback mechanism preventing *UBA2* expression whilst promoting *ULP2* expression may lower the level of global sumo conjugates after the initial accumulation of HMW sumo conjugates in the response to cold temperatures. However, this model is purely speculative and would require further characterisation.

In addition to the sensitivity to cold temperatures, it has been identified that strains expressing the *smt3* allele are also much more sensitive to oxidative stress (Fig 3.6). Increased sensitivity observed in the *smt3-allR* strain to H₂O₂ treatment also suggests that polysumoylation is important for the response to ROS. Interestingly, data in this chapter demonstrates that the findings from Golebiowski et al. (2006) in which polysumoylation accounts for the majority of sumoylation in heat shock can also be observed in the responses to cold temperatures and oxidative stress. Taken together, these results suggest that the induction of HMW polysumoylated substrates is a key, conserved feature in the conserved response to cellular stress. Moreover, in agreement with the findings that inhibition of sumo proteases is important in the responses to cold and oxidative stress, Lewicki et al (2015) also suggest that Ulp2 activity is the main inactivator of the SSR. Indeed, it could be proposed that cold temperature and H₂O₂ treatment induce Ulp2 inhibition, although Fig 3.4 also indicates that Ulp1 inhibition may also be important in the response to cold temperature.

Finally, it can be concluded that ubiquitination can also be seen to increase in response to cold conditions. However, this ubiquitination is not as rapid as sumoylation. Indeed, this ubiquitination may be recruited to polysumoylated proteins for targeted degradation after the SSR is no longer required. Notably, ubiquitin levels are much higher at basal levels within

smt3 cells, suggesting that co-ordination between sumo and ubiquitin levels may be closely linked. PTMs often compete for the same modification sites. It may be the case that lower levels of Smt3 within *smt3* cells allow ubiquitination of sites which would usually be subject to sumoylation. However, this is purely speculative and would involve further investigation.

To conclude, it has been identified that sumo levels are vital to induce the SSR in cold temperature and oxidative stresses. Polysumoylation appears to be a key feature of the SSR, although it does not appear to be essential for these responses.

Chapter Four: Investigation of the functions of sumoylation in cell cycle progression

4.1 Introduction

Previous studies have shown that sumoylation is important for the regulation of the cell cycle. For example, studies in *S. cerevisiae* revealed that mutations of *SMT3* or of *UBC9* cause cells to arrest in G2/M phase of the cell cycle (Li and Hochstrasser, 1999a, Johnson and Blobel, 1999). Furthermore, *S. cerevisiae* cells expressing the *smt3::DAmP* allele in either the BY4741 or the W303 strain backgrounds have significant growth defects (Chapter 3, section 3.3.1, (Lewis, 2016)). Indeed, initial DNA content analyses of *smt3::DAmP* mutant cells in the BY4741 strain background (GC16) revealed that cells with reduced levels of Smt3 display increased levels of aneuploidy compared to wild type cells (Lewis, 2016). Aneuploidy, characterised by an atypical number of chromosomes, often arises through mitotic defects and is usually associated with a detrimental impact to cells. However, several recent studies have suggested that aneuploidy may also be utilised as an important adaptative mechanism to improve cellular fitness. For example, the opportunistic pathogen *C. albicans* has been shown to induce aneuploidy in order to confer resistance against anti-fungal agents (Selmecki et al., 2006). Duplication of chromosome V in *C. albicans* cells enables resistance against the anti-fungal agent fluconazole, promoting *C. albicans* survival and maintaining the fungal infection in human cells (Selmecki et al., 2006). Hence, it is possible that the increased aneuploidy displayed in *smt3* mutant cells is not a cause of the detected growth defects but rather is an adaptation by the mutant cells to allow them to cope with reduced sumo function. Interestingly, as described in Chapter 1, section 1.4.2, the SGA screen identified several mutations that, when crossed with the *smt3* mutant strain, suppressed the poor growth associated with loss of Smt3 function ((Lewis, 2016)). However, the effects of many of these mutations on the cell cycle and aneuploidy associated with the *smt3* mutation have not been characterised. Thus, to gain further insight into the relationship between sumo and the cell cycle, the work described in this chapter focusses on investigations of the effects of loss of sumo function on cell cycle progression and aneuploidy in the different strain backgrounds.

In addition, the roles of polysumoylation and some of the top suppressor mutations on the cell cycle functions of sumo are also explored.

4.2 Results and Discussion

4.2.1 *smt3* cells display defects in G2/M phase progression

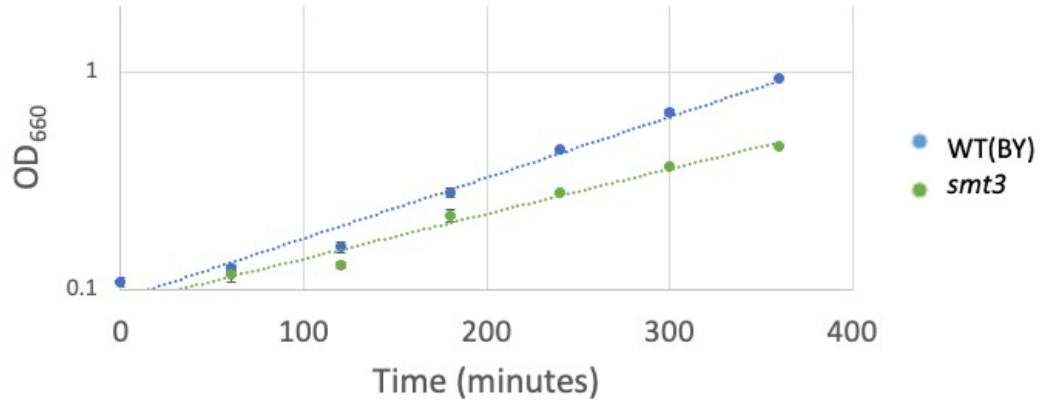
Previous work from the laboratory demonstrated that *smt3* mutant cells (GC16) in the BY4741 strain background are predominately large budded cells and exhibit nuclear morphology defects indicative of problems in mitosis (Lewis, 2016). In addition, *smt3* cells displayed substantial aneuploidy when compared to wild type cells, with a significant proportion of *smt3* cells found to have >2C DNA content (Lewis, 2016). However, these cell cycle defects were not characterised further in the previous study. Hence, in this study the cell cycle parameters and aneuploidy of *smt3* cells were investigated in more detail. In agreement with the original observations by Dr. Lewis, analysis of the growth of *smt3* mutant cells in the BY4741 strain background confirmed that cells with reduced levels of Smt3 grow considerably slower than wild type cells (Figure 4.1A). Indeed, growth rate analyses suggests that the doubling time of the *smt3* mutant is 144 ± 3 minutes compared to a doubling time of 108 ± 2 minutes for the wild type control strain. It was possible that the much longer apparent doubling time of the *smt3* mutant might be linked to severe loss of viability rather than slow growth. However, although there is significantly reduced viability observed in cultures of the *smt3* mutant, this is not sufficient to explain the large increase in doubling time (Fig. 4.1B). Next, DNA content analysis was performed on cultures of the mid-log phase growing wild type (GC1) and *smt3* mutant (GC16) strains. As expected, the FACS analyses revealed that a significant proportion of *smt3* cells ($\sim 6\%$, $p=0.005$) show >2C DNA content compared to the wild type control cells, confirming that *smt3* cells do indeed show aneuploidy (Figure 4.1C/D). To further analyse the cell cycle defects associated with the *smt3* mutant the proportion of cells in each cell cycle phase was combined with the doubling times of the wild type and *smt3* mutant strains to calculate the approximate time that wild type and *smt3* cells spend in each phase of the cell cycle (Morgan et al., 1991). Strikingly, this analysis revealed that *smt3* cells spend an increased amount of time in G2/M phases compared to wild type cells (Fig. 4.1E). In particular, *smt3* cells were found to spend ~ 72 minutes in G2/M phases in comparison to wild type cells which spend ~ 40 minutes in G2/M phases (Fig. 4.1E). As mentioned previously,

midlog growing cultures of the *smt3* mutant contain significant numbers of budded cells that are larger than normal, a phenotype of which is indicative of late cell cycle and mitotic defects. Hence, the DNA content analysis is consistent with these cell phenotypes and, furthermore, suggest that *smt3* cells are much larger than normal due to a delay in cell cycle progression through G2/M phases (Li and Hochstrasser, 1999a).

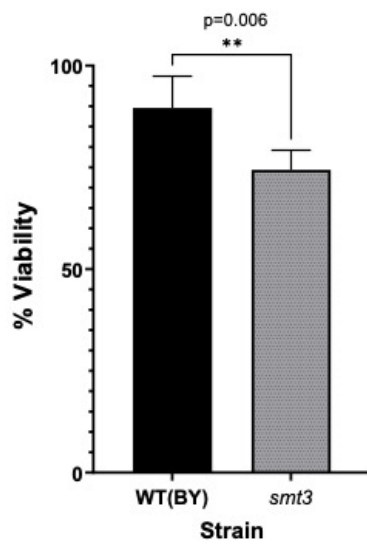
4.2.2 Duplication of specific chromosomes contribute to *smt3* aneuploidy

As described above, DNA content analyses revealed that a significant proportion of growing *smt3* mutant cells show aneuploidy, possibly linked to the detected problems in progressing through G2/M phases (Fig. 4.1C/D). However, whilst there is evidence of aneuploidy displayed in *smt3* cells, it was not clear if this was a general defect associated with all of the chromosomes or rather was associated with a specific subset of chromosomes, as the DNA content analysis is only a rough analysis of aneuploidy and does not provide insights into the chromosomal dynamics. To investigate these different possibilities, the aneuploidy of the *smt3* mutant (GC16) was examined by determining which chromosomes displayed increased numbers. Interestingly, at the beginning of the thesis project, analysis of an *ulp2Δ* mutant revealed that *ulp2Δ* cells also exhibit aneuploidy (Ryu et al., 2016). Furthermore, disomy of chromosomes I and XII were characteristic of *ulp2Δ* cells (Ryu et al., 2016). Ryu et al. (2016) suggested that overexpression of specific genes located on these chromosomes may compensate for the loss of Ulp2 function and that the aneuploidy associated with *ulp2Δ* mutant cells could be suppressed by overexpression of the *CLN3* and *CCR4* genes, both located on Chromosome I. Moreover, the *ulp2Δ* aneuploidy associated with chromosome XII was rapidly reversed after ~50 generations of growth illustrating that aneuploidy of chromosome XII was not permanent phenotype and could be rapidly reversed *in vivo* (Ryu et al., 2016). Hence, this study suggested that chromosome I aneuploidy may be an adaptive response to the loss of Ulp2 function. Nevertheless, strains expressing reduced sumo function were not examined in the Ryu et al. (2016) study so it was unclear whether loss of sumo function would have the same influence on aneuploidy as preventing desumoylation in the *ulp2Δ* mutant (Ryu et al., 2016).

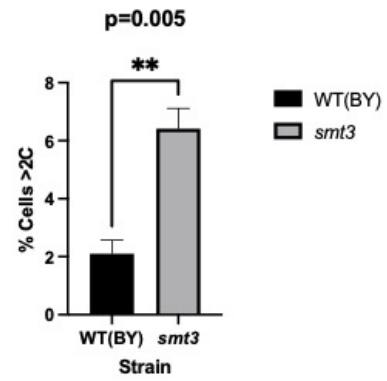
A.



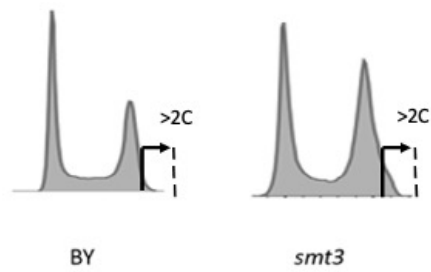
B.



C.



D.



E.

Strain	Doubling Time	G1	S	G2/M
WT(BY)	108±2	36±3	32±1	40±3
<i>smt3</i>	144±3	30±1	39±2	72±2

Figure 4.1 *smt3* cells have cell cycle defects. (A) Growth curves of mid-log phase growing cultures of wild type (GC1) and *smt3* (GC16) cells. Error bars represent SD from 3 biological repeats. (B) An equal number of cells from mid-log phase growing cultures of wild type (GC1) and *smt3* (GC16) strains were plated on to YPD plates and incubated at 30°C. Colonies were counted after 3 days. Error bars represent the SD from 5 biological repeats. (C) Gating analysis of the DNA content analyses in (D) of cells containing >2C DNA content. P values were derived from an unpaired T-test (D) DNA content analysis was performed on mid-log phase growing cultures of wild type (GC1) and *smt3* (GC16) cells and presented as indicated. Arrows indicate cells with >2C content. (E) Gating analysis of the DNA content analyses in (D) of the time (in minutes) cells spent in each stage of the cell cycle.

Next, to determine the chromosomal profile of *smt3* cells, the same qPCR chromosomal ploidy assay used by Ryu et al. (2016) was utilised to analyse the 16 chromosomes of the *smt3* mutant (GC16) (Fig. 4.2). Briefly, *smt3* cultures were grown to midlog phase, DNA extracted and 5µg DNA was subject to analysis by qPCR. Primers within the non-coding regions specific to the left arm of each chromosome were used to analyse the copy number of each chromosome (Pavelka et al., 2010). The sequences of the oligonucleotide primers used were specific for each chromosome and were identical to those used by Ryu et al. (2016) (Ryu et al., 2016). The chromosomal assay was also applied to DNA extracted from wild type (GC1) cells and *ulp2* (GC30) cells which contain an *ulp2::DAmP* allele, rather than a deletion of the *ULP2* gene, to determine whether reduced Ulp2 function has the same effect on aneuploidy as a complete deletion of the *ULP2* gene.

As can be seen in Fig. 4.2, *ulp2* cells clearly show significant duplication of chromosome I, consistent with the previous analysis of *ulp2Δ* cells (Ryu et al., 2016)). Interestingly, chromosome XII does not appear to be duplicated in *ulp2* mutant cells and may actually be present at slightly lower levels in the *ulp2* population compared to wild type cells (Fig. 4.2). However, it is worth noting that the *ulp2* mutant strain used in this study is from a commercially available library of DAmP mutations of essential genes and thus has likely been grown over many generations before it was obtained for the present study. Ryu et al (2016) found that the increased levels of chromosome XII detected after construction of the *ulp2Δ* mutant disappeared after ~50 generations of growth (Ryu et al., 2016). Hence, it is possible that increased levels of chromosome XII were originally present in the *ulp2* mutant cells under investigation in the present study but that this increase disappeared upon outgrowth of the strain. Although there is some evidence that chromosome XII may be present at slightly lower levels than normal in *ulp2* mutant cells compared to wild type cells (Fig. 4.2), and compared to the studies of the *ulp2Δ* mutant (Ryu et al., 2016), given that it is unclear how many generations of growth the *ulp2* mutant has undergone it would be interesting to compare the chromosome complement of *ulp2Δ* cells grown for an equivalent number of generations. However, it also possible that these differences between the *ulp2* mutant strains are linked to the fact that the previous study used a null mutant of Ulp2 versus a reduced Ulp2 function mutant in the present study (Ryu et al., 2016). Importantly, in agreement with Ryu et al.

(2016), chromosome I was the only chromosome with significantly enhanced levels in *ulp2* cells (Fig. 3.2).

Interestingly, the chromosome profiles of the *smt3* mutant strain were found to be distinctly different from both wild type cells and from the two different *ulp2* mutants (Fig. 4.2). In particular, analyses of *smt3* mutant cells revealed ~2 fold increases in the levels of several chromosomes. Indeed, chromosomes I, II, IV, VI, VII, X, XI and XVI were significantly increased compared to wild type cells (Fig. 4.2). Hence, although the levels of chromosome I were increased in *smt3* mutant cells similar to *ulp2* mutant cells, the levels of other specific chromosomes were also increased (Fig. 4.2). However, the basis of these changes is not clear. It is possible that *smt3* cells, like *ulp2* mutant cells, compensate for the partial loss of sumo function by increasing the levels of specific chromosomes, thereby increasing specific gene expression on these chromosomes. However, if this is the case then compensation of loss of sumo function likely involves gene expression that is not linked to suppression of the growth defects of *ulp2* mutants. Nevertheless, it is also possible that the aneuploidy detected in the *smt3* mutant cells is not adaptive but rather is a mitotic defect that is associated with loss of sumo function. Indeed, *smt3* mutants spend almost twice as long in G2/M compared to wild type cells (Fig. 4.1.E) suggestive that loss of sumo function impacts the timely progression through mitosis. However, it is unclear why only specific chromosomes would be affected by such a mitotic defect. Indeed, although the sixteen chromosomes of *S. cerevisiae* vary in size, from 0.23Mb to 1.53Mb, there does not appear to be any correlation between chromosome size and increased levels in the *smt3* mutant. For example, the levels of both chromosomes I and IV, which are the smallest (0.23Mb) and largest (1.53Mb) respectively, are increased in *smt3* mutant cells (Fig. 4.2). It must also be noted that the qPCR ploidy assay does not represent the chromosomal dynamics of an individual cell, rather the average chromosomal arrangement within a population of cells. Hence, it may be the case that individual *smt3* cells display different chromosomal dynamics, with Fig. 4.2 illustrating the average chromosomal arrangement observed in cells lacking sumo function.

Interestingly, recent evidence has also identified that dysregulation within the sumo conjugation pathway can lead to chromosomal duplications, suggesting that accurate sumo regulation is crucial for genomic integrity (Ryu and Hochstrasser, 2017). In agreement with

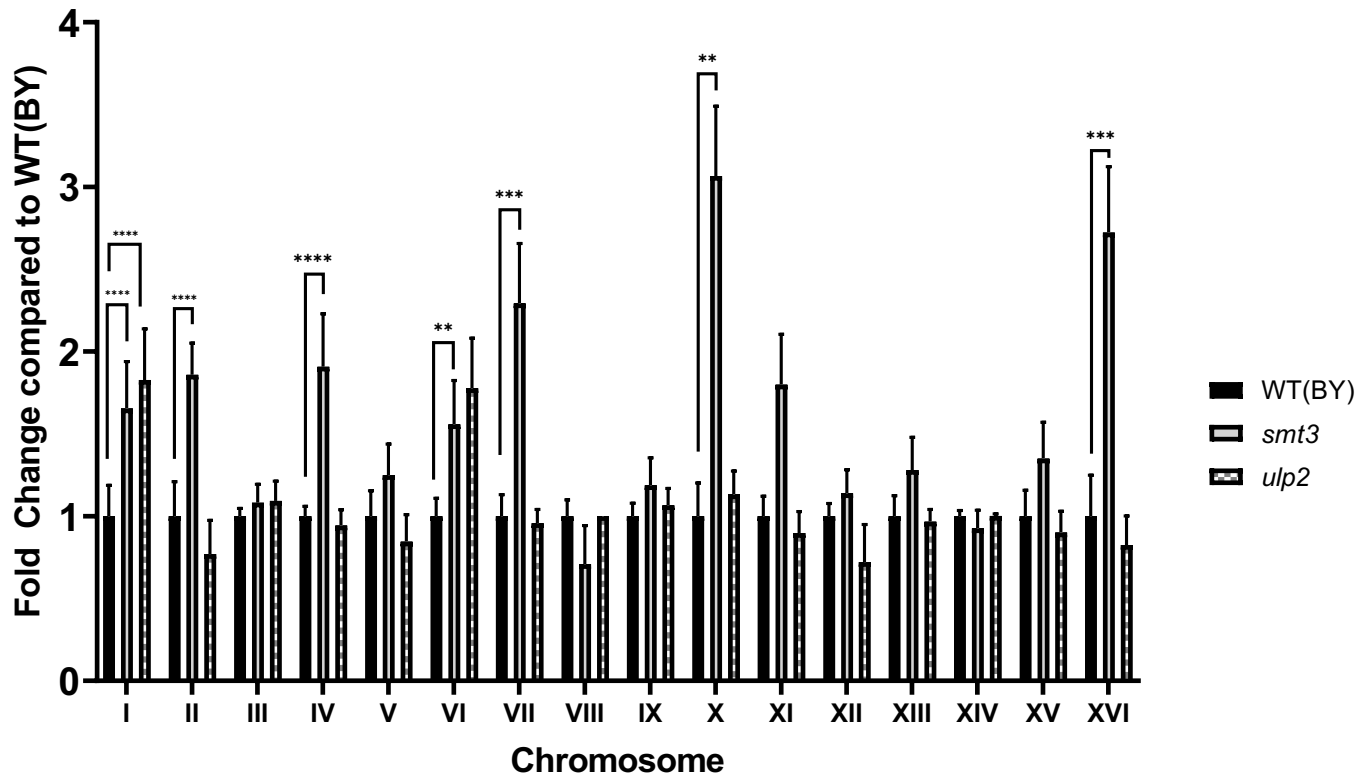


Figure 4.2 Loss of Smt3 function causes specific multichromosome aneuploidy. A chromosomal qPCR assay (ref) was performed on DNA extracted from mid-log phase growing wild type (GC1), *smt3* (GC16) and *ulp2* (GC30) cells using an alkaline lysis method adapted from Pavelka et al. (2010). 2.5µg of DNA was used in each qPCR reaction with primers specific for each chromosome (see Pavelka et al., 2010). Samples were normalised to the levels of *ALG9* and compared to the wild type control (BY) which was set at 1. Error bars represent SD from 3 biological repeats. P values were derived from an unpaired T-test.

these findings, Fig. 4.2 suggests that cells expressing reduced sumo function can also lead to chromosomal duplications. Taken together, our data suggest that reduced sumo function leads to specific chromosome aneuploidy that is different to the aneuploidy observed in response to loss of function of the Ulp2 desumoylase. In conclusion, our data suggests that accurate sumo function is critical for G2/M progression in addition to preventing aneuploidy.

4.2.3 The chromosomal location of the top 100 *smt3* suppressor proteins does not appear to correlate with aneuploidy in the *smt3* mutant

Previous work revealed that overexpression of specific genes on chromosome I were linked to the aneuploidy associated with the *ulp2Δ* strain (Ryu et al., 2016). Our investigation into the function(s) of Smt3 using an SGA screen have also identified specific genes whose expression influences the phenotypes associated with the loss of Smt3 function (see Chapter 1, section 1.4). In particular, the SGA screen revealed a number of mutations which suppressed or enhanced the slow growth defect associated with the DAMP allele of the *SMT3* gene (Lewis, 2016). Hence, it was possible that the specific aneuploidy associated with the *smt3* mutant was linked to some of these suppressors and/or enhancers. To investigate this possibility the chromosome locations of the top 100 suppressors and the top 100 enhancers were examined to reveal which, if any, of these genes are located on the six chromosomes whose levels were increased in *smt3* mutant cells (Fig. 4.3).

Of the eight chromosomes (I, II, IV, VI, VII, X, XI and XVI) whose levels were significantly increased in *smt3* mutant cells, surprisingly several of these chromosomes contain none of the top 100 suppressors. For example, none of the top 100 *smt3* suppressors are located on chromosomes I (Fig. 4.3) and only 2 out of the top 100 *smt3* suppressors are located on chromosome II. Furthermore, many suppressors are located on chromosomes whose levels were not increased in the *smt3* mutant (Fig. 4.3). For example, 16 of the top 100 *smt3* suppressors are located on chromosome XII which was unaffected in the *smt3* mutant (compare Figs. 4.2 and 4.3). With respect to the top 100 enhancers, although all of the chromosomes which displayed increased levels in *smt3* mutant cells contained some enhancers, there did not seem to be increased numbers of enhancers on these chromosomes

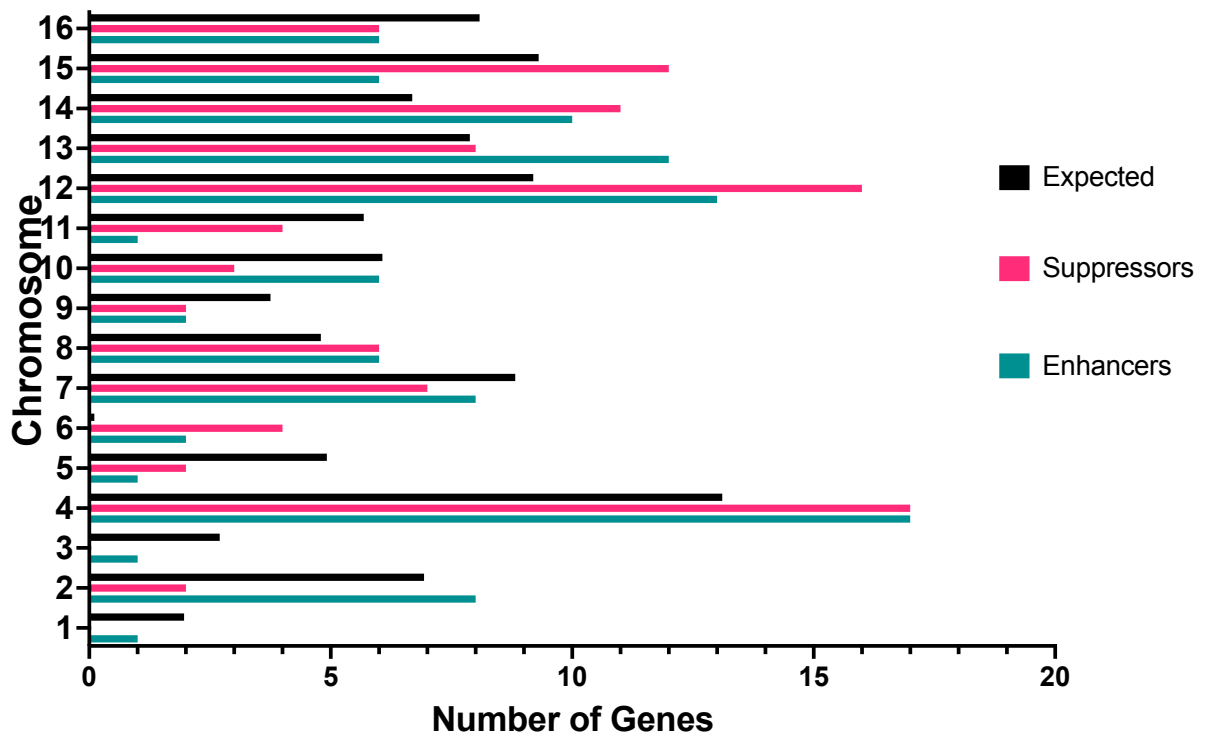
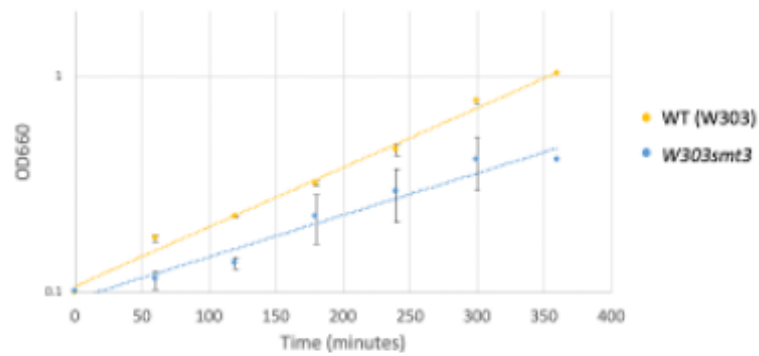
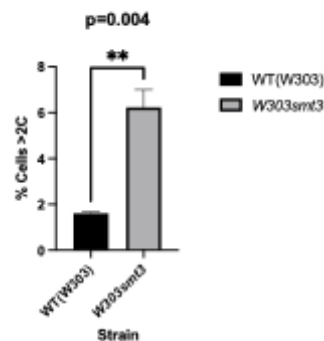


Figure 4.3 Analysis of the chromosomal locations of the top 100 suppressor and enhancer mutations identified in the *smt3* SGA screen. The chromosomal locations of the top 100 suppressor and enhancer mutations were compared to the “expected” predictions of numbers of suppressor and enhancer mutations for each chromosome based on chromosome size. The “expected” numbers for each chromosome were calculated using the formula: chromosome size/genome size x 100.

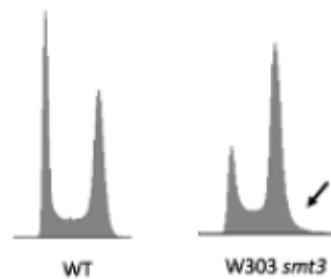
A.



B.



C.



D.

Strain	Doubling Time	G1	S	G2/M
WT(W303)	110±4	36±1	33±1	40.±2
W303 <i>smt3</i>	154±9	23±3	74±1	57±6

Figure 4.4 *smt3* mutant cells display similar cell cycle defects in different strain backgrounds. (A) Growth curves of mid-log phase growing cultures of wild type (GC2) and W303*smt3* (GC50) cells. Error bars represent SD from 3 biological repeats. (B) Gating analysis of the DNA content analyses in cells containing >2C DNA content. (C) DNA content analysis was performed on mid-log phase growing cultures of wild type (GC2) and W303*smt3* (GC50) cells and presented as indicated. P values were derived from an unpaired T-test. (D) Gating analysis of the DNA content analyses in (D) of the time cells spent in each stage of the cell cycle.

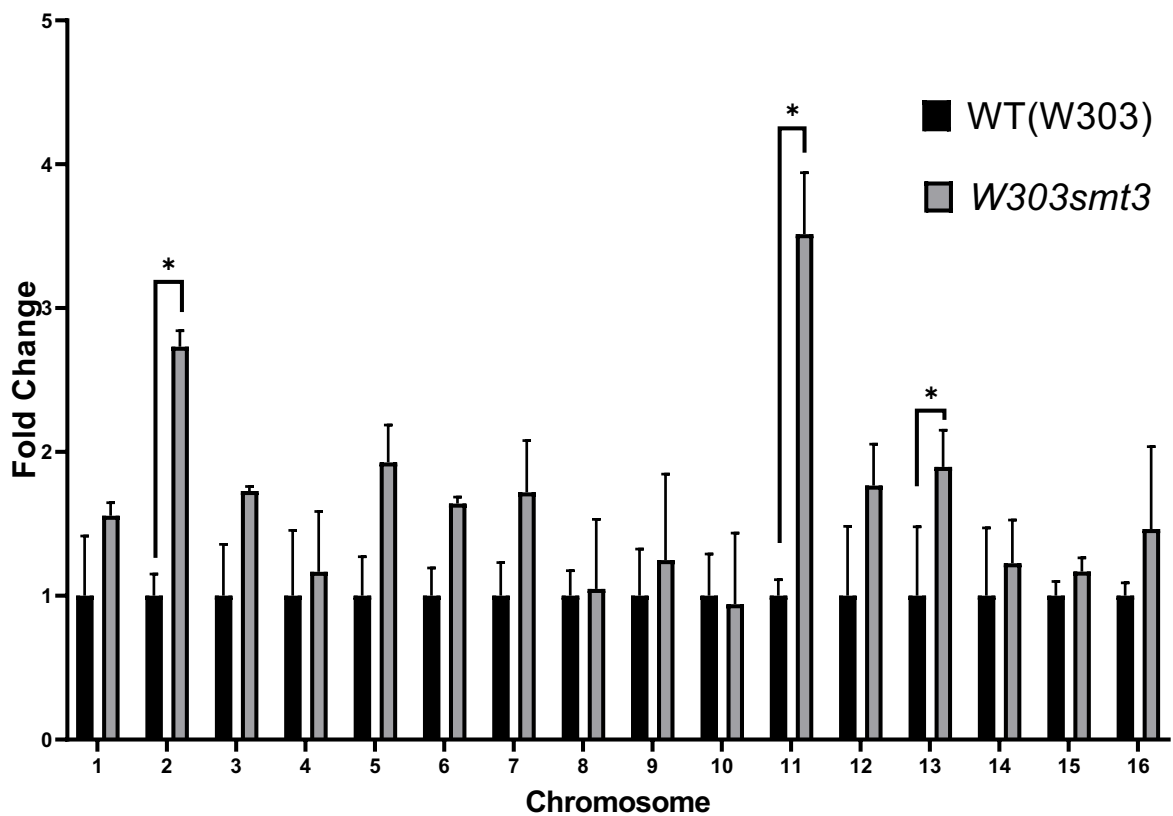


Figure 4.5 *smt3* mutant cells display similar multichromosome aneuploidy in different strain backgrounds. A chromosomal qPCR assay (Pavelka et al., 2010) was performed on DNA extracted from mid-log phase growing wild type (GC2) and *W303smt3* (GC50) cells using an alkaline lysis method adapted from Pavelka et al. (2010). 2.5 μ g of DNA was used in each qPCR reaction with primers specific for each chromosome (see Pavelka et al., 2010). Samples were normalised to the levels of *ALG9* and compared to the wild type control (GC2) which was set at 1. Error bars represent SD from 3 biological repeats. P values were derived from an unpaired T-test.

compared to other chromosomes whose levels were not affected in *smt3* mutant cells (compare Figs. 4.2 and 4.3). Hence, in conclusion, there is no clear evidence to suggest that the increased expression of any of the enhancers or suppressors is linked to the aneuploidy in the *smt3* mutant, although it is important to point that the analyses also does not exclude this possibility.

4.2.4 Loss of Smt3 function causes cell cycle defects in different strain backgrounds

As described in Chapter 3 the *smt3::DAmP* allele causes similar but also different phenotypes when expressed in different strain backgrounds (for example see Fig. 3.1 and Fig. 3.2). Hence, to gain further insights into the phenotypes associated with loss of Smt3 function, the cell cycle profile of the *smt3* mutant strain (GC50) in the W303 genetic background was explored. Similar to *smt3* mutant cells in BY4741 strain background, analysis of the growth of *smt3* mutant cells in the W303 background confirmed that cells with reduced levels of Smt3 grow considerably slower than wild type cells (Figure 4.4A). Interestingly, the growth rate analyses suggests that the doubling time of the *smt3* mutant in the W303 strain background (GC50) is 154 ± 9 minutes compared to a doubling time of 110 ± 4 minutes for the wild type control strain (GC2). Interestingly, the *W303smt3* (GC50) strain grew slightly slower than the BY4741 *smt3* (GC16) strain (compare Fig. 4.1E and 4.4E). However, it must also be noted that the BY4741 WT strain (GC1) grew marginally better than the W303 WT strain (GC2) (108 ± 2 minutes compared to 110 ± 4 minutes respectively) which may account for the *W303smt3* (GC50) strain growing slightly slower than the BY4741 *smt3* (GC16) strain. Nevertheless, *W303smt3* cells do show different sensitivities compared to the BY4741 *smt3* strain (Fig. 3.1C) which may also account for the differences in doubling times between the two *smt3* mutants.

Next, DNA content analysis was performed on cultures of the mid-log phase growing wild type (GC2) and *W303smt3* mutant (GC50) strains. As expected, these data revealed that a significant proportion of *W303smt3* cells (~6%, $p=0.004$) show >2C DNA content compared to the wild type control cells, confirming aneuploidy in dividing *W303smt3* cells (Figure 4.4). Hence, a significant level of aneuploidy is conserved in *smt3* mutants in different strain backgrounds (compare Figs. 4.1C/D and 4.4C/D). To further analyse the cell cycle defects associated with the *smt3* mutant in the W303 strain background the proportion of cells in each cell cycle phase was combined with the doubling times of the wild type (GC2) and *smt3*

(GC50) mutant strains to calculate the approximate time that wild type and *smt3* cells spend in each phase of the cell cycle (Fig. 4.4B). Similar to the *smt3* mutant in the BY4741 strain background, the *smt3* mutant in the W303 strain background also spends much longer in G2/M phases compared to wild type cells (compare Figs. 4.1E and 4.4B). In particular, *W303smt3* cells were found to spend ~57 minutes in G2/M phases in comparison to wild type cells which spend ~40 minutes in G2/M phases (Fig. 4.4B). In contrast to the BY4741 *smt3* (GC16) strain which spends ~72 minutes in G2/M phases, *W303smt3* (GC50) cells show a reduced mitotic delay, spending ~57 minutes in G2/M. (compare Fig.4.1E and 4.4B). Hence, the DNA content analyses suggest that *smt3* cells have similar defects in cell cycle progression through G2/M phases in different strain backgrounds, although the mitotic delay does appear to be greater in BY4741 *smt3* cells. Strikingly, dissimilar to BY4741 *smt3* cells, the *W303smt3* strain spends almost twice as long in S Phase compared to the respective wild type strain (Fig. 4.4B). This S phase delay is noticeable in Fig. 4.4D and may explain the differences in sensitivities between the *smt3* mutants in different strain backgrounds.

The next step was to investigate the similarities and differences in the aneuploidy of the *smt3* mutants in the BY4741 and W303 strain backgrounds. Hence, the qPCR chromosomal ploidy assay described above (see section 4.2.2) was applied to DNA extracted from W303 wild type (GC2) cells and *W303smt3* (GC50) cells (Fig. 4.5).

Interestingly, the chromosomal profiles of *smt3* mutant in the W303 strain background were found to overlap with, but also display differences to, the chromosome profiles of the *smt3* mutant in the BY4741 strain background. Indeed, the *smt3* mutant in the W303 strain background had increased levels of chromosomes I, II, V, VI, VII, XI, XII, XIII, and XVI, although only chromosomes II, XI and XIII were significantly increased (Fig. 4.5). Thus, increased levels of chromosomes I, II, XI, and XVI appears to be conserved between the two *smt3* mutants in different genetic backgrounds (compare Figs. 4.2 and 4.5). However, there are also differences in aneuploidy between the two *smt3* mutants. For example, the levels of chromosome IV are specifically increased in the *smt3* mutant in the BY4741 genetic background, whilst chromosomes III, V, XII and XIII are specifically increased in the *smt3* mutant in the W303 genetic background. The basis for these similarities and differences in aneuploidies between the two different *smt3* mutants is unclear. However, these results are consistent with the characterisation of the phenotypes of the *smt3* mutants in the BY4741

and W303 strain backgrounds which display both similarities and differences (compare Fig. 3.1 and Fig. 3.2/ compare Fig. 4.1 and Fig. 4.4). Although the relationships between these similarities and differences in phenotypes and aneuploidy between the *smt3* mutants, it is intriguing to speculate that they are interconnected. For example, perhaps altered expression of specific genes contributes to the differences in phenotypes that were detected. Furthermore, the conserved duplication of chromosomes I, II, VII and XI suggests that there are conserved links between sumo function and these chromosomes in these *smt3* mutants.

4.2.5 Polysumoylation mutants also show cell cycle defects

As described above, the loss of sumo function affects cell cycle progression and results in specific aneuploidy. However, it was not clear which aspects of sumoylation are linked to these cell cycle defects. Interestingly, previous studies revealed that cells lacking the ability to polysumoylate substrates had a much higher proportion of cells with >2N content compared to WT cells, although no further analysis was carried out to further characterise these cell cycle defects (Srikumar et al., 2013a). Hence, to gain further insight into the links between sumoylation and cell cycle progression the cell cycle parameters and aneuploidy of the *smt3-allR* mutant, which is unable to polysumoylate substrates, were investigated. Growth analysis of *smt3-allR* (GC57) mutant cells confirmed that cells where polysumoylation is prevented grow considerably slower than wild type (GC55) cells (Figure 4.6A). Indeed, comparison of growth rate analyses suggests that the doubling time of the *smt3-allR* mutant is 165 ± 7 minutes compared to a doubling time of 117 ± 3 minutes for the wild type control strain (Fig. 4.6E). Interestingly, the *smt3-allR* (GC55) strain grew slower than the *smt3* mutant in either strain background (compare Fig.4.6A with 4.1A/4.3A). Taken together, these growth analyses suggest that the type of sumo modification, polysumoylation, rather than mono or multisumoylation, is important for timely cell cycle progression.

Next, DNA content analysis was performed on cultures of the mid-log phase growing wild type (GC55) and *smt3-allR* mutant (GC57) strains. Consistent with the previous published work (Srikumar et al., 2013a), these data revealed that a significant proportion of *smt3-allR* cells (~6%, $p=0.0013$) show >2C DNA content compared to the wild type control cells, confirming aneuploidy in dividing *smt3-allR* cells (Fig. 4.6C/D). To further analyse the cell cycle defects

associated with the *smt3-allR* mutant the proportion of cells in each cell cycle phase was combined with the doubling times of the wild type and *smt3-allR* mutant strains to calculate the approximate time that wild type and *smt3-allR* cells spend in each phase of the cell cycle (Fig. 4.6B). Similar to the analyses of the *smt3* mutants in the BY4741 and W303 strain backgrounds, the *smt3-allR* mutant also spends much longer in G2/M phases compared to wild type cells (compare Figs. 4.1E and 4.4B with Fig 4.6B). Indeed, *smt3-allR* cells were found to spend ~54 minutes in G2/M phases in comparison to wild type cells which spend ~40 minutes in G2/M phases (Fig. 4.6B). Thus, the DNA content analyses suggest that *smt3* mutants have similar defects in cell cycle progression through G2/M phases in different strain backgrounds. However, it must be noted that the three different *smt3* mutant strains show differences in the time spent in G2/M phases. For example, BY4741 *smt3* (GC16) cells spend ~72 minutes in G2/M compared to ~57 and ~54 minutes in the *W303smt3* (GC50) and *smt3-allR* (GC57) strains, respectively. Hence, these data suggest that loss of sumo function contributes more towards the G2/M delay than the loss of polysumoylation (compare Figs. 4.1E and 4.4B with Fig 4.6B). Furthermore, although BY4741 *smt3* (GC16) cells do not display a severe S Phase delay (~39 minutes compared to ~32 minutes in the respective wild type), both *W303smt3* (GC50) and *smt3-allR* (GC57) strains show considerable delays in S Phase. For example, *W303smt3* (GC50) cells spend ~74 minutes in S Phase compared to ~33 minutes in wild type W303 cells (GC2) (Fig. 4.4E). In addition, *smt3-allR* (GC57) cells take ~64 minutes to complete S Phase compared to ~35 minutes in wild type (GC55) cells (Fig. 4.6E). Taken together, these results indicate that substrate polysumoylation is important for S Phase progression, whilst sumo function is critical for timely G2/M progression.

The next step in the characterisation of the *smt3-allR* mutant was to investigate the similarities and differences in the aneuploidy of the *smt3* and *smt3-allR* mutants in order to understand to the extent to which loss of polysumoylation contributes to the aneuploidy of the *smt3* mutants. Hence, the qPCR chromosomal ploidy assay described above (Fig. 4.2/4.5) was applied to DNA extracted from wild type (GC55) cells and *smt3-allR* (GC57) cells (Fig. 4.7). Interestingly, the chromosomal profiles of the *smt3-allR* mutant were found to overlap with, but also display differences to, the chromosomal profiles of the *smt3* mutants in both the BY4741 and W303 backgrounds (compare Figs. 4.2 and 4.5 with Fig. 4.7). For example, the *smt3-allR* mutant displayed increased levels of chromosomes II, III, IV, V, VI, VII, XI, XII (of

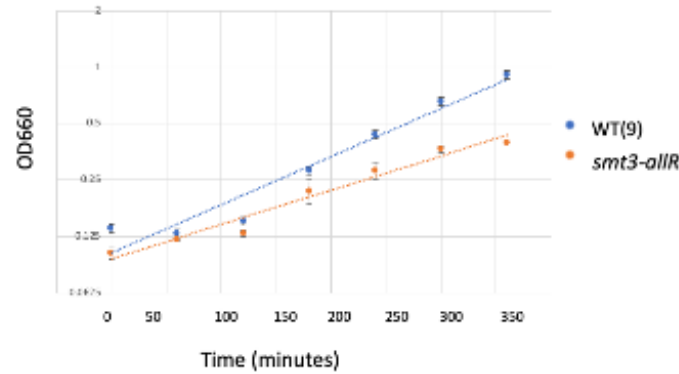
which chromosomes II, V, VI, VII and XII are significantly increased), but *smt3-allR* cells also showed decreased levels of chromosomes XIV and XV (Fig. 4.7). Chromosomes increased in either or both *smt3* mutants, chromosomes II, IV, VI, VII, and XI are also increased in the *smt3-allR* mutant although chromosomes I and XIII which are increased in both *smt3* mutants are not increased in the *smt3-allR* mutant (compare Figs. 4.2 and 4.5 with Fig. 4.7). Furthermore, chromosomes XIV, XV and XVI are decreased in the *smt3-allR* mutant but in neither *smt3* mutant. However, the basis for these differences between the various *smt3/smt3-allR* mutants is not clear. Nevertheless, these data suggest that the aneuploidy associated with the *smt3* mutants is not simply associated with loss of polysumoylation, although clearly the aneuploidy of several of the chromosomes is affected in all the different *smt3/smt3-allR* mutants. It is also interesting to note that several chromosomes in the *smt3-allR* mutant are present in more copies compared to the two *smt3* mutants (compare Figs. 4.2/4.5 with Fig. 4.7). For example, more copies of chromosome II were detected in the *smt3-allR* mutant compared to both *smt3* mutants. The explanation for this observation is unclear but it is interesting to speculate that the residual polysumoylation present in the *smt3* mutants inhibits this increased ploidy detected in the *smt3-allR* mutant.

Interestingly, one key difference between the *smt3* mutant in the BY4741 background and the *W303smt3* and *smt3-allR* strains is the time spent in S Phase. For example, the *W303smt3* and *smt3-allR* mutants both show an S phase delay, but this is not observed in the BY4741 *smt3* strain (compare Fig. 4.1D/E with Fig. 4.4D/E and 4.6D/E). Importantly, Smt3 levels are not altered in the *smt3-allR* strain (Srikumar et al., 2013a), confirming that it is the inability to form polysumo chains rather than the cellular levels of *smt3-allR* which contribute to the observed cell cycle delays. Interestingly, our results strongly suggest that it is not only the downregulation of Smt3 which leads to aneuploidy, but also that the inhibition of polysumo chain formation can influence chromosomal copy number (Figure 4.7). Consistent with the correlation between the inhibition of polysumoylation and the observed S phase delay (Fig. 4.6E), Srikumar et al. (2013) identified that ~144 proteins involved in the DNA replication and DNA damage repair pathways were found to be mislocalised in *smt3-allR* cells (Srikumar et al., 2013a). Hence, in agreement with Fig. 4.6, it appears that polysumoylation is critical for the timely progression through S Phase, although the role of polysumoylation in S Phase remains unclear (Srikumar et al., 2013a). Interestingly, the *W303smt3* (GC50) mutant also

shows a considerable S Phase delay (Fig. 4.4E). Thus, it would be interesting to identify whether, similar to the *smt3-allR* strain, the localisation of proteins associated with DNA replication and/or DNA damage pathways are altered in *W303smt3* cells. However, this will not be investigated further in this study.

Studies investigating the cell cycle dynamics of the STUbL mutants, *slx5Δ* and *slx8Δ*, revealed that *slx5Δ* and *slx8Δ* mutants display extensive aneuploidy and appear as large, budded cells showing a severe mitotic delay (van de Pasch et al., 2013). Furthermore, *slx8Δ* mutants show defective positioning of the mitotic spindle, typically spending ~80 minutes in G2/M phases (van de Pasch et al., 2013). Interestingly, *smt3* cells spend a similar amount of time in G2/M as *slx8Δ* mutants (*smt3* spends ~72 minutes in G2/M compared to ~80 minutes in *slx8Δ* and ~40 minutes in wild type cells (Fig. 4.1E)(van de Pasch et al., 2013)), thus it is tempting to speculate whether spindle defects in the *smt3* strain also contribute to the G2/M delay (van de Pasch et al., 2013). Indeed, Dr. Lewis identified that microtubule length is reduced in *smt3* cells, resulting in mitotic spindles unable to attach to opposite poles of the cell (Lewis, 2016). Hence, the aberrant microtubule dynamics associated with the loss of sumo function may contribute to the mitotic delay observed in *smt3* (GC16) cells. Similar to the *smt3* mutants characterised in this study, *slx8Δ* cells also display aneuploidy (van de Pasch et al., 2013). However, *slx8Δ* cells show a >2C DNA content of ~16.5%, which is significantly higher than the ~6% >2C DNA content associated with the *smt3/ smt3-allR* mutants analysed in this thesis. Although the extent of *slx8Δ* chromosomal duplications were not analysed by van de Pasche et al. (2013), microarray analysis of *slx8Δ* mutants indicated that gene expression is significantly upregulated throughout the genome of *slx8Δ* cells, although almost all of the genes located on chromosomes XI and XIII are significantly upregulated >3 fold compared to wild type cells (van de Pasch et al., 2013). Interestingly, our data suggests that chromosomes XI and XIII are also duplicated in *smt3*, *w303smt3* and *smt3-allR* cells (Fig. 4.2, Fig. 4.5 and Fig. 4.7), suggesting that both inhibiting and enhancing the levels of polysumo chains in the cell results in similar patterns of aneuploidy. It must also be noted that *slx8Δ* mutants are isogenic to the S288c strain background, an *S. cerevisiae* strain background not analysed in this study. Hence, these data suggest that sumo mutants in the S288c strain background in addition to the three different strain backgrounds analysed in Fig. 4.1/2, Fig. 4.4/5 and Fig. 4.6/7 are associated with aneuploidy.

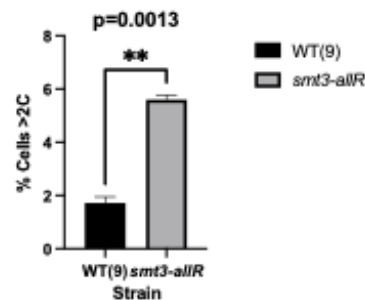
A.



B.

Strain	Doubling Time	G1	S	G2/M
WT(9)	117±3	38±3	35±1	40±2
<i>smt3-allR</i>	165±7	31±1	64±1	54±1

C.



D.

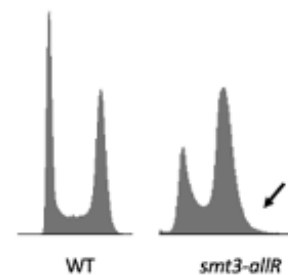


Figure 4.6 *smt3* cell cycle phenotypes are conserved in the *smt3-allR* strain. (A) Growth curves of mid-log phase growing cultures of wild type (GC55) and *smt3-allR* (GC57) cells. Error bars represent standard error from 3 biological repeats. (B) Gating analysis of the DNA content analyses in (D) of the time cells spent in each stage of the cell cycle. (C) Gating analysis of the DNA content analyses in cells containing >2C DNA content. P values were derived from an unpaired T-test. (D) DNA content analysis was performed on mid-log phase growing cultures of wild type (GC2) and W303*smt3* (GC50) cells and presented as indicated.

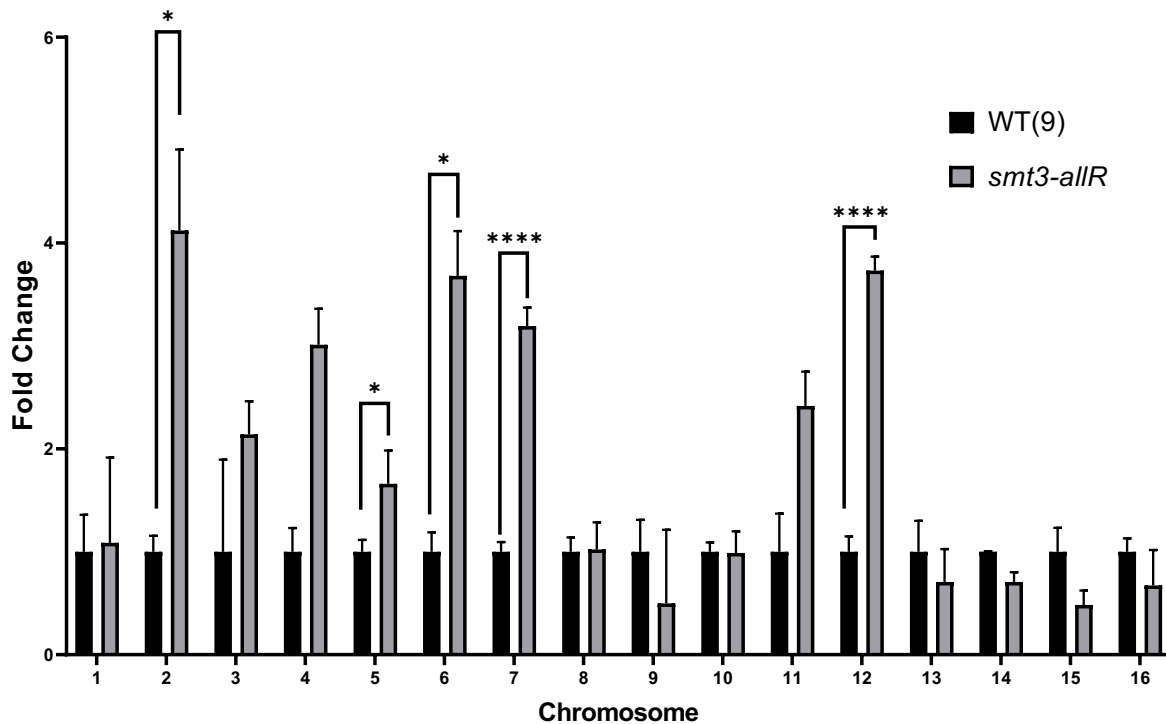


Figure 4.7 Loss of polysumoylation causes specific multichromosome aneuploidy. A chromosomal qPCR assay (Pavelka et al., 2010) was performed on DNA extracted from mid-log phase growing wild type (GC55) and *smt3-allR* (GC57) cells using an alkaline lysis method adapted from Pavelka et al. (2010). 2.5µg of DNA was used in each qPCR reaction with primers specific for each chromosome (see Pavelka et al., 2010). Samples were normalised to the levels of *ALG9* and compared to the wild type control (GC2) which was set at 1. Error bars represent SD from 3 biological repeats. P values were derived from an unpaired T-test.

In conclusion, from the above results, data in this chapter has characterised the aneuploidy associated with the loss of sumo function and the loss of polysumoylation. Our data suggests that *smt3* aneuploidy is conserved in different strain backgrounds whilst the inhibition of polysumoylation in the *smt3-allR* mutant is also associated with cells with significantly higher >2C DNA content compared to wild type cells (Fig. 4.1, Fig. 4.4, Fig. 4.6). Interestingly, the DNA content analyses suggest that the *smt3/smt3allR* mutants have similar defects in cell cycle progression through G2/M phases, although the *W303smt3* (GC50) and *smt3-allR* (GC57) mutants also show S Phase delays which are not observed in the *smt3* (GC16) strain. Furthermore, chromosomal ploidy assays indicate that duplications of chromosomes II, III and XI are conserved between the *smt3/smt3allR* mutants analysed in this study, although the basis of these specific chromosomal duplications remain unclear. Loss of sumo function appears to be connected with a delay in G2/M phases, whereas inhibition of polysumoylation appears to be more closely associated with an S Phase delay, suggesting that polysumoylation is important during S Phase (compare Fig 4.1 with Fig. 4.6). However, it must also be noted that although polysumoylation is prevented in *smt3allR* cells, *smt3* mutants in the BY471 and W303 strain backgrounds will also have a reduction in polysumoylation. Hence, these results suggest that polysumoylation in addition to sumo function appears to be important for timely progression through the cell cycle. To conclude, it appears that the loss of sumo function and the loss of polysumoylation both contribute to the aneuploidy and cell cycle defects observed in the *smt3* mutant (GC16, GC50 and GC57) strains.

4.2.6 Suppression of *smt3* associated defects by mutations of the Arp2/3 complex and the CCT complex

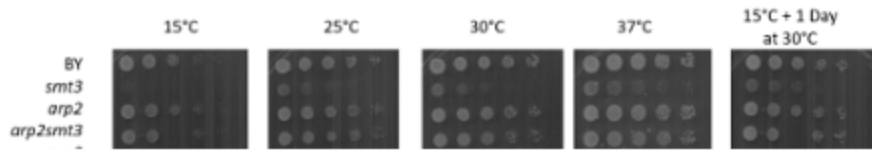
As described earlier in this thesis, an SGA screen performed in the laboratory identified multiple novel suppressors of the slow growth defects associated with the *smt3::DAmP* allele (see section 1.4). Notably, several independent mutations in the conserved Arp2/3 complex or the conserved CCT complex when combined with the *smt3* allele recovered the sumo-linked growth defects (Lewis, 2016). The results described earlier in this chapter revealed that the *smt3* mutant in the BY4741 strain background has cell cycle defects progressing through G2/M phases and displays specific multichromosome aneuploidy (Fig. 4.1 and Fig. 4.2). Hence

it was possible that the mutations of the Arp2/3 and/or CCT complexes may suppress some or all of these cell cycle and aneuploidy defects associated with the *smt3* allele.

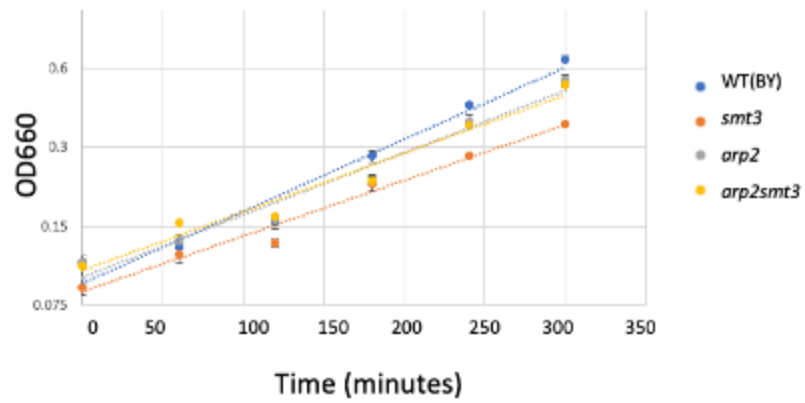
4.2.6.1 Investigation of mutations of the Arp2/3 complex

The highly conserved seven protein Arp2/3 complex binds to actin to enable the branching of actin filaments (see Chapter 1, section 1.4.2.3) (Goley and Welch, 2006). Remarkably, DAmP alleles of the genes encoding three of the Arp2/3 complex subunits, Arp2, Arp3 and Arc35, were very good suppressors of the growth defects associated with the *smt3::DAmP* allele (see section 1.4.2, Fig. 4.8A, Fig 4.9A). All seven Arp2/3 complex subunits are essential in *S. cerevisiae*, thus only DAmP alleles were available for study in the *smt3* SGA screen (see Chapter 1, section 1.4.2.3). In addition, these DAmP alleles of the Arp2/3 complex rescue the growth defects of the *smt3* mutant at a range of temperatures (Fig. 4.8A, Fig4.9A). In agreement with the SGA analysis (Lewis, 2016), growth curves confirmed that the *arp2smt3* and *arp3smt3* double mutants grow much better than the single *smt3* mutant (Fig. 4.8B, Fig4.9B). Furthermore, the growth of *arc35smt3* was also found to improve growth compared to the *smt3* single mutant (data not shown). Indeed, the growth rate analyses suggests that the doubling times of the *arp2* (GC10), *arp3* (GC11), *arp2smt3* (GC17) and *arp3smt3* (GC19) mutants are 126 ± 7 minutes, 12 ± 2 minutes, 133 ± 2 minutes, and 128 ± 2 minutes respectively compared to a doubling time of 108 ± 2 minutes and 144 ± 3 minutes for the wild type control strain (GC1) and the *smt3* mutant, respectively. Interestingly, both the *arp2* and *arp3* single mutants grew slightly slower compared to the wild type control, although the reason for this slower growth is unclear (Fig 4.8A, Fig4.9A). Nevertheless, although the growth of the double mutants *arp2smt3* and *arp3smt3* were slightly slower compared to the *arp2* and *arp3* single mutants (~ 126 minutes for *arp2* compared to ~ 133 minutes for *arp2smt3* and ~ 124 minutes for *arp3* compared to ~ 118 minutes for *arp3smt3*), both *arp2smt3* and *arp3smt3* grew significantly better compared to the single *smt3* mutant (~ 144 minutes). Thus, these analyses suggest that a reduction in *ARP2* or *ARP3* expression improves the fitness of the single *smt3* mutant strain. Interestingly, Dr. Lewis analysed *SMT3* expression in the *arp2smt3* and *arp3smt3* double mutants to identify whether *SMT3* expression was rescued in either of the double mutant strains (Dr. Lewis, personal communication). Strikingly, *SMT3* expression was

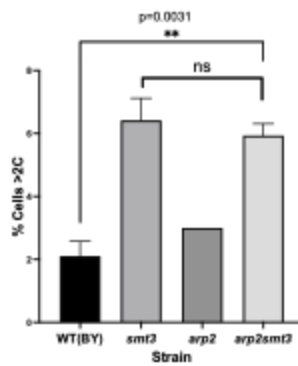
A.



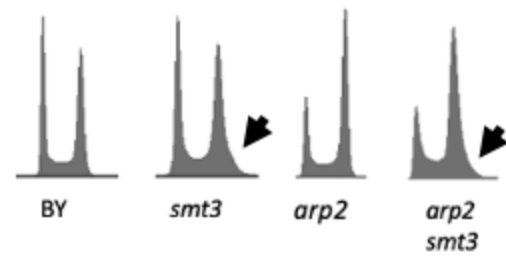
B.



C.



D.

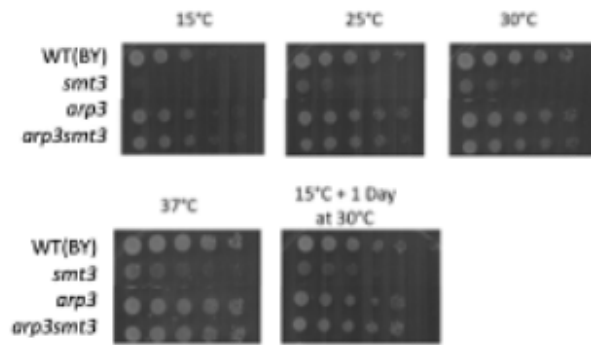


E.

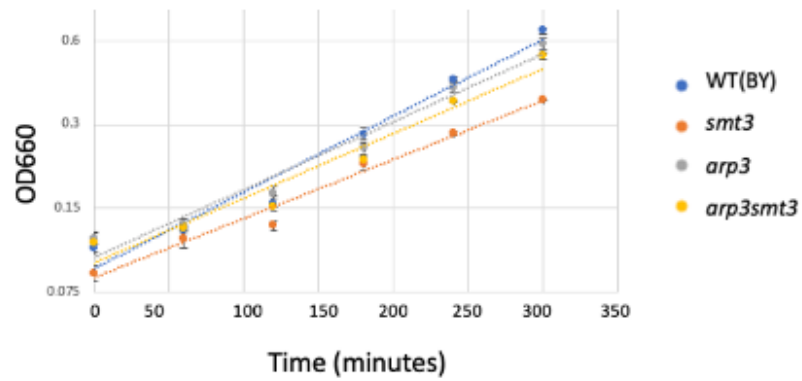
Strain	Doubling Time	G1	S	G2/M
WT(BY)	108±2	36±3	32±1	40±3
<i>smt3</i>	144±3	30±1	39±2	72±2
<i>arp2</i>	126±7	34	35	50
<i>arp2smt3</i>	133±2	42±1	43±1	39

Figure 4.8 *smt3* cell cycle phenotypes are rescued in the *arp2smt3* double mutant. (A) Five-fold serial dilutions of mid-log growing cultures GC1, GC16, GC10 and GC17 cells were spotted onto YPD plates using a 48-pin tool and then incubated at the indicated temperatures. (B) Growth curves of mid-log phase growing cultures of GC1, GC16, GC10 and GC17 cells. Error bars represent SD from 3 biological repeats. (C) Gating analysis of the DNA content analyses in (D) of cells containing >2C DNA content. (D) DNA content analysis was performed on mid-log phase growing cultures GC1, GC16, GC10 and GC17 cells and presented as indicated. (E) Gating analysis of the DNA content analyses in (D) of the time cells spent in each stage of the cell cycle.

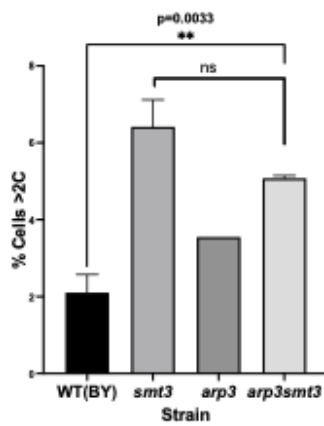
A.



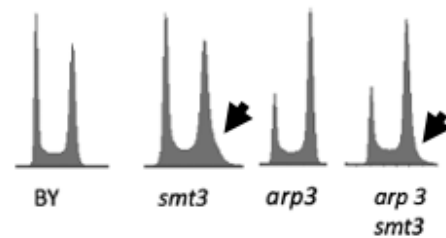
B.



C.



D.



E.

Strain	Doubling Time	G1	S	G2/M
WT(BY)	108±2	36±3	32±1	40±3
<i>smt3</i>	144±3	30±1	39±2	72±2
<i>arp3</i>	124±2	33	33	53
<i>arp3smt3</i>	128±2	44	40±1	35±4

Figure 4.9 *smt3* cell cycle phenotypes are rescued in the *arp3smt3* double mutant. (A) Five-fold serial dilutions of mid-log growing cultures GC1, GC16, GC11 and GC19 cells were spotted onto YPD plates using a 48-pin tool and then incubated at the indicated temperatures. (B) Growth curves of mid-log phase growing cultures of GC1, GC16, GC11 and GC19 cells. Error bars represent SD from 3 biological repeats. (C) Gating analysis of the DNA content analyses in (D) of cells containing >2C DNA content. (D) DNA content analysis was performed on mid-log phase growing cultures GC1, GC16, GC11 and GC19 cells and presented as indicated. (E) Gating analysis of the DNA content analyses in (D) of the time cells spent in each stage of the cell cycle.

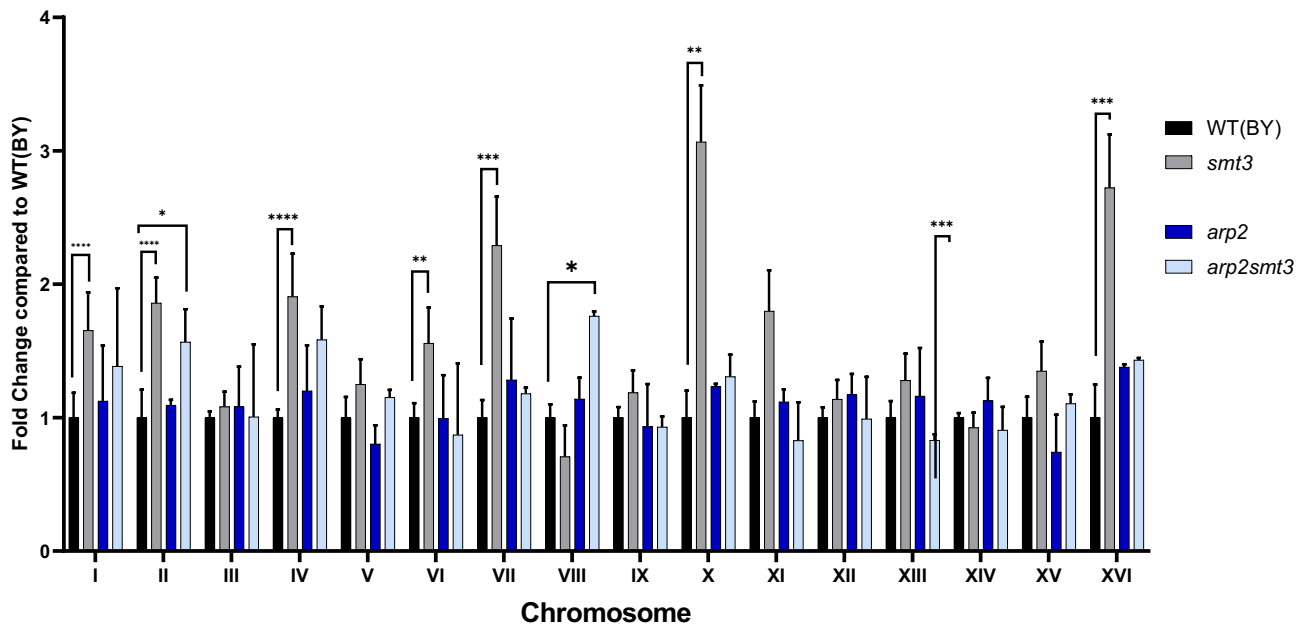


Figure 4.10 The *arp2smt3* mutant displays specific aneuploidy. A chromosomal qPCR assay (Pavelka et al., 2010) was performed on DNA extracted from mid-log phase growing wild type (GC1), *smt3* (GC16), *arp2* (GC10) and *arp2smt3* (GC17) cells using an alkaline lysis method adapted from Pavelka et al. (2010). 2.5mg of DNA was used in each qPCR reaction with primers specific for each chromosome (see Pavelka et al., 2010). Samples were normalised to the levels of *ALG9* and compared to the wild type control (GC2) which was set at 1. Error bars represent SD from 3 biological repeats. P values were derived from an unpaired T-test, (*) indicates $p < 0.05$, (**) indicates $p < 0.01$ and (***) indicates $p < 0.001$.

not rescued in either *arp2smt3* or *arp3smt3* strains, remaining at ~10% of *SMT3* expression observed in wild type cells (Dr. Lewis, personal communication). Hence these results suggest that the rescue of *smt3* growth in the *arp2smt3* and *arp3smt3* double mutants is not due to increased expression of *SMT3* in these cells. Next, DNA content analysis was performed on cultures of the mid-log phase growing wild type (GC1), *smt3* (GC16), *arp2* (GC10), *arp3* (GC11), *arp2smt3* (GC17), and *arp3smt3* (GC19) strains (Fig. 4.8C/D, Fig. 4.9C/D). As expected, the DNA content analyses also revealed that a larger proportion of *smt3* cells (~6%) show >2C DNA content compared to the wild type control cells (Fig. 4.8C, Fig. 4.9C). Interestingly, a slight increase in aneuploidy was detected in the single *arp2* and *arp3* single mutants, although it must be noted that only one biological repeat was performed on these strains, thus further repeats are required to determine whether this aneuploidy is consistent with the single *arp2* and *arp3* single mutants. Nevertheless, significant aneuploidy was detected in both the *arp2smt3* and *arp3smt3* double mutants, with ~6% and ~5% >2C DNA content displayed in *arp2smt3* and *arp3smt3* strains respectively (Fig. 4.8C, Fig. 4.9C). Strikingly, both the *arp2smt3* and *arp3smt3* >2C DNA content are not significantly different to the *smt3* >2C DNA content (Fig. 4.8C, Fig. 4.9C). Thus, in conclusion, it appears that neither *arp2smt3* nor *arp3smt3* double mutants are able to rescue the aneuploidy displayed in the *smt3* mutant.

To further analyse the cell cycle defects associated with the *arp2*, *arp3*, *arp2smt3* and *arp3smt3* mutants, the proportion of cells in each cell cycle phase was combined with the doubling times of the *Arp2/3* single and double mutants in addition to *smt3* and the wild type control to calculate the approximate time that each strain spends in each phase of the cell cycle (Fig. 4.8E, Fig. 4.9E). Strikingly, both the *arp2smt3* and *arp3smt3* double mutants spend less time in G2/M compared to the *smt3* single mutant (~72 minutes in *smt3* cells compared to ~39 minutes and ~35 minutes in *arp2smt3* and *arp3smt3* cells respectively). Indeed, the time spent in G2/M in the *arp2smt3* and *arp3smt3* double mutants is extremely similar to that of wild type cells (~40 minutes). Thus, the *arp2smt3* and *arp3smt3* double mutants have increased fitness compared to the *smt3* single mutant whilst also rescuing the G2/M delay associated with the *smt3* strain (Fig 4.8E, Fig. 4.9E). It is also interesting to note that the *arp2smt3* and *arp3smt3* mutants show a slight delay in G1 and S Phase compared to the *smt3* mutant (Fig 4.8E, Fig. 4.9E). *smt3* cells complete G1 in ~30 minutes and S Phase in ~39 minutes compared to ~42 minutes and ~43 minutes in *arp2smt3* cells and ~44 minutes and ~40

minutes in *arp3smt3* cells (Fig 4.8E, Fig. 4.9E). Hence, these data suggest that although *arp2smt3* and *arp3smt3* reduce the *smt3* G2/M delay, the doubling times of *arp2smt3* and *arp3smt3* are slightly slower than wild type cells due to a slight delay in G1 and S Phase (Fig 4.8A/E, Fig. 4.9A/E).

The above results suggest that mutations of the Arp2/3 complex do not significantly influence the aneuploidy associated with loss of sumo function (Fig. 4.8C, Fig. 4.9C). Hence, to confirm this hypothesis, the qPCR chromosomal ploidy assay described above (see section 4.2.2) was applied to DNA extracted from wild type (GC1), *smt3* (GC16), *arp2* (GC10) and *arp2smt3* (GC17) cells (Fig. 4.10). As expected, the *smt3* mutant in the BY4741 background had increased levels of chromosomes I, II, IV, VI, VII, X, XI and XVI (Fig. 4.10). Furthermore, there was only slight aneuploidy in the single *arp2* mutant, confirming the DNA content analysis, suggesting that chromosome XVI was present in slightly higher levels compared to the wild type, although this was not significantly increased (Fig. 4.10). Surprisingly, only the levels of chromosome II, XIII and XVI were increased in the *arp2smt3* double mutant (chromosomes II and XIII were significantly increased), whilst the levels of chromosomes I, III, IV, and XI were not significantly different from the wild type control (Fig. 4.10). Taken together, although the DNA content analysis suggested that the *smt3* and *arp2smt3* strains have almost identical levels of >2C DNA content, the pattern of aneuploidy is distinctly different (compare Figs. 4.8C and 4.10). However, it must be noted that the qPCR ploidy assay represents a population of cells, rather than the chromosomal profile of a single cell. Thus, individual cells may have slightly different chromosomal profiles to one another dependant on the number of generations in which the cells have passed through. Although the *arp2smt3* double mutant was obtained by Dr. Lewis from the SGA screen, it is unknown how many generations this strain has passed through prior to the use of the *arp2smt3* double mutant in this study. Nevertheless, it can be concluded that *arp2smt3* cells show a pattern of chromosomal duplications different to the *smt3/smt3allR* strains.

Interestingly, the results from Figs. 4.8, 4.9 and 4.10 suggest that the Arp2/3 complex is linked to the nuclear defects associated with loss of sumo and, furthermore, that the growth defects associated with loss of sumo is linked to the aneuploidy in *smt3* mutant cells. Although the function(s) of the Arp2/3 complex has largely been characterised in the cytoplasm, several studies have also proposed a nuclear role for the Arp2/3 complex. For example, it has been

suggested that the Arp2/3 complex may localise to sites of DNA damage (Yoo et al., 2007, Schrank et al., 2018). Hence, the nuclear role of the Arp2/3 complex (or of specific Arp2/3 subunits) may be important in S Phase, suggestive as to why the *arp2smt3* and *arp3smt3* mutants show a slight S Phase delay. However, the basis for this S Phase delay in the *arp2smt3* and *arp3smt3* strains remains unclear.

It is also intriguing to note that the levels of chromosome II are significantly increased in the *arp2smt3* mutant (Fig. 4.10), both of the *smt3* mutants in the different genetic backgrounds (Figs. 4.2 and 4.5) and also in the *smt3-allR* mutant (Fig. 4.7). Hence, this observation raises the possibility that increased levels of chromosome II, perhaps through upregulation of gene(s) located on this chromosome, may be crucial for viability in cells containing the *smt3* allele.

In conclusion, it appears that whilst mutations of Arp2/3 complex rescue the poor growth associated with the *smt3* single mutant, the *smt3* aneuploidy is not rescued in either *arp2smt3* or *arp3smt3* double mutants (Fig. 4.10). Hence, these results suggest that the loss of sumo is linked to aneuploidy in *smt3* cells and that restoration of growth in the *arp2smt3* and *arp3smt3* mutants does not significantly alter the >2C DNA content (Fig. 4.8C/ 9C). Surprisingly, the pattern of aneuploidy differs in the *arp2smt3* and *arp3smt3* mutants compared to the *smt3* single mutant, whilst the fitness of the *arp2smt3* and *arp3smt3* double mutants is vastly improved compared to the *smt3* single mutant, reducing the G2/M delay back to wild type levels (Fig. 4.8A/B/E, Fig. 4.9A/B/E).

4.2.6.2 Investigation of mutation of the CCT complex

The evolutionarily conserved CCT complex is a double octameric complex that consists of eight proteins, Cct1-8 (see section 1.4.2.2) (Stoldt et al., 1996). The CCT complex functions as a molecular chaperonin which facilitates protein folding, with substrates including cytoskeleton proteins such as tubulin and actin (see section 1.4.2.2) (Llorca et al., 2001). All eight subunits of the CCT complex are essential in *S. cerevisiae*, thus only DAmP alleles were available for study in the *smt3* SGA screen (see section 1.4.2). Interestingly, the DAmP allele of the gene encoding the CCT complex subunit Cct8, was a very good suppressor of the growth defects associated with the *smt3::DAmP* allele (see section 1.4.2). As mentioned in section

4.2.6.1, although the *arp2smt3* and *arp3smt3* double mutants rescue the poor growth of the *smt3* mutant, *SMT3* expression is not restored in either of the *arp2smt3* and *arp3smt3* double mutants (Dr. Lewis, personal communication). Hence, as the *cct8::DAMP* (*cct8*) allele was an extremely good suppressor of *smt3* identified from the SGA, it was important to characterise *SMT3* expression in both the *cct8* single and *cct8smt3* double mutant strains. Therefore the levels of *SMT3* RNA were examined in *his3* (GC51), *smt3* (GC16), *cct8* (GC97) and *cct8smt3* cells (GC99). As expected, the levels of *SMT3* RNA were significantly reduced in *smt3* cells (Fig. 4.11). Furthermore, the levels of *SMT3* RNA did not significantly increase in the *cct8smt3* double mutant suggesting that the ability of the *cct8* allele to recover growth phenotypes associated with the *smt3* allele are not linked to any effect of the *cct8* allele on *SMT3* gene expression (Fig. 4.11). Surprisingly, although not as low as the *smt3* mutant, the levels of *SMT3* RNA were found to be lower in the single *cct8* mutant (Fig. 4.11). The basis of this effect of the *cct8* allele on *SMT3* expression is not clear, although it must be noted that analysis of *SMT3* expression in the *cct8* mutant has only been performed once and will require further biological repeats.

Interestingly, levels of the CCT ϵ subunit have been shown to influence transcription of the cytoskeletal protein actin in mammalian cells (Elliott et al., 2015). Hence it has been proposed that the CCT complex may regulate transcription in addition to the established chaperonin function of the CCT complex (Elliott et al., 2015). Additionally, Kane et al. (2004) identified that RNA levels of *CCT8* and *SUMO-1* in mammalian cells were both decreased when cells were treated with nicotine (Kane et al., 2004). Hence, this study provides a link between the regulation of *CCT8* and *SMT3* expression, although the regulation of nicotine-induced gene expression remains unclear. Nevertheless, it is interesting to note that our data also suggests that downregulation of *SMT3* may influence *CCT8* expression (Fig. 4.11). Taken together, these data suggest that the regulation of *CCT8* and *SMT3* may be linked, although further studies are required to test this hypothesis.

Consistent with the SGA analyses, the *cct8* allele was an extremely good suppressor of the growth defects associated with the *smt3* allele at a range of temperatures (Fig. 4.12A). Furthermore, in agreement with the SGA analysis (Lewis, 2016), growth curves confirmed that the *cct8smt3* double mutant grows much better than the single *smt3* mutant (Fig. 4.12B).

Indeed, the growth rate analyses suggests that the doubling times of the *cct8* and *cct8smt3* mutants are 126 ± 1 minute and 124 ± 6 minutes respectively, compared to a doubling time of 108 ± 2 and 144 ± 3 minutes for the wild type control strain and the *smt3* mutant, respectively (Fig. 4.12E). Similar to the *arp2* and *arp3* single mutants, *cct8* grows slightly slower than wild type cells (~ 126 minutes for *cct8* compared to ~ 108 minutes in the wild type) (Fig. 4.12A/E compared to Fig. 8A/E and Fig. 9A/E). Nevertheless, the poor growth of the *smt3* strain is improved in the *cct8smt3* double mutant (~ 144 minutes doubling time in the *smt3* strain compared to ~ 124 minutes in the *cct8smt3* strain). However, it must be noted that the rescue of *smt3* growth in the *cct8smt3* double mutant is not restored back to wild type levels, but instead is restored to the level of growth displayed by the *cct8* single mutant (Fig. 4.12E).

Next, DNA content analysis was performed on cultures of the mid-log phase growing wild type (GC1), *smt3* (GC16), *cct8* (GC97) and *cct8smt3* (GC99) strains (Fig. 4.12 C/D). To assess the effects of the mutation of the CCT complex on the cell cycle defects associated with the *smt3* mutant the proportion of cells in each cell cycle phase was combined with the doubling times of the wild type, *smt3*, *cct8* and *cct8smt3* strains to calculate the approximate time that each strain spends in each phase of the cell cycle (see section 4.2.2, Fig. 4.12E). Interestingly, the *smt3* G2/M delay is greatly reduced in the *cct8smt3* double mutant (~ 72 minutes for *smt3* compared to ~ 47 minutes for *cct8smt3*) (Fig. 4.12E). However, in contrast to the *arp2smt3* and *arp3smt3* double mutants which reduce the *smt3* G2/M delay back to wild type levels (Fig. 4.8E, Fig. 4.9E), the *smt3* G2/M delay is only reduced to ~ 47 minutes in the *cct8smt3* double mutant, which is strikingly similar to the G2/M delay associated with the *cct8* single mutant (~ 48 minutes). Thus, to conclude, it appears that the *smt3* G2/M delay and slow growth are improved in the *cct8smt3* double mutant, but these cell cycle defects are not restored back to wild type levels (Fig, 4.12A/B/E).

As expected, the DNA content analyses also revealed that a larger proportion of *smt3* cells ($\sim 6\%$) show $>2C$ DNA content compared to the wild type control cells (Figure 4.12C). Interestingly, no increase in aneuploidy was detected in the single *cct8* single mutant and, moreover, similar levels of aneuploidy to the *smt3* mutant were detected in the *cct8smt3* double mutant (Fig. 4.12C). Hence, these results suggest that the *cct8* mutation of the CCT complex does not influence the aneuploidy associated with loss of sumo function (Fig. 4.12C). However, to confirm this suggestion the qPCR chromosomal ploidy assay described above

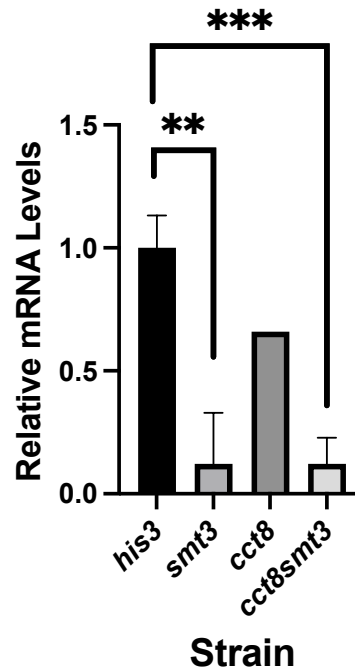


Figure 4.11 *SMT3* gene expression is not rescued in the *cct8smt3* double mutant. The relative expression of *SMT3* was analysed in indicated strains (GC51, GC16, GC97 and GC99). RNA was extracted from midlog growing cultures, RT-qPCR analyses performed using *SMT3* Forward and *SMT3* Reverse primers (Table 2.4) and transcripts normalised to the RNA levels of the *ALG9* gene. Error bars represent SD based on three biological repeats (n=1 for *cct8*). P values were derived from an unpaired T-test, (*) indicates $p < 0.05$, (**) indicates $p < 0.01$ and (***) indicates $p < 0.001$.

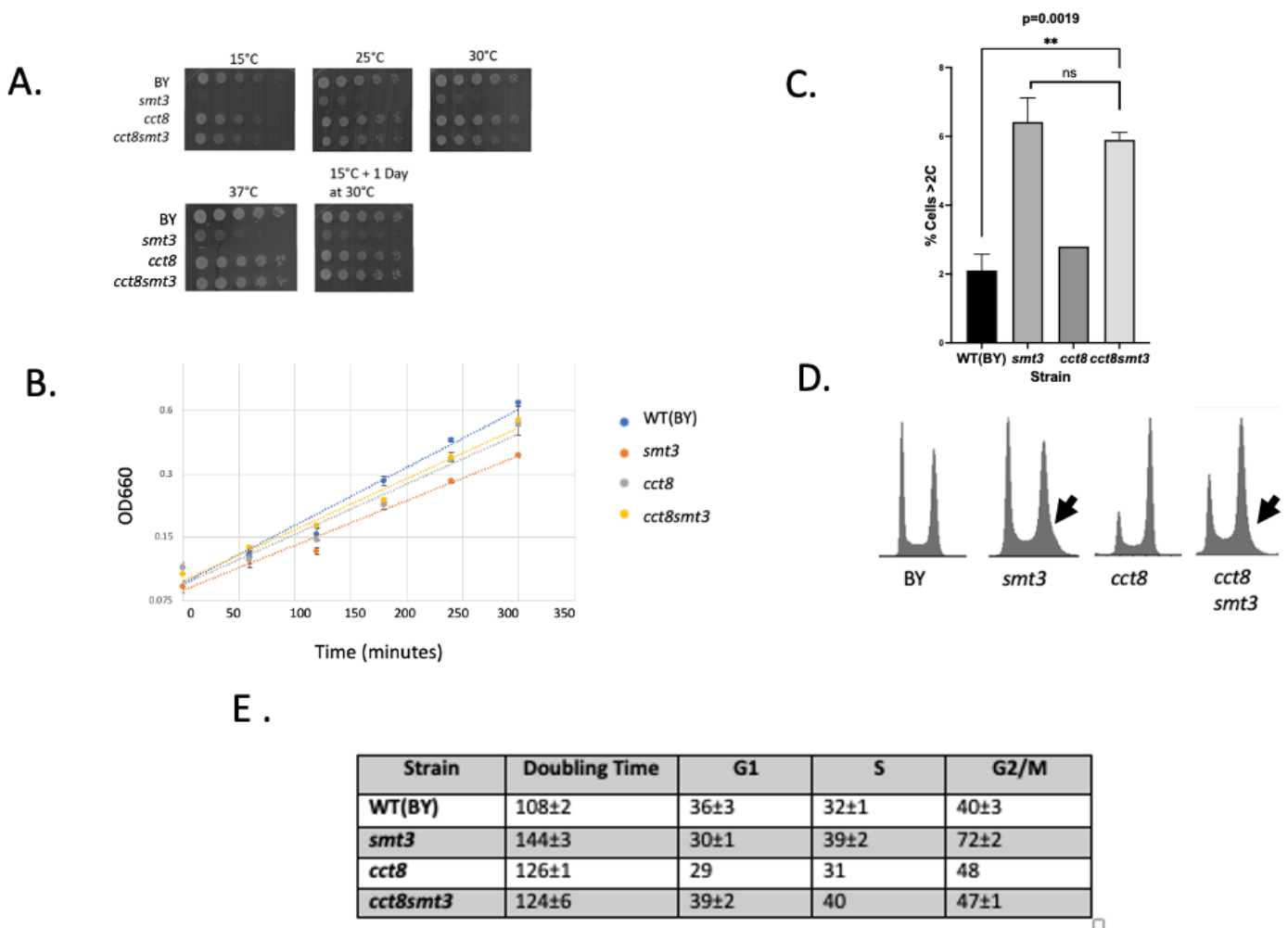


Figure 4.12 *smt3* cell cycle phenotypes are rescued in the *cct8smt3* double mutant. (A) Five-fold serial dilutions of mid-log growing cultures GC1, GC16, GC97 and GC99 cells were spotted onto YPD plates using a 48-pin tool and then incubated at the indicated temperatures. (B) Growth curves of mid-log phase growing cultures of GC1, GC16, GC97 and GC99 cells. Error bars represent SD from 3 biological repeats. (C) Gating analysis of the DNA content analyses in (D) of cells containing >2C DNA content. (D) DNA content analysis was performed on mid-log phase growing cultures GC1, GC16, GC97 and GC99 cells and presented as indicated. (E) Gating analysis of the DNA content analyses in (D) of the time cells spent in each stage of the cell cycle.

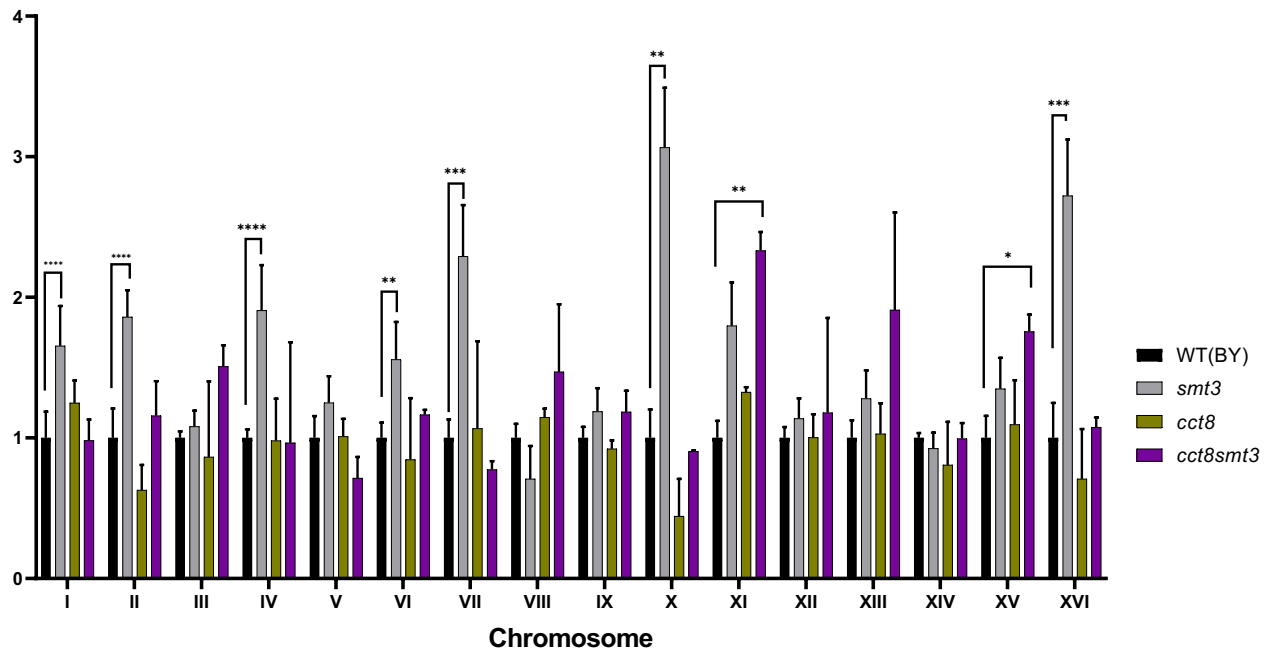


Figure 4.13 The *cct8* mutant and the *cct8smt3* double mutant display specific aneuploidy.

A chromosomal qPCR assay (Pavelka et al., 2010) was performed on DNA extracted from mid-log phase growing wild type (GC1), *smt3* (GC16), *cct8* (GC97) and *cct8smt3* (GC99) cells using an alkaline lysis method adapted from Pavelka et al. (2010). 2.5µg of DNA was used in each qPCR reaction with primers specific for each chromosome (see Pavelka et al., 2010). Samples were normalised to the levels of *ALG9* and compared to the wild type control (GC2) which was set at 1. Error bars represent SD from 3 biological repeats. P values were derived from an unpaired T-test, (*) indicates $p < 0.05$, (**) indicates $p < 0.01$ and (***) indicates $p < 0.001$.

	WT(BY)	<i>smt3</i>	<i>ulp2</i>	WT(W303)	W303 <i>smt3</i>	WT(9)	<i>smt3-allR</i>	<i>arp2</i>	<i>arp2smt3</i>	<i>cct8</i>	<i>cct8smt3</i>
Chr I	-	+	+	-	+	-	-	-	-	-	-
Chr II	-	+	-	-	+	-	+	-	+	-	-
Chr III	-	-	-	-	+	-	+	-	-	-	+
Chr IV	-	+	-	-	-	-	+	-	+	-	-
Chr V	-	-	-	-	+	-	-	-	-	-	-
Chr VI	-	+	+	-	-	-	+	-	-	-	-
Chr VII	-	+	-	-	+	-	+	-	-	-	-
Chr VIII	-	-	-	-	-	-	-	-	+	-	+
Chr IX	-	-	-	-	-	-	-	-	-	-	-
Chr X	-	+	-	-	-	-	-	-	-	-	-
Chr XI	-	+	-	-	+	-	+	-	-	+	+
Chr XII	-	-	-	-	+	-	+	-	-	-	-
Chr XIII	-	-	-	-	+	-	-	-	-	-	+
Chr XIV	-	-	-	-	-	-	-	-	-	-	-
Chr XV	-	-	-	-	-	-	-	-	-	-	+
Chr XVI	-	+	-	-	-	-	-	-	-	-	-

Table 4.1 Analysis of the chromosomal profiles of the *smt3* mutants. The chromosomal profiles of the indicated strains were collated. Grey boxes represent chromosomal increases and orange boxes represent chromosomal loss.

(see section 4.2.2) was applied to DNA extracted from wild type (GC1), *smt3* (GC16), *cct8* (GC97) and *cct8smt3* (GC99) cells (Fig. 4.13). As expected, the *smt3* mutant in the BY4741 background displayed increased levels of chromosomes I, II, IV, VI, VII, X, XI and XVI (Fig. 4.13). However, interestingly, there were detectable changes in the levels of chromosomes in the *cct8* mutant (Fig. 4.13). Whilst the levels of chromosomes II and X appeared to be lower than normal in the cell population, the levels of chromosome XI appeared to be higher than normal, although this was not a significant increase (Fig. 4.11). Nevertheless, the level of chromosome XI in the *cct8smt3* double mutant was significantly increased, similar to that of ChrXI in *smt3* cells. These alterations in the levels of specific chromosomes were not detected in the DNA content analyses of *cct8* cells (Fig. 4.12C), possibly as the reduction of chromosomes II and X masked the higher levels of chromosome XI, leading to the DNA content analyses identifying WT levels of >2N DNA content in *cct8* cells. Importantly, the DNA content analyses also suggested that the *smt3* and *cct8smt3* mutants had similar levels of aneuploidy (Fig. 4.12C), comparable to the *arp2smt3* and *arp3smt3* mutants (Fig. 4.8C, Fig. 4.9C). However, intriguingly, the levels of the chromosomes present in the *cct8smt3* double mutant, although not wild type, were not identical to the patterns detected in either the *smt3* or the *cct8* single mutant (Fig. 4.13). For example, the aberrant levels of chromosomes I, II, III and IV in the *smt3* mutant and chromosomes II, X and XVI in the *cct8* mutant were not significantly different from wild type in the *cct8smt3* double mutant (Fig. 4.13). Moreover, the levels of chromosome XI, which were significantly increased in both the *smt3* and *cct8* mutants, and chromosome XIII, which were increased in the *smt3* mutant, were also increased in the *cct8smt3* double mutant (Fig. 4.13). Finally, the levels of chromosomes VIII and XV were increased in the *cct8smt3* double mutant but were not increased in the *smt3* and the *cct8* single mutants (Fig. 4.13). Therefore, although the DNA content analysis suggested that the *smt3* and *cct8smt3* strains have almost identical levels of >2C DNA content, the pattern of aneuploidy is distinctly different (compare Figs. 4.12C and 4.13). Taken together, these results suggest that the CCT complex is linked to the nuclear defects associated with loss of sumo and, furthermore, provides more evidence that the growth defects associated with loss of sumo is linked to the aneuploidy in *smt3* mutant cells. It is also intriguing to note that the levels of chromosome XI are increased in the *cct8* single mutant (Table 4.1). The levels of chromosome XI are also significantly increased in the *cct8smt3* mutant (Table 4.1), both of the *smt3* mutants in the different genetic backgrounds (Figs. 4.2

and 4.5) and also in the *smt3-allR* mutant (Fig. 4.7). Hence, this observation raises the possibility that increased levels of chromosome XI is linked to shared functions of sumo and the CCT complex.

Interestingly, Smt3 protein levels do not appear to be reduced in *cct8* mutant cells compared to wild type cells although Smt3 levels are indeed lower in *cct8smt3* double mutants compared to wild type cells (data not shown). Taken together, these data suggest that the loss of sumo function associated with the *smt3* allele (and subsequent reduction in cellular Smt3 levels) contributes to the *smt3* aneuploidy (Fig. 4.12C). As mentioned in section 4.2.6.1, mutations in the Arp2/3 complex appear to be linked to the nuclear defects associated with loss of sumo. Analysis of the *cct8* allele also suggests a nuclear role for the CCT complex when sumo function is reduced. Interestingly, Huang et al., (2012) identified interactions between the mammalian CCT complex and the spliceosome, a large complex which catalyses intron splicing to enable mRNA maturation (Huang et al., 2012). Hence, the CCT complex may have an alternative, nuclear role in regulating mRNA maturation and RNA processing.

As shown in the results above, I have characterised that the aneuploidy associated with the *smt3* mutant is still present, but different, in the *cct8smt3* double mutant (Fig. 4.12C). Interestingly, the chromosomal profiles of *arp2smt3* and *cct8smt3* are different from each other and to the *smt3/ smt3allR* mutants (compare Fig. 4.2, Fig. 4.5, Fig. 4.7, Fig. 4.10 and Fig.4.13) (Table 4.1). Similar to the *arp2smt3* and *arp3smt3* mutants, the *cct8smt3* double mutant increases the fitness of the *smt3* mutant whilst reducing the *smt3* G2/M delay (Fig. 4.12). Furthermore, *cct8smt3*, *arp2smt3* and *arp3smt3* mutants also display a slight S Phase delay, although the basis of this delay unclear (Fig. 4.12). Additionally, Fig. 4.11 proposes that regulation of the expression of *SMT3* and *CCT8* may be linked, although it can be concluded that the recovery of *smt3* growth in the *cct8smt3* double mutant is not linked to *SMT3* expression. In conclusion, the data above has identified that although the top *smt3* SGA suppressors in the Arp2/3 and CCT complexes improve the fitness of the *smt3* strain, *arp2smt3* and *cct8smt3* mutants do not rescue the aneuploidy associated with the *smt3* allele.

4.3 Summary

This chapter has identified and characterised both the cell cycle progression and chromosomal dynamics in the *smt3*, *W303smt3 smt3-allr* strains, based on the initial findings by Dr. Lewis suggesting that loss of sumo function resulted in cell cycle defects (Lewis, 2016). Indeed, the results in this chapter confirm that cell cycle defects are conserved between *smt3/smt3-allR* mutants, with *smt3*, *W303smt3 smt3-allr* strains exhibiting G2/M delays and significant aneuploidy compared to wild type cells (Fig. 4.1, Fig. 4.4, Fig. 4.6). However, the above data revealed that *smt3-allR* and, to a lesser extent, *W303smt3* cells also display S Phase delays, suggestive that polysumoylation has an important role during S Phase, although this role remains unclear (Fig. 4.4E, Fig. 4.6E). Nevertheless, these results highlight the importance of sumoylation to ensure timely progression through the cell cycle. Furthermore, chromosomal profiling of the *smt3*, *W303smt3* and *smt3-allr* strains revealed that the pattern of aneuploidy observed between the *smt3/smt3-allR* mutants is not identical. For example, an increase of chromosomes I, III and XI appear to be conserved across the three *smt3* mutants, whereas chromosome XII is increased in *W303smt3* and *smt3-allR* but not *smt3* (Table 4.1). Hence, it may be suggested that an increase chromosome XII may be associated with a delayed S Phase. However, it must be noted that in both the DNA content analysis and chromosomal ploidy assays it is a population of cells that is being examined, rather than an individual cell. Thus the results presented in this chapter represent an average across the population of cells. It is possible that no one cell may have all the aneuploidy, or that the higher or lower levels of chromosomal duplications could be concentrated in a relatively small number of cells. Nevertheless, we can conclude that as a population, *smt3/smt3-allR* mutants show significant aneuploidy compared to wild type cells. It must also be noted that although the aneuploidy observed in the *smt3* mutants was confirmed in the chromosomal qPCR assays, 6 chromosomes appear to be amplified in the *smt3* strain, whilst only ~6% of *smt3* cells analysed by FACs showed aneuploidy. The reasons underlying this discrepancy remain unclear, but further experiments, such as carrying out the FACs analysis with differently stained WT and *smt3* cells simultaneously may provide further insights into the aneuploidy associated with the *smt3* strain. For example, it would allow the same gating analysis to be used on the WT and mutant cells from a single FACs experiment in order to determine the >2C DNA shift in the mutants relative to the respective wildtype strain. In addition, synchronised cells could be used, rather than the asynchronous cells used in this study, which would allow FACs analysis to be performed on different populations of cells.

As mentioned previously, the same chromosomal primers used by Ryu et al. (2016) and Pavelka (2010) were also used in the chromosomal ploidy assays in this study (Ryu et al., 2016, Pavelka et al., 2010). Ryu et al. (2016) used two primers pairs per chromosome; one primer pair specific for the left arm of each chromosome and one primer pair specific for the right arm of each chromosome (Ryu et al., 2016). However, due to time constraints and limited resources, only the primers specific to the left arm of each chromosome were used in this study. Therefore further chromosomal ploidy assays using the primers specific to the right arms of the chromosomes will be required. Importantly, these assays would allow identification of whether the >2C DNA content associated with the *smt3/smt3-allR* strains is due to an increase of entire chromosomes or an increase of fragments of certain chromosomes.

One proposed model based on the above findings is that loss of sumo function promotes an adaptive aneuploidy response, by the upregulation of key genes located on chromosomes I, III and XI are vital for survival. However, the G2/M delay associated with the *smt3/smt3-allR* strains is indicative of a mitotic defect. Thus, an alternative hypothesis may be that the aneuploidy associated with the loss of sumo function/ loss of polysumoylation is present due to errors in chromosomal segregation during anaphase. Ryu et al (2016) identified that aneuploidy developed rapidly with the deletion of the *ULP2* gene (Ryu et al., 2016). Hence the use of a temperature sensitive *smt3* allele could provide insights into adaptive aneuploidy induced by the loss of Smt3 function when this strain is placed at the non-permissive temperature. Chromosomal profiling of this strain after a set number of generations would identify the generation(s) at which specific chromosomes are increased which may provide insights into the importance of certain chromosomes associated with the loss of sumo function. Nevertheless, it is clear that further studies are required to investigate the aneuploidy associated with the *smt3/smt3-allR* mutants.

Interestingly, studies investigating the chromosomal profiles of stable aneuploid *S. cerevisiae* strains identified that duplication of chromosome II was shown to be the most frequent chromosome attributing to aneuploidy in *S. cerevisiae* (Pavelka et al., 2010). Thus, it is intriguing that chromosome II was one of the most frequently duplicated chromosomes

identified in four of the strains characterised in this study (Table 4.1). Indeed, chromosome II duplication appears to be conserved in *smt3*, *W303smt3* and *smt3-allR* mutants, supporting the hypothesis that upregulation of genes located on chromosome II are required for loss of sumo function.

As discussed earlier, the duplication of chromosomes I, III and XI appear to be conserved between the *smt3/smt3-allR* mutants. Interestingly, Beaupere et al. (2018) identified that *S. cerevisiae* cells induce aneuploidy on chromosomes II and XIII to enable resistance to ER stress (Beaupere et al., 2018). Furthermore, upregulation of several key genes within the N-glycan synthesis pathway were located on these duplicated chromosomes, with deletion of these genes rendering the cells sensitive to ER stress. In parallel with our findings that loss of sumo function impacts chromosomal dynamics differently in different strain backgrounds, Beaupere et al. (2018) identified that the pattern of aneuploidy to ER stress induced by the antibiotic tunicamycin differed within different strain backgrounds (Beaupere et al., 2018). For example, the aneuploidy induced by tunicamycin varied between the duplication of two to five chromosomes dependant on the strain background (Beaupere et al., 2018). However, the authors concluded that the critical genes conferring tunicamycin resistance were located on chromosome II, suggesting that aneuploidy is an adaptive response to tunicamycin resistance. Hence, it may also be the case that key genes important for survival in cells expressing reduced sumo function may be located on chromosome I, III and XI, with the aneuploidy associated with the other chromosomes in different strains having a specific protective effect within that particular strain background. Moreover, analogous to this study, the two strain *S. cerevisiae* backgrounds used by Beaupere et al. (2018) were BY4741 and W303, illustrating that the pattern of aneuploidy in response to the same stress condition differs within these two strain backgrounds (Beaupere et al., 2018). Taken together, the results from this chapter suggest that adaptive aneuploidy enables survival of the *smt3* mutants by upregulating key genes, although different strain backgrounds may influence the pattern of this aneuploidy. Interestingly, activation of ER stress response pathways in mammalian cells is facilitated by the desumoylation of the transcription factor XBP1, providing a link between the sumo pathway and the ER stress response (Enserink, 2015). Furthermore, Sumo mRNA is degraded during ER stress in *Drosophila melanogaster* cells, suggesting that downregulation of the sumo conjugation pathway is important in the

response to ER stress (Enserink, 2015). Considering that ER stress is induced by the accumulation of misfolded proteins, it is perhaps not surprising that data in this chapter suggests a connection between Smt3 and subunits of the CCT complex, a major protein chaperonin complex.

Data in this chapter has also revealed that the top cytoskeletal suppressors from the Arp2/3 complex and the CCT complex identified in the *smt3* SGA screen are not able to reverse the *smt3* aneuploidy (Fig. 4.10 and Fig. 4.13). Suppressors found in these two separate molecular complexes did not eliminate the aneuploidy associated with the *smt3* allele, although the pattern of chromosomal duplication in both the *arp2smt3* and *cct8smt3* double mutants differed from the *smt3* strain (compare Fig. 4.2 with Fig. 4.10 and Fig. 4.13). Although it was not possible during the duration of this study, it would be interesting to identify which genes are upregulated on chromosomes I, III and XI within the *smt3* mutants. It would also be important to assess if aneuploidy helps or hinders the phenotype(s) associated with other mutants in the Sumo pathway. This would allow identification of key pathways which are affected by changes to the sumo pathway, providing further insights into the essential nature of sumo in eukaryotes.

To conclude, this chapter has identified cell cycle delays associated with the loss of the sumo function which are conserved between different strain backgrounds. Furthermore, characterisation of aneuploidy in the *smt3/ smt3-allR* strains suggests that although the duplication of several chromosomes are conserved, there are differences in the pattern of aneuploidy between the different mutants. Finally, data in this chapter confirmed that several top scoring *smt3* cytoskeletal suppressor proteins improve the growth and cell cycle delays associated with the *smt3* mutant, although these suppressor proteins appear to induce a different, distinct pattern of aneuploidy compared to the *smt3* single mutant.

Chapter Five: Characterisation of the relationship between Tub2 and Smt3

5.1 Introduction

Previous studies and the work described in Chapter 4 revealed that inhibition of either sumoylation or deconjugation leads to cell cycle defects and aneuploidy (Srikumar et al., 2013a, Ryu and Hochstrasser, 2017, van de Pasch et al., 2013). Although the mechanisms underlying the influence of sumoylation on cell cycle progression and chromosome dynamics are unclear, it is interesting to note that several studies revealed that important components of the kinetochore and centromere are sumo substrates (Wan et al., 2012, Montpetit et al., 2006). In addition, the Slx5 and Slx8 proteins of the Slx5-Slx8 STUbL in *S. cerevisiae* localise at the centromere, and deletion of the gene that encodes either Slx5 or Slx8 results in extensive aneuploidy (van de Pasch et al., 2013). Furthermore, the mitotic spindle, comprising of tubulin dimers, is mispositioned in *slx5Δ* and *slx8Δ* cells, possibly accounting for the aneuploidy associated with these mutants. To date little is known about the relationship between sumo and tubulin. Surprisingly, a DAmP allele of *TUB2* (*tub2::DAmP*), the sole gene encoding β -tubulin in *S. cerevisiae*, was the 4th highest suppressor of the growth defects associated with the *smt3* allele in the SGA screen, indicative that there is a strong genetic interaction between the two genes (see Chapter 1, section 1.4, (Lewis, 2016)). Analysis of the literature revealed that there is currently relatively limited evidence that shows that Tub2 is indeed a sumo substrate. Nevertheless, mass spectrometry data obtained from several large scale sumo screens have suggested that Tub2 is sumoylated in *S. cerevisiae* cells (Panse et al., 2004). In a more recent study, Greenlee et al. (2018) used a yeast two hybrid system to provide evidence that Tub2 may interact with Smt3 (Greenlee et al., 2018). Interestingly, there is also some limited evidence that links between sumo and β -tubulin may be conserved. For example, β -tubulin pulldowns in mammalian cells overexpressing SUMO-1 suggested that β -tubulin is indeed sumoylated (Feng et al., 2021). However, the authors were unable to repeat this experiment in endogenous conditions, which might indicate that sumoylation of β -tubulin is extremely dynamic, with only very small fraction of β -tubulin in a sumoylated

state, or alternatively that sumoylated β -tubulin is unstable (see Chapter 1, section 1.4.2.1, (Feng et al., 2021)).

Several previous studies have also found that α -tubulin is a sumo substrate (Feng et al., 2021, Greenlee et al., 2018, Di Genova et al., 2017). For example, cytoplasmic α -tubulin subunits were identified as sumo substrates in mammalian cells (Feng et al., 2021). Additional studies using the unicellular protozoan *Giardia lamblia* identified that α -tubulin immunoprecipitated with sumo (Di Genova et al., 2017), suggesting that the sumoylation of α -tubulin is conserved throughout eukaryotes.

It is also interesting to note that α -tubulin is encoded by two genes, *TUB1* and *TUB3*, in *S. cerevisiae*. The *TUB1* gene is essential and no mutant allele of this gene was available for the SGA screen that was performed with the *smt3* mutant. However, the deletion of the *TUB3* gene is viable and interestingly the *tub3 Δ* was a weak suppressor (150/4998), further strengthening the connection between tubulin and the growth defects associated with the *smt3* allele. Hence, a range of studies suggest that the functions of sumo and tubulin are connected in eukaryotes.

Following on from the identification of the *tub2::DAmP* allele as a strong suppressor, and *tub3 Δ* as weak suppressor, initial analysis of the growth defects associated with the *smt3* performed to begin to better understand the relationships between tubulin and Smt3 (Lewis, 2016). In particular, an antibody against α -tubulin was used to reveal that *smt3* cells display microtubule spindle morphology defects (Lewis, 2016). For example, analysis of spindle length in *smt3* cells revealed that microtubule spindles are shorter than those in wild type cells (Lewis, 2016). In addition, it was also observed that exposure of wild type cells to cold temperature resulted in a rapid, transient increase in tubulin staining and that this induction was lost in *smt3* cells (Lewis, 2016). Hence, taken together, these results suggest that Smt3 influences microtubule dynamics in *S. cerevisiae*.

However, despite these observations that link α - and β -tubulin with sumo, the functions of sumoylation in microtubule function and structure are not understood. Hence, the aims of

this chapter are to build on these previous studies to investigate the links between tubulin and sumo functions in cell cycle progression and on chromosome dynamics, and to initiate studies to explore the relationships between sumo and the function(s) of β -tubulin.

5.2 Results and discussion

5.2.1 Suppression of *smt3* and *tub2* associated defects in the *tub2smt3* double mutant

As mentioned in Chapter 1, section 1.4, the SGA screen revealed that the *tub2::DAMP* (*tub2*) allele was an extremely good suppressor of the *smt3* poor growth (Lewis, 2016). Furthermore, the *tub2smt3* double mutant reduced the F-actin morphological defects associated with the *smt3* strain, whilst the benomyl sensitivity of the *tub2* strain was rescued in *tub2smt3* cells (Lewis, 2016). Although these results indicate that *tub2* allele improves defects associated with the *smt3* allele, it remains unclear how this is achieved. Thus, to gain further insights into the rescue of the *smt3* growth in the *tub2smt3* strain, cell cycle analysis was carried out in the *tub2* and *tub2smt3* strain backgrounds.

5.2.1.1 *smt3* growth defects are restored in the *tub2smt3* double mutant

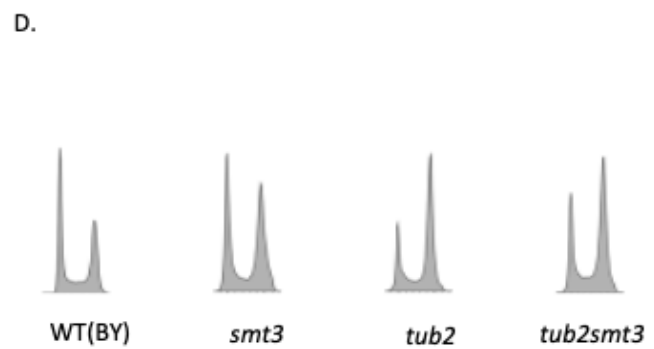
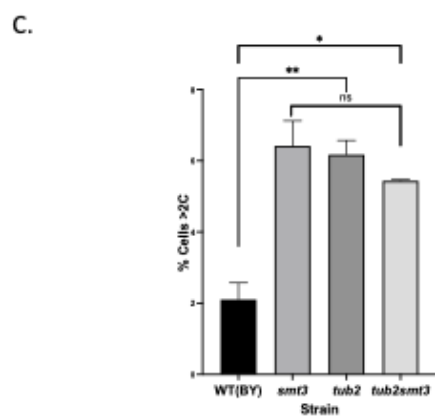
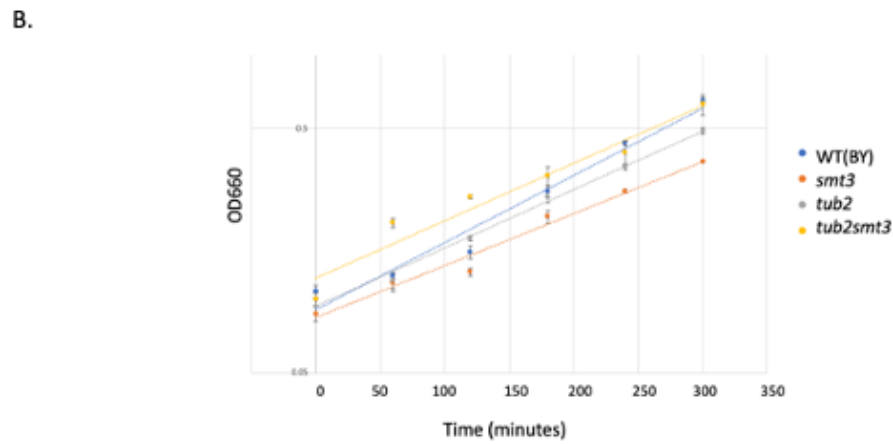
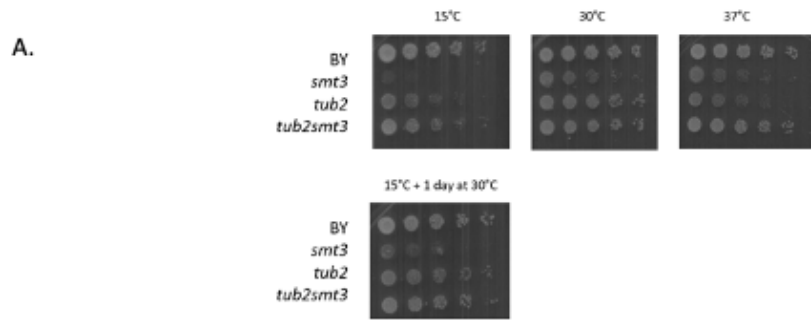
As described in Chapter 4, the *smt3* mutants in the BY4741 and W303 backgrounds have cell cycle progression defects with delays during G2/M in addition to these mutants displaying specific multichromosome aneuploidy. Hence it was possible that the *tub2* mutation may suppress some or all of these cell cycle and aneuploidy defects. The *tub2* mutation was an excellent suppressor of the growth defects associated with the *smt3::DAmP* allele (see section 1.4, Fig. 5.1A). In addition, the *tub2* mutation rescues the growth defects of the *smt3* mutant at a range of temperatures (Lewis, 2016) (Fig. 5.1A). Furthermore, in agreement with the SGA analysis, growth curves confirmed that the *tub2smt3* double mutant grows much better than the single *smt3* mutant (Fig. 5.1B). Additionally, the *tub2* single mutant was found to grow slower than the wild type and this growth defect was also rescued in the *tub2smt3* double mutant (Fig. 5.1B). Indeed, the growth rate analyses suggests that the doubling times of the *tub2* (GC44) and *tub2smt3* (GC49) mutants are 126 ± 9 minutes and 117 ± 6 minutes

respectively compared to a doubling time of 108 ± 2 and 144 ± 3 minutes for the wild type control strain (GC1) and the *smt3* (GC16) mutant, respectively. Although the *tub2* single mutant grew slightly better than the *smt3* mutant (126 ± 9 minutes compared to 144 ± 3 minutes respectively), both strains showed considerable growth defects compared to the wild type strain (108 ± 2 minutes) (Fig. 5.1B/E). Strikingly, growth rate analysis of *tub2smt3* cells revealed that *tub2smt3* doubling times are more similar to the growth rate of wild type cells than the single *tub2* or *smt3* strains (117 ± 6 minutes in *tub2smt3* compared to 108 ± 2 minutes in wild type cells). Thus, in agreement with Fig. 5.A, *tub2smt3* appears to reduce the growth defects associated with the single *tub2* or *smt3* alleles, restoring growth back to almost wildtype levels (Fig. 5.1B/E).

5.2.1.2 Cell cycle analysis of the *tub2* and *tub2smt3* double mutants

Next, DNA content analysis was performed on cultures of the mid-log phase growing wild type (GC1), *smt3* (GC16), *tub2* (GC44) and *tub2smt3* (GC49) strains (Fig. 5.1C/D). As expected, *smt3* cells had a ~6% >2C DNA content (Fig. 5.1C). Strikingly, *tub2* cells also displayed significant aneuploidy compared to wild type cells (~6% >2C DNA content in *tub2* compared to ~2% >2C DNA content in wild type cells), with the >2C DNA content of *tub2* cells remarkably similar to that of *smt3* cells (Fig. 5.1C). Interestingly, although the >2C DNA content associated with *tub2smt3* cells was slightly lower than both *tub2* and *smt3* single mutants (~5.5% in *tub2smt3* cells compared to ~6 in both *tub2* and *smt3* cells, Fig. 5.C), the >2C DNA content associated with the *tub2smt3* strain was not significantly different to that of the *smt3* single mutant (Fig. 5.1C). Thus, these results are consistent with the observation that the *tub2smt3* double mutant grows better than either of the *tub2* and *smt3* single mutants and further supports the conclusion that reduced Tub2 function suppresses phenotypes associated with reduced sumo function and that reduced Smt3 function suppresses phenotypes associated with reduced Tub2 function.

To assess the effects of the *tub2* allele on the cell cycle defects associated with the *smt3* mutant, the proportion of cells in each cell cycle phase was combined with the doubling times



E.

Strain	Doubling Time	G1	S	G2/M
WT(BY)	108±2	36±3	32±1	40±3
<i>smt3</i>	144±3	30±1	39±2	72±2
<i>tub2</i>	126±9	23±3	38±2	69±4
<i>tub2smt3</i>	117±6	26±4	35±3	51±2

Figure 5.1 The *tub2* allele suppresses cell cycle and aneuploidy phenotypes associated with the *smt3* allele. (A) Five-fold serial dilutions of mid-log growing cultures wild type (GC1), *smt3* (GC16), *tub2* (GC44) and *tub2smt3* (GC49) cells were spotted onto YPD plates using a 48-pin tool and then incubated at the indicated temperatures. (B) Growth curves of mid-log phase growing cultures of wild type (GC1), *smt3* (GC16), *tub2* (GC44) and *tub2smt3* (GC49) cells. Error bars represent SD from 3 biological repeats. (C) Gating analysis of the DNA content analyses in (D) of cells containing >2C DNA content. P values were derived from an unpaired T-test, (*) indicates $p < 0.05$, (**) indicates $p < 0.01$ and (***) indicates $p < 0.001$. (D) DNA content analysis was performed on mid-log phase growing cultures of wild type (GC1), *smt3* (GC16), *tub2* (GC44) and *tub2smt3* (GC49) cells and presented as indicated. (E) Gating analysis of the DNA content analyses in (D) of the time cells spent in each stage of the cell cycle.

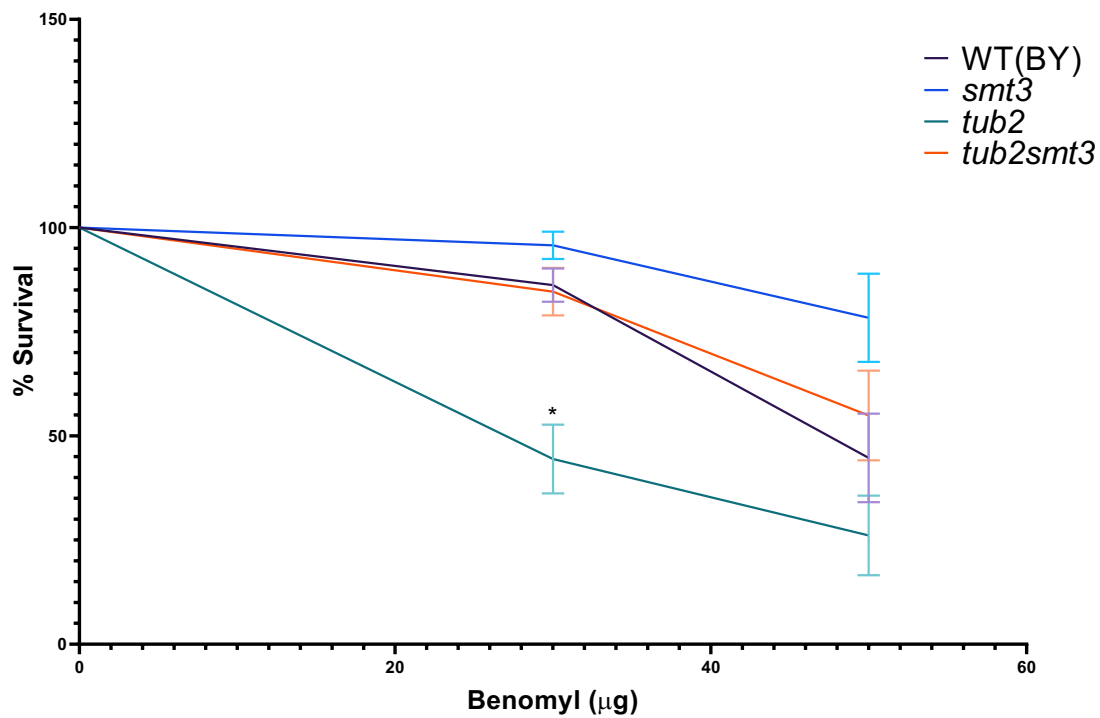


Figure 5.2 The *smt3* mutation suppresses the sensitivity of the *tub2* mutant to a microtubule depolymerising drug. Equal numbers of mid-log phase growing wild type (GC1), *smt3* (GC16), *tub2* (GC44) and *tub2smt3* (GC49) cells were plated on YPD plates containing the indicated benomyl concentrations. Plates were incubated at 30°C until colonies formed. % survival was calculated based on the colonies formed on the 0µg/ml benomyl plates. Error bars represent SD from 5 biological replicates (n=4 for *smt3*). P values were derived from an unpaired T-test, (*) indicates p<0.05.

of the wild type, *smt3*, *tub2* and *tub2smt3* strains to calculate the approximate time that each strain spends in each phase of the cell cycle (Morgan et al., 1991), Fig. 5.1E). Interestingly, *tub2* cells spent a significant amount of time in G2/M compared to wild type cells (~69 minutes in G2/M compared to ~40 minutes for *tub2* and wild type cells respectively). This is perhaps unsurprising considering the importance of tubulin during mitosis and the role of tubulin within the mitotic spindle (see Chapter 1, section 1.4.3). Nevertheless, the observed *tub2* G2/M delay was almost identical to the in G2/M delay associated with the *smt3* mutant (~69 minutes in G2/M compared to ~72 minutes for *tub2* and *smt3* cells respectively). Furthermore, *tub2smt3* cells show a reduced G2/M delay compared to either *tub2* or *smt3* (*tub2smt3* spends ~51 minutes in G2/M compared to ~69 minutes and ~72 minutes for *tub2* and *smt3* cells respectively) (Fig.5.1E). However, although the G2/M delay is reduced in *tub2smt3* cells, *tub2smt3* cells do appear to spend slightly longer in G2/M compared to wild type cells (~51 minutes compared to ~40 minutes in *tub2smt3* and wild type cells, respectively), suggestive that these double mutants do still have cell cycle defects (Fig. 5.1E).

Furthermore, both *tub2* and *tub2smt3* spend less time in G1 than wild cells or *smt3* (~23 minutes and ~26 minutes in *tub2* and *tub2smt3* respectively compared to ~36 minutes in wild type cells and ~30 minutes in *smt3* cells) (Fig. 5.1E). However, although *tub2* and *tub2smt3* strains appear to complete G1 faster than wild type cells, the reason for this remains unclear.

Interestingly, knockdown of β 3-tubulin, one of the seven β -tubulin genes expressed in mammalian cells, results in a severe G2/M delay in human melanoma cells (Altonsty et al., 2020). Tubulin is a critical component of the mitotic spindle, thus it could be proposed that modifying proteins found within the mitotic spindle may result in cell cycle defects. Intriguingly, the results from Altonsty et al. (2020) suggest that the 6 other β -tubulin genes expressed in mammalian cells are unable to compensate for the loss of β 3-tubulin, emphasising the specificity of the different isoforms. Nevertheless, analogous with our data, in which *tub2* cells show G2/M delays, a reduction of β 3-tubulin also results in a G2/M delay in mammalian cells. Taken together, these results are consistent with the hypothesis that accurate tubulin expression is required for timely progression through G2/M.

5.2.1.3 *smt3* cells are extremely resistant to microtubule depolymerising agents

The growth analysis presented in Fig. 5.1 suggested that the functions of Smt3 and Tub2 are linked. Interestingly, this hypothesis was also consistent with preliminary analysis of the sensitivity of wild type, *smt3*, *tub2* and *tub2smt3* strains to the microtubule depolymerising agent benomyl (Lewis, 2016). This sensitivity data indicated that, unsurprisingly, *tub2* cells are extremely sensitive to benomyl and suggested that this increased sensitivity was suppressed in the *smt3tub2* double mutant (Lewis, 2016). Hence, to further characterise the extent of this suppression and assess the benomyl sensitivity of the *smt3* single mutant, viability assays were performed on the wild type (GC1), *smt3* (GC16), *tub2* (GC44) and *tub2smt3* (GC49) strains using increasing concentrations of benomyl (Fig. 5.2). Consistent with the initial studies (Lewis, 2016) the *tub2* mutant was found to be significantly sensitive to increasing concentrations of benomyl (Fig. 5.2). Furthermore, the increased sensitivity of the *tub2* single mutant was restored to wild type sensitivity in the *tub2smt3* double mutant (Fig. 5.2). Unexpectedly, however, the *smt3* single mutant was found to be extremely resistant to benomyl compared to the wild type control, with almost 80% of *smt3* cells retaining viability at 50µg/ml benomyl (Fig. 5.2). Importantly, the initial experiments performed on the *smt3* mutant did not examine whether the *smt3* mutant was more resistant than wild type cells to benomyl (Lewis, 2016). Microtubule polymerisation and depolymerisation is a highly dynamic process during the cell cycle (see Chapter 1, section 1.4.2.1). Since benomyl directly induces microtubule depolymerisation these results suggest that reduced levels of Smt3 promotes microtubule stability. Interestingly, microtubules are only partially depolymerised using 50µg/ml of benomyl treatment and complete microtubule depolymerisation is not achieved until *S. cerevisiae* cells are treated with concentrations of ~120µg/ml benomyl (Hochwagen et al., 2005). Hence, it remains to be determined whether the reduction of Smt3 levels in the *smt3* mutant prevents microtubule depolymerisation at much higher benomyl concentrations. However, it must be noted that microtubules present in *smt3*, *tub2* and *tub2smt3* cells are of aberrant length, typically much shorter than microtubules expressed in wild type cells (Lewis, 2016). Thus, as both *tub2* and *tub2smt3* strain do not show benomyl resistance, it can be concluded that microtubule length does not influence sensitivity to benomyl. Hence, the nature of *smt3* benomyl resistance remains unclear. Taken together,

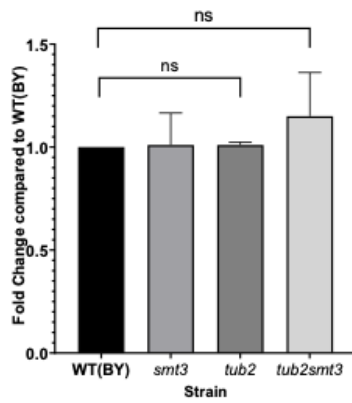
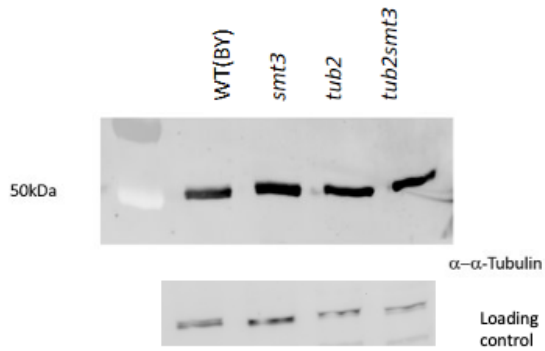
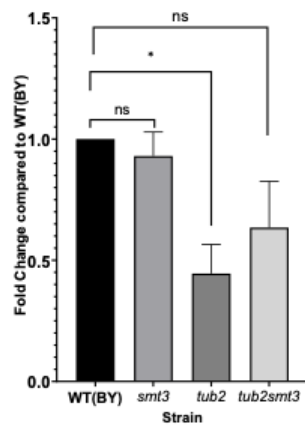
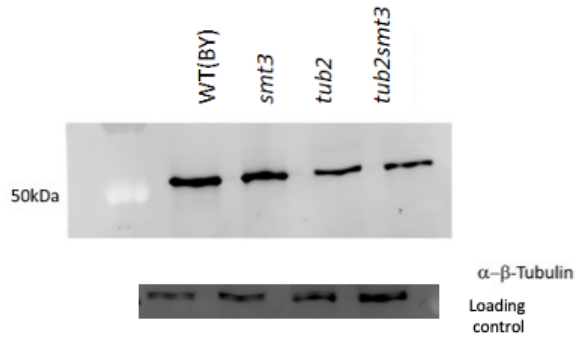


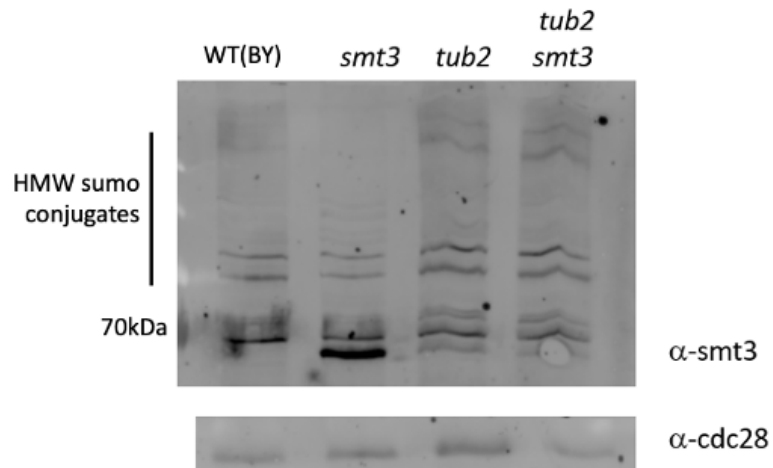
Figure 5.3. The levels of sumo do not affect the levels of α - and β -tubulin (A) Proteins were TCA extracted from mid-log phase growing wild type (GC1), *smt3* (GC16), *tub2* (GC44) and *tub2smt3* (GC49) cells and analysed by western blotting using an anti- β -tubulin antibody. A representative blot of three biological repeats is shown. (B) Blots were stripped, re-probed with anti-Cdc28 antibody as a loading control (lower panel in (A)) and quantified using ImageQuant software (GE Healthcare). Bars represent β -tubulin levels normalised to the wild type control (GC1). Error bars represent SD with P values derived from an unpaired T-test, (*) indicates $p < 0.05$. (C) Strains described in (A) were also analysed by western blotting using an anti- α -tubulin antibody. A representative blot of three biological repeats is shown. Blots were stripped, re-probed with anti-Cdc28 as a loading control (lower panel in (C)). (D) Blots were quantified using ImageQuant software (GE Healthcare). Bars represent α -tubulin levels normalised to the wild type control (GC1). Error bars represent SD with P values derived from an unpaired T-test.

these results suggest that reducing Smt3 levels promotes microtubule stability in cells containing the wild type *TUB2* gene and in cells expressing the *tub2* allele.

5.2.1.4 *smt3* mutants express Tub2 at wild type levels

The fact that the *tub2smt3* double mutant restored benomyl sensitivity to that observed in wild type cells raises the possibility that the balance of levels of Smt3 and Tub2 determines microtubule stability. Tubulin exists as dimers of α -tubulin and β -tubulin, hence it was possible that Smt3 influences microtubule stability by regulating the expression and/or stability of α - and β -tubulin. To examine this possibility, proteins were extracted from growing cultures of wild type (GC1), *smt3* (GC16), *tub2* (GC44) and *tub2smt3* (GC49) strains and western blot analysis was performed using antibodies specific to α - and β -tubulin (Figure 5.3). Confirming the phenotypes associated with the *tub2* mutant are linked to the mutant allele, the levels of β -tubulin, but not α -tubulin, are significantly lower in *tub2* cells compared to the wild type control (Fig. 5.3). Indeed, Tub2 levels in *tub2* cells are ~42% of the levels found in wild type cells (Fig. 5.3A,B). Interestingly, reducing *SMT3* gene expression by ~90% in the *smt3* mutant, which results in extremely low levels of Smt3 protein, did not appear to significantly affect the levels of α - and β -tubulin compared to wild type cells (Fig. 5.3). Hence, the increased resistance of the *smt3* single mutant to benomyl is not due to higher levels than normal of α - and β -tubulin. Furthermore, although there appeared to be a modest, but not significant, increase in α -tubulin levels in the *tub2smt3* double mutant, there was no significant recovery of β -tubulin levels detected (Fig. 5.3). It is worth noting here that there are two genes, *TUB1* and *TUB3*, that encode slightly different variants of α -tubulin in *S. cerevisiae* and it is unclear which of these proteins is recognised by the α -tubulin antibody which was used in Figure 5.3C. Hence, future work using two different α -tubulin antibodies specific to Tub1 and Tub3 could determine whether there are differences between the two α -tubulin isoforms in any of the *tub2* mutants. However, taken together, these data suggest that the range of sensitivities to benomyl observed in the wild type, *smt3*, *tub2* and *smt3tub2* strains is unlikely to be due to regulation of the expression and/or stability of α - and β -tubulin by Smt3.

A.



B.

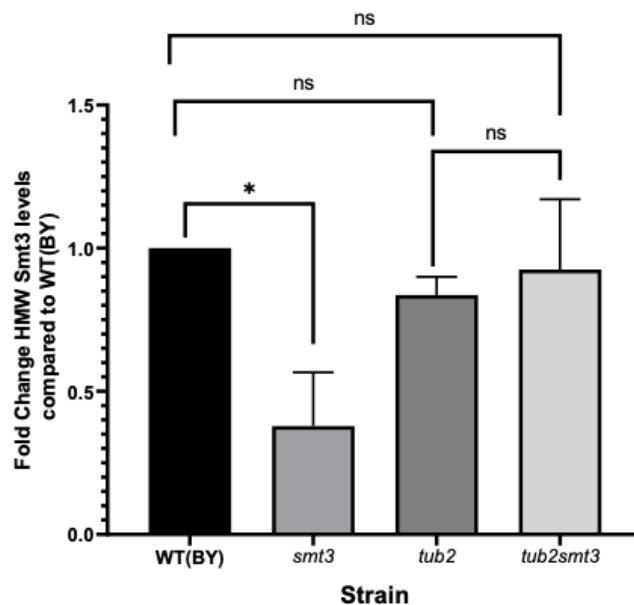


Figure 5.4. HMW sumo conjugates are rescued in *tub2smt3* double mutants. (A) Proteins were TCA extracted from mid-log phase growing wild type (GC1), *smt3* (GC16), *tub2* (GC44) and *tub2smt3* (GC49) cells and analysed by western blotting using an anti-Smt3 antibody. A representative blot of two biological repeats is shown. (B) Blots were stripped, re-probed with anti-Cdc28 antibody as a loading control (lower panel in (A)) and quantified using ImageQuant (GE Healthcare). Error bars represent SD. Bars represent Smt3 levels normalised to the wild type (GC1) control. P values were derived from an unpaired T-test, (*) indicates $p < 0.05$.

5.2.1.5 HMW sumo conjugates are rescued in *tub2smt3* cells

As identified by Dr. Lewis, a number of the double mutants which were able to rescue the *smt3* growth defect (including *arp2smt3* and *cct8smt3*) are not able to rescue the low abundance of HMW sumo conjugates present in *smt3* cells (personal communication, data not shown). Fig. 5.1 and Fig. 5.2 revealed that several phenotypes associated with the *smt3* allele were suppressed in the *tub2smt3* double mutant. Hence, it was possible that reduced levels of β -tubulin affected sumoylation. To examine this possibility protein extracts were isolated from wild type (GC1), *smt3* (GC16), *tub2* (GC44) and *tub2smt3* (GC49) and analysed by western blotting (Fig. 5.4). The levels of HMW Smt3 conjugates appeared to be relatively unaffected in the *tub2* strain, suggesting that the phenotypes observed in *tub2* cells are not due to any major changes in sumoylation. Unexpectedly, however, the levels of HMW Smt3 conjugates were not significantly different in *tub2smt3* cells when compared to the wild type control (Fig. 5.4). Interestingly, previous studies indicated that the levels of *SMT3* RNA were similar in the *smt3* mutant and the *tub2smt3* double mutant (Dr. Lewis, personal communication). Hence, these results suggest that the effects of the *tub2* allele on Smt3 conjugates in *tub2smt3* cells occurs post-transcriptionally. Nevertheless, it is possible that the effect of the *tub2* allele on the levels of Smt3 conjugates in the *tub2smt3* double mutant explains the suppression of phenotypes associated with the *smt3* allele.

5.2.1.6 *tub2smt3* double mutants display specific aneuploidy

As described above the *tub2* mutant displayed increased levels of aneuploidy and, moreover, the *tub2* allele appeared to at least partially suppress some of the aneuploidy associated with the *smt3* allele in the *tub2smt3* double mutant (Fig. 5.1C). However, to confirm and extend these observations the qPCR chromosomal ploidy assay (see Chapter 4 section 4.2.2) was applied to DNA extracted from wild type (GC1), *smt3* (GC16), *tub2* (GC44) and *tub2smt3* (GC49) cells (Fig. 5.5). As expected, the *smt3* mutant in the BY4741 strain background had increased levels of chromosomes I, II, IV, VI, VII, X, XI and XVI (Fig. 5.5).

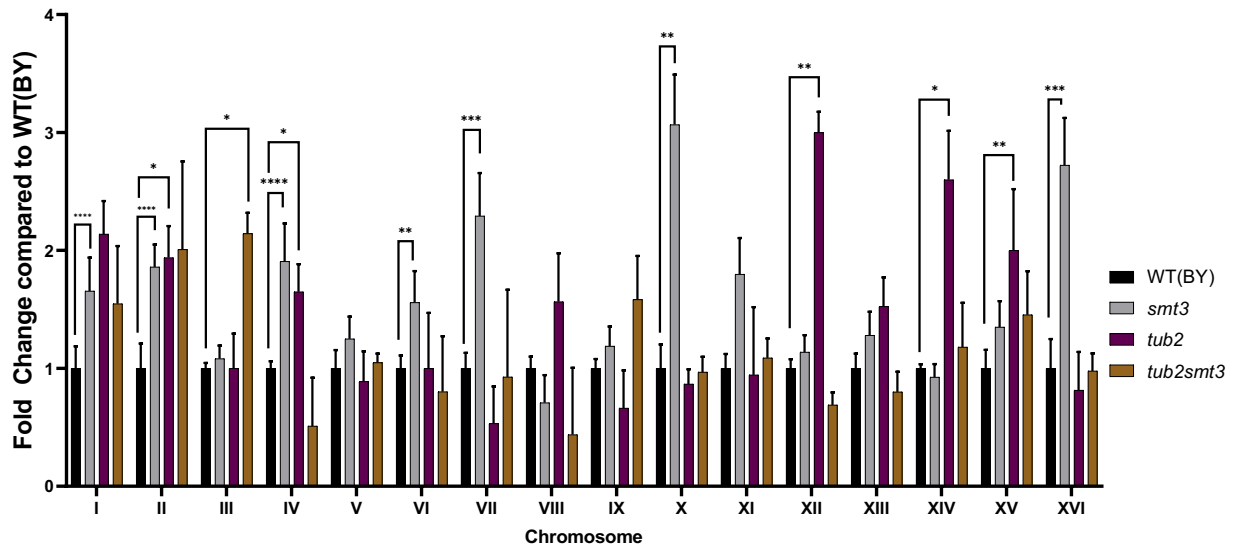


Figure 5.5 The *tub2* and *smt3* single mutants and the *tub2smt3* double mutant display specific aneuploidy. A chromosomal qPCR assay (Pavelka et al., 2010) was performed on DNA extracted from mid-log phase growing wild type (GC1), *smt3* (GC16), *tub2* (GC44) and *tub2smt3* (GC49) cells using an alkaline lysis method adapted from Pavelka et al. (2010). 2.5µg of DNA was used in each qPCR reaction with primers specific for each chromosome (see Pavelka et al., 2010). Samples were normalised to the levels of *ALG9* and compared to the wild type control (BY) which was set at 1. Error bars represent SD from 5 biological repeats.

	WT(BY)	<i>smt3</i>	<i>ulp2</i>	<i>tub2</i>	<i>tub2smt3</i>
Chr I	-	+	+	+	+
Chr II	-	+	-	+	+
Chr III	-	-	-	-	+
Chr IV	-	+	-	+	
Chr V	-	-	-		
Chr VI	-	+	+		+
Chr VII	-	+	-		
Chr VIII	-	-	-	+	
Chr IX	-	-	-		
Chr X	-	+	-		
Chr XI	-	+	-		
Chr XII	-	-	-	+	+
Ch XIII	-	-	-		
Chr XIV	-	-	-	+	+
Chr XV	-	-	-	+	+
Chr XVI	-	+	-		

Table 5.1 Analysis of the chromosomal profiles of the *smt3*, *tub2* and *tub2smt3* mutants.

The chromosomal profiles of the indicated strains from Fig. 5.5. Grey boxes represent an increase in the indicated chromosome.

Furthermore, the qPCR assay revealed aneuploidy of chromosomes I, II, III, VIII, XII, XIII, XIV and XV in the *tub2* mutant, confirming the DNA content analysis (Figs. 5.1C, 5.5, Table 5.1). Interestingly, analysis of the *tub2smt3* double mutant revealed that the levels of chromosomes I, II, III, XIV and XV were increased whilst the levels of chromosomes VIII and IV were decreased when compared to the wild type control (Figs. 5.5 and Table 5.1). Therefore, consistent with the DNA content analysis, these data show that some of the aneuploidy detected in the *smt3* mutant is suppressed in the *tub2smt3* double mutant (compare Fig.5.1C and Fig. 5.5, Table 5.1). However, these data also reveal that some of the aneuploidy detected in the *tub2* mutants suppressed in the *tub2smt3* double mutant and, moreover, that specific aneuploidy not detected in either the *smt3* or the *tub2* single mutants is present in the *tub2smt3* double mutant (Fig. 5.5 and Table 5.1). It is also very interesting to note that many of the chromosomes that are aneuploid in the *smt3* single mutant are also aneuploid in the *tub2* single mutant (Fig. 5.5 and Table 5.1). Hence, given the key role of microtubules in chromosome dynamics, these results support the hypothesis that mutations in either sumo or β -tubulin may promote problems in chromosome dynamics during anaphase.

Taken together these analyses suggest there is a functional relationship between sumo and microtubules. For example, aneuploidy is reduced in the *tub2smt3* strain compared to the *smt3* and *tub2* single mutants (Fig. 5.5) whilst the *tub2* benomyl sensitivity is rescued back to wild type levels in the *tub2smt3* double mutant (Fig. 5.2). Furthermore, the G2/M delays associated with either the *tub2* or *smt3* single mutants is significantly reduced in *tub2smt3* cells (Fig. 5.1.E).

5.2.2 Investigation of Tub2 as a sumo substrate

The results described above suggest that sumo and β -tubulin functions are linked in the regulation of normal cell cycle progression. Interestingly, as described in the introduction to the chapter several large scale studies of sumoylated proteins in *S. cerevisiae* have suggested that α - and β -tubulin may be sumoylated and other work in other eukaryotes suggested that β -tubulin interacts with sumo (Di Genova et al., 2017, Greenlee et al., 2018, Feng et al., 2021). Hence, to further explore the relationship between sumo and β -tubulin it was important to

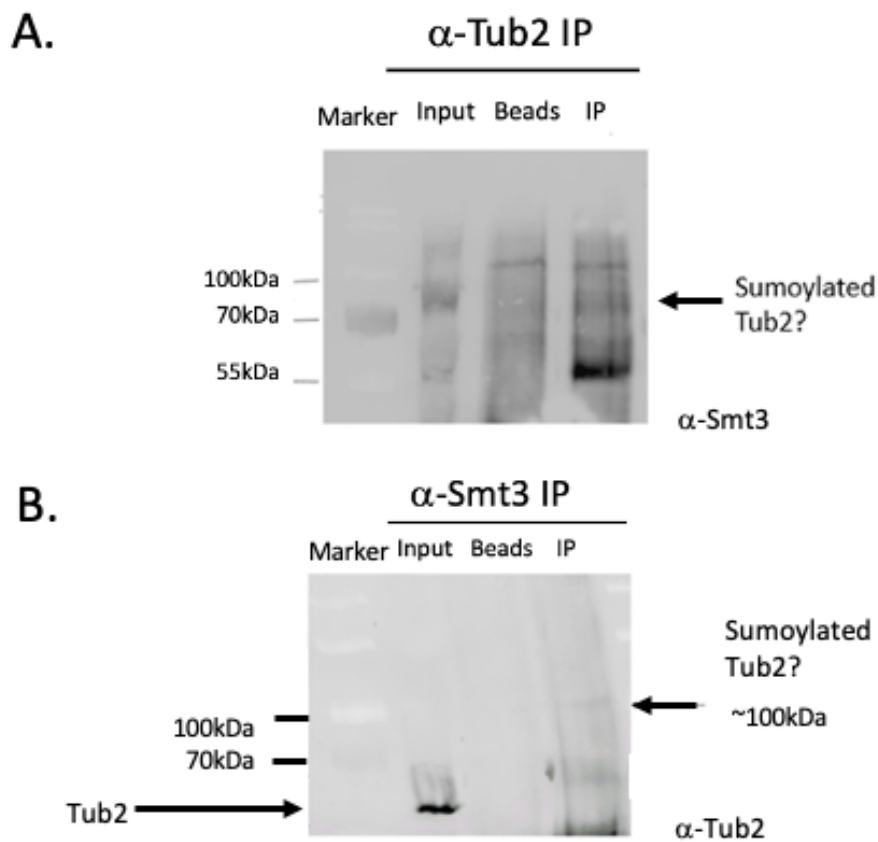


Figure 5.6 Tub2 is sumoylated in *S. cerevisiae*. (A) Protein extracts were isolated from mid-log phase growing wild type cells (GC1). Tubulin was immunoprecipitated with anti-Tub2 antibody and analysed by western blotting using an anti-Smt3 antibody. (B) The experiment described in (A) was repeated except immunoprecipitation was performed with anti-Smt3 antibody and western blot analysis used anti- β -tubulin. “Beads” indicates protein extract incubated with beads with no conjugated anti-Smt3/ anti- β -tubulin antibody as a control and input (5%) is indicated. Arrows indicate Tub2 in (B) and potentially sumoylated Tub2 (A and B). Western blots are representative of two biological repeats.

determine whether β -tubulin is indeed sumoylated in *S. cerevisiae*. Protein extracts were isolated from mid-log phase growing wild type (GC1) cells and sumoylated proteins were immunoprecipitated with either anti-Smt3 antibody-conjugated beads or anti- β -tubulin-conjugated beads (Fig. 5.6).

Immunoprecipitated proteins were then analysed by western blot analysis with either anti- β -tubulin antibody (Figure 5.6A) or anti-Smt3 antibody (Figure 5.6B), respectively. The predicted molecular weight of Tub2 is ~51kDa and a band was detected with slightly slower mobility around the expected region of the gel in the "Input" lane in the western performed with the anti- β -tubulin antibody of the anti-Smt3 IP (Figure 5.6B, lane 2). A faint band indicating possible modification(s) of Tub2, with a size of 100kDa, was observed in the "IP" lane (Figure 5.6B, lane 4). Moreover, the mobilities of these two bands are consistent with them representing mono (~68kDa) and multi- or polysumoylation of Tub2 (Figure 3.6A). It is also interesting to note that two bands of ~60kDa and ~75kDa were also detected using the anti-Smt3 antibody following immunoprecipitation with the anti- β -tubulin antibody (Figure 3.7A). Although it was not possible to include control cells in the immunoprecipitation/western analyses that lacked the Tub2 protein, which is an essential protein, or expressed an epitope-tagged version of Tub2 that altered the mobility of the protein, taken together, these results suggest that Tub2 may indeed be sumoylated in growing *S. cerevisiae* cells. Nevertheless, it must be heavily caveated that a control IgG antibody was not used (only the beads and extract were used as controls, lanes 2 and 3 in each blot) and the 50kDa bands observed in the IP lanes may be a result of heavy chain cross reactivity. Therefore, repeats of these IPs are required to determine the nature of the ~50-60kDa bands. In addition, the potential sumoylated versions of Tub2 detected represented a relatively small amount of the Tub2 present in cells. However, the cells used in the immunoprecipitation experiment were growing asynchronously and it is possible that Tub2 is only sumoylated during a limited time frame in the cell cycle. However, studies of sumoylation of other proteins have shown this to be a highly dynamic modification and hence it can be difficult to detect the sumoylated forms of proteins. It is also interesting in this respect that although Feng et al. (2021) identified an interaction between Smt3 and Tub2 the authors found it very challenging to demonstrate the

interaction in wild type cells, leading to the proposal that this interaction may be transient and/or weak (Feng et al., 2021).

5.2.3 Construction of a “plasmid shuffle” strain to enable studies of Tub2 mutations

As outlined above, the data suggests that the functions of β -tubulin (Tub2) and sumo (Smt3) act together to regulate cell cycle progression. Hence, to allow further studies of the relationships between Tub2 and Smt3 it would be very useful to be able to make specific mutations of *TUB2* that may impact on sumo function. However, as described earlier (see Chapter 1 section 1.4.2.1) the *TUB2* gene is essential and hence the wild type gene cannot be deleted from the genome in the absence of another source of the *TUB2* gene. Previous studies in *S. cerevisiae* developed a technique, known as the plasmid shuffle technique (Fan and Xiao, 2021), which allows straightforward construction and testing of mutations in essential genes. Hence, the plasmid shuffle technique was utilised to begin to study specific mutations of *TUB2*. The first step in the procedure involved constructing a single copy *URA3* plasmid that expresses the wild type *TUB2* gene from its own promoter. Hence, the *TUB2* gene with the complete promoter and 3' regions of the gene was amplified by PCR using the PRS316TUB2 Forward and PRS316TUB2 Reverse primers and genomic DNA from the wild type (GC1) strain as template (Figure 5.7). Next, the PCR product was co-transformed into GC1 cells with the pRS316 plasmid (Sikorski and Hieter, 1989) that had been digested with Xba1 and Sac1 restriction enzymes and transformed cells were plated on media lacking uracil (Figure 5.10A). The PRS316 Forward and PRS316 Reverse primers contain a short region of homology at the 5' end of each primer with the regions of the plasmid located next to the Xba1 and Sac1 restriction enzymes (Fig. 5.8, 5.9). Hence, this allows the construction of the pRS316-*TUB2* plasmid by homologous recombination between the PCR product and the Xba1/Sac1 digested pRS316 plasmid (Fig. 5.7, 5.9). After 3-5 days, Ura⁺ yeast colonies were checked by PCR to confirm the presence of pRS316-*TUB2* (data not shown). Plasmids were extracted from PCR positive colonies and the DNA sequence was obtained to confirm the sequence of pRS316-*TUB2*. Two individual yeast colonies yielded pRS316-*TUB2* plasmids that did not contain any mutations within the PCR fragment insert and one was used for all the subsequent work in this thesis.

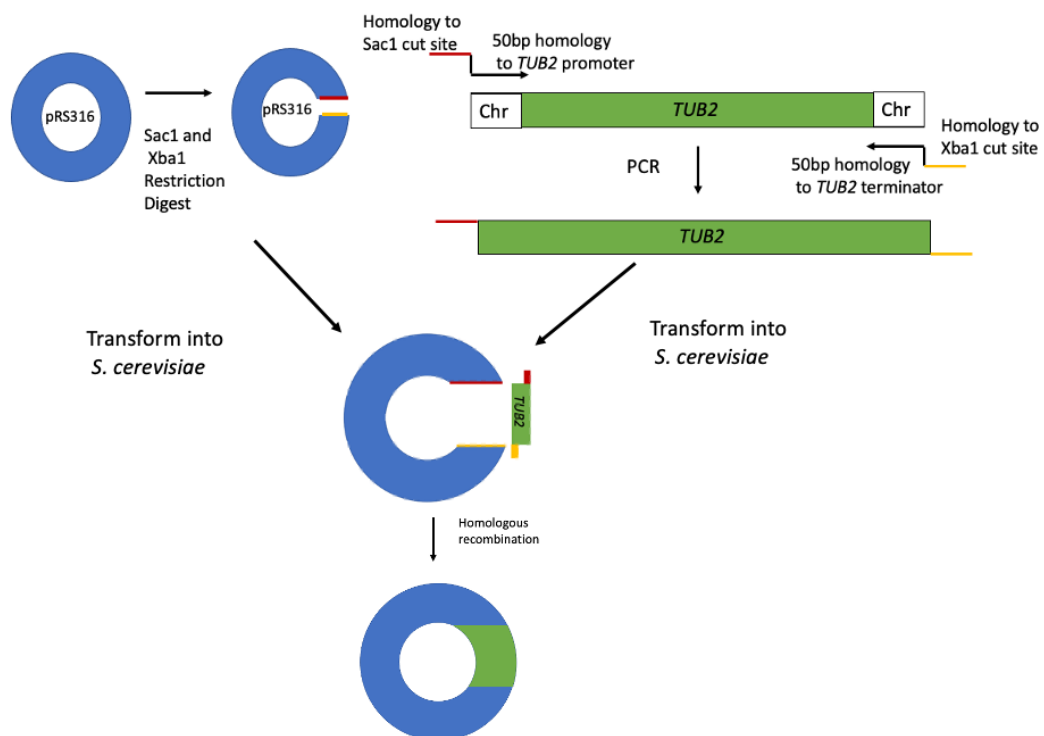


Figure 5.7 Strategy to create the pRS316-*TUB2* plasmid. Schematic diagram of pRS316 WT-*TUB2* plasmid construction in *S. cerevisiae*. Forward primers were designed with 20bp homology to the pRS316 *SacI* cut site and the first 20bp of the *TUB2* promoter (Sikorski and Hieter, 1989). Reverse primers were designed with 20bp homology to the last 20bp of the *TUB2* terminator and 20bp homology to the pRS316 *XbaI* cut site. A PCR reaction (see Chapter 2 section 2.2.1) containing both the forward and reverse primers along with *S. cerevisiae* genomic DNA (taken from a plated colony of GC1) as template was performed to generate a cassette containing the *TUB2* gene including the promoter and terminator regions and with 20bp homology upstream and downstream to the *XbaI* and *SacI* restriction enzyme cut sites respectively in YCplac111. The *TUB2* cassette was run on a 1% agarose gel (see Chapter 2 section 2.2.2) to confirm the fragment size, transformed into *S. cerevisiae* cells and plated onto plates lacking uracil.

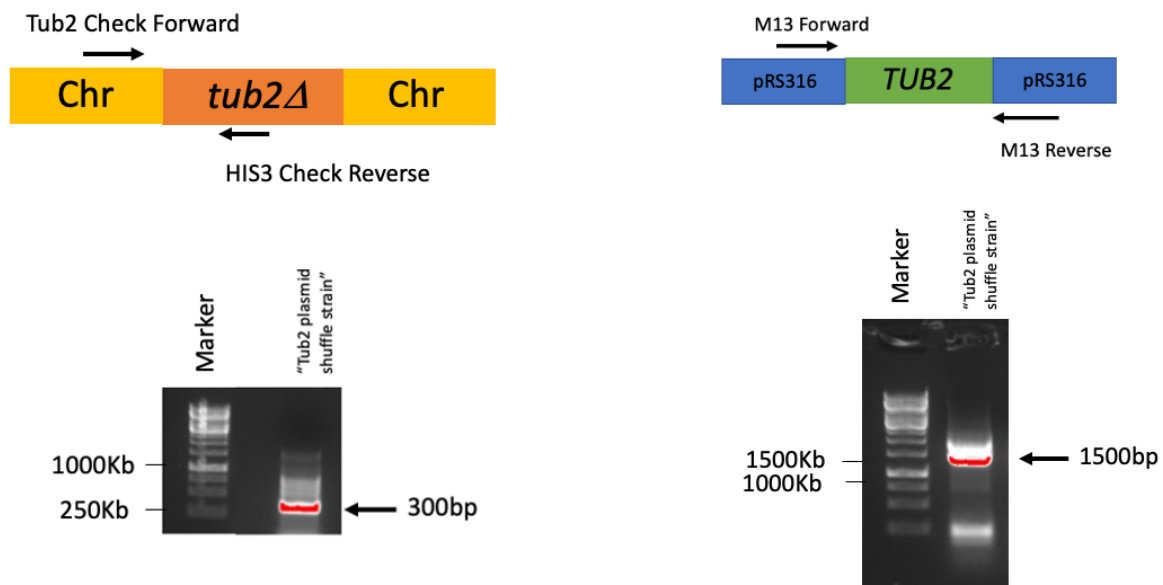


Figure 5.8 Verification of the Tub2 “Plasmid Shuffle Starting Strain”. (A) Tub2 Check Forward primers were designed with 20bp homology to the promoter region upstream of *TUB2* and HIS3 Check Reverse primers were designed with 20bp homology to the *HIS3* deletion cassette. To confirm the integration of the Tub2 Δ cassette from HIS3+ growing colonies, a PCR reaction was set up (see Chapter 2 section 2.2.1) containing both the forward and reverse primers along with *S. cerevisiae* genomic DNA (taken from growing GC55 colonies transformed with the Tub2 Δ cassette and pRS316 plasmid) as a template. A fragment of \sim 300bp (indicated by the arrow) confirmed the presence of the Tub2 Δ cassette. (B) M13 Forward and M13 Reverse Primers have homology to two sites located on opposite sides of the *TUB2* gene insert in the pRS316-*TUB2* plasmid. To confirm the presence of the pRS316-*TUB2* plasmid from URA3+ growing colonies, a PCR reaction was set up (see Chapter 2 section 2.2.1) containing both the M13 Forward and M13 Reverse primers along with *S. cerevisiae* genomic DNA (taken from growing GC55 colonies transformed with the Tub2 Δ cassette and pRS316-*TUB2* plasmid) as a template. A fragment of \sim 1500bp (indicated by the arrow) confirmed the presence of the pRS316-*TUB2* plasmid.

Step 1

"Tub2 plasmid shuffle strain" created by co-transformation of the *TUB2* deletion cassette and the *URA3* plasmid expressing the WT Tub2 protein.

Step 2

Transform *LEU2* plasmids expressing the different Tub2 mutations into the "Tub2 plasmid shuffle strain"

Step 3

Remove the *URA3* plasmid expressing the WT Tub2 protein, leaving only the *LEU2* plasmid expressing the different Tub2 mutation to be expressed.

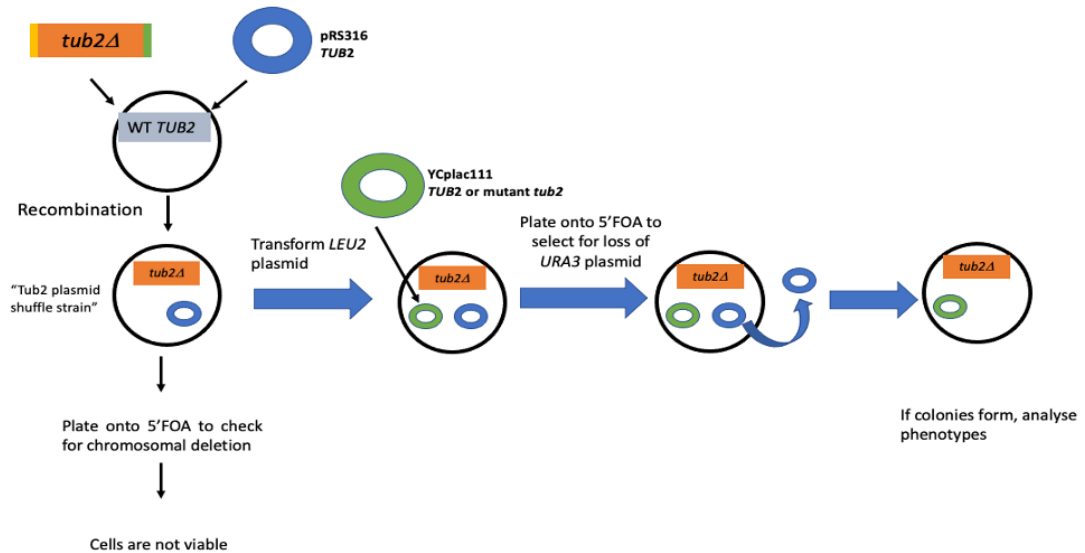


Figure 5.9 Tub2 Plasmid Shuffle Strategy. The first step in the development of the Tub2 plasmid shuffle strategy is to create the starting strain. Briefly, the *TUB2Δ* cassette along with the *pRS316-TUB2* plasmid are co-transformed into midlog growing wild type (GC55) cells and plated onto *-HIS3 -URA3* plates. Plates are incubated for 3-5 days, or until visible colonies formed. Colonies are subsequently streaked out onto plates containing 5'FOA, with the loss of viability in these colonies indicating that cells were selected for loss of the *URA3 pRS316-TUB2* plasmid. Next, *LEU2* plasmids (*YCplac111*) expressing either mutant *tub2* or wildtype *TUB2* are transformed into the Plasmid Shuffle Starting Strain and plated onto media containing 5'FOA. Cells are selected for the loss of the *URA3* plasmid, leaving the *LEU2* plasmid expressing the mutant *tub2* or wildtype *TUB2*. If colonies are formed in cells expressing a mutated *tub2*, phenotypes of these *tub2* mutations can now be analysed.

At the same time as the pRS316-*TUB2* plasmid was constructed, a single copy *LEU2* plasmid that expresses the wild type *TUB2* gene from its own promoter was also constructed, using the same techniques as described above. Briefly, the *TUB2* gene with the complete promoter and 3' regions of the gene was amplified by PCR using the TUB2YCplac111 Forward and TUB2YCplac111 Reverse primers and genomic DNA from the wild type (GC1) strain as a template. Next, the PCR product was co-transformed into GC1 cells with the YCplac111 plasmid that had been digested with Nhe1 and Sac1 restriction enzymes and transformed cells were plated on media lacking leucine. The TUB2YCplac111 Forward and TUB2YCplac111 Reverse primers contain a short region of homology at the 5' end of each primer with the regions of the plasmid located next to the Nhe1 and Sac1 restriction enzymes, enabling the construction of the YCplac111-*TUB2* plasmid by homologous recombination between the PCR product and the Nhe1/Sac1 digested YCplac111 plasmid. After 3-5 days, Leu²⁺ yeast colonies were checked by PCR to confirm the presence of YCplac111-*TUB2* (data not shown). Plasmids were extracted from colonies and DNA sequencing confirmed that the YCplac111-*TUB2* did not contain any mutations within the PCR fragment insert. Hence, now two plasmids had been constructed, both expressing the *TUB2* gene with the complete promoter and 3' regions.

The next step in the strategy to mutagenise *TUB2* was to construct a haploid strain in which the wild type *TUB2* gene was completely deleted from the genome and also contained the pRS316-*TUB2* plasmid to maintain viability (Figure 5.9, step 1). Hence a *TUB2* gene deletion *HIS3* cassette was obtained by PCR using the primers Tub2Delete Forward and Tub2Delete Reverse and the YDp-*HIS3* (Berben et al., 1991) plasmid as template. This creates a gene deletion cassette which has 50bp at the ends of the cassette that are homologous to the regions adjacent to the *TUB2* promoter and terminator regions (see Chapter 2 section 2.1.2). A PCR product of ~1300kb was produced which matched the predicted size of 1300kb for the gene deletion cassette (data not shown). To create the strain with a deletion of the *TUB2* gene on the genome and containing pRS316-*TUB2* (Figure 5.19, step 1) the *TUB2* gene deletion cassette and pRS316-*TUB2* were co-transformed into the wild type strain background, BY4741 (GC1), used in the original SGA screen and transformed cells were plated on media lacking uracil and histidine. Curiously, although the strain construction of a *tub2Δ* mutant containing pRS316-*TUB2* was viable and successful as confirmed by PCR (data not shown), microscopic analyses of the cells revealed that they were much larger than normal

and displayed morphological defects (data not shown). Furthermore, western blot analysis of the β -tubulin protein expressed in this mutant from the pRS316-*TUB2* plasmid indicated that the protein had a much faster mobility than wild type control cells (data not shown). The explanation for the phenotypes detected in this mutant strain is not clear but indicated that this strain would not be suitable for further experiments using a plasmid shuffle approach.

It was possible that the BY4741 genetic background might be influencing the ability to create the *tub2 Δ* plasmid shuffle strain. Consequently, it was decided to attempt to create the required *tub2 Δ* plasmid shuffle mutant in a different wild type strain (GC55), the control strain for the *smt3-allR* mutant which was studied extensively in Chapters 3 and 4. This wild type strain is closely related to the BY4742 strain background (Srikumar et al., 2013a). Hence, the *TUB2* gene deletion cassette and pRS316-*TUB2* were co-transformed into GC55 cells and transformed cells were plated on media lacking uracil and histidine (Figure 5.9, step 1). One colony was obtained after several attempts and was picked for further analysis and named strain GC134 (Plasmid shuffle starting strain). First, the integration of the *TUB2* gene deletion cassette in GC134 was confirmed by PCR (Figure 5.8A). The detection of a \sim 300bp PCR product confirmed correct integration of the *TUB2* gene deletion cassette (Figure 5.8A). To confirm the presence of the pRS316-*TUB2* plasmid in GC134 a PCR reaction was performed using the standard M13 forward and M13 reverse primers whose binding sites are located on opposite sides of the *TUB2* gene insert in the pRS316-*TUB2* plasmid. The presence of pRS316-*TUB2* in the GC134 strain was confirmed by the detection of a PCR product of expected size \sim 1500bp (Figure 5.9B). Importantly, microscopic analysis confirmed that cells of the new strain displayed normal morphologies (data not shown).

Next, to confirm that the strain was ready for use in the plasmid shuffle technique, GC134 cells were transformed with the single copy *LEU2* plasmid, YCplac111, and plated onto 5'FOA media. Overexpression of Tub2 is lethal in *S. cerevisiae* cells (Katz et al., 1990, Burke et al., 1989), so it was uncertain whether colonies would form with the transformation of the new plasmid, as the levels of Tub2 in the cells would be elevated. As expected, GC134 cells transformed with the YCplac111 empty vector (EV) were unable to grow on 5'FOA media confirming that cells cannot lose the pRS316-*TUB2* plasmid and retain viability (Figure 5.11A). Conversely, GC134 cells transformed with the YCplac111-WT-*TUB2* plasmid (strain GC136

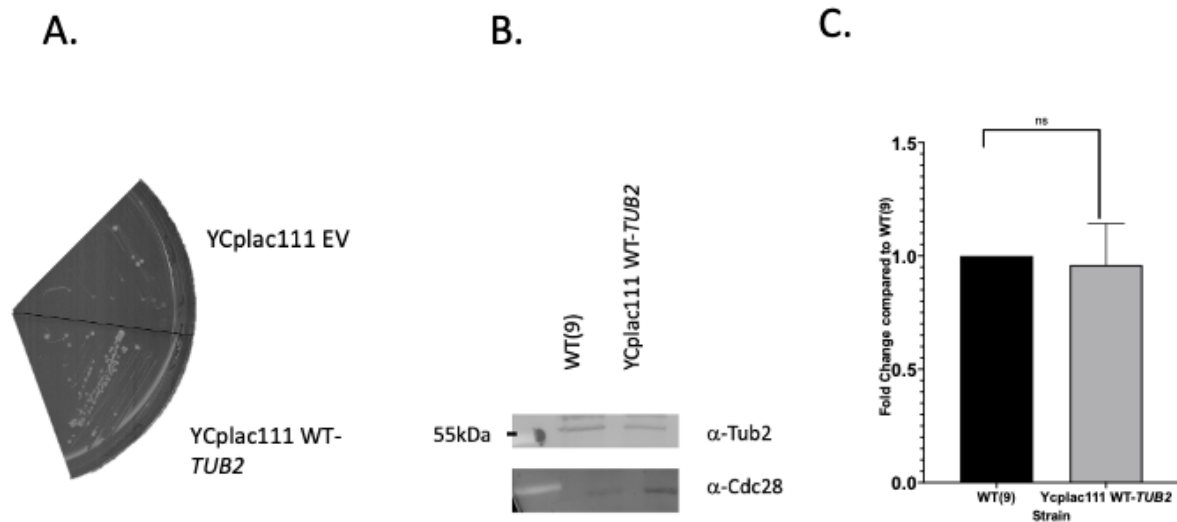
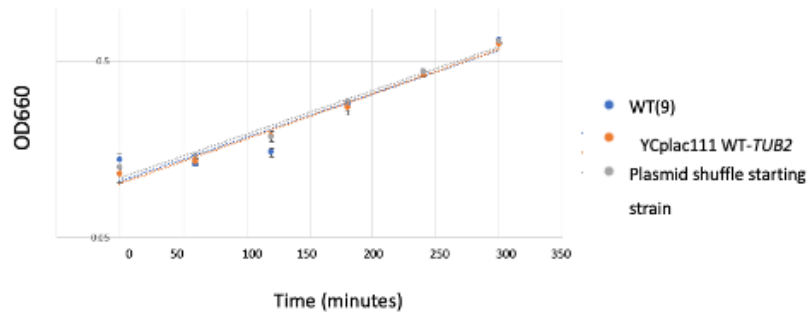


Figure 5.10. GC136 cells express wild type Tub2 levels. (A) GC136 and a control strain expressing the YC plac111 empty vector (EV) were streaked onto 5'FOA plates and images after 5 days. (B) Proteins were TCA extracted from mid-log phase growing wild type (GC55), and YCplac111-*TUB2* (GC136) cells and analysed by western blotting using an anti- β -tubulin antibody. A representative blot of three biological repeats is shown. (C) Blots were stripped, re-probed with anti-Cdc28 antibody as a loading control and quantified using ImageQuant (GE Healthcare). Error bars represent SD. Bars represent β -tubulin levels normalised to the wild type control (GC55). P values were derived from an unpaired T-test.

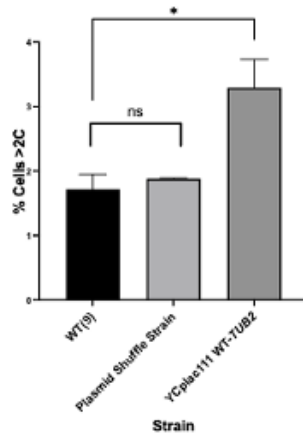
A.



B.

Strain	Doubling Time	G1	S	G2/M
WT(9)	117±3	38±3	35±1	40±2
Plasmid Shuffle Strain	122±1	40±1	36±1	44±3
YCplac111 WT-TUB2	117±2	37±2	35±1	44±2

C.



D.

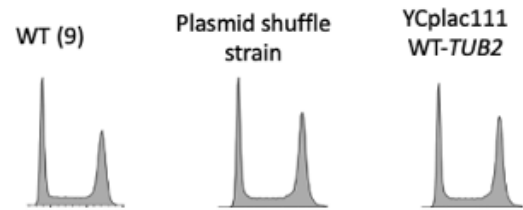


Figure 5.11 Cell cycle analysis of the YCplac111-TUB2 (GC136) strain. (A) Growth curves of mid-log phase growing cultures of wild type (GC55), Plasmid Shuffle Strain (GC134), and YCplac111-TUB2 (GC136) cells. Error bars represent SD from 3 biological repeats. (B) (C) Gating analysis of the DNA content analyses in (D) of cells containing >2C DNA content. P values were derived from an unpaired T-test, (*) indicates $p < 0.05$, (**) indicates $p < 0.01$ and (***) indicates $p < 0.001$. (D) DNA content analysis was performed on mid-log phase growing cultures of wild type (GC55), Plasmid Shuffle Strain (GC134) and YCplac111-TUB2 (GC136) cells and presented as indicated. (E) Gating analysis of the DNA content analyses in (C) of the time cells spent in each stage of the cell cycle.

were viable. Excitingly, this now meant that the plasmid shuffle strain had been successfully constructed and would enable any *tub2* mutants to be analysed in future. Next, it was important to confirm that that Tub2 protein expressed by the YCplac111-WT-*TUB2* plasmid was stable and expressed *TUB2* at levels similar to wild type cells. Indeed, the western blot analyses of midlog growing GC136 cells revealed that that β -tubulin was expressed at similar levels which were not significantly different to wild type control cells (Figure 5.10B/C). Importantly, growth rate analysis confirmed that YCplac111-WT-*TUB2* (GC136) cells grew almost identical to wild type cells (GC55) (117 \pm 3 minutes in GC136 compared to 117 \pm 2 minutes in GC134). Next, DNA content analysis was performed on performed on mid-log phase growing cultures of wild type (GC55), Plasmid Shuffle Strain (GC134) and YCplac111-*TUB2* (GC136) cells. Surprisingly, YCplac111-*TUB2* cells appear to show slight aneuploidy compared to the wild type control strain (3.2% >2C DNA content compared to \sim 1.8 >2C DNA content, respectively). Indeed, CEN plasmids, such as YCPlac111, are present in a single copy in the cell and are replicated analogous to an additional yeast chromosome. However, it is estimated that \sim 5% of plasmids are lost during replication, which may explain the slight increase in aneuploidy associated with the GC136 strain (Fig. 5.12C). Nevertheless, the reason behind the YCplac111-*TUB2* is unclear.

Next, the proportion of cells in each cell cycle phase was combined with the doubling times of the wild type (GC55), Plasmid Shuffle Strain (GC134) and YCplac111-*TUB2* (GC136) strains to calculate the approximate time that each strain spends in each phase of the cell cycle (Morgan et al., 1991), Fig. 5.11E). Importantly, although the DNA content analysis indicated that the YCplac111-*TUB2* strain showed slight aneuploidy compared to wild type cells, YCplac111-*TUB2* cells do not appear to show any cell cycle defects, with G1, S and G2/M phases almost identical to wild type cells (Fig. 5.11E).

5.2.4 Investigation of covalent and non-covalent interactions of sumo with Tub2

As described above the *tub2* Δ plasmid shuffle strain was successfully constructed and, moreover, the 5'FOA selection procedure was shown to work successfully to “swap” the

pRS316-*TUB2* plasmid with the YCplac111-*TUB2* plasmid. Having obtained these reagents, the next step was to utilise them to begin to investigate the relationships between sumo and the function of Tub2. As described previously, earlier studies have suggested that Tub2 is sumoylated and that Tub2 can interact with sumo through non-covalent interactions (Greenlee et al., 2018). With respect to potential sumoylation site(s) in Tub2 the sumo consensus motif has been relatively well characterised (Chapter 1, section 1.2.1 and 1.3.1). However, this consensus sequence does not predict 100% of sumoylated residues (Chapter 1 section 1.2.3.5). Nevertheless, several sumo prediction software packages have been developed to allow the identification of potential sumo sites in a protein of interest (Zhao et al., 2014, Beauclair et al., 2015). With respect to the detected non-covalent interactions between Tub2 and sumo these results suggested that Tub2 may contain a SIM domain(s) (Greenlee et al., 2018)(Chapter 1, section 1.3.1). SIM domains are often present in large protein complexes and have been proposed to act as a molecular “glue” that stabilises interactions within the complex (Matunis et al., 2006) (Chapter 1 section 1.3.6). Based on this proposal, it is possible that a SIM domain(s) in Tub2 acts to stabilise microtubule filaments. Significantly, similar to the sumo consensus motif, software packages have been developed to identify potential SIM domains in proteins (Zhao et al., 2014, Beauclair et al., 2015)(<http://sumosp.biocuckoo.org/showResult.php>). Hence, it was decided to apply these software packages to identify potential SIM domain consensus sequence(s) and sumoylation site consensus sequence(s) in Tub2 and then utilise the plasmid shuffle technique with the newly constructed *tub2Δ* reagents to study the functions of any identified sites.

5.2.4.1 Investigation of non-covalent interactions of sumo with Tub2

To begin to investigate potential non-covalent interactions between sumo and Tub2, the protein sequence of Tub2 was subjected to a high-stringency search for potential SIM domains using the prediction tool, GPS-SUMO, developed by Zhao et al. (Zhao et al., 2014)(<http://sumosp.biocuckoo.org/showResult.php>) Excitingly, several potential SIM domains were identified in Tub2, with the IIHI sequence located extremely close to the Tub2 N terminal domain classified as the most statistically significant SIM domain ($p=0.003$) (Fig. 5.12A). SIM domains have characteristic motifs, including the V/I-X-V/I-V/I motif, which

A.

Amino Acid Position in Tub2	Sequence	P Value
4-7	MRE IIHI STGQCGNQ	0.003
149-152	GGTGSGMG TLLI SKIREEFP	0.01
255-258	NSDLRKLAV NLV PFPR LHFF	0.081

← Inverted SIM motif.
Most significant SIM domain in Tub2.

B.

V/I-V/I-X -V/I Song et al. (2005)

C.

WT MRE**IIHI**STG
 ↓
 SIM MRE**AAAA**STG

Figure 5.12 Identification of a putative Tub2 SIM domain. (A) The sequence of Tub2 was subjected to a high-stringency search for potential SIM domains using the sumo site prediction tool available at <http://sumosp.biocuckoo.org/>. The location, sequence and P values of potential SIM domains are detailed in the table. (B) Sequence of the SIM domain, as characterised by (Song et al., 2005). (C) Amino acid alignment of the IIHI SIM domain in Tub2 with the sequence of the proposed SIM mutation. The Tub2 IIHI SIM domain was mutated to AAAA to remove the negatively charged sumo binding site, as in (Kung et al., 2014).

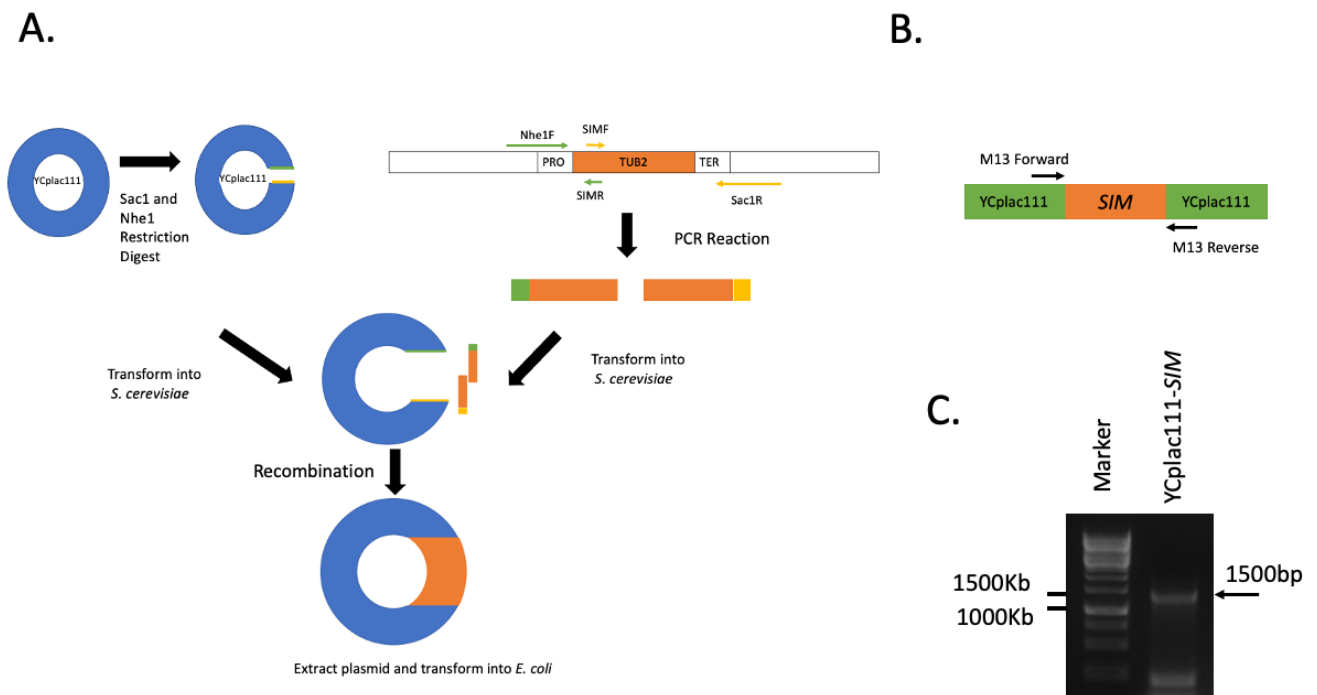


Figure 5.13 Construction of the YCplac111-SIM strain. (A) To construct the YCplac111-SIM plasmid expressing the *tub2-SIM* mutant protein two primers were designed, NHE1F and SAC1R, with 50bp homology to the *TUB2* promoter and terminator regions of the *TUB2* gene, respectively, followed by either a Nhe1 or a Sac1 restriction site, respectively. Internal primers, SIMR and SIMF, were designed to mutate the I1H1 amino acids located at the N-terminus of Tub2 to AAAA (Kung et al., 2014). Two PCR reactions were set up with either the NHE1F and SIMR primers or the SAC1R and SIMF primers, using wild type (GC55) genomic DNA as a template in both PCR reactions. The two PCR fragments were analysed on a 1% agarose gel to confirm the fragment sizes (data not shown). PCR products were isolated from the agarose gel, transformed into the GC55 strain with Nhe1/Sac1 digested YCplac111 and plated onto plates lacking leucine. (B) M13 Forward and M13 Reverse Primers have homology to two sites located on opposite sides of the *SIM* insert in the YCplac111 plasmid. To confirm the presence of the YCplac111-SIM plasmid from LEU2+ growing colonies, a PCR reaction was set up (see Chapter 2 section 2.2.1) containing both the forward and reverse primers along with *S. cerevisiae* genomic DNA (taken from growing GC55 colonies transformed with the YCplac11-SIM plasmid) as a template. (C) A fragment of ~1500bp (indicated by the arrow) confirmed the presence of the *SIM* insert in the YCplac111 plasmid. Plasmids were subsequently extracted from yeast colonies (see Chapter 2 section 2.2.4) and sequenced.

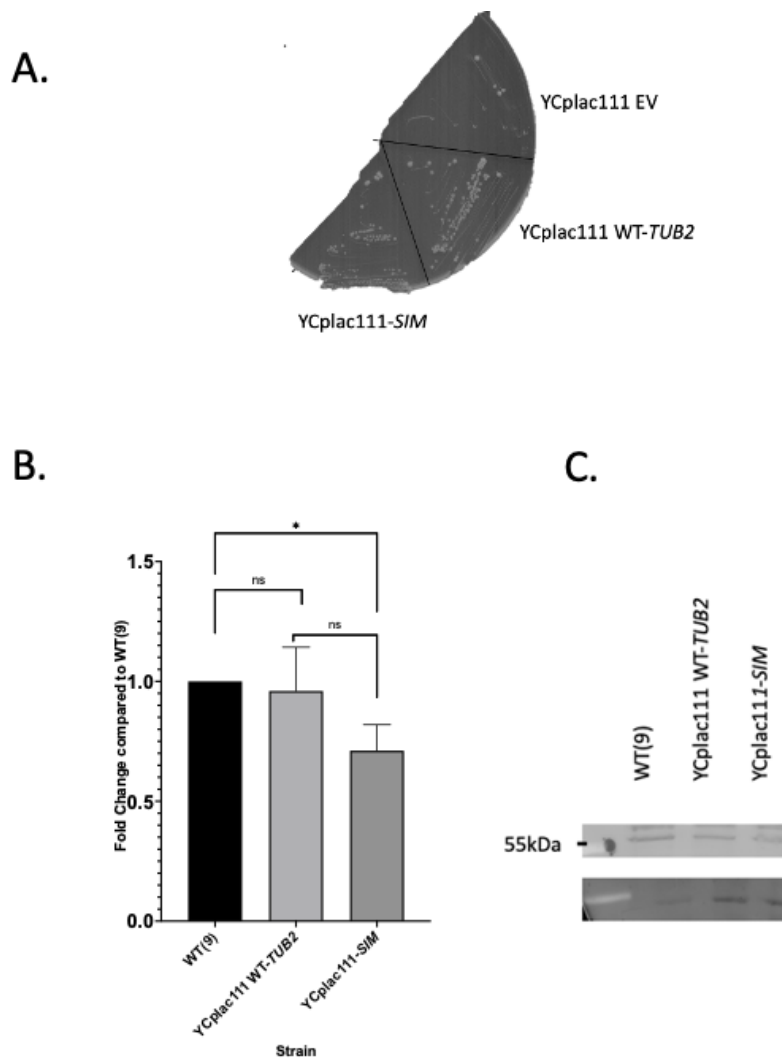


Figure 5.14. Mutations of the Tub2 SIM domain are not lethal. (A) GC136, GC138 and a control strain expressing the YC *plac111* empty vector (EV) were streaked onto 5'FOA plates and images after 5 days. (B) Proteins were TCA extracted from mid-log phase growing wild type (GC55), YC*plac111-TUB2* (GC136) and YC*plac111-SIM* (GC138) cells and analysed by western blotting using an anti- β -tubulin antibody. A representative blot of three biological repeats is shown. (C) Blots were stripped, re-probed with anti-Cdc28 antibody as a loading control and quantified using ImageQuant (GE Healthcare). Error bars represent SD. Bars represent β -tubulin levels normalised to the wild type control. P values were derived from an unpaired T-test.

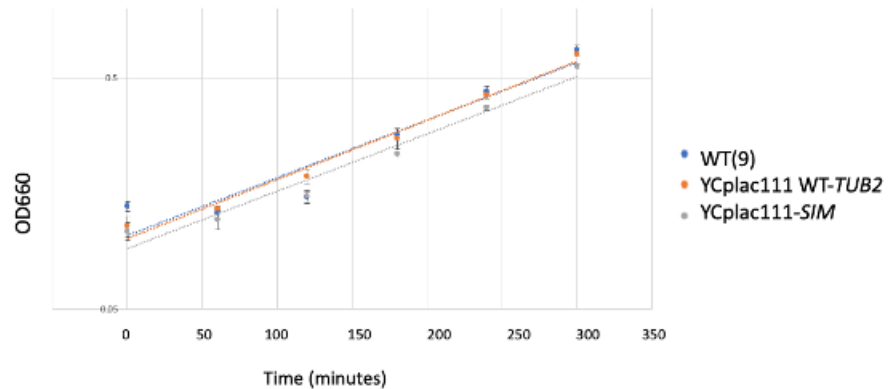
interact with the sumo β -sheet in either parallel or antiparallel confirmations (Kung et al., 2014, Sun et al., 2007) (Fig. 5.12A). Interestingly, the IIHI SIM domain identified in Tub2 represents an inverted SIM motif V/I-V/I-X-V/I, suggesting that it may interact with sumo in an antiparallel manner. Previous studies investigating the binding properties of SIM domains revealed that mutating amino acids within the SIM consensus sequence to alanine residues prevented the sumo-SIM interaction, hence we also decided to substitute the Tub2 IIHI motif with four alanine amino acids (Kung et al., 2014) (Fig. 5.12C). To substitute the IIHI motif located at the N-terminus of Tub2 with four alanine amino acids, a PCR mutagenesis and plasmid construction strategy was designed to express the mutant version of the Tub2 protein from the single copy *LEU2* YCplac111 plasmid from its own promoter (YCplac111-SIM, Figure 5.13A). Specifically, two PCR fragments spanning the *TUB2* gene with the complete promoter and 3' regions of the gene, and that included the DNA sequence substitutions to mutate the IIHI motif, were amplified by PCR (data not shown) using the NHE1F/SIMR primers and the SAC1R/SIMF primers respectively and genomic DNA from the GC55 wild type strain as a template (Figure 5.13A). Next, the PCR products were co-transformed into GC55 cells with the YCplac111 plasmid that had been digested with Nhe1 and Sac1 restriction enzymes and transformed cells were plated on media lacking leucine (Figure 5.13A). The NHE1F and SAC1R primers contain a short region of homology at the 5' end of each primer with the regions of the plasmid located next to the Nhe1 and Sac1 restriction enzymes (Figure 5.13A). Hence, this allowed the construction of the YCplac111-SIM plasmid by homologous recombination between the PCR products and the Nhe1/Sac1-digested YCplac111 plasmid (Figure 5.13A). After 3-5 days, Leu⁺ yeast colonies were checked by PCR (Figure 5.13B) and restriction digest analysis of plasmids recovered from *S. cerevisiae* into *E. coli* (data not shown) to confirm construction of YCplac111-SIM. Finally, DNA sequence analyses confirmed the successful mutation of the sequences encoding the IIHI motif and also that no other changes in the *TUB2* gene had arisen in the construction of the plasmid. The YCplac111-SIM plasmid was subsequently extracted from yeast cells and transformed into the Plasmid Shuffle strain (GC134) (Fig. 5.9, step 2).

Next, the viability of the SIM mutation was assessed. Colonies from the YCplac111-SIM plasmid transformation were streaked onto 5'FOA media to assess the ability of the YCplac111-SIM plasmid to replace the pRS316-TUB2 plasmid in the Plasmid Shuffle strain

(Figure 5.14). As expected, the YCplac111 EV was unable to replace pRS316-*TUB2* whilst the YCplac111-*TUB2* enabled growth on 5-FOA media (Figures 5.11A and 5.14A). Excitingly, the YCplac111-*SIM* plasmid was also able to replace the pRS316-*TUB2* plasmid, indicating that the mutant version of Tub2 expressed from the YCplac111-*SIM* is functional (Figure 5.14A). It was also important to confirm that that mutated Tub2 expressed by the YCplac111-*SIM* plasmid was stable and expressed at levels similar to wild type cells. Indeed, the western blot analyses of midlog growing GC138 cells revealed that the *SIM* mutant was expressed at lower levels than cells expressing the YCplac111-*TUB2* plasmid (Figure 5.14B/C). Although the levels of β -tubulin appear to be lower in GC138 cells, this is not significantly different to the level of β -tubulin expressed in cells expressing the YCplac111-*TUB2* plasmid. Hence, it could be confirmed that the *SIM* mutant was viable and that the mutation did not significantly affect the stability of β -tubulin protein levels. Interestingly, Tub2 autoregulation is a mechanism used by the cell to ensure that there is a finely regulated pool of free tubulin dimers available in the cytosol of eukaryotic cells. This autoregulation is achieved in mammalian cells by recognition of the N-terminal MREI sequence in Tub2 by an unknown mediator protein, resulting in the destabilisation of Tub2 transcripts (Gay et al., 1989). Surprisingly, the Tub2 SIM domain identified in this study lies adjacent to this conserved MREI sequence (Fig. 5.12C), hence it is surprising that mutation of the SIM domain does not appear significantly alter Tub2 protein levels (Fig. 5.14C). However, this may explain the slightly lower levels of Tub2 expressed in cells dependant on the YCplac111-*SIM* plasmid. Nevertheless, as the stability and viability had been confirmed, the YCplac111-*SIM* mutant was subject to further phenotype analysis.

Next, the growth of YCplac111-*SIM* (GC138) cells were compared with YCplac111-*TUB2* (GC136) cells (Fig. 5.15A). Interestingly, growth rate analyses indicated that the doubling time of the cells dependent on YCplac111-*TUB2* is 117 ± 2 minutes compared to a doubling time of 128 ± 3 minutes for the cells dependent on YCplac111-*SIM* (Fig. 5.15A/B). Hence it appears that cells dependant on the YCplac111-*SIM* grow slower than cells expressing the wild type Tub2. Next, DNA content analysis was performed on cultures of the mid-log phase growing cells dependent on either the YCplac111-*TUB2* plasmid (GC136) or the YCplac111-*SIM* plasmid (GC138). Interestingly, these data revealed that mutation of the potential SIM domain of Tub2 did not cause any significant increase in aneuploidy (Figure 5.15C/D). This contrasts with

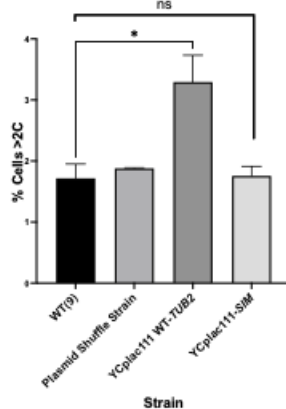
A.



B.

Strain	Doubling Time	G1	S	G2/M
WT(9)	117±3	38±3	35±1	40±2
Plasmid Shuffle Strain	122±1	40±1	36±1	44±3
YCplac111 WT-TUB2	117±2	37±2	35±1	44±2
YCplac111-SIM	128±3	39±3	41±2	47±1

C.



D.

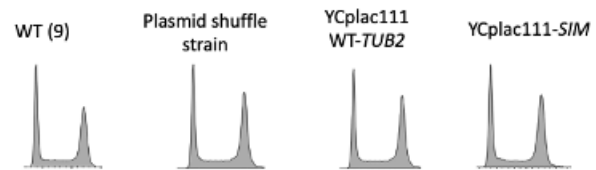


Figure 5.15 Cell cycle analysis of the YCplac111-SIM (GC138) strain. (A) Growth curves of mid-log phase growing cultures of wild type (GC55), YCplac111-*TUB2* (GC136) and YCplac111-*SIM* (GC138) cells. Error bars represent SD from 3 biological repeats. (B) Gating analysis of the DNA content analyses in (C) of the time cells spent in each stage of the cell cycle. (C) DNA content analysis was performed on mid-log phase growing cultures of wild type (GC55), Plasmid Shuffle Strain (GC134), YCplac111-*TUB2* (GC136) and YCplac111-*SIM* (GC138) cells and presented as indicated. (E) (D) Gating analysis of the DNA content analyses in (C) of wild type (GC55), Plasmid shuffle strain (GC134), YCplac111-*TUB2* (GC136) and YCplac111-*SIM* (GC138) cells containing >2C DNA content. P values were derived from an unpaired T-test, (*) indicates $p < 0.05$.

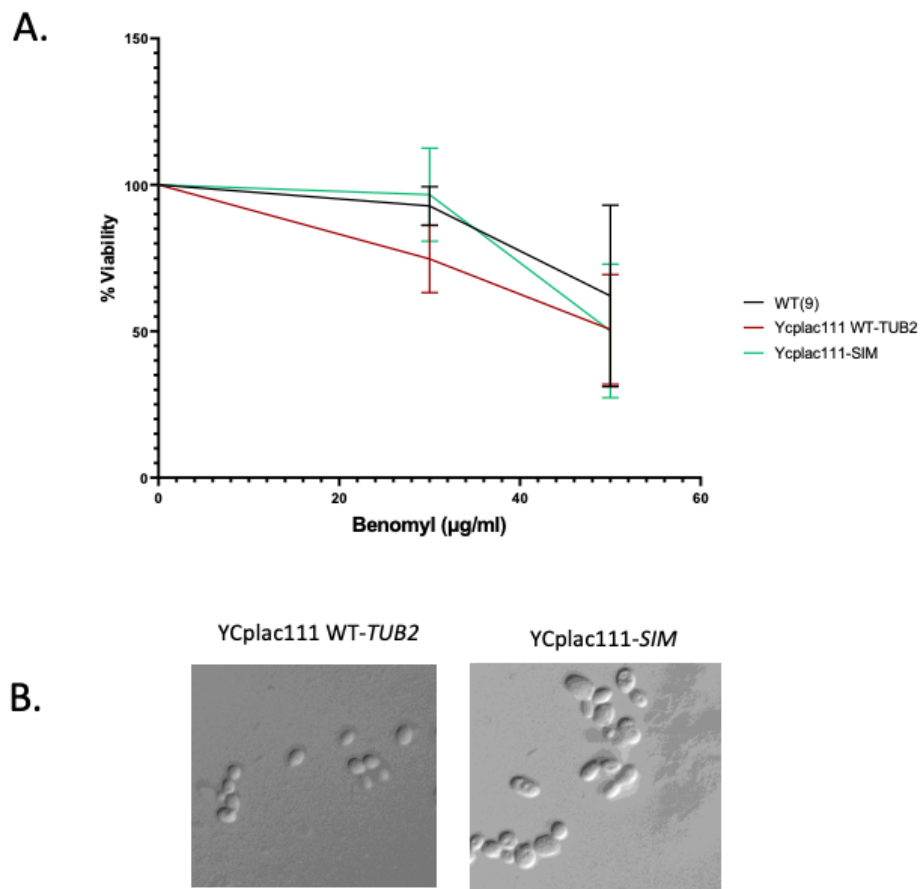


Figure 5.16 *SIM* mutants are not sensitive to microtubule depolymerisation agents. (A) Equal numbers of mid-log phase growing wild type (GC55) cells and cells containing either YCplac111-*TUB2* (GC136) or YCplac111-*SIM* (GC138), were plated on YPD plates containing the indicated benomyl concentrations. Plates were incubated at 30°C until colonies formed. % survival was calculated based on the colonies formed on the 0µg/ml benomyl plates. Error bars represent SD from 3 biological replicates. P values were derived from an unpaired T-test, all samples are not significantly different compared to WT(9). (B) Cells containing either YCplac111-*TUB2* (GC136) or YCplac111-*SIM* (GC138) were grown to mid-log phase in minimal media lacking leucine and visualised by DIC.

the analyses of the *tub2* mutant strain (see section 5.2.1.2) which displays significantly increased levels of aneuploidy (Fig. 5.1C/D, Fig. 5.5). To further analyse the cell cycle defects associated with cells dependent on YCplac111-*SIM*, the proportion of cells in each cell cycle phase was combined with the doubling times of the cells dependent on either the YCplac111-*TUB2* or YCplac111-*SIM* plasmids to calculate the approximate time that these cells spend in each phase of the cell cycle (Morgan et al., 1991). One striking result from this analysis was the increase in time that YCplac111-*SIM* dependent cells spend in S Phase compared to YCplac111-*TUB2* dependent cells (Fig. 5.15B). In particular, cells dependent on YCplac111-*SIM* were found to spend ~47 minutes in S Phase in comparison to cells dependent on YCplac111-*TUB2* which spend ~35 minutes in S Phase (Fig. 5.15B). Hence, it can be concluded that the mutation of the potential SIM domain compromises the normal function of Tub2. In contrast to *tub2* cells, which have a severe G2/M delay (Fig. 5.1E), YCplac111-*SIM* cells do not appear to have mitotic defects (Fig. 5.15B) suggesting that a reduction of Tub2 contributes to the *tub2* G2/M delay. Furthermore, these results also suggest that the Tub2 SIM domain mutated in this study does not have a key role in the progression through mitosis.

As described above (section 5.2.1.3, Fig. 5.2) the *tub2* mutant which expresses lower levels of β -tubulin exhibited increased sensitivity to benomyl. Hence, given the defects of cell cycle progression associated with the mutation of the potential SIM domain of Tub2, the benomyl sensitivity of cells expressing this mutant version of Tub2 was investigated. Interestingly, the resistance of cells containing the YCplac111-*SIM* plasmid to benomyl was not significantly different to cells containing the YCplac111-*TUB2* (Fig. 5.16A). Hence, as β -tubulin protein levels are not significantly different in cells containing the YCplac111-*SIM* plasmid compared to containing the YCplac111-*TUB2* plasmid (Fig. 5.14C), these results suggest that it is the reduced level of Tub2 in *tub2* cells which contributes to the *tub2* benomyl sensitivity.

Cells dependent on YCplac111-*SIM* were found to be larger than the control cells dependent on YCplac111-*TUB2* (Figure 5.16B). However, cells dependent on YCplac111-*SIM* are not as large as *tub2* or *smt3* cells (data not shown). These findings are consistent with Fig. 5.15B, suggesting that the YCplac111-*SIM* strain does not show significant mitotic delays, unlike the *tub2* strain (Fig.5.15B). Taken together, these results suggested that the potential SIM

domain located at the N-terminus of Tub2, although not essential for viability, appears to be important during S Phase, although this role remains unclear.

Interestingly, recent studies have suggested a role for microtubules during S Phase (Laflamme et al., 2019). For example, Laflamme et al. revealed that Tub2 mutants which are sensitive to DNA damaging agents showed cell cycle delays which were independent of the S-Phase checkpoint response (Laflamme et al., 2019). Interestingly, the authors suggest that during S Phase microtubules are able to detect lesions in DNA, preventing errors in DNA replication prior to entry into mitosis (Laflamme et al., 2019). Hence, cells dependent on YCplac111-*SIM* may have problems detecting DNA lesions in S Phase, leading to an S Phase delay. However, this is purely speculative and would require further characterisation.

Taken together, the analyses of the phenotypes associated with the Tub2 *SIM* mutant protein suggest that a SIM domain may indeed be located near the N-terminus of Tub2 which is important for the stability and function of β -tubulin/microtubules and, moreover, that this potential domain is important for normal cell cycle progression. However, it is not possible at present to discount the possibility that these amino acid substitutions of Tub2 act to destabilise Tub2 in a sumo-independent manner. Hence, further work should focus on investigations of the influence of the amino acid changes on the non-covalent interactions between Tub2 and sumo.

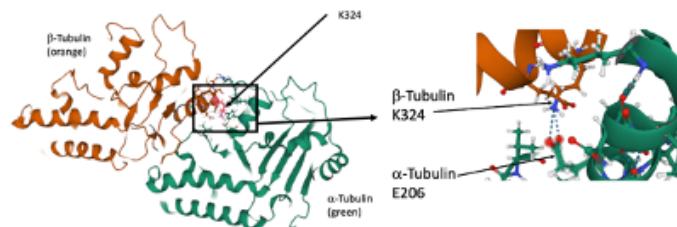
Sumo-SIM interactions are often regarded as a “molecular glue” providing large molecular complexes with additional stability (see Chapter 1, section 1.3.1)(Chatterjee et al., 2019). Therefore it may be the case that mutation of the Tub2 SIM domain may destabilise interactions between tubulin and other MAPs or protein complexes. However, although we identified that mutation of the Tub2 SIM domain led to an S Phase delay, it is unclear whether the stability of large multiprotein complexes or the interaction(s) between specific proteins are altered in cells expressing the YCplac111-*SIM* plasmid. Nevertheless, the potential Tub2 SIM domain investigated in this study appears to be conserved in eukaryotes, highlighting its importance. Indeed, sequence analysis of β -tubulin expressed in human cells revealed that

A.

Lysine Residue	Sequence	P Value
K44	HGHDDIQKERLNVYF	0.578
K58	FNEASSGKVVPRISIN	0.913
K103	SAGNVWAKGHYTEGA	0.872
K154	MGTLISKIREEFPD	0.176
K174	FSVLPSPKTSDTVVE	0.977
K216	DICQRTLKLNQPSYG	0.566
K252	QLNSDLRKLAVNLVP	0.561
K297	TQQMFDAKNMMAAAD	0.224
K320	VAAFFRGKVSVEVE	0.047
K324	FRGKVSVEVEDEM	0.051
K332	EVEDEMHKVSQKNSD	0.059
K336	EMHKVQKNSDYFVE	0.652
K379	TSIQELFKRVGDQFS	0.731
K390	DQFSAMFKRKAFLHW	0.049
K392	FSAMFKRKAFLHWYT	0.5

Cluster of lysine residues

B.



C.

K324
↓

S. cerevisiae TUB2 301 AAADPRNGRYLTVAFFRGKVSVEVEDEMHKVSQKN:
AA DPR+GRYLTVA FRG++S+KEV+++M +QSKN:

Homo sapiens TUBB3 301 AACDPRHGRYLTVATVFRGRMSMKEVDEQMLAIQSKN:

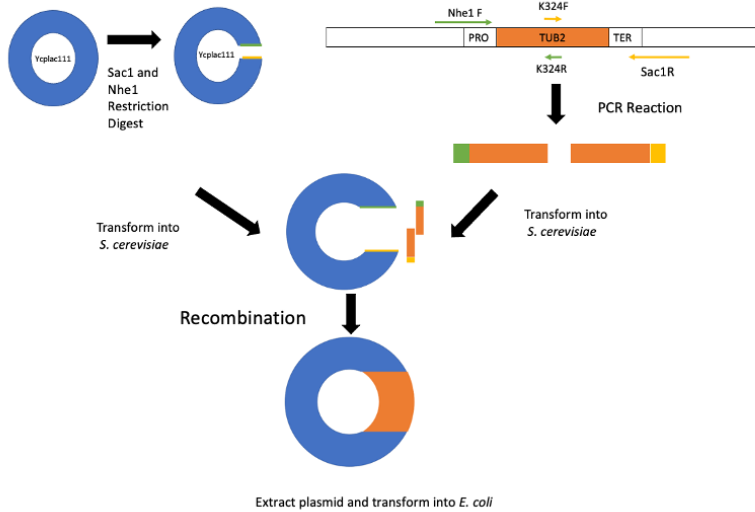
D.

WT FRGKVSVEVEDEM

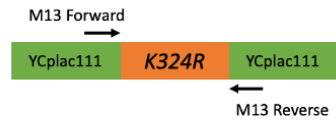
K324R FRGKVSREVEDEM

Figure 5.17 Identification of covalent sumo binding site in Tub2. (A) The Tub2 sequence was subject to a high-stringency search for potential sumo sites using the sumo site prediction tool developed by (Zhao et al., 2014). P values indicate the statistical significance of the lysine residue indicated in red. (B) The location of Tub2 K324 relative to the structure of *S. cerevisiae* α/β tubulin dimers (Howes et al., 2017) (DOI:[10.2210/pdb5w3f/pdb](https://doi.org/10.2210/pdb5w3f/pdb)). (C) Conservation of the Tub2 K324 residue between *S. cerevisiae* and *H. sapiens* β -tubulin. (D) Amino acid sequence of the Tub2 K234R mutation compared to the wild type Tub2 sequence.

A.



B.



C.

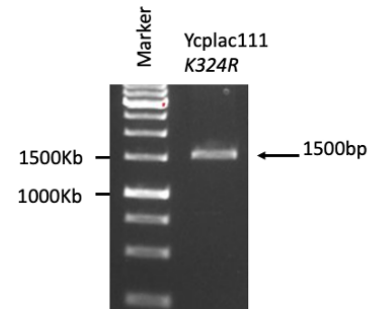


Figure 5.18 Construction of the YCplac111-K324R (GC137) strain. (A) To construct the YCplac111-K324R plasmid expressing the *tub2*-K324R mutant protein two primers were designed, NHE1F and SAC1R, with 50bp homology to the *TUB2* promoter and terminator regions of the *TUB2* gene, respectively, followed by either a Nhe1 or a Sac1 restriction site, respectively. Internal primers, K324R and K324F, were designed to mutate K324 to an arginine residue. Two PCR reactions were set up with either the NHE1F and K324R primers or the SAC1R and K324F primers, using wild type (GC55) genomic DNA as a template in both PCR reactions. The two PCR fragments were analysed on a 1% agarose gel to confirm the fragment sizes (data not shown). PCR products were isolated from the agarose gel, transformed into the GC55 strain with Nhe1/Sac1 digested YCplac111 and plated onto plates lacking leucine. (B) M13 Forward and M13 Reverse Primers have homology to two sites located on opposite sides of the *K324R* insert in the YCplac111 plasmid. To confirm the presence of the YCplac111-*K324R* plasmid from LEU2+ growing colonies, a PCR reaction was set up (see Chapter 2 section 2.2.1) containing both the forward and reverse primers along with *S. cerevisiae* genomic DNA (taken from growing GC55 colonies transformed with the YCplac11-K324R plasmid) as a template. (C) A fragment of ~1500bp (indicated by the arrow) confirmed the presence of the K32R insert in the YCplac111 plasmid. Plasmids were subsequently extracted from yeast colonies (see Chapter 2 section 2.2.4) and sequenced.

five of the β -tubulin isoforms expressed in human cells have a potential SIM domain present at exactly the same location as the SIM domain identified in Tub2. Interestingly, the human Tub2 SIM domain has a slightly different sequence when compared to the Tub2 SIM domain investigated in this study (IIHI in *S. cerevisiae* compared to IVHI in *H. sapiens*). Nevertheless, the human IVHI SIM domain still fits within the inverted SIM consensus sequence, suggesting that β -tubulin does indeed contain a conserved SIM domain (Song et al., 2005). Hence we speculate that this highly conserved SIM domain may be important for β -tubulin function, especially during S Phase. Furthermore, analysis of the Tub1 sequence, the major α -tubulin expressed in budding yeast, identified 10 potential SIM domains. Thus, it may be the case that sumo-SIM interactions between α/β -tubulin dimers may promote stabilisation of tubulin structures. Indeed, cells dependant on YCplac111-SIM grew slower than wild type cells and showed specific S Phase delays, indicative that the Tub2 SIM domain is important for growth in *S. cerevisiae* cells.

5.2.4.2 Investigation of covalent interactions of sumo with Tub2

To begin to investigate covalent interactions between sumo and Tub2, the protein sequence of Tub2 was analysed and found to contain 15 lysine residues, the target amino acid in substrates for sumoylation. However, to identify possible lysines that may be sumoylated the protein sequence of Tub2 was analysed using the same sumo prediction software used for the identification of the potential SIM domain of Tub2 (Zhao et al., 2014). Excitingly, several lysine residues were identified in Tub2 as potential sumoylation sites (Fig.5.17A). Indeed, out of the 15 lysines present in the Tub2 sequence, two statistically significant lysine residues at positions K320 and K390 were identified, with p values of 0.047 and 0.049 respectively (Fig. 5.17A). Two additional lysine residues K324 and K332 had p values of 0.051 and 0.059 respectively. Intriguingly, K320, K324 and K332 reside in a cluster of four lysine residues (the nearby K336 was not identified as a potential sumoylation site, p=0.652). Indeed, numerous studies have shown that sumoylation of adjacent lysine residues often occurs when the normally sumoylated lysine residue is mutated. For example, the sumo E2 enzyme Ubc9 is usually sumoylated on residue K153 during meiosis (Klug et al., 2013). However, mutation of Ubc9 K153 (Ubc9^{K153R}) does not inhibit Ubc9 sumoylation in budding yeast cells (Klug et al.,

2013). Instead, in cells expressing the Ubc9^{K153R} mutation, the sumoylation of an alternative, nearby lysine residue, K157, is sumoylated instead to compensate for the loss of K153 (Klug et al., 2013). Furthermore, mutants expressing Ubc9^{K153R/K157R} completely abolished Ubc9 sumoylation, resulting in these cells displaying severe meiotic defects (Klug et al., 2013). Hence, these data suggest that sumoylation of nearby lysine residues may compensate for the loss of a lysine residue usually subject to sumoylation. Thus, with respect to our findings, that three out of four lysine residues residing within a cluster of lysine residues are significant candidates for sumoylation, it was possible that one of these lysine residues may indeed be sumoylated (Fig. 5.14A). Thus residues K320, K332, K324 were investigated further.

Tub2 K324 (p=0.051) resides within an inverted sumo consensus sequence (Matic et al., 2010). Significantly, other studies have shown that the equivalent lysine residue within this consensus sequence is sumoylated in five other proteins (data not shown). In addition, the Tub2 K324 residue directly interacts with the E206 residue of α -tubulin within the α/β -tubulin dimer (Fig. 5.17B). Thus, it is possible that sumoylation of Tub2 K324 may influence the stability of the interaction between α -tubulin and β -tubulin, although this is purely speculative. In addition, sequence alignment of *S. cerevisiae* TUB2 with *H. sapiens* TUBB3 (one of the β -tubulin isoforms expressed in human cells) revealed that K324 is conserved between species (Fig. 5.17C). In comparison, neither K320 nor K332 appear to be conserved, suggesting that K324 may be the most important lysine residue with the cluster (Fig. 5.17C). It must also be noted that K390 (p=0.049) was also a candidate for sumoylation (Fig. 5.15A). However, taken together, the location of K324 within a cluster of lysine residues in Tub2 and the interaction between K324 and α -tubulin E206, suggested that K324 was highly probable to be an important sumo target.

5.2.4.2.1 Analysis of the role of K324 in the function of Tub2

The first step to investigate the potential role of sumoylation in the regulation of tubulin was to mutate K324 to an arginine residue in order to test the potential role of this amino acid in the function of Tub2. To substitute K324 with an arginine residue a PCR mutagenesis and plasmid construction strategy was designed to express the mutant version of the Tub2 protein from the single copy *LEU2* YCplac111 plasmid from its own promoter (YCplac111-K324R,

Figure 5.18A). Specifically, two PCR fragments spanning the *TUB2* gene with the complete promoter and 3' regions of the gene, and that included the DNA sequence substitutions to mutate K324, were amplified by PCR (data not shown) using the NHE1F/K324R primers and the SAC1R/K324F primers respectively and genomic DNA from the GC55 wild type strain as template (Figure 5.15A). Next, the PCR products were co-transformed into GC55 cells with the YCplac111 plasmid that had been digested with Nhe1 and Sac1 restriction enzymes and transformed cells were plated on media lacking leucine (Figure 5.18A). The NHE1F and SAC1R primers contain a short region of homology at the 5' end of each primer with the regions of the plasmid located next to the Nhe1 and Sac1 restriction enzymes (Figure 5.18A). Hence, this allowed the construction of the YCplac111-K324R plasmid by homologous recombination between the PCR products and the Nhe1/Sac1-digested YCplac111 plasmid (Figure 5.15A). After 5 days, Leu⁺ yeast colonies were checked by PCR (Figure 5.15B) and restriction digest analysis of plasmids recovered from *S. cerevisiae* into *E. coli* (data not shown) to confirm construction of YCplac111-K324R. Finally, DNA sequence analyses confirmed the successful mutation of the sequences encoding K324 and also that no other changes in the *TUB2* gene had arisen in the construction of the plasmid.

In order to investigate the effect of the K324R mutation of Tub2 the YCplac111 vector, YCplac111-*TUB2* and YCplac111-K324R plasmids were transformed into the plasmid shuffle strain (GC134) and the cells were plated onto media lacking leucine (Figure 5.10, Step 2). Transformants were obtained from all three plasmids following incubation of the plates for 2-3 days. Next, colonies from each plate were re-streaked onto media lacking leucine to confirm selection of viable transformants. Finally, colonies from each of the individual plasmid transformations were streaked from this media onto 5'FOA media to assess the ability of each plasmid to replace the pRS316-*TUB2* plasmid in the plasmid shuffle strain (Figure 5.19A). As expected, the YCplac111 vector was unable to replace pRS316-*TUB2* and the YCplac111-*TUB2* enabled growth on 5-FOA media (Figure 5.19A). Importantly, the YCplac111-K324R plasmid was also able to replace the pRS316-*TUB2* plasmid, indicating that the mutant version of Tub2 expressed from the YCplac111-K324R plasmid is functional (GC137)(Figure 5.19A).

It was also important to confirm that that mutant Tub2 expressed by the YCplac111-*K324R* plasmid was stable and expressed at levels similar to wild type cells. Indeed, the western blot analyses of midlog growing GC137 cells revealed that the *K324R* mutant was expressed at similar levels to cells expressing the YCplac111-*TUB2* plasmid (Figure 5.19B/C). Furthermore, the level of β -tubulin expressed by the YCplac111-*K324R* plasmid is not significantly different to the level of β -tubulin expressed in cells expressing the YCplac111-*TUB2* plasmid. Hence, it could be concluded that the *K324R* mutant was viable and that the lysine mutation did not significantly affect the stability of β -tubulin protein levels. Thus, the YCplac111-*K324R* mutant was subject to further phenotype analysis.

Next, the growth of the cells dependent on either YCplac111-*TUB2* (GC136) or YCplac111-*K324R* (GC137) was compared (Figure 5.20A). Interestingly, growth rate analyses indicated that the doubling time of the cells dependent on YCplac111-*TUB2* is 117 ± 2 minutes compared to a doubling time of 133 ± 4 minutes for the cells dependent on YCplac111-*K324R* (Figure 5.20B). Thus, cells dependent on YCplac111-*K324R* appear to have growth defects compared to cells dependent on YCplac111-*TUB2*. Furthermore, the YCplac111-*K324R* cells appear to grow at a similar rate to YCplac111-*SIM* cells (~ 133 minutes doubling time compared to ~ 128 minutes respectively), suggestive that mutation of Tub2 K324 is no more important for growth than mutation of the SIM domain (compare Fig. 5.20A/B with Fig. 5.15A/B).

Next, DNA content analysis was performed on cultures of the mid-log phase growing cells dependent on either the YCplac111-*TUB2* plasmid (GC134) or the YCplac111-*K324R* plasmid (GC137). Interestingly, these data revealed that mutation of K324 of Tub2 did not cause a significant increase in aneuploidy (Figure 5.20C/D). This contrasts with the cell cycle analyses of the *tub2* mutant strain (see section 5.2.1.2) which displays significantly increased levels of aneuploidy (Figures 5.1C/D). To further characterise the cell cycle defects associated with the cells dependent on YCplac111-*K324R*, the proportion of cells in each cell cycle phase was combined with the doubling times of the cells dependent on either the YCplac111-*TUB2* or YCplac111-*K324R* plasmids to calculate the approximate time that these cells spend in each phase of the cell cycle (Morgan et al., 1991). A striking result from this analysis was the increased time that YCplac111-*K324R* dependent cells spend in S phase compared to control cells dependant on YCplac111-*TUB2* (Fig. 5.20B). For example, cells dependent on YCplac111-

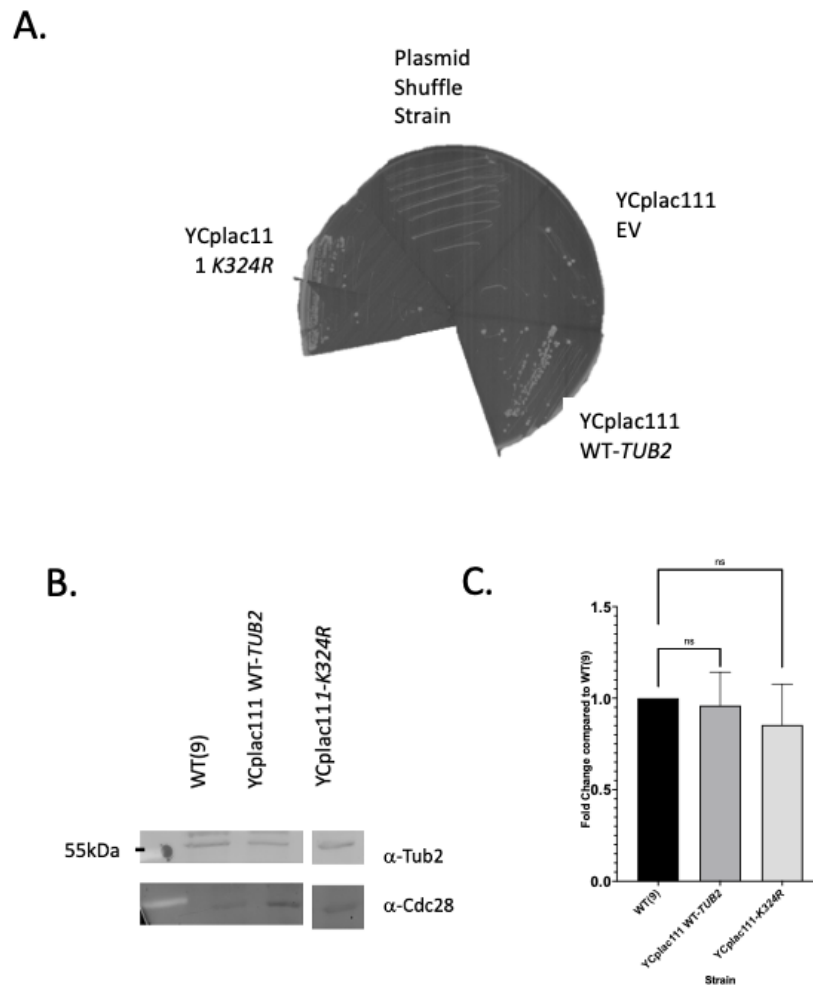
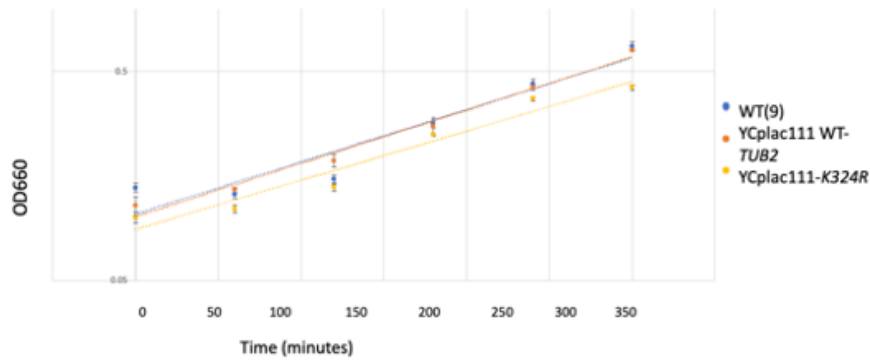


Figure 5.19. The Tub2 K324R mutation is not lethal. (A) GC136, GC137 and a control strain expressing the YC plac111 empty vector (EV) were streaked onto 5'FOA plates and images after 5 days. (B) Proteins were TCA extracted from mid-log phase growing wild type (GC55), YCplac111-*TUB2* (GC136) and YCplac111-*K324R* (GC137) cells and analysed by western blotting using an anti- β -tubulin antibody. A representative blot of three biological repeats is shown. (C) Blots were stripped, re-probed with anti-Cdc28 antibody as a loading control and quantified using ImageQuant (GE Healthcare). Error bars represent SD. Bars represent β -tubulin levels normalised to the wild type control. P values were derived from an unpaired T-test.

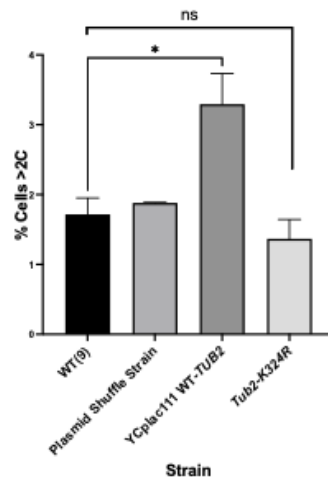
A.



B.

Strain	Doubling Time	G1	S	G2/M
WT(9)	117±3	38±3	35±1	40±2
Plasmid Shuffle Strain	122±1	40±1	36±1	44±3
YCplac111 WT-TUB2	117±2	37±2	35±1	44±2
YCplac111-K324R	133±4	37±3	47±2	47±2

C.



D.

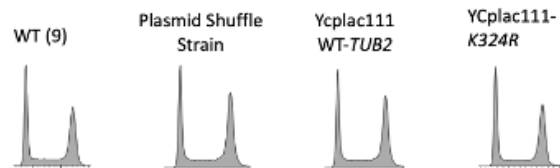


Figure 5.20 Cell cycle analysis of the YCplac111-K324R (GC137) strain. (A) Growth curves of mid-log phase growing cultures of wild type (GC55), YCplac111-*TUB2* (GC136) and YCplac111-*K324R* (GC137) cells. Error bars represent SD from 3 biological repeats. (B) Gating analysis of the DNA content analyses in (C) of the time cells spent in each stage of the cell cycle. (C) DNA content analysis was performed on mid-log phase growing cultures of wild type (GC55), Plasmid Shuffle Strain (GC134), YCplac111-*TUB2* (GC136) and YCplac111-*K324R* (GC137) cells and presented as indicated. (E) (D) Gating analysis of the DNA content analyses in (C) of wild type (GC55), Plasmid shuffle strain (GC134), YCplac111-*TUB2* (GC136) and YCplac111-*K324R* (GC137) cells containing >2C DNA content. P values were derived from an unpaired T-test, (*) indicates p<0.05.

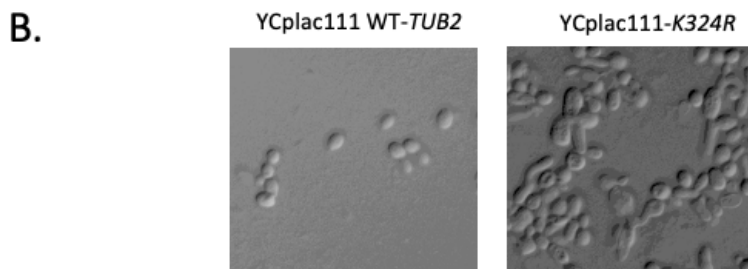
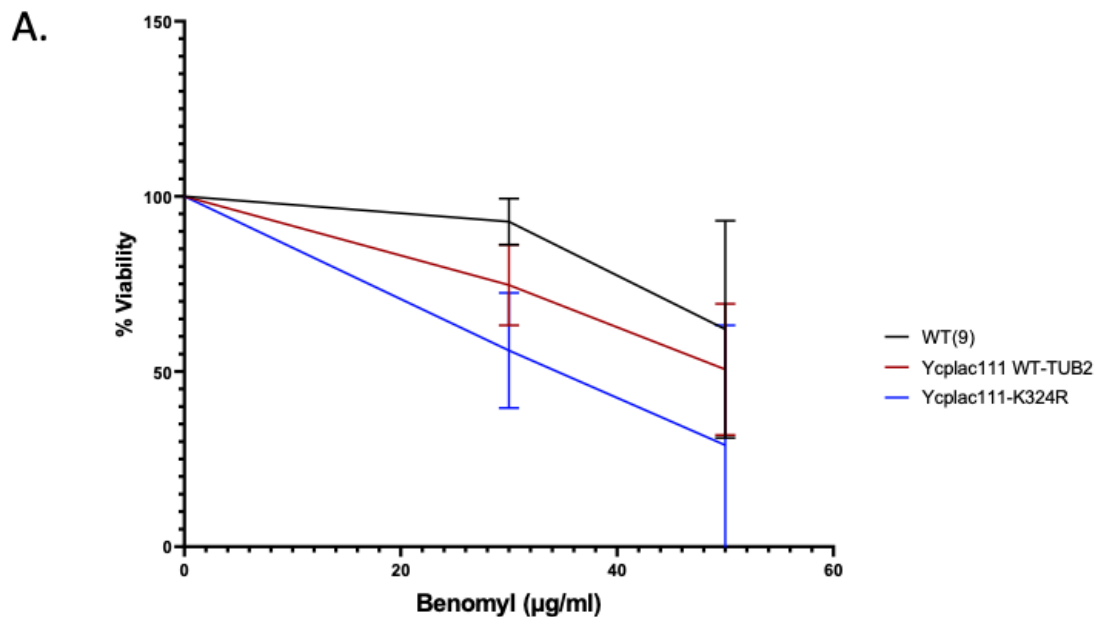


Figure 5.21 *K324R* mutants are not sensitive to microtubule depolymerisation agents. (A) Equal numbers of mid-log phase growing wild type (GC55) cells and cells containing either YCplac111-*TUB2* (GC136) or YCplac111-*K324R* (GC137), were plated on YPD plates containing the indicated benomyl concentrations. Plates were incubated at 30°C until colonies formed. % survival was calculated based on the colonies formed on the 0µg/ml benomyl plates. Error bars represent SD from 3 biological replicates. P values were derived from an unpaired T-test, all samples are not significantly different compared to WT(9). (B) Cells containing either YCplac111-*TUB2* (GC136) or YCplac111-*K324R* (GC137) were grown to mid-log phase in minimal media lacking leucine and visualised by DIC.

K324R were found to spend ~47 minutes in S Phase in comparison to cells dependent on YCplac111-*TUB2* which spend just ~35 minutes S Phase (Fig. 5.20B). Strikingly, this S Phase delay is extremely similar to that of cells dependent on YCplac111-*SIM*. Indeed, both YCplac111-*SIM* and cells YCplac111-*K324R* spend ~47 minutes in S Phase compared to ~35 minutes in cells dependant on YCplac111-*TUB2* (compare Fig. 5.20B with Fig. 5.15B). Taken together, these data suggest that the *K324R* mutation compromises the normal function of Tub2. Furthermore, cell cycle analysis also indicates that mutation of either covalent or non-covalent sumoylation sites in Tub2 result in a delayed S Phase, although the reason for this delay is unclear.

Given the relationship between β -tubulin function and benomyl sensitivity described above, and the defects of cell cycle progression associated with cells dependant on YCplac111-*K324R*, the benomyl sensitivity of cells expressing YCplac111-*K324R* was investigated (Fig. 5.21A). Interestingly, cells dependant on the YCplac111-*K324R* plasmid did not show any significant sensitivity to benomyl compared to cells dependant on YCplac111-*TUB2* (Figure 5.21A). Furthermore, cells dependant on the YCplac111-*K324R* plasmid showed a similar rate of survival when plated on 50ug benomyl compared to dependant on the YCplac111-*SIM* plasmid (compare Fig. 5.21A and Fig.5.16A). In contrast, *tub2* cells are extremely sensitive to benomyl (Fig. 5.2). Thus, these results are consistent with the cell cycle analysis, suggesting that, unlike *tub2*, cells dependant on either the YCplac111-*K324R* or YCplac111-*SIM* plasmids do not show mitotic defects. Immunoprecipitations carried out during this study indicate that Tub2 is a putative sumo substrate in *S. cerevisiae* cells, hence we attempted to investigate the importance of both covalent Tub2 sumoylation and non-covalent sumo interactions. Efforts to identify essential Tub2 lysine residues through mutagenesis of *K324R* and the adjacent lysine residues suggest that although *K324* sumoylation is not essential, *K324* is critical for cellular growth. β -tubulin *K324* is a conserved residue between budding yeast and humans (Fig. 5.17C), hence it would be interesting to further characterise the Tub2 *K324R* mutation in mammalian cells. Furthermore, analysis of the cell cycle identified that the *SIM* and *K324R* mutants both displayed significant S Phase delays when compared to cells expressing wild

type Tub2. Sensitivity tests using DNA damaging agents such as HU or UV would identify whether the SIM and K324R mutants in this study are sensitive to replication stress. Previous

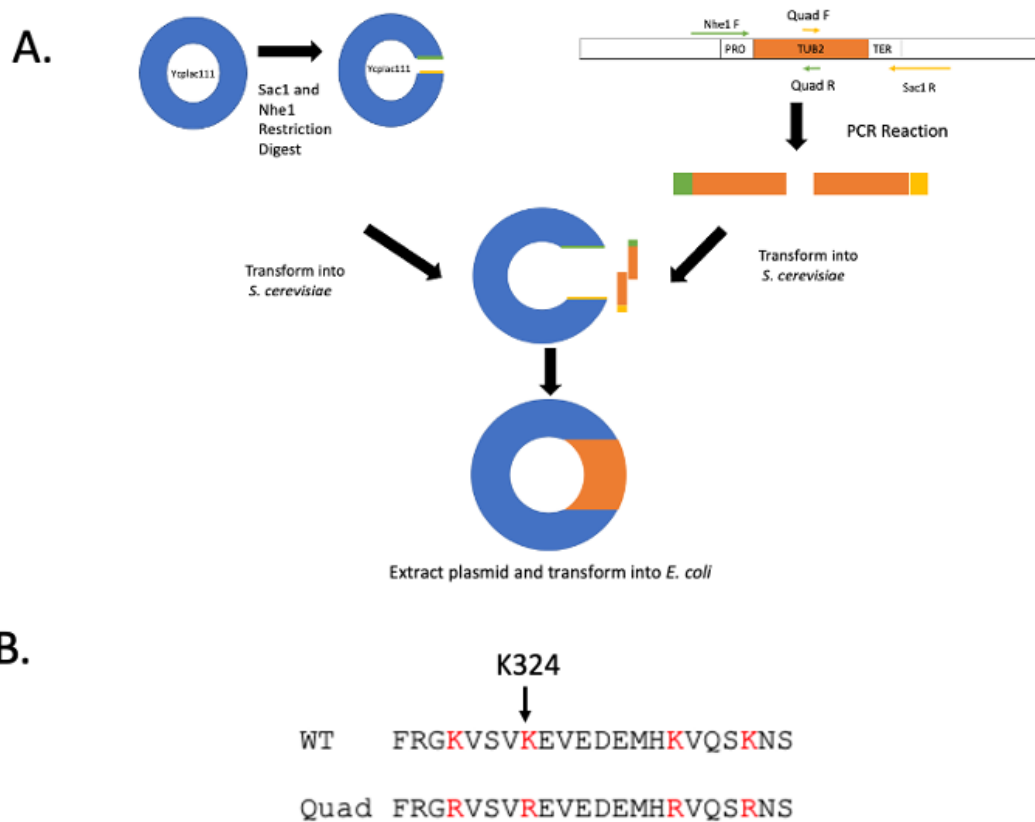
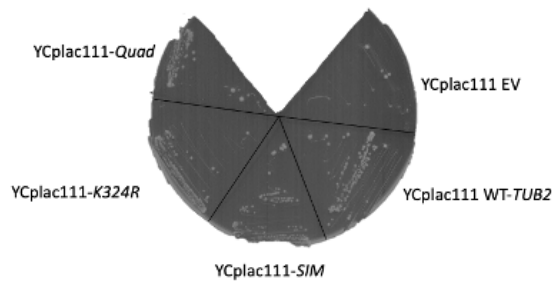


Figure 5.22 Construction of the YCplac111-Quad strain. (A) To construct the YCplac111-Quad plasmid expressing the Quad mutant protein, two primers were designed, NHE1F and SAC1R, with 50bp homology to the TUB2 promoter and terminator regions of the TUB2 gene, respectively, followed by either a Nhe1 or a Sac1 restriction site, respectively. Internal primers, QuadR and QuadF, were designed to mutate K324 to an arginine residue. Two PCR reactions were set up with either the NHE1F and QuadR primers or the SAC1R and QuadF primers, using wild type (GC55) genomic DNA as a template in both PCR reactions. The two PCR fragments were analysed on a 1% agarose gel to confirm the fragment sizes (data not shown). PCR products were isolated from the agarose gel, transformed into the GC55 strain with Nhe1/Sac1 digested YCplac111 and plated onto plates lacking leucine. Primer design and PCR reactions were carried out by Z. Richards. Plasmids were PCR checked using the M13F and M13R primers to confirm the size of the insert. Plasmids were subsequently extracted from yeast colonies (see Chapter 2 section 2.2.4) and sequenced. (B) Amino acid sequence of

the Tub2 Quad mutation compared to the wild type (WT) Tub2 sequence. Lysine residues to be mutated are highlighted in red.

A.



B.



C.

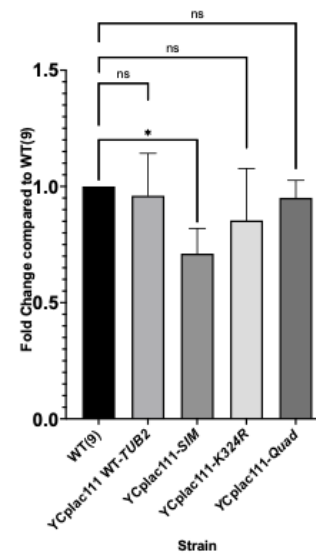
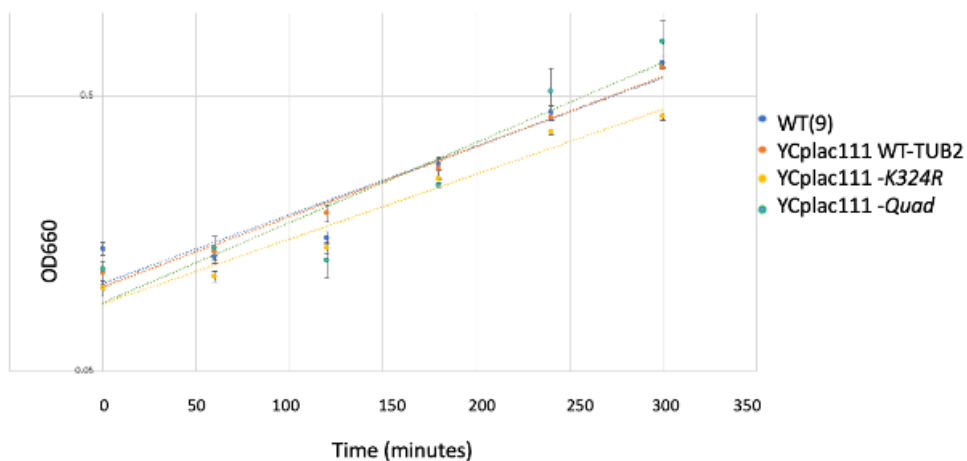


Figure 5.23. The Tub2 quad mutation is not lethal. (A) GC136, GC137, GCV138 and a control strain expressing the YC plac111 empty vector (EV) were streaked onto 5'FOA plates and images after 5 days. (B) Proteins were TCA extracted from mid-log phase growing wild type (GC55), YCplac111-*TUB2* (GC136), YCplac111-*K324R* (GC137) and YCplac111-*Quad* (GC139) cells and analysed by western blotting using an anti- β -tubulin antibody. A representative blot of three biological repeats is shown. (C) Blots were stripped, re-probed with anti-Cdc28 antibody as a loading control and quantified using ImageQuant (GE Healthcare). Error bars represent SD. Bars represent β -tubulin levels normalised to the wild type control. P values were derived from an unpaired T-test.

A.



B.

Strain	Doubling Time	G1	S	G2/M
WT(9)	117±3	38±3	35±1	40±2
Plasmid Shuffle Strain	122±1	40±1	36±1	44±3
YCplac111 WT-TUB2	117±2	37±2	35±1	42±2
YCplac111-SIM	128±3	39±3	41±2	47±1
YCplac111-K324R	133±4	37±3	47±2	47±2
YCplac111-Quad	103±7			

Figure 5.24 Cell cycle analysis of the YCplac111-Quad strain. (A) Growth curves of mid-log phase growing cultures of wild type (GC55), YCplac111-TUB2 (GC136), YCplac111-K324R (GC137) and YCplac111-Quad (GC139) cells. Error bars represent standard error from 3 biological repeats. (B) Doubling times of the strains in (A).

studies by Reijo et al. (1994) investigated the phenotypes associated with >50 strains expressing Tub2 point mutations introduced onto the chromosome of *S. cerevisiae* (Reijo et al., 1994). Interestingly, this study identified that cells expressing a Tub2 K324A mutation were cold sensitive when placed at 25°C, whilst a K324A E325A double mutant was temperature sensitive (Reijo et al., 1994). Interestingly, in disagreement with Reijo et al., our data indicates that the K324R mutant does not appear to be sensitive to cold temperatures. However, it must be noted that a K324R mutation is not identical to K324A, thus this may account for the discrepancy between the two results, suggesting that a positively charged amino acid at position 324 may be important for Tub2 growth.

Nevertheless, consistent with the findings that the K324R mutation results in cell cycle defects, cells dependent on YCplac111-*K324R* cells were found to have aberrant morphologies compared to the control cells dependent on YCplac111-*TUB2* (Figure 5.21B). For example, YCplac111-*K324R* cells appear larger and more elongated than control cells dependent on YCplac111-*TUB2* (Fig. 5.21B). Furthermore, cells dependant on YCplac111-*K324R* cells appear to be a mixed population of cells. This is in contrast to *tub2* cells which are large, budded cells, indicative of G2/M delays (data not shown). Although cells dependant on YCplac111-*SIM* show a similar S Phase delay to cells dependant on YCplac111-*K324R*, YCplac111-*SIM* cells are not elongated (compare Fig. 5.21B with 5.16B). Nevertheless, similar to YCplac111-*K324R*, YCplac111-*SIM* cells do appear to be larger than the YCplac111-*TUB2* control cells, (compare Fig. 5.21B with 5.16B). Hence, the DNA content analyses are consistent with YCplac111-*K324R* cell phenotypes, suggesting that the S Phase delay attributes to the morphological defects displayed in YCplac111-*K324R* cells. Taken together, these results suggested that Tub2 K324, although not essential for viability, is important for cell cycle progression.

5.2.4.2.2 Analysis of the role of K320, K324, K332 and K336 in the function of Tub2

The results presented above suggest that the K324 residue of Tub2 is important for the function of Tub2. However, K324 is not absolutely essential for function (Fig. 5.19A). Nevertheless, if K324 is in fact the main, possibly sole, sumoylated residue in Tub2 then perhaps the retention of some Tub2 function is due, as described above, to the sumoylation

of an adjacent lysine(s) when K324 is unavailable. Indeed, analysis of the Tub2 sequence revealed that two lysine residues (K320 and K332) located extremely close to K324 were also possible sumo sites (K320 $p=0.047$ and K332 $p=0.059$). Therefore, to test this hypothesis a strategy was developed in collaboration with an MRes student, Zack Richards, to substitute multiple lysine residues at positions 320, 332 and 336 (K320, K332, K336), which cluster around K324 in the Tub2 polypeptide chain, with arginine residues. To substitute each of the four K320, K324, K332 and K336 residues with an arginine residue a PCR mutagenesis and plasmid construction strategy was designed to express the mutant version of the Tub2 protein from the single copy *LEU2* YCplac111 plasmid from its own promoter (YCplac111-*Quad*, Figure 5.22A). This PCR mutagenesis and plasmid construction was performed as part of Zack Richard's MRes laboratory-based project and hence the details of only the strategy are shown in Figure 5.20A as I directly contributed to developing the strategy for the design of the YCplac111-*Quad* plasmid. However, the plasmid was constructed and initially PCR checked by Zack Richards as described above for the YCplac111-*K324R* plasmid. I then carried out the DNA sequencing, plasmid transformation and subsequent phenotyping of cells dependant on the YCplac111-*Quad* plasmid.

Hence, to investigate the effect of the "*Quad*" mutant version of Tub2, the YCplac111 vector, YCplac111-*TUB2*, YCplac111-*K324R* and YCplac111-*Quad* plasmids were transformed into the plasmid shuffle strain (GC134) and the cells were plated onto media lacking leucine (Figure 5.9, Step 2). Transformants were obtained from all four plasmids following incubation of the plates for 2-3 days. Next, colonies from each plate were re-streaked onto media lacking leucine to confirm selection of viable transformants. Finally, colonies from each of the individual plasmid transformations were streaked from this media onto 5'FOA media to assess the ability of each plasmid to replace the pRS316-*TUB2* plasmid in the plasmid shuffle strain (Figure 5.23A). As expected, the YCplac111 vector was unable to replace pRS316-*TUB2* whilst the YCplac111-*TUB2*, YCplac111-*SIM* and the YCplac111-*K324R* plasmids enabled growth on 5'FOA media (Figure 5.23A). Interestingly, cells dependant on the YCplac111-*Quad* plasmid were also able to replace the pRS316-*TUB2* plasmid, indicating that the mutant version of Tub2 expressed from the YCplac111-*Quad* plasmid is functional (Figure 5.23A). Importantly, the level of Tub2 expressed by the YCplac111-*Quad* plasmid was not significantly different to Tub2 expressed by the YCplac111-*TUB2* plasmid. Hence, as the *Quad* mutant has stable, wild

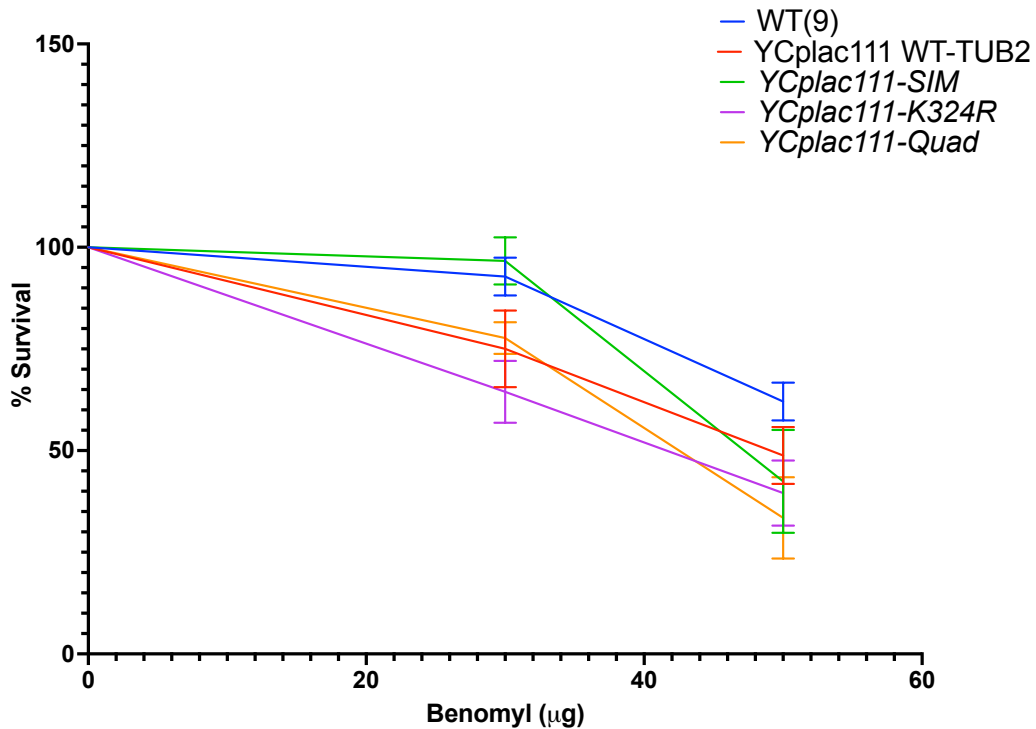


Figure 5.25 *Quad* mutants are not sensitive to microtubule depolymerisation agents. (A) Equal numbers of mid-log phase growing wild type (GC55) cells and cells containing either YCplac111-*TUB2* (GC136), YCplac111-*K324R* (GC137) or YCplac111-*Quad* (GC139) cells were plated on YPD plates containing the indicated benomyl concentrations. Plates were incubated at 30°C until colonies formed. % survival was calculated based on the colonies formed on the 0µg/ml benomyl plates. Error bars represent SD from 3 biological replicates. P values were derived from an unpaired T-test, all samples are not significantly different compared to WT(9).

type levels of Tub2, phenotype analysis of cells dependant on the YCplac111-*Quad* plasmid could now be carried out. First, the growth of the cells dependent on either YCplac111-*TUB2* (GC136), YCplac111-*K324R* (GC137) were compared to cells dependant on YCplac111-*Quad* (GC139) (Figure 5.24A/B). Interestingly, growth rate analyses indicated that the doubling time of the cells dependent on YCplac111-*TUB2* was 117 ± 2 minutes compared to a doubling time of 133 ± 4 minutes for the cells dependent on YCplac111-*K324R* and a doubling time of 103 ± 7 minutes for the cells dependent on YCplac111-*Quad*. Hence, unexpectedly this data revealed that mutation of K320, K332 and K336 to arginine residues partially suppressed the slow growth phenotype associated with the *K324R* mutation. Unfortunately, due to the Covid-19 lockdown period and restricted laboratory access it was not possible to perform DNA content analyses on the cells expressing the YCplac111-*Quad* protein. Hence it remains unclear which aspect(s) of the cell cycle were altered in the cells containing or YCplac111-*Quad* versus cells containing or YCplac111-*K324R*. Future DNA content analysis of the YCplac111-*Quad* is crucial, as it would identify whether the S Phase delay associated with cells expressing the YCplac111-*SIM* or *K324R* mutants is reduced or rescued in the YCplac111-*Quad* mutant.

Next, the benomyl sensitivity of cells expressing the YCplac111-*Quad* mutant version of Tub2 was investigated. Interestingly, cells expressing the YCplac111-*Quad* plasmid were not found to show significant sensitivity to benomyl compared to cells containing the YCplac111-*TUB2* plasmid (Fig. 5.25). These results are consistent with the earlier findings that neither the YCplac111-*SIM* or YCplac111-*K324R* mutations appear to affect the sensitivity to benomyl compared to the YCplac111-*TUB2* control strain (compare Fig. 5.25, Fig. 5.16A and Fig 5.21A). In contrast, *tub2* cells are extremely sensitive to benomyl (Fig. 5.2). Thus, taken together, it could be suggested that YCplac111-*SIM* and YCplac111-*K324R* mutants are not sensitive to benomyl as these strains, unlike *tub2*, do not show any delays within G2/M phases.

Unexpectedly, mutation of the three lysine residues adjacent to K324 appears to partially rescue growth of the single mutant, suggesting that this cluster of lysine residues are not vital for growth. However, although the *K324R* mutant does not appear to show aneuploidy (although this requires confirmation using chromosomal qPCR assays), it remains to be determined whether the quad mutant shows an increased $>2N$ DNA content.

In conclusion, the hypothesis that the effects of blocking potential sumoylation of K324 could be partially suppressed by shifting sumoylation to a neighbouring lysine residue is not supported by these initial analyses of cells dependent on the YCplac111-*Quad* plasmid. Nevertheless, the data does indicate that there is a functional relationship between the K320, K324, K332, and K336 residues that cannot simply be explained by the charge associated with each of these amino acids. Hence, future studies should focus on a detailed analyses of the sumoylation status of the cells expressing the YCplac111-*K324R* and YCplac111-*Quad* plasmids *in vivo*, combined with detailed studies of the microtubules/spindle structures associated with these mutant proteins. Attempts were made during the course of this study to repeat the IPS using the YCplac111-*SIM*, YCplac111-*K324R* and YCplac111-*Quad* strains, although these were not achieved due to time constraints. However, preliminary experiments do suggest that YCplac111-*Quad* is indeed sumoylated similar to wild type cells, although further repeats are required to verify these preliminary results (data not shown). Nevertheless, it is clear that further work is required to determine the sumoylation status of the Tub2 mutants in this study.

5.3 Summary

The *smt3* SGA screen identified *tub2* as an excellent suppressor of the growth defects associated with the *smt3* single mutant (Lewis, 2016). In addition, previous studies suggested that β -tubulin may be a potential target for sumoylation (Greenlee et al., 2018). However, despite these connections, the relationship between tubulin and sumo remain unclear. This study has built on these preliminary findings to begin to investigate the relationships between sumo and β -tubulin. DNA content analysis suggested that although the poor growth of the *smt3* strain is rescued in the *tub2smt3* double mutant, neither the aneuploidy nor the *SMT3* expression are significantly different when compared to the *smt3* single mutant. Moreover, our data suggests a model in which reduced sumo function hyper-stabilises microtubules, strengthening the links between tubulin and sumo functions. In addition, data in this thesis suggests that *S. cerevisiae* β -tubulin may be a sumo substrate *in vivo*, with the subsequent development of a plasmid shuffle strategy in order to investigate mutations of potential

covalent and non-covalent sumo sites in Tub2. Indeed, mutations of both covalent and non-covalent sumoylation sites in Tub2 resulted in growth defects and specific S Phase delays. Hence, taken together, it appears that sumoylation of β -tubulin may be important for progression through S Phase, although the specific role(s) of tubulin during S Phase remains unclear.

In agreement with a recent study by Altonsy et al. (2020) which identified that a reduction of β 3 tubulin in mammalian cells lead to a G2/M delay, our findings also indicate that reducing Tub2 levels in the *tub2* strain leads to a severe G2/M delay (Altonsy et al., 2020). Furthermore, the G2/M delay associated with the *tub2* allele is partially rescued by the *tub2smt3* double mutant, suggesting that a balance between tubulin and sumo levels in the cell may be critical for timely cell division. Additionally, we confirmed that *tub2* mutants have an increased >2N DNA content, almost identical to the >2N DNA content associated with the *smt3* strain (Fig. 5.1C). Remarkably, although the *smt3* growth is rescued in the *tub2smt3* strain, the aneuploidy displayed *tub2smt3* cells is not significantly different to the aneuploidy shown by *smt3* cells (Fig. 5.1C). However, the chromosomal profile of *tub2smt3* cells is strikingly different to *smt3* cells, suggesting that these chromosomal differences between the two strains may account for the improved phenotypes observed in the *tub2smt3* double mutant. Nevertheless, taken together, these results strongly suggest a synergistic relationship between the *smt3* and *tub2* alleles.

Considering that the survival curves revealed that *smt3* cells are extremely resistant to benomyl treatment, these results suggest that reducing sumo levels may directly enhance microtubule stability (Fig. 5.2). Our current hypothesis is that sumo may play a key role in promoting microtubule depolymerisation, although this requires further biochemical confirmation. Nevertheless, the *smt3* benomyl results appear to conflict with a number of recent studies which suggest that sumoylation of kinetochore proteins stabilises, rather than destabilises, the mitotic spindle (Pelisch et al., 2014, Zhang et al., 2008b). However, it must be noted that these studies have focussed on the sumoylation of centromere and kinetochore associated proteins and have not investigated the sumoylation of tubulin itself. For example, the microtubule motor protein CENP-E in mammalian cells is subject to both covalent and non-covalent sumoylation, which are crucial for the localisation of CENP-E at the kinetochore

(Zhang et al., 2008b). Mutation of CENP-E sumo sites lead to a prometaphase arrest, highlighting the importance of sumoylation for timely mitosis (Zhang et al., 2008a). Hence, microtubule staining of GC156, GC137, GC138 and GC139 strains could identify whether any of the Tub2 mutants created in this study affect either the mitotic spindle or the assembly of microtubule filaments. This analysis was not carried out during the course of this study due to time constraints and limited access to facilities, but future microtubule staining analyses would address some important questions. For example, this would confirm whether microtubules formed within the SIM or lysine mutants showed aberrant structures. Previous findings by Dr. Lewis revealed that *smt3* cells displayed an increase in F-actin staining in addition to actin morphology defects when compared to wild type cells (Lewis, 2016). Furthermore, *tub2* and *tub2smt3* mutants both displayed reduced F-actin staining compared to *smt3* cells. Thus, it would be interesting to repeat the F-actin staining in the Tub2 SIM or lysine mutants created in this study to identify actin structures are affected in these mutants. Taken together these data suggest that the reducing Tub2 levels rescue the aberrant F-actin levels associated with the *smt3* allele, although how this is achieved remains to be determined. Thus, at present, the relationship between sumo, actin and tubulin remains unclear. Remarkably, two high-scoring suppressors identified in the SGA screen, *cct8* and *cct3*, are subunit of the CCT1-8 chaperonin complex. Considering that two major substrates of the CCT complex are actin and tubulin, it is tempting to speculate that sumoylation of the CCT complex may regulate actin and tubulin dynamics. *smt3* cells show defects in both actin and tubulin morphologies (Lewis, 2016), suggestive that these defects attribute to the growth problems associated with the *smt3* allele. Hence it would be interesting to repeat the actin and tubulin immunofluorescence in the *cct8*, *cct3*, *cct8smt3* and *cct3smt3* mutant strains to identify whether *cct* mutants display cytoskeletal defects.

To conclude, data in this chapter has strengthened the connection(s) between tubulin regulation and sumoylation in regulating cell cycle progression. The aneuploidy associated with the *tub2* and *tub2smt3* strains has been characterised, with the results suggesting that *smt3* aneuploidy is improved, but not completely rescued, in the *tub2smt3* double mutant (Fig. 5.5). Moreover, *tub2smt3* mutants reduce the G2/M delays displayed in the *tub2* and *smt3* single mutants, although the mechanisms attributing to this cell cycle rescue remain unclear. Additionally, immunoprecipitations suggest that Tub2 is targeted for sumoylation in

S. cerevisiae cells, hence we attempted to identify and characterise potential sumoylation sites. Although mutation of K324 was not lethal, growth defects associated with this mutant highlight the importance of sumoylation for appropriate growth. Unexpectedly, mutation of three lysine residues adjacent to K324 improved growth compared to K324 single mutant. The reason for this rescue of growth is unclear, hence DNA content analysis will allow further insights into the cell cycle dynamics of this mutant. SIM domains are often associated with the increased stability of large protein complexes (Matunis et al., 2006). Thus, it was not surprising that sequence analysis revealed potential SIM domains both in Tub2 and Tub1 (data not shown), which we propose may stabilise α/β -tubulin structures. Mutation of the N-terminal Tub2 SIM domain resulted in cells growing slower than cells expressing wild type Tub2, suggestive that the SIM domain is important for growth. Nevertheless, it is clear that further characterisation of the lysine and SIM mutants is critical to improve our understanding of the relationship(s) between sumo and tubulin.

Chapter Six: Final Discussion

6.1 Highlights of this study

Sumoylation is a highly conserved post-translational modification which is essential in the majority of eukaryotic cells. Despite the large number of studies investigating sumoylation over the last 25 years, linking sumo to a diverse range of cellular processes, the fundamental nature of sumoylation remains largely unknown. Hence, the aim of this thesis was to investigate the important role(s) of sumoylation in *S. cerevisiae* cells based on the novel *smt3* cytoskeletal suppressors identified in an SGA screen previously carried out in our lab. Specific aims of this study were to characterise the sumo-mediated stress responses to cold temperature and oxidative stress in *S. cerevisiae*, to identify and characterise cell cycle defects associated with polysumo and reduced sumo function mutants and finally to investigate the putative interactions of Smt3 with β -tubulin and characterise the potential Tub2 covalent and non-covalent sumoylation sites.

Excitingly, work in this thesis revealed that there are strain specific differences in the sumo-mediated response to different cellular stresses. Furthermore, we propose a novel role for sumo in the response to cold temperatures, with data suggesting that a cold-induced increase in sumo conjugates is facilitated by the sumo E3 enzymes Siz1 and Siz2, whilst inhibition of the two Smt3 deconjugases, Ulp1 and Ulp2, maintain this increased level of cellular sumoylation. In addition, we demonstrate that reduced sumo function in the W303 strain background results in increased stress sensitivities compared to reduced sumo function in the BY4741 strain background. For example, W303*smt3* cells are much more sensitive to oxidative stress than BY4741 *smt3* cells, although the reason for the difference in sensitivities is unclear. However, it must be noted that the pathways regulating activation of the stress-induced transcription factor YAP1 during the response to oxidative stress are different in the W303 strain background compared to the BY4741 strain background, which may contribute to increased sensitivity to oxidative stress in W303*smt3* cells (Maeta et al., 2004). Data in this study also indicates that polysumo mutants show increased sensitivity to oxidative stress compared to wild type cells, suggestive that the type of sumo modification is critical for the appropriate stress response(s). Furthermore, preliminary data suggests that sumo-mediated

ubiquitination is an important aspect of the response to cold temperatures, although the cellular consequences of cold-induced ubiquitination remain to be determined.

Interestingly, data in this study indicates that a fundamental role of sumoylation is to enable progression through the eukaryotic cell cycle. For example, data in Chapter 3 indicate that cells with reduced Smt3 function display severe G2/M delays, with the identification of a novel role for sumo during S Phase specific to the W303 strain background. Thus, taken together, these data highlight the strain specific differences which contribute to cell cycle defects in cells with compromised sumo function. Moreover, cell cycle analysis of a polysumo mutant also revealed that these cells display significant S Phase delays, suggestive that different types of sumo modifications are also important for cell cycle progression. In order to further characterise the aneuploidy associated with the *smt3* allele, this study shows that the chromosomal profiles of the *smt3/smt3-allR* mutants are significantly different to that of *ulp2Δ* cells, although the basis of these differences remain unclear (Ryu et al., 2016). Strikingly, despite the similar levels of aneuploidy exhibited between the *smt3/smt3t-allR* mutants, the chromosomal profiles of these mutants are not identical. Thus, although an increase in chromosomes II, III and XI appear to be conserved between the *smt3/smt3t-allR* mutants, it is clear that the strain background and lack of polysumoylation influence the individual chromosomal dynamics within each of these strains.

Finally, work in this thesis aimed to characterise the sumoylation of Tub2, one of the strongest *smt3* suppressors identified from the SGA screen. Indeed, this study supports the proposed hypothesis that Tub2 is a sumo substrate, with IPs indicating that Tub2 is indeed modified by sumo *in vivo*. In addition, the development of a novel plasmid shuffle technique has enabled investigation of mutations in Tub2, allowing the characterisation of potential sumoylation sites in Tub2. For example, the mutation of a conserved lysine residue (K324) in Tub2 revealed that although K324 is not an essential lysine residue, Tub2 K324R mutants show growth defects and a notable S Phase delay. Moreover, cells expressing a mutation of an identified conserved N-terminal SIM domain in Tub2 also display growth defects and an S Phase delay, consistent with our model in which sumoylation is important for tubulin function. Hence, although neither the lysine nor SIM mutation in Tub2 are not lethal, taken together these data do suggest an important, but unclear, role for these residues during S Phase.

6.2 Sumo and Disease

It is interesting to note that sumo, the CCT complex, tubulin and F-actin are all linked to a number of human diseases, including cancer, neurodegenerative diseases and viral infections (Binarová and Tuszynski, 2019, Broadley and Hartl, 2009, Eckermann, 2013, Eifler and Vertegaal, 2015, Wimmer et al., 2012). Results in this thesis strongly suggest that combining F-actin, tubulin and cct mutants with the *smt3* strain improve the phenotypes associated with the loss of sumo function. Hence it is tempting to speculate that the pathology of diseases caused by the downregulation of components in F-actin, microtubules or the CCT complex may be improved when combined with reduced sumo function. For example, synthetic lethal screens could identify genes which, when combined with cancerous cells, cause lethality but do not affect wild type cells (Huang et al., 2020). Hence it would be extremely interesting to identify whether mutations of sumo (or the sumo conjugation system) would be synthetically lethal with cells from diseases associated with actin or tubulin mutations. Remarkably, a novel finding from this thesis proposes that lowering cellular sumo levels promotes the increased stability of microtubules. Interestingly, the anti-cancer drug, Taxol, which specifically binds to β -tubulin, remains one of the most frequently used drugs in cancer treatment. Cancerous cells grow and divide uncontrollably, hence Taxol stabilises the mitotic spindle to promote metaphase arrest, thus inhibiting cells from dividing by activation of the spindle checkpoint (Löwe et al., 2001) (Brito et al., 2008). However, microtubule-targeted drugs often have unwanted side-effects, such as hair loss and anaemia and are often not specific to just cancer cells. Hence, it would be interesting to identify whether cells expressing lower levels of sumo are more sensitive to treatment with Taxol. If so, prior to Taxol administration, cancer cells from patients could be screened and the sumo levels analysed. This would allow patients with reduced sumo levels to be offered lower doses of Taxol, which may alleviate some of the unwanted side effects. Nevertheless, this is purely hypothetical but highlights how this study could provide insights into potential therapeutic drug treatments.

Bacterial infections often target the sumo pathway to enhance pathogenicity (Wimmer et al., 2012). One such pathogen, the bacteria *L. monocytogenes*, targets the sumo E2 Ubc9 for degradation, inhibiting global sumoylation to facilitate entry into host cells (Citro and Chiocca,

2010, Ribet et al., 2010). Interestingly, separate observations suggest that activation of the Arp2/3 complex enables the formation of *L. monocytogenes* actin-rich comet tails to enhance bacterial motility. Furthermore, siRNA knockdown of the ARPC1 subunit of the mammalian Arp2/3 complex significantly reduces the rate of *L. monocytogenes* entry into cells, suggestive that Arp2/3 dependant actin remodelling is critical for *L. monocytogenes* infection (Lambrechts et al., 2008). Hence, it is intriguing that data from this study suggests a functional link between sumo and F-actin remodelling by the Arp2/3 complex, although the relationship between sumo and the Arp2/3 complex during *L. monocytogenes* infection remain to be determined. Nevertheless, it is clear that further research is required to investigate whether the Arp2/3 complex is subject to sumo modifications during *L. monocytogenes* infection which may provide insights into future drug targets for bacterial infections.

6.3 Final Remarks

In conclusion, this study has provided key insights into the fundamental roles of sumoylation in *S. cerevisiae*. Taken together, findings in this thesis indicate a model in which sumoylation is functionally linked to the cytoskeleton by the interaction of sumo with microtubules and F-actin (Fig. 6.1). Indeed, investigation of the relationships between *smt3* and the novel cytoskeletal suppressor proteins revealed that although these *smt3* suppressors partially suppress the *smt3* growth defects, these growth defects are not restored back to wildtype levels. Additionally, the *smt3* strain also partially suppresses several phenotypes associated with the cytoskeletal suppressors, suggesting that there is a synergistic relationship between sumo, F-actin and microtubules. Thus, the current model based on results in this thesis suggests that sumo individually regulates F-actin and tubulin (Fig. 6.1). Furthermore, siRNA knockdown of Ubc9 in mammalian cells results in aberrant F-actin structures, similar to those observed in *smt3* cells (Dr. Lewis, personal communication). Taken together, these data suggest that the functional relationship between sumo, actin and tubulin are highly conserved throughout eukaryotes. Although several subunits of the CCT complex were identified as top suppressors in the SGA, it is intriguing to note that, unlike F-actin or microtubules, to date no studies have identified components of the CCT complex as sumo substrates. Therefore, as actin and tubulin are two major substrates of the CCT complex, one hypothesis is that downregulation of the CCT complex may reduce the folding efficiency of actin and

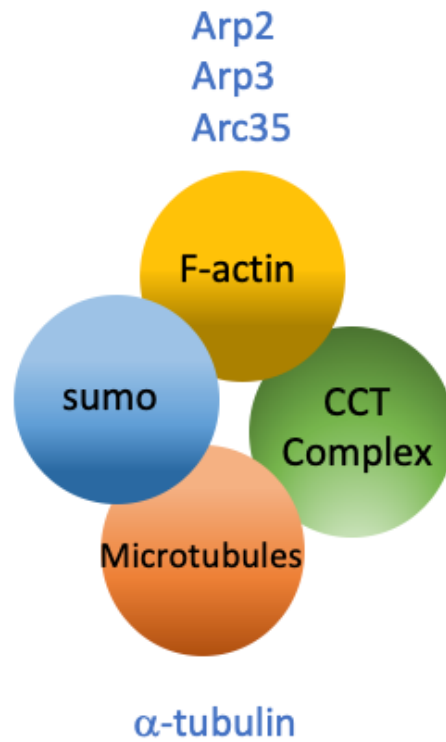


Figure 6.1 Sumo is functionally linked to the cytoskeleton by interaction(s) with microtubules and F-actin. The proposed model in which sumo is functionally linked to the cytoskeleton via interaction(s) with F-actin and microtubules. Proteins from each complex which have been shown to physically interact with sumo in mammalian cells are labelled in blue next to the appropriate complex (Wen et al., 2014, Feng et al., 2021). Overlaps indicate physical interactions between the indicated proteins/ complexes.

tubulin, resulting in lower levels of actin and tubulin in the cell. Collectively, this may suggest why *cct8* and *cct3* were identified as strong *smt3* suppressors in the SGA screen. Nevertheless, in conclusion, finding in this thesis support a model in which sumo is linked to the function of actin and microtubules in eukaryotic cells.

References

- AGUILAR-MARTINEZ, E., CHEN, X., WEBBER, A., MOULD, A. P., SEIFERT, A., HAY, R. T. & SHARROCKS, A. D. 2015. Screen for multi-SUMO-binding proteins reveals a multi-SIM-binding mechanism for recruitment of the transcriptional regulator ZMYM2 to chromatin. *Proc Natl Acad Sci U S A*, 112, E4854-63.
- AGUILAR-MARTINEZ, E., GUO, B. & SHARROCKS, A. D. 2016. RNF4 interacts with multiSUMOylated ETV4. *Wellcome Open Res*, 1, 3.
- AGUILERA, J., RANDEZ-GIL, F. & PRIETO, J. A. 2007. Cold response in *Saccharomyces cerevisiae*: new functions for old mechanisms. *FEMS Microbiol Rev*, 31, 327-41.
- ALTONSY, M. O., GANGULY, A., AMREIN, M., SURMANOWICZ, P., LI, S. S., LAUZON, G. J. & MYDLARSKI, P. R. 2020. Beta3-Tubulin is Critical for Microtubule Dynamics, Cell Cycle Regulation, and Spontaneous Release of Microvesicles in Human Malignant Melanoma Cells (A375). *Int J Mol Sci*, 21.
- AMIN, M. A., AGARWAL, S. & VARMA, D. 2019. Mapping the kinetochore MAP functions required for stabilizing microtubule attachments to chromosomes during metaphase. *Cytoskeleton (Hoboken)*, 76, 398-412.
- AMIT, M., WEISBERG, S. J., NADLER-HOLLY, M., MCCORMACK, E. A., FELDMESSER, E., KAGANOVICH, D., WILLISON, K. R. & HOROVITZ, A. 2010. Equivalent mutations in the eight subunits of the chaperonin CCT produce dramatically different cellular and gene expression phenotypes. *J Mol Biol*, 401, 532-43.
- ARAVA, Y., WANG, Y., STOREY, J. D., LIU, C. L., BROWN, P. O. & HERSCHLAG, D. 2003. Genome-wide analysis of mRNA translation profiles in *Saccharomyces cerevisiae*. *Proc Natl Acad Sci U S A*, 100, 3889-94.
- ARCHAMBAULT, V. & GLOVER, D. M. 2009. Polo-like kinases: conservation and divergence in their functions and regulation. *Nat Rev Mol Cell Biol*, 10, 265-75.
- ARMSTRONG, A. A., MOHIDEEN, F. & LIMA, C. D. 2012. Recognition of SUMO-modified PCNA requires tandem receptor motifs in Srs2. *Nature*, 483, 59-63.
- ASLANUKOV, A., BHOWMICK, R., GURUJU, M., OSWALD, J., RAZ, D., BUSH, R. A., SIEVING, P. A., LU, X., BOCK, C. B. & FERREIRA, P. A. 2006. RanBP2 modulates Cox11 and hexokinase I activities and haploinsufficiency of RanBP2 causes deficits in glucose metabolism. *PLoS Genet*, 2, e177.
- BALLARD, C., GAUTHIER, S., CORBETT, A., BRAYNE, C., AARSLAND, D. & JONES, E. 2011. Alzheimer's disease. *Lancet*, 377, 1019-31.
- BAN, R., NISHIDA, T. & URANO, T. 2011. Mitotic kinase Aurora-B is regulated by SUMO-2/3 conjugation/deconjugation during mitosis. *Genes Cells*, 16, 652-69.
- BARNA, J., CSERMELY, P. & VELLAI, T. 2018. Roles of heat shock factor 1 beyond the heat shock response. *Cell Mol Life Sci*, 75, 2897-2916.
- BASELER, L., CHERTOW, D. S., JOHNSON, K. M., FELDMANN, H. & MORENS, D. M. 2017. The Pathogenesis of Ebola Virus Disease. *Annu Rev Pathol*, 12, 387-418.
- BATES, G. P., DORSEY, R., GUSELLA, J. F., HAYDEN, M. R., KAY, C., LEAVITT, B. R., NANCE, M., ROSS, C. A., SCAHILL, R. I., WETZEL, R., WILD, E. J. & TABRIZI, S. J. 2015. Huntington disease. *Nat Rev Dis Primers*, 1, 15005.

- BEAUCLAIR, G., BRIDIER-NAHMIAS, A., ZAGURY, J. F., SAÏB, A. & ZAMBORLINI, A. 2015. JASSA: a comprehensive tool for prediction of SUMOylation sites and SIMs. *Bioinformatics*, 31, 3483-91.
- BEAUPERE, C., DINATTO, L., WASKO, B. M., CHEN, R. B., VANVALKENBURG, L., KIFLEZGHI, M. G., LEE, M. B., PROMISLOW, D. E. L., DANG, W., KAEBERLEIN, M. & LABUNSKYY, V. M. 2018. Genetic screen identifies adaptive aneuploidy as a key mediator of ER stress resistance in yeast. *Proc Natl Acad Sci U S A*, 115, 9586-9591.
- BECKER, J., BARYSCH, S. V., KARACA, S., DITTNER, C., HSIAO, H. H., BERRIEL DIAZ, M., HERZIG, S., URLAUB, H. & MELCHIOR, F. 2013. Detecting endogenous SUMO targets in mammalian cells and tissues. *Nat Struct Mol Biol*, 20, 525-31.
- BERBEN, G., DUMONT, J., GILLIQUET, V., BOLLE, P. A. & HILGER, F. 1991. The YDp plasmids: a uniform set of vectors bearing versatile gene disruption cassettes for *Saccharomyces cerevisiae*. *Yeast*, 7, 475-7.
- BERNIER-VILLAMOR, V., SAMPSON, D. A., MATUNIS, M. J. & LIMA, C. D. 2002. Structural basis for E2-mediated SUMO conjugation revealed by a complex between ubiquitin-conjugating enzyme Ubc9 and RanGAP1. *Cell*, 108, 345-56.
- BIGGINS, S. & MURRAY, A. W. 2001. The budding yeast protein kinase Ipl1/Aurora allows the absence of tension to activate the spindle checkpoint. *Genes Dev*, 15, 3118-29.
- BINAROVÁ, P. & TUSZYNSKI, J. 2019. Tubulin: Structure, Functions and Roles in Disease. *Cells*, 8.
- BOEHM, E. M., GILDENBERG, M. S. & WASHINGTON, M. T. 2016. The Many Roles of PCNA in Eukaryotic DNA Replication. *Enzymes*, 39, 231-54.
- BOSSIS, G. & MELCHIOR, F. 2006. Regulation of SUMOylation by reversible oxidation of SUMO conjugating enzymes. *Mol Cell*, 21, 349-57.
- BRACKLEY, K. I. & GRANTHAM, J. 2009. Activities of the chaperonin containing TCP-1 (CCT): implications for cell cycle progression and cytoskeletal organisation. *Cell Stress Chaperones*, 14, 23-31.
- BREHME, M., VOISINE, C., ROLLAND, T., WACHI, S., SOPER, J. H., ZHU, Y., ORTON, K., VILLELLA, A., GARZA, D., VIDAL, M., GE, H. & MORIMOTO, R. I. 2014. A chaperome subnetwork safeguards proteostasis in aging and neurodegenerative disease. *Cell Rep*, 9, 1135-50.
- BRESLOW, D. K., CAMERON, D. M., COLLINS, S. R., SCHULDINER, M., STEWART-ORNSTEIN, J., NEWMAN, H. W., BRAUN, S., MADHANI, H. D., KROGAN, N. J. & WEISSMAN, J., .S. 2008. A comprehensive strategy enabling high-resolution functional analysis of the yeast genome. *Nature Methods*, 5, 711-718.
- BRITO, D. A., YANG, Z. & RIEDER, C. L. 2008. Microtubules do not promote mitotic slippage when the spindle assembly checkpoint cannot be satisfied. *J Cell Biol*, 182, 623-9.
- BROADLEY, S. A. & HARTL, F. U. 2009. The role of molecular chaperones in human misfolding diseases. *FEBS Lett*, 583, 2647-53.
- BURKE, D., GASDASKA, P. & HARTWELL, L. 1989. Dominant effects of tubulin overexpression in *Saccharomyces cerevisiae*. *Mol Cell Biol*, 9, 1049-59.
- BYLEBYL, G. R., BELICHENKO, I. & JOHNSON, E. S. 2003. The SUMO isopeptidase Ulp2 prevents accumulation of SUMO chains in yeast. *J Biol Chem*, 278, 44113-20.
- CAMASSES, A., BOGDANOVA, A., SHEVCHENKO, A. & ZACHARIAE, W. 2003. The CCT chaperonin promotes activation of the anaphase-promoting complex through the generation of functional Cdc20. *Mol Cell*, 12, 87-100.
- CAPPADOCIA, L. & LIMA, C. D. 2017. Ubiquitin-like Protein Conjugation: Structures, Chemistry, and Mechanism. *Chem Rev*.

- CHATTERJEE, K. S., TRIPATHI, V. & DAS, R. 2019. A conserved and buried edge-to-face aromatic interaction in small ubiquitin-like modifier (SUMO) has a role in SUMO stability and function. *J Biol Chem*, 294, 6772-6784.
- CITRO, S. & CHIOCCA, S. 2010. *Listeria monocytogenes*: a bacterial pathogen to hit on the SUMO pathway. *Cell Res*, 20, 738-40.
- COSTA, A. C., CARVALHO, F., CABANES, D. & SOUSA, S. 2019. Stathmin recruits tubulin to *Listeria monocytogenes*-induced actin comets and promotes bacterial dissemination. *Cell Mol Life Sci*, 76, 961-975.
- COSTANZO, M., BARYSHNIKOVA, A., BELLAY, J., KIM, Y., SPEAR, E. D., SEVIER, C. S., DING, H., KOH, J. L., TOUFIGHI, K., MOSTAFAVI, S., PRINZ, J., ST ONGE, R. P., VANDERSLUIJ, B., MAKHNEVYCH, T., VIZEACOMAR, F. J., ALIZADEH, S., BAHR, S., BROST, R. L., CHEN, Y., COKOL, M., DESHPANDE, R., LI, Z., LIN, Z. Y., LIANG, W., MARBACK, M., PAW, J., SAN LUIS, B. J., SHUTERIQUI, E., TONG, A. H., VAN DYK, N., WALLACE, I. M., WHITNEY, J. A., WEIRAUCH, M. T., ZHONG, G., ZHU, H., HOURY, W. A., BRUDNO, M., RAGIBIZADEH, S., PAPP, B., PÁL, C., ROTH, F. P., GIAEVER, G., NISLOW, C., TROYANSKAYA, O. G., BUSSEY, H., BADER, G. D., GINGRAS, A. C., MORRIS, Q. D., KIM, P. M., KAISER, C. A., MYERS, C. L., ANDREWS, B. J. & BOONE, C. 2010. The genetic landscape of a cell. *Science*, 327, 425-31.
- COTTO-RIOS, X. M., BÉKÉS, M., CHAPMAN, J., UEBERHEIDE, B. & HUANG, T. T. 2012. Deubiquitinases as a signaling target of oxidative stress. *Cell Rep*, 2, 1475-84.
- CRAIG, E. A. 1985. The heat shock response. *CRC Crit Rev Biochem*, 18, 239-80.
- DAWLATY, M. M., MALUREANU, L., JEGANATHAN, K. B., KAO, E., SUSTMANN, C., TAHK, S., SHUAI, K., GROSSCHEDL, R. & VAN DEURSEN, J. M. 2008. Resolution of sister centromeres requires RanBP2-mediated SUMOylation of topoisomerase IIalpha. *Cell*, 133, 103-15.
- DI BACCO, A., OUYANG, J., LEE, H. Y., CATIC, A., PLOEGH, H. & GILL, G. 2006. The SUMO-specific protease SENP5 is required for cell division. *Mol Cell Biol*, 26, 4489-98.
- DI GENOVA, B. M., DA SILVA, R. C., DA CUNHA, J. P. C., GARGANTINI, P. R., MORTARA, R. A. & TONELLI, R. R. 2017. Protein SUMOylation is Involved in Cell-cycle Progression and Cell Morphology in *Giardia lamblia*. *J Eukaryot Microbiol*, 64, 491-503.
- DIECKHOFF, P., BOLTE, M., SANCAK, Y., BRAUS, G. H. & IRNIGER, S. 2004. Smt3-SUMO and Ubc9 are required for efficient APC-C-mediated proteolysis in budding yeast. *Molecular Microbiology*, 51, 1375-1387.
- DOBRYNSKI, J. K., STERNLICHT, M. L., FARR, G. W. & STERNLICHT, H. 1996. Newly-Synthesized β -Tubulin Demonstrates Domain-Specific Interactions with the Cytosolic Chaperonin. *Biochemistry*, 35, 15870-15882.
- DOHMEN, R. J. 2004. SUMO protein modification. *Biochim Biophys Acta*, 1695, 113-31.
- DORIS, K. S., RUMSBY, E. L. & MORGAN, B. A. 2012. Oxidative stress responses involve oxidation of a conserved ubiquitin pathway enzyme. *Mol Cell Biol*, 32, 4472-81.
- DORVAL, V. & FRASER, P. E. 2007. SUMO on the road to neurodegeneration. *Biochim Biophys Acta*, 1773, 694-706.
- DU, L., LI, Y. J., FAKIH, M., WIATREK, R. L., DULDULAO, M., CHEN, Z., CHU, P., GARCIA-AGUILAR, J. & CHEN, Y. 2016. Role of SUMO activating enzyme in cancer stem cell maintenance and self-renewal. *Nat Commun*, 7, 12326.
- ECKERMANN, K. 2013. SUMO and Parkinson's disease. *Neuromolecular Med*, 15, 737-59.

- EIFLER, K., CUIJPERS, S. A. G., WILLEMSTEIN, E., RAAIJMAKERS, J. A., EL ATMIOUI, D., OVAA, H., MEDEMA, R. H. & VERTEGAAL, A. C. O. 2018. SUMO targets the APC/C to regulate transition from metaphase to anaphase. *Nature Communications*, 9, 1119.
- EIFLER, K. & VERTEGAAL, A. C. O. 2015. SUMOylation-Mediated Regulation of Cell Cycle Progression and Cancer. *Trends Biochem Sci*, 40, 779-793.
- EL MOTIAM, A., VIDAL, S., SEOANE, R., BOUZAHER, Y. H., GONZÁLEZ-SANTAMARÍA, J. & RIVAS, C. 2020. SUMO and Cytoplasmic RNA Viruses: From Enemies to Best Friends. *Adv Exp Med Biol*, 1233, 263-277.
- ELLIOTT, K. L., SVANSTRÖM, A., SPIESS, M., KARLSSON, R. & GRANTHAM, J. 2015. A novel function of the monomeric CCT ϵ subunit connects the serum response factor pathway to chaperone-mediated actin folding. *Mol Biol Cell*, 26, 2801-9.
- ENSERINK, J. M. 2015. Sumo and the cellular stress response. *Cell Div*, 10, 4.
- FAN, L. & XIAO, W. 2021. Study Essential Gene Functions by Plasmid Shuffling. *Methods Mol Biol*, 2196, 53-62.
- FELDMAN, D. E., SPIESS, C., HOWARD, D. E. & FRYDMAN, J. 2003. Tumorigenic mutations in VHL disrupt folding in vivo by interfering with chaperonin binding. *Mol Cell*, 12, 1213-24.
- FENG, W., LIU, R., XIE, X., DIAO, L., GAO, N., CHENG, J., ZHANG, X., LI, Y. & BAO, L. 2021. SUMOylation of α -tubulin is a novel modification regulating microtubule dynamics. *J Mol Cell Biol*.
- FINLEY, D., SADIS, S., MONIA, B. P., BOUCHER, P., ECKER, D. J., CROOKE, S. T. & CHAU, V. 1994. Inhibition of proteolysis and cell cycle progression in a multiubiquitination-deficient yeast mutant. *Mol Cell Biol*, 14, 5501-9.
- FORMAN, H. J., URSINI, F. & MAIORINO, M. 2014. An overview of mechanisms of redox signaling. *J Mol Cell Cardiol*, 73, 2-9.
- FRA, A., YOBOUE, E. D. & SITIA, R. 2017. Cysteines as Redox Molecular Switches and Targets of Disease. *Frontiers in Molecular Neuroscience*, 10.
- FRADELIZI, J., NOIREAUX, V., PLASTINO, J., MENICHI, B., LOUVARD, D., SYKES, C., GOLSTEYN, R. M. & FRIEDERICH, E. 2001. ActA and human zyxin harbour Arp2/3-independent actin-polymerization activity. *Nat Cell Biol*, 3, 699-707.
- GALI, H., JUHASZ, S., MOROCZ, M., HAJDU, I., FATYOL, K., SZUKACSOV, V., BURKOVICS, P. & HARACSKA, L. 2012. Role of SUMO modification of human PCNA at stalled replication fork. *Nucleic Acids Res*, 40, 6049-59.
- GARCIA-DOMINGUEZ, M. & REYES, J. C. 2009. SUMO association with repressor complexes, emerging routes for transcriptional control. *Biochim Biophys Acta*, 1789, 451-9.
- GAY, D. A., SISODIA, S. S. & CLEVELAND, D. W. 1989. Autoregulatory control of beta-tubulin mRNA stability is linked to translation elongation. *Proc Natl Acad Sci U S A*, 86, 5763-7.
- GIETZ, R. D. & SCHIESTL, R. H. 2007. High-efficiency yeast transformation using the LiAc/SS carrier DNA/PEG method. *Nat Protoc*, 2, 31-4.
- GILL, G. 2005. Something about SUMO inhibits transcription. *Curr Opin Genet Dev*, 15, 536-41.
- GOLEBIOWSKI, F., MATIC, I., TATHAM, M. T., COLE, C., YIN, Y., NAKAMURA, A., COX, J., BARTON, G. J. & HAY, R. T. 2009. System-Wide Changes to SUMO Modifications in Response to Heat Shock. *Science Signalling*, 2.
- GOLEY, E. D. & WELCH, M. D. 2006. The ARP2/3 complex: an actin nucleator comes of age. *Nat Rev Mol Cell Biol*, 7, 713-26.

- GÓMEZ-PUERTAS, P., MARTÍN-BENITO, J., CARRASCOSA, J. L., WILLISON, K. R. & VALPUESTA, J. M. 2004. The substrate recognition mechanisms in chaperonins. *J Mol Recognit*, 17, 85-94.
- GOODSON, H. V. & JONASSON, E. M. 2018. Microtubules and Microtubule-Associated Proteins. *Cold Spring Harb Perspect Biol*, 10.
- GOUIN, E., EGILE, C., DEHOUX, P., VILLIERS, V., ADAMS, J., GERTLER, F., LI, R. & COSSART, P. 2004. The RickA protein of *Rickettsia conorii* activates the Arp2/3 complex. *Nature*, 427, 457-61.
- GRANTHAM, J. 2020. The Molecular Chaperone CCT/TRiC: An Essential Component of Proteostasis and a Potential Modulator of Protein Aggregation. *Frontiers in Genetics*, 11.
- GRANTHAM, J., BRACKLEY, K. I. & WILLISON, K. R. 2006. Substantial CCT activity is required for cell cycle progression and cytoskeletal organization in mammalian cells. *Exp Cell Res*, 312, 2309-24.
- GREENLEE, M., ALONSO, A., RAHMAN, M., MEEDNU, N., DAVIS, K., TABB, V., COOK, R. & MILLER, R. K. 2018. The TOG protein Stu2/XMAP215 interacts covalently and noncovalently with SUMO. *Cytoskeleton (Hoboken)*, 75, 290-306.
- GUTIERREZ, G. J. & RONAI, Z. 2006. Ubiquitin and SUMO systems in the regulation of mitotic checkpoints. *Trends Biochem Sci*, 31, 324-32.
- HALL, A. 2009. The cytoskeleton and cancer. *Cancer Metastasis Rev*, 28, 5-14.
- HAMON, M. A., RIBET, D., STAVRU, F. & COSSART, P. 2012. Listeriolysin O: the Swiss army knife of *Listeria*. *Trends Microbiol*, 20, 360-8.
- HAN, Z. J., FENG, Y. H., GU, B. H., LI, Y. M. & CHEN, H. 2018. The post-translational modification, SUMOylation, and cancer (Review). *Int J Oncol*, 52, 1081-1094.
- HAY, R. T. 2005. SUMO: a history of modification. *Mol Cell*, 18, 1-12.
- HAY, R. T. 2013. Decoding the SUMO signal. *Biochem Soc Trans*, 41, 463-73.
- HENDRIKS, I. A., LYON, D., YOUNG, C., JENSEN, L. J., VERTEGAAL, A. C. & NIELSEN, M. L. 2017. Site-specific mapping of the human SUMO proteome reveals co-modification with phosphorylation. *Nat Struct Mol Biol*, 24, 325-336.
- HENDRIKS, I. A. & VERTEGAAL, A. C. 2015. SUMO in the DNA damage response. *Oncotarget*, 6, 15734-5.
- HENDRIKS, I. A. & VERTEGAAL, A. C. 2016. A comprehensive compilation of SUMO proteomics. *Nat Rev Mol Cell Biol*, 17, 581-95.
- HERRMANN, J., LERMAN, L. O. & LERMAN, A. 2007. Ubiquitin and ubiquitin-like proteins in protein regulation. *Circ Res*, 100, 1276-91.
- HIETAKANGAS, V., ANCKAR, J., BLOMSTER, H. A., FUJIMOTO, M., PALVIMO, J. J., NAKAI, A. & SISTONEN, L. 2006. PDSM, a motif for phosphorylation-dependent SUMO modification. *Proc Natl Acad Sci U S A*, 103, 45-50.
- HOCHSTRASSER, M. 2001. SP-RING for SUMO: new functions bloom for a ubiquitin-like protein. *Cell*, 107, 5-8.
- HOCHSTRASSER, M. 2009. Origin and function of ubiquitin-like proteins. *Nature*, 458, 422-9.
- HOCHWAGEN, A., WROBEL, G., CARTRON, M., DEMOUGIN, P., NIEDERHAUSER-WIEDERKEHR, C., BOSELLI, M. G., PRIMIG, M. & AMON, A. 2005. Novel response to microtubule perturbation in meiosis. *Mol Cell Biol*, 25, 4767-81.
- HOEGE, C., PFANDER, B., MOLDOVAN, G. L., PYROWOLAKIS, G. & JENTSCH, S. 2002. RAD6-dependent DNA repair is linked to modification of PCNA by ubiquitin and SUMO. *Nature*, 419, 135-41.

- HONG, Y., ROGERS, R., MATUNIS, M. J., MAYHEW, C. N., GOODSON, M. L., PARK-SARGE, O. K. & SARGE, K. D. 2001. Regulation of heat shock transcription factor 1 by stress-induced SUMO-1 modification. *J Biol Chem*, 276, 40263-7.
- HOWES, S. C., GEYER, E. A., LAFRANCE, B., ZHANG, R., KELLOGG, E. H., WESTERMANN, S., RICE, L. M. & NOGALES, E. 2017. Structural differences between yeast and mammalian microtubules revealed by cryo-EM. *J Cell Biol*, 216, 2669-2677.
- HUANG, A., GARRAWAY, L. A., ASHWORTH, A. & WEBER, B. 2020. Synthetic lethality as an engine for cancer drug target discovery. *Nat Rev Drug Discov*, 19, 23-38.
- HUANG, R., YU, M., LI, C. Y., ZHAN, Y. Q., XU, W. X., XU, F., GE, C. H., LI, W. & YANG, X. M. 2012. New insights into the functions and localization of nuclear CCT protein complex in K562 leukemia cells. *Proteomics Clin Appl*, 6, 467-75.
- HUNTER, T. & SUN, H. 2008. Crosstalk between the SUMO and ubiquitin pathways. *Ernst Schering Found Symp Proc*, 1-16.
- IMPENS, F., RADOSHEVICH, L., COSSART, P. & RIBET, D. 2014. Mapping of SUMO sites and analysis of SUMOylation changes induced by external stimuli. *PNAS*, 111, 12432-12437.
- IWAYA, K., OIKAWA, K., SEMBA, S., TSUCHIYA, B., MUKAI, Y., OTSUBO, T., NAGAO, T., IZUMI, M., KURODA, M., DOMOTO, H. & MUKAI, K. 2007. Correlation between liver metastasis of the colocalization of actin-related protein 2 and 3 complex and WAVE2 in colorectal carcinoma. *Cancer Sci*, 98, 992-9.
- JARDIN, C., HORN, A. H. & STICHT, H. 2015. Binding properties of SUMO-interacting motifs (SIMs) in yeast. *J Mol Model*, 21, 50.
- JOHNSON, E. S. & BLOBEL, G. 1999. Cell cycle-regulated attachment of the ubiquitin-related protein SUMO to the yeast septins. *J Cell Biol*, 147, 981-94.
- JOHNSON, E. S. & GUPTA, A. A. 2001a. An E3-like factor that promotes SUMO conjugation to the yeast. *Cell*, 106, 735-744
- JOHNSON, E. S. & GUPTA, A. A. 2001b. An E3-like factor that promotes SUMO conjugation to the yeast septins. *Cell*, 106, 735-44.
- JOHNSON, E. S., SCHWEIENHORST, I., DOHMEN, R. J. & BLOBEL, G. 1997. The ubiquitin-like protein Smt3p is activated for conjugation to other proteins by an Aos1p Uba2p heterodimer. *The EMBO Journal*, 16, 5509-5519.
- JOHNSON, V., AYAZ, P., HUDDLESTON, P. & RICE, L. M. 2011. Design, overexpression, and purification of polymerization-blocked yeast α -tubulin mutants. *Biochemistry*, 50, 8636-44.
- JUNTILLA, M. M., PATIL, V. D., CALAMITO, M., JOSHI, R. P., BIRNBAUM, M. J. & KORETZKY, G. A. 2010. AKT1 and AKT2 maintain hematopoietic stem cell function by regulating reactive oxygen species. *Blood*, 115, 4030-8.
- KAHYO, T., NISHIDA, T. & YASUDA, H. 2001. Involvement of PIAS1 in the sumoylation of tumor suppressor p53. *Mol Cell*, 8, 713-8.
- KANE, J. K., KONU, O., MA, J. Z. & LI, M. D. 2004. Nicotine coregulates multiple pathways involved in protein modification/degradation in rat brain. *Brain Res Mol Brain Res*, 132, 181-91.
- KARVONEN, U., JÄÄSKELÄINEN, T., RYTINKI, M., KAIKKONEN, S. & PALVIMO, J. J. 2008. ZNF451 is a novel PML body- and SUMO-associated transcriptional coregulator. *J Mol Biol*, 382, 585-600.

- KATZ, W., WEINSTEIN, B. & SOLOMON, F. 1990. Regulation of tubulin levels and microtubule assembly in *Saccharomyces cerevisiae*: consequences of altered tubulin gene copy number. *Mol Cell Biol*, 10, 5286-94.
- KAYUKAWA, T. & ISHIKAWA, Y. 2009. Chaperonin contributes to cold hardiness of the onion maggot *Delia antiqua* through repression of depolymerization of actin at low temperatures. *PLoS One*, 4, e8277.
- KEITEN-SCHMITZ, J., SCHUNCK, K. & MÜLLER, S. 2019. SUMO Chains Rule on Chromatin Occupancy. *Front Cell Dev Biol*, 7, 343.
- KELLEY, R. & IDEKER, T. 2005. Systematic interpretation of genetic interactions using protein networks. *Nat Biotechnol*, 23, 561-6.
- KIM, T. & GARTNER, A. 2021. Bub1 kinase in the regulation of mitosis. *Anim Cells Syst (Seoul)*, 25, 1-10.
- KIM, W. Y. & KAELIN, W. G. 2004. Role of VHL gene mutation in human cancer. *J Clin Oncol*, 22, 4991-5004.
- KLUG, H., XAVER, M., CHAUGULE, V. K., KOIDL, S., MITTLER, G., KLEIN, F. & PICHLER, A. 2013. Ubc9 sumoylation controls SUMO chain formation and meiotic synapsis in *Saccharomyces cerevisiae*. *Mol Cell*, 50, 625-36.
- KNIPSCHEER, P., FLOTHO, A., KLUG, H., OLSEN, J. V., VAN DIJK, W. J., FISH, A., JOHNSON, E. S., MANN, M., SIXMA, T. K. & PICHLER, A. 2008. Ubc9 sumoylation regulates SUMO target discrimination. *Mol Cell*, 31, 371-82.
- KOMANO, J., MIYAUCHI, K., MATSUDA, Z. & YAMAMOTO, N. 2004. Inhibiting the Arp2/3 complex limits infection of both intracellular mature vaccinia virus and primate lentiviruses. *Mol Biol Cell*, 15, 5197-207.
- KROONEN, J. S. & VERTEGAAL, A. C. O. 2020. Targeting SUMO Signaling to Wrestle Cancer. *Trends Cancer*.
- KUNG, C. C., NAIK, M. T., WANG, S. H., SHIH, H. M., CHANG, C. C., LIN, L. Y., CHEN, C. L., MA, C., CHANG, C. F. & HUANG, T. H. 2014. Structural analysis of poly-SUMO chain recognition by the RNF4-SIMs domain. *Biochem J*, 462, 53-65.
- KUNZ, K., PILLER, T. & MÜLLER, S. 2018. SUMO-specific proteases and isopeptidases of the SENP family at a glance. *J Cell Sci*, 131.
- LAFLAMME, G., SIM, S., LEARY, A., PASCARIU, M., VOGEL, J. & D'AMOURS, D. 2019. Interphase Microtubules Safeguard Mitotic Progression by Suppressing an Aurora B-Dependent Arrest Induced by DNA Replication Stress. *Cell Rep*, 26, 2875-2889.e3.
- LAI, W. F. & WONG, W. T. 2020. Roles of the actin cytoskeleton in aging and age-associated diseases. *Ageing Res Rev*, 58, 101021.
- LAKE, M. W., WUEBBENS, M. M., RAJAGOPALAN, K. V. & SCHINDELIN, H. 2001. Mechanism of ubiquitin activation revealed by the structure of a bacterial MoeB-MoaD complex. *Nature*, 414, 325-9.
- LAMBRECHTS, A., GEVAERT, K., COSSART, P., VANDEKERCKHOVE, J. & VAN TROYS, M. 2008. *Listeria* comet tails: the actin-based motility machinery at work. *Trends Cell Biol*, 18, 220-7.
- LARA-GONZALEZ, P., WESTHORPE, F. G. & TAYLOR, S. S. 2012. The spindle assembly checkpoint. *Curr Biol*, 22, R966-80.
- LAUER, P., THERIOT, J. A., SKOBLE, J., WELCH, M. D. & PORTNOY, D. A. 2001. Systematic mutational analysis of the amino-terminal domain of the *Listeria monocytogenes* ActA protein reveals novel functions in actin-based motility. *Mol Microbiol*, 42, 1163-77.

- LE, J., EL-ASSAL SEL, D., BASU, D., SAAD, M. E. & SZYMANSKI, D. B. 2003. Requirements for Arabidopsis ATARP2 and ATARP3 during epidermal development. *Curr Biol*, 13, 1341-7.
- LEACH, M. D., STEAD, D. A., ARGO, E. & BROWN, A. J. 2011. Identification of sumoylation targets, combined with inactivation of SMT3, reveals the impact of sumoylation upon growth, morphology, and stress resistance in the pathogen *Candida albicans*. *Mol Biol Cell*, 22, 687-702.
- LEE, C. C., LI, B., YU, H. & MATUNIS, M. J. 2018. Sumoylation promotes optimal APC/C Activation and Timely Anaphase. *Elife*, 7.
- LEE, Y. J., MIYAKE, S., WAKITA, H., MCMULLEN, D. C., AZUMA, Y., AUH, S. & HALLENBECK, J. M. 2007. Protein SUMOylation is massively increased in hibernation torpor and is critical for the cytoprotection provided by ischemic preconditioning and hypothermia in SHSY5Y cells. *J Cereb Blood Flow Metab*, 27, 950-62.
- LEISNER, C., KAMMERER, D., DENOTH, A., BRITSCHI, M., BARRAL, Y. & LIAKOPOULOS, D. 2008. Regulation of mitotic spindle asymmetry by SUMO and the spindle-assembly checkpoint in yeast. *Curr Biol*, 18, 1249-55.
- LEITNER, A., JOACHIMIAK, L. A., BRACHER, A., MÖNKEMEYER, L., WALZTHOENI, T., CHEN, B., PECHMANN, S., HOLMES, S., CONG, Y., MA, B., LUDTKE, S., CHIU, W., HARTL, F. U., AEBERSOLD, R. & FRYDMAN, J. 2012. The molecular architecture of the eukaryotic chaperonin TRiC/CCT. *Structure*, 20, 814-25.
- LEVY, D. E. & DARNELL, J. E., JR. 2002. Stats: transcriptional control and biological impact. *Nat Rev Mol Cell Biol*, 3, 651-62.
- LEWICKI, M. C., SRIKUMAR, T., JOHNSON, E. & RAUGHT, B. 2015. The *S. cerevisiae* SUMO stress response is a conjugation-deconjugation cycle that targets the transcription machinery. *J Proteomics*, 118, 39-48.
- LEWIS, C. 2016. *Investigation into the function of Sumoylation in yeast.*, University of Newcastle
- LI, S. & HOCHSTRASSER, M. 1999a. A new protease required for cell-cycle progression in yeast. *Nature*, 398, 246-251.
- LI, S. & HOCHSTRASSER, M. 2000. The Yeast ULP2 (SMT4) Gene Encodes a Novel Protease Specific for the Ubiquitin-Like Smt3 Protein. *Molecular and Cellular Biology*, 20, 2367-2377.
- LI, S. J. & HOCHSTRASSER, M. 1999b. A new protease required for cell-cycle progression in yeast. *Nature*, 398, 246-51.
- LI, S. J. & HOCHSTRASSER, M. 2003. The Ulp1 SUMO isopeptidase: distinct domains required for viability, nuclear envelope localization, and substrate specificity. *J Cell Biol*, 160, 1069-81.
- LIEBELT, F., SEBASTIAN, R. M., MOORE, C. L., MULDER, M. P. C., OVAA, H., SHOULDERS, M. D. & VERTEGAAL, A. C. O. 2019. SUMOylation and the HSF1-Regulated Chaperone Network Converge to Promote Proteostasis in Response to Heat Shock. *Cell Rep*, 26, 236-249.e4.
- LIMA, C. D. & REVERTER, D. 2008. Structure of the human SENP7 catalytic domain and poly-SUMO deconjugation activities for SENP6 and SENP7. *J Biol Chem*, 283, 32045-55.
- LIN, H. & CAROLL, K. S. 2018. Introduction: Posttranslational Protein Modification. *Chem Rev*, 118, 887-888.
- LITTLE, M. & SEEHAUS, T. 1988. Comparative analysis of tubulin sequences. *Comp Biochem Physiol B*, 90, 655-70.

- LIU, C., ZHAO, H., XIAO, S., HAN, T., CHEN, Y., WANG, T., MA, Y., GAO, H., XIE, Z., DU, L. L., LI, J., LI, G. & LI, W. 2020. Slx5p-Slx8p Promotes Accurate Chromosome Segregation by Mediating the Degradation of Synaptonemal Complex Components during Meiosis. *Adv Sci (Weinh)*, 7, 1900739.
- LIU, F., WANG, X., SU, M., YU, M., ZHANG, S., LAI, J., YANG, C. & WANG, Y. 2015. Functional characterization of DnSIZ1, a SIZ/PIAS-type SUMO E3 ligase from *Dendrobium*. *BMC Plant Biology*, 15, 225.
- LIU, X., LIN, C. Y., LEI, M., YAN, S., ZHOU, T. & ERIKSON, R. L. 2005. CCT chaperonin complex is required for the biogenesis of functional Plk1. *Mol Cell Biol*, 25, 4993-5010.
- LLORCA, O., MARTÍN-BENITO, J., GÓMEZ-PUERTAS, P., RITCO-VONSOVICI, M., WILLISON, K. R., CARRASCOSA, J. L. & VALPUESTA, J. M. 2001. Analysis of the interaction between the eukaryotic chaperonin CCT and its substrates actin and tubulin. *J Struct Biol*, 135, 205-18.
- LLORCA, O., MCCORMACK, E. A., HYNES, G., GRANTHAM, J., CORDELL, J., CARRASCOSA, J. L., WILLISON, K. R., FERNANDEZ, J. J. & VALPUESTA, J. M. 1999. Eukaryotic type II chaperonin CCT interacts with actin through specific subunits. *Nature*, 402, 693-6.
- LOIS, L. M. & LIMA, C. D. 2005. Structures of the SUMO E1 provide mechanistic insights into SUMO activation and E2 recruitment to E1. *Embo j*, 24, 439-51.
- LOMAKINA, M. E., LALLEMAND, F., VACHER, S., MOLINIE, N., DANG, I., CACHEUX, W., CHIPYSHEVA, T. A., ERMILOVA, V. D., DE KONING, L., DUBOIS, T., BIÈCHE, I., ALEXANDROVA, A. Y. & GAUTREAU, A. 2016. Arpin downregulation in breast cancer is associated with poor prognosis. *Br J Cancer*, 114, 545-53.
- LONDON, N. & BIGGINS, S. 2014. Mad1 kinetochore recruitment by Mps1-mediated phosphorylation of Bub1 signals the spindle checkpoint. *Genes Dev*, 28, 140-52.
- LONGTINE, M. S., DEMARINI, D. J., VALENCIK, M. L., AL-AWAR, O. S., FARES, H., DE VIRGILIO, C. & PRINGLE, J. R. 1996. The septins: roles in cytokinesis and other processes. *Curr Opin Cell Biol*, 8, 106-19.
- LOPEZ-FANARRAGA, M., AVILA, J., GUASCH, A., COLL, M. & ZABALA, J. C. 2001. Review: postchaperonin tubulin folding cofactors and their role in microtubule dynamics. *J Struct Biol*, 135, 219-29.
- LORICK, K. L., JENSEN, J. P., FANG, S., ONG, A. M., HATAKEYAMA, S. & WEISSMAN, A. M. 1999. RING fingers mediate ubiquitin-conjugating enzyme (E2)-dependent ubiquitination. *Proc Natl Acad Sci U S A*, 96, 11364-9.
- LÖWE, J., LI, H., DOWNING, K. H. & NOGALES, E. 2001. Refined structure of alpha beta-tubulin at 3.5 Å resolution. *J Mol Biol*, 313, 1045-57.
- LUCHNIAK, A., FUKUDA, Y. & GUPTA, M. L., JR. 2013. Structure-function analysis of yeast tubulin. *Methods Cell Biol*, 115, 355-74.
- LUMPKIN, R. J., GU, H., ZHU, Y., LEONARD, M., AHMAD, A. S., CLAUSER, K. R., MEYER, J. G., BENNETT, E. J. & KOMIVES, E. A. 2017. Site-specific identification and quantitation of endogenous SUMO modifications under native conditions. *Nat Commun*, 8, 1171.
- LUO, H. B., XIA, Y. Y., SHU, X. J., LIU, Z. C., FENG, Y., LIU, X. H., YU, G., YIN, G., XIONG, Y. S., ZENG, K., JIANG, J., YE, K., WANG, X. C. & WANG, J. Z. 2014. SUMOylation at K340 inhibits tau degradation through deregulating its phosphorylation and ubiquitination. *Proc Natl Acad Sci U S A*, 111, 16586-91.
- LUSCAN, R., MECHAUSIER, S., PAUL, A., TIAN, G., GÉRARD, X., DEFOORT-DELLHEMMES, S., LOUNDON, N., AUDO, I., BONNIN, S., LEGARGASSON, J. F., DUMONT, J., GOUDIN, N., GARFA-TRAORÉ, M., BRAS, M., POULIET, A., BESSIÈRES, B., BODDAERT, N., SAHEL, J.

- A., LYONNET, S., KAPLAN, J., COWAN, N. J., ROZET, J. M., MARLIN, S. & PERRAULT, I. 2017. Mutations in TUBB4B Cause a Distinctive Sensorineural Disease. *Am J Hum Genet*, 101, 1006-1012.
- MACEK, B., FORCHHAMMER, K., HARDOUIN, J., WEBER-BAN, E., GRANGEASSE, C. & MIJAKOVIC, I. 2019. Protein post-translational modifications in bacteria. *Nat Rev Microbiol*, 17, 651-664.
- MACRAE, T. H. 1997. Tubulin post-translational modifications--enzymes and their mechanisms of action. *Eur J Biochem*, 244, 265-78.
- MAETA, K., IZAWA, S., OKAZAKI, S., KUGE, S. & INOUE, Y. 2004. Activity of the Yap1 transcription factor in *Saccharomyces cerevisiae* is modulated by methylglyoxal, a metabolite derived from glycolysis. *Mol Cell Biol*, 24, 8753-64.
- MAGIERA, M. M. & JANKE, C. 2014. Post-translational modifications of tubulin. *Curr Biol*, 24, R351-4.
- MAGIERA, M. M., SINGH, P., GADADHAR, S. & JANKE, C. 2018. Tubulin Posttranslational Modifications and Emerging Links to Human Disease. *Cell*, 173, 1323-1327.
- MAHAJAN, R., DELPHIN, C., GUAN, T., GERACE, L. & MELCHIOR, F. 1997. A small ubiquitin-related polypeptide involved in targeting RanGAP1 to nuclear pore complex protein RanBP2. *Cell*, 88, 97-107.
- MAKHNEVYCH, T., SYDORSKYY, Y., XIN, X., SRIKUMAR, T., VIZEACOUMAR, F. J., JERAM, S. M., LI, Z., BAHR, S., ANDREWS, B. J., BOONE, C. & RAUGHT, B. 2009. Global map of SUMO function revealed by protein-protein interaction and genetic networks. *Mol Cell*, 33, 124-35.
- MATIC, I., SCHIMMEL, J., HENDRIKS, I. A., VAN SANTEN, M. A., VAN DE RIJKE, F., VAN DAM, H., GNAD, F., MANN, M. & VERTEGAAL, A. C. 2010. Site-specific identification of SUMO-2 targets in cells reveals an inverted SUMOylation motif and a hydrophobic cluster SUMOylation motif. *Mol Cell*, 39, 641-52.
- MATUNIS, M. J., COUTAVAS, E. & BLOBEL, G. 1996. A novel ubiquitin-like modification modulates the partitioning of the Ran-GTPase-activating protein RanGAP1 between the cytosol and the nuclear pore complex. *J Cell Biol*, 135, 1457-70.
- MATUNIS, M. J., ZHANG, X. D. & ELLIS, N. A. 2006. SUMO: the glue that binds. *Dev Cell*, 11, 596-7.
- MAY, R. C. 2001. The Arp2/3 complex: a central regulator of the actin cytoskeleton. *Cell Mol Life Sci*, 58, 1607-26.
- MAY, R. C., HALL, M. E., HIGGS, H. N., POLLARD, T. D., CHAKRABORTY, T., WEHLAND, J., MACHESKY, L. M. & SECHI, A. S. 1999. The Arp2/3 complex is essential for the actin-based motility of *Listeria monocytogenes*. *Curr Biol*, 9, 759-62.
- MCCORMACK, E. A., LLORCA, O., CARRASCOSA, J. L., VALPUESTA, J. M. & WILLISON, K. R. 2001. Point mutations in a hinge linking the small and large domains of beta-actin result in trapped folding intermediates bound to cytosolic chaperonin CCT. *J Struct Biol*, 135, 198-204.
- MEEK, K., DANG, V. & LEES-MILLER, S. P. 2008. Chapter 2 DNA-PK: The Means to Justify the Ends? *Advances in Immunology*. Academic Press.
- MELUH, P. B. & KOSHLAND, D. 1995. Evidence that the MIF2 gene of *Saccharomyces cerevisiae* encodes a centromere protein with homology to the mammalian centromere protein CENP-C. *Molecular Biology of the Cell*, 6, 793-807.

- MELVILLE, M. W., MCCLELLAN, A. J., MEYER, A. S., DARVEAU, A. & FRYDMAN, J. 2003. The Hsp70 and TRiC/CCT chaperone systems cooperate in vivo to assemble the von Hippel-Lindau tumor suppressor complex. *Mol Cell Biol*, 23, 3141-51.
- MINTY, A., DUMONT, X., KAGHAD, M. & CAPUT, D. 2000. Covalent modification of p73alpha by SUMO-1. Two-hybrid screening with p73 identifies novel SUMO-1-interacting proteins and a SUMO-1 interaction motif. *J Biol Chem*, 275, 36316-23.
- MIURA, K., JIN, J. B., LEE, J., YOO, C. Y., STIRM, V., MIURA, T., ASHWORTH, E. N., BRESSAN, R. A., YUN, D. J. & HASEGAWA, P. M. 2007. SIZ1-mediated sumoylation of ICE1 controls CBF3/DREB1A expression and freezing tolerance in Arabidopsis. *Plant Cell*, 19, 1403-14.
- MONTPETIT, B., HAZBUN, T. R., FIELDS, S. & HIETER, P. 2006. Sumoylation of the budding yeast kinetochore protein Ndc10 is required for Ndc10 spindle localization and regulation of anaphase spindle elongation. *J Cell Biol*, 174, 653-63.
- MOREAU, V., MADANIA, A., MARTIN, R. P. & WINSON, B. 1996. The *Saccharomyces cerevisiae* actin-related protein Arp2 is involved in the actin cytoskeleton. *J Cell Biol*, 134, 117-32.
- MORGAN, B. A., MITTMAN, B. A. & SMITH, M. M. 1991. The highly conserved N-terminal domains of histones H3 and H4 are required for normal cell cycle progression. *Mol Cell Biol*, 11, 4111-20.
- MORRELL, R. & SADANANDOM, A. 2019. Dealing With Stress: A Review of Plant SUMO Proteases. *Front Plant Sci*, 10, 1122.
- MUKHOPADHYAY, D. & DASSO, M. 2010. The fate of metaphase kinetochores is weighed in the balance of SUMOylation during S phase. *Cell Cycle*, 9, 3194-201.
- MUKHOPADHYAY, D. & DASSO, M. 2017. The SUMO Pathway in Mitosis. *Adv Exp Med Biol*, 963, 171-184.
- MULLEN, J. R. & BRILL, S. J. 2008. Activation of the Slx5-Slx8 ubiquitin ligase by poly-small ubiquitin-like modifier conjugates. *J Biol Chem*, 283, 19912-21.
- MULLEN, J. R., DAS, M. & BRILL, S. J. 2011. Genetic evidence that polysumoylation bypasses the need for a SUMO-targeted Ub ligase. *Genetics*, 187, 73-87.
- MULLINS, R. D., STAFFORD, W. F. & POLLARD, T. D. 1997. Structure, subunit topology, and actin-binding activity of the Arp2/3 complex from *Acanthamoeba*. *J Cell Biol*, 136, 331-43.
- MUNK, S., SIGURÐSSON, J. O., XIAO, Z., BATH, T. S., FRANCIOSA, G., VON STECHOW, L., LOPEZ-CONTRERAS, A. J., VERTEGAAL, A. C. O. & OLSEN, J. V. 2017. Proteomics Reveals Global Regulation of Protein SUMOylation by ATM and ATR Kinases during Replication Stress. *Cell Rep*, 21, 546-558.
- MUSACCHIO, A. 2015. The Molecular Biology of Spindle Assembly Checkpoint Signaling Dynamics. *Curr Biol*, 25, R1002-18.
- MUSACCHIO, A. & SALMON, E. D. 2007. The spindle-assembly checkpoint in space and time. *Nat Rev Mol Cell Biol*, 8, 379-93.
- NACERDDINE, K., LEHEMBRE, F., BHAUMIK, M., ARTUS, J., COHEN-TANNOUDJI, M., BABINET, C., PANDOLFI, P. P. & DEJEAN, A. 2005. The SUMO pathway is essential for nuclear integrity and chromosome segregation in mice. *Dev Cell*, 9, 769-79.
- NAGAI, S., DUBRANA, K., TSAI-PFLUGFELDER, M., DAVIDSON, M. B., ROBERTS, T. M., BROWN, G. W., VARELA, E., HEDIGER, F., GASSER, S. M. & KROGAN, N. J. 2008. Functional targeting of DNA damage to a nuclear pore-associated SUMO-dependent ubiquitin ligase. *Science*, 322, 597-602.

- NANDI, D., TAHILIANI, P., KUMAR, A. & CHANDU, D. 2006. The ubiquitin-proteasome system. *J Biosci*, 31, 137-55.
- NASERI, N. N., WANG, H., GUO, J., SHARMA, M. & LUO, W. 2019. The complexity of tau in Alzheimer's disease. *Neurosci Lett*, 705, 183-194.
- NATHAN, D., INGVARSDOTTIR, K., STERNER, D. E., BYLEBYL, G. R., DOKMANOVIC, M., DORSEY, J. A., WHELAN, K. A., KRSMANOVIC, M., LANE, W. S., MELUH, P. B., JOHNSON, E. S. & BERGER, S. L. 2006. Histone sumoylation is a negative regulator in *Saccharomyces cerevisiae* and shows dynamic interplay with positive-acting histone modifications. *Genes Dev*, 20, 966-76.
- NEEF, D. W., JAEGER, A. M., GOMEZ-PASTOR, R., WILLMUND, F., FRYDMAN, J. & THIELE, D. J. 2014. A direct regulatory interaction between chaperonin TRiC and stress-responsive transcription factor HSF1. *Cell Rep*, 9, 955-66.
- NEWMAN, H. A., MELUH, P. B., LU, J., VIDAL, J., CARSON, C., LAGESSE, E., GRAY, J. J., BOEKE, J. D. & MATUNIS, M. J. 2017. A high throughput mutagenic analysis of yeast sumo structure and function. *PLoS Genet*, 13, e1006612.
- NIE, M., VASHISHT, A. A., WOHLSCHLEGEL, J. A. & BODDY, M. N. 2015. High Confidence Fission Yeast SUMO Conjugates Identified by Tandem Denaturing Affinity Purification. *Sci Rep*, 5, 14389.
- NOVATCHKOVA, M., TOMANOV, K., HOFMANN, K., STUIBLE, H. P. & BACHMAIR, A. 2012. Update on sumoylation: defining core components of the plant SUMO conjugation system by phylogenetic comparison. *New Phytologist*, 195, 23-31.
- OLSEN, S. K., CAPILI, A. D., LU, X., TAN, D. S. & LIMA, C. D. 2010. Active site remodelling accompanies thioester bond formation in the SUMO E1. *Nature*, 463, 906-12.
- OLSEN, S. K. & LIMA, C. D. 2013. Structure of a ubiquitin E1-E2 complex: insights to E1-E2 thioester transfer. *Mol Cell*, 49, 884-96.
- OTSUBO, T., IWAYA, K., MUKAI, Y., MIZOKAMI, Y., SERIZAWA, H., MATSUOKA, T. & MUKAI, K. 2004. Involvement of Arp2/3 complex in the process of colorectal carcinogenesis. *Mod Pathol*, 17, 461-7.
- PADRICK, S. B., DOOLITTLE, L. K., BRAUTIGAM, C. A., KING, D. S. & ROSEN, M. K. 2011. Arp2/3 complex is bound and activated by two WASP proteins. *Proc Natl Acad Sci U S A*, 108, E472-9.
- PANG, Y., YAMAMOTO, H., SAKAMOTO, H., OKU, M., MUTUNGI, J. K., SAHANI, M. H., KURIKAWA, Y., KITA, K., NODA, N. N., SAKAI, Y., JIA, H. & MIZUSHIMA, N. 2019. Evolution from covalent conjugation to non-covalent interaction in the ubiquitin-like ATG12 system. *Nature Structural & Molecular Biology*, 26, 289-296.
- PANSE, V. G., HARDELAND, U., WERNER, T., KUSTER, B. & HURT, E. 2004. A proteome-wide approach identifies sumoylated substrate proteins in yeast. *J Biol Chem*, 279, 41346-51.
- PARKER, J. L., BUCCERI, A., DAVIES, A. A., HEIDRICH, K., WINDECKER, H. & ULRICH, H. D. 2008. SUMO modification of PCNA is controlled by DNA. *EMBO J*, 27, 2422-31.
- PARKER, J. L. & ULRICH, H. D. 2012. A SUMO-interacting motif activates budding yeast ubiquitin ligase Rad18 towards SUMO-modified PCNA. *Nucleic Acids Res*, 40, 11380-8.
- PAVEL, M., IMARISIO, S., MENZIES, F. M., JIMENEZ-SANCHEZ, M., SIDDIQI, F. H., WU, X., RENNA, M., O'KANE, C. J., CROWTHER, D. C. & RUBINSZTEIN, D. C. 2016. CCT complex restricts neuropathogenic protein aggregation via autophagy. *Nat Commun*, 7, 13821.

- PAVELKA, N., RANCATI, G., ZHU, J., BRADFORD, W. D., SARAF, A., FLORENS, L., SANDERSON, B. W., HATTEM, G. L. & LI, R. 2010. Aneuploidy confers quantitative proteome changes and phenotypic variation in budding yeast. *Nature*, 468, 321-5.
- PELISCH, F., SONNEVILLE, R., POURKARIMI, E., AGOSTINHO, A., BLOW, J. J., GARTNER, A. & HAY, R. T. 2014. Dynamic SUMO modification regulates mitotic chromosome assembly and cell cycle progression in *Caenorhabditis elegans*. *Nat Commun*, 5, 5485.
- PETREZSELYOVA, S., ZAHRADKA, J. & SYCHROVA, H. 2010. *Saccharomyces cerevisiae* BY4741 and W303-1A laboratory strains differ in salt tolerance. *Fungal Biol*, 114, 144-50.
- PICHLER, A., FATOUROS, C., LEE, H. & EISENHARDT, N. 2017. SUMO conjugation - a mechanistic view. *Biomol Concepts*, 8, 13-36.
- PIETILÄ, M., VIJAY, G. V., SOUNDARARAJAN, R., YU, X., SYMMANS, W. F., SPHYRIS, N. & MANI, S. A. 2016. FOXC2 regulates the G2/M transition of stem cell-rich breast cancer cells and sensitizes them to PLK1 inhibition. *Sci Rep*, 6, 23070.
- PINTO, M. P., CARVALHO, A. F., GROU, C. P., RODRIGUEZ-BORGES, J. E., SA-MIRANDA, C. & AZEVEDO, J. E. 2012. Heat shock induces a massive but differential inactivation of SUMO-specific proteases. *Biochim Biophys Acta*, 1823, 1958-66.
- PISITHKUL, T., PATEL, N. M. & AMADOR-NOGUEZ, D. 2015. Post-translational modifications as key regulators of bacterial metabolic fluxes. *Curr Opin Microbiol*, 24, 29-37.
- PIZARRO-CERDA, J., CHOREV, D. S., GEIGER, B. & COSSART, P. 2017. The Diverse Family of Arp2/3 Complexes. *Trends Cell Biol*, 27, 93-100.
- PIZARRO-CERDÁ, J., CHOREV, D. S., GEIGER, B. & COSSART, P. 2017. The Diverse Family of Arp2/3 Complexes. *Trends Cell Biol*, 27, 93-100.
- PLECHANOVOVÁ, A., JAFFRAY, E. G., TATHAM, M. H., NAISMITH, J. H. & HAY, R. T. 2012. Structure of a RING E3 ligase and ubiquitin-loaded E2 primed for catalysis. *Nature*, 489, 115-20.
- PRINCZ, A. & TAVERNARAKIS, N. 2020. SUMOylation in Neurodegenerative Diseases. *Gerontology*, 66, 122-130.
- RAMAN, N., NAYAK, A. & MULLER, S. 2013. The SUMO system: a master organizer of nuclear protein assemblies. *Chromosoma*, 122, 475-85.
- REIJO, R. A., COOPER, E. M., BEAGLE, G. J. & HUFFAKER, T. C. 1994. Systematic mutational analysis of the yeast beta-tubulin gene. *Mol Biol Cell*, 5, 29-43.
- REINDLE, A., BELICHENKO, I., BYLEBYL, G. R., CHEN, X. L., GANDHI, N. & JOHNSON, E. S. 2006. Multiple domains in Siz SUMO ligases contribute to substrate selectivity. *J Cell Sci*, 119, 4749-57.
- REN, Y., JIANG, H., HU, Z., FAN, K., WANG, J., JANOSCHKA, S., WANG, X., GE, S. & FENG, J. 2015. Parkin mutations reduce the complexity of neuronal processes in iPSC-derived human neurons. *Stem Cells*, 33, 68-78.
- REN, Y., ZHAO, J. & FENG, J. 2003. Parkin binds to alpha/beta tubulin and increases their ubiquitination and degradation. *J Neurosci*, 23, 3316-24.
- REVERTER, D. & LIMA, C. D. 2005. Insights into E3 ligase activity revealed by a SUMO-RanGAP1-Ubc9-Nup358 complex. *Nature*, 435, 687-92.
- RIBET, D., HAMON, M., GOUIN, E., NAHORI, M. A., IMPENS, F., NEYRET-KAHN, H., GEVAERT, K., VANDEKERCKHOVE, J., DEJEAN, A. & COSSART, P. 2010. *Listeria monocytogenes* impairs SUMOylation for efficient infection. *Nature*, 464, 1192-5.
- RICHARDS, K. L., ANDERS, K. R., NOGALES, E., SCHWARTZ, K., DOWNING, K. H. & BOTSTEIN, D. 2000. Structure-Function Relationships in Yeast Tubulins. *Molecular Biology of the Cell*, 11, 1887-1903.

- RODRIGUEZ, M. S., DARGEMONT, C. & HAY, R. T. 2001. SUMO-1 conjugation in vivo requires both a consensus modification motif and nuclear targeting. *J Biol Chem*, 276, 12654-9.
- RODRIGUEZ-VARGAS, S., ESTRUCH, F. & RANDEZ-GIL, F. 2002. Gene expression analysis of cold and freeze stress in Baker's yeast. *Appl Environ Microbiol*, 68, 3024-30.
- RONAU, J. A., BECKMANN, J. F. & HOCHSTRASSER, M. 2016. Substrate specificity of the ubiquitin and Ubl proteases. *Cell Research*, 26, 441-456.
- ROSONINA, E., AKHTER, A., DOU, Y., BABU, J. & SRI THEIVAKADADCHAM, V. S. 2017. Regulation of transcription factors by sumoylation. *Transcription*, 8, 220-231.
- ROY, D. & SADANANDOM, A. 2021. SUMO mediated regulation of transcription factors as a mechanism for transducing environmental cues into cellular signaling in plants. *Cell Mol Life Sci*, 78, 2641-2664.
- RYTZ, T. C., MILLER, M. J., MCLOUGHLIN, F., AUGUSTINE, R. C., MARSHALL, R. S., JUAN, Y. T., CHARNG, Y. Y., SCALF, M., SMITH, L. M. & VIERSTRA, R. D. 2018. SUMOylome Profiling Reveals a Diverse Array of Nuclear Targets Modified by the SUMO Ligase SIZ1 during Heat Stress. *Plant Cell*, 30, 1077-1099.
- RYU, H. Y. & HOCHSTRASSER, M. 2017. Adaptive aneuploidy counters a dysregulated SUMO system. *Cell Cycle*, 16, 383-385.
- RYU, H. Y., WILSON, N. R., MEHTA, S., HWANG, S. S. & HOCHSTRASSER, M. 2016. Loss of the SUMO protease Ulp2 triggers a specific multichromosome aneuploidy. *Genes Dev*, 30, 1881-94.
- SAITOH, H. & HINCHEY, J. 2000. Functional heterogeneity of small ubiquitin-related protein modifiers SUMO-1 versus SUMO-2/3. *J Biol Chem*, 275, 6252-8.
- SANTAGUIDA, S. & MUSACCHIO, A. 2009. The life and miracles of kinetochores. *Embo j*, 28, 2511-31.
- SCHAERER-BRODBECK, C. & RIEZMAN, H. 2003. Genetic and biochemical interactions between the Arp2/3 complex, Cmd1p, casein kinase II, and Tub4p in yeast. *FEMS Yeast Res*, 4, 37-49.
- SCHAKS, M., GIANNONE, G. & ROTTNER, K. 2019. Actin dynamics in cell migration. *Essays Biochem*, 63, 483-495.
- SCHATZ, P. J., PILLUS, L., GRISAFI, P., SOLOMON, F. & BOTSTEIN, D. 1986. Two functional alpha-tubulin genes of the yeast *Saccharomyces cerevisiae* encode divergent proteins. *Mol Cell Biol*, 6, 3711-21.
- SCHRANK, B. R., APARICIO, T., LI, Y., CHANG, W., CHAIT, B. T., GUNDERSEN, G. G., GOTTESMAN, M. E. & GAUTIER, J. 2018. Nuclear ARP2/3 drives DNA break clustering for homology-directed repair. *Nature*, 559, 61-66.
- SCHULTE, J. & LITTLETON, J. T. 2011. The biological function of the Huntingtin protein and its relevance to Huntington's Disease pathology. *Curr Trends Neurol*, 5, 65-78.
- SCHWIENHORST, I., JOHNSON, E. S. & DOHMEN, R. J. 2000. SUMO conjugation and deconjugation. *Mol Gen Genet*, 263, 771-86.
- SCHWOB, E., BÖHM, T., MENDENHALL, M. D. & NASMYTH, K. 1994. The B-type cyclin kinase inhibitor p40SIC1 controls the G1 to S transition in *S. cerevisiae*. *Cell*, 79, 233-44.
- SEELER, J. S. & DEJEAN, A. 2017. SUMO and the robustness of cancer. *Nat Rev Cancer*, 17, 184-197.
- SELMECKI, A., FORCHE, A. & BERMAN, J. 2006. Aneuploidy and isochromosome formation in drug-resistant *Candida albicans*. *Science*, 313, 367-70.

- SEU, C. S. & CHEN, Y. 2009. Identification of SUMO-binding motifs by NMR. *Methods Mol Biol*, 497, 121-38.
- SHINBO, Y., NIKI, T., TAIRA, T., OOE, H., TAKAHASHI-NIKI, K., MAITA, C., SEINO, C., IGUCHI-ARIGA, S. M. & ARIGA, H. 2006. Proper SUMO-1 conjugation is essential to DJ-1 to exert its full activities. *Cell Death Differ*, 13, 96-108.
- SIKORSKI, R. S. & HIETER, P. 1989. A system of shuttle vectors and yeast host strains designed for efficient manipulation of DNA in *Saccharomyces cerevisiae*. *Genetics*, 122, 19-27.
- SILVER, H. R., NISSLEY, J. A., REED, S. H., HOU, Y. M. & JOHNSON, E. S. 2011. A role for SUMO in nucleotide excision repair. *DNA Repair (Amst)*, 10, 1243-51.
- SKOBLE, J., AUERBUCH, V., GOLEY, E. D., WELCH, M. D. & PORTNOY, D. A. 2001. Pivotal role of VASP in Arp2/3 complex-mediated actin nucleation, actin branch-formation, and *Listeria monocytogenes* motility. *J Cell Biol*, 155, 89-100.
- SOMER, L., SHMULMAN, O., DROR, T., HASHMUELI, S. & KASHI, Y. 2002a. The eukaryote chaperonin CCT is a cold shock protein in *Saccharomyces cerevisiae*. *Cell Stress Chaperones*, 7, 47-54.
- SOMER, L., SHMULMAN, O., DROR, T., HASHMUELI, S. & KASHI, Y. 2002b. The eukaryote chaperonin CCT is a cold shock protein in *Saccharomyces cerevisiae*. *Cell Stress and Chaperones*, 7, 47-54
- .
- SONG, J., ZHANG, Z., HU, W. & CHEN, Y. 2005. Small ubiquitin-like modifier (SUMO) recognition of a SUMO binding motif: a reversal of the bound orientation. *J Biol Chem*, 280, 40122-9.
- SPEAR, M., GUO, J., TURNER, A., YU, D., WANG, W., MELTZER, B., HE, S., HU, X., SHANG, H., KUHN, J. & WU, Y. 2014. HIV-1 triggers WAVE2 phosphorylation in primary CD4 T cells and macrophages, mediating Arp2/3-dependent nuclear migration. *J Biol Chem*, 289, 6949-6959.
- SPENCE, J., SADIS, S., HAAS, A. L. & FINLEY, D. 1995. A ubiquitin mutant with specific defects in DNA repair and multiubiquitination. *Mol Cell Biol*, 15, 1265-73.
- SRIKUMAR, T., LEWICKI, M. C., COSTANZO, M., TKACH, J. M., VAN BAKEL, H., TSUI, K., JOHNSON, E. S., BROWN, G. W., ANDREWS, B. J., BOONE, C., GIAEVER, G., NISLOW, C. & RAUGHT, B. 2013a. Global analysis of SUMO chain function reveals multiple roles in chromatin regulation. *J Cell Biol*, 201, 145-63.
- SRIKUMAR, T., LEWICKI, M. C. & RAUGHT, B. 2013b. A global *S. cerevisiae* small ubiquitin-related modifier (SUMO) system interactome. *Mol Syst Biol*, 9, 668.
- SRIRAMACHANDRAN, A. M. & DOHMEN, R. J. 2014. SUMO-targeted ubiquitin ligases. *Biochim Biophys Acta*, 1843, 75-85.
- STINDT, M. H., CARTER, S., VIGNERON, A. M., RYAN, K. M. & VOUSDEN, K. H. 2011. MDM2 promotes SUMO-2/3 modification of p53 to modulate transcriptional activity. *Cell Cycle*, 10, 3176-88.
- STOLDT, V., RADEMACHER, F., KEHREN, V., ERNST, J. F., PEARCE, D. A. & SHERMAN, F. 1996. Review: the Cct eukaryotic chaperonin subunits of *Saccharomyces cerevisiae* and other yeasts. *Yeast*, 12, 523-9.
- STREICH, F. C., JR. & LIMA, C. D. 2014. Structural and functional insights to ubiquitin-like protein conjugation. *Annu Rev Biophys*, 43, 357-79.
- SUN, H., LEVERSON, J. D. & HUNTER, T. 2007. Conserved function of RNF4 family proteins in eukaryotes: targeting a ubiquitin ligase to SUMOylated proteins. *Embo j*, 26, 4102-12.

- SUN, S. C., WANG, Z. B., XU, Y. N., LEE, S. E., CUI, X. S. & KIM, N. H. 2011. Arp2/3 complex regulates asymmetric division and cytokinesis in mouse oocytes. *PLoS One*, 6, e18392.
- SUNG, M. K., LIM, G., YI, D. G., CHANG, Y. J., YANG, E. B., LEE, K. & HUH, W. K. 2013. Genome-wide bimolecular fluorescence complementation analysis of SUMO interactome in yeast. *Genome Res*, 23, 736-46.
- SVITKINA, T. 2018. The Actin Cytoskeleton and Actin-Based Motility. *Cold Spring Harb Perspect Biol*, 10.
- TAKAHASHI, Y., IWASE, M., KONISHI, M., TANAKA, M., TOH-E, A. & KIKUCHI, Y. 1999. Smt3, a SUMO-1 homolog, is conjugated to Cdc3, a component of septin rings at the mother-bud neck in budding yeast. *Biochem Biophys Res Commun*, 259, 582-7.
- TAKAHASHI, Y. & KIKUCHI, Y. 2005. Yeast PIAS-type Ull1/Siz1 is composed of SUMO ligase and regulatory domains. *J Biol Chem*, 280, 35822-8.
- TAMMSALU, T., MATIC, I., JAFFRAY, E. G., IBRAHIM, A. F. M., TATHAM, M. H. & HAY, R. T. 2014. Proteome-wide identification of SUMO2 modification sites. *Sci Signal*, 7, rs2.
- TAN, W., WANG, Z. & PRELICH, G. 2013. Physical and Genetic Interactions Between Uls1 and the Slx5-Slx8 SUMO-Targeted Ubiquitin Ligase. *G3 (Bethesda)*, 3, 771-780.
- TANAKA, K., NISHIDE, J., OKAZAKI, K., KATO, H., NIWA, O., NAKAGAWA, T., MATSUDA, H., KAWAMUKAI, M. & MURAKAMI, Y. 1999. Characterization of a fission yeast SUMO-1 homologue, pmt3p, required for multiple nuclear events, including the control of telomere length and chromosome segregation. *Mol Cell Biol*, 19, 8660-72.
- TATHAM, M. H., GEOFFROY, M. C., SHEN, L., PLECHANOVOVA, A., HATTERSLEY, N., JAFFRAY, E. G., PALVIMO, J. J. & HAY, R. T. 2008. RNF4 is a poly-SUMO-specific E3 ubiquitin ligase required for arsenic-induced PML degradation. *Nat Cell Biol*, 10, 538-46.
- TOMASI, M. L. & RAMANI, K. 2018. SUMOylation and phosphorylation cross-talk in hepatocellular carcinoma. *Transl Gastroenterol Hepatol*, 3, 20.
- TONG, A. H. & BOONE, C. 2006. Synthetic genetic array analysis in *Saccharomyces cerevisiae*. *Methods Mol Biol*, 313, 171-92.
- TORRE, L. A., SIEGEL, R. L., WARD, E. M. & JEMAL, A. 2016. Global Cancer Incidence and Mortality Rates and Trends--An Update. *Cancer Epidemiol Biomarkers Prev*, 25, 16-27.
- TRINIDAD, A. G., MULLER, P. A., CUELLAR, J., KLEJNOT, M., NOBIS, M., VALPUESTA, J. M. & VOUSDEN, K. H. 2013. Interaction of p53 with the CCT complex promotes protein folding and wild-type p53 activity. *Mol Cell*, 50, 805-17.
- UZUNOVA, K., GÖTTSCHE, K., MITEVA, M., WEISSHAAR, S. R., GLANEMANN, C., SCHNELLHARDT, M., NIESSEN, M., SCHEEL, H., HOFMANN, K., JOHNSON, E. S., PRAEFCKE, G. J. & DOHMEN, R. J. 2007. Ubiquitin-dependent proteolytic control of SUMO conjugates. *J Biol Chem*, 282, 34167-75.
- VADLAMUDI, R. K., LI, F., BARNES, C. J., BAGHERI-YARMAND, R. & KUMAR, R. 2004. p41-Arc subunit of human Arp2/3 complex is a p21-activated kinase-1-interacting substrate. *EMBO Rep*, 5, 154-60.
- VAN DE PASCH, L. A., MILES, A. J., NIJENHUIS, W., BRABERS, N. A., VAN LEENEN, D., LIJNZAAD, P., BROWN, M. K., OUELLET, J., BARRAL, Y., KOPS, G. J. & HOLSTEGE, F. C. 2013. Centromere binding and a conserved role in chromosome stability for SUMO-dependent ubiquitin ligases. *PLoS One*, 8, e65628.
- VAN NGUYEN, T., ANGKASEKWINAI, P., DOU, H., LIN, F. M., LU, L. S., CHENG, J., CHIN, Y. E., DONG, C. & YEH, E. T. 2012. SUMO-specific protease 1 is critical for early lymphoid development through regulation of STAT5 activation. *Mol Cell*, 45, 210-21.

- VAN RECHEM, C., BOULAY, G., PINTE, S., STANKOVIC-VALENTIN, N., GUÉRARDEL, C. & LEPRINCE, D. 2010. Differential regulation of HIC1 target genes by CtBP and NuRD, via an acetylation/SUMOylation switch, in quiescent versus proliferating cells. *Mol Cell Biol*, 30, 4045-59.
- VEAL, E. A., DAY, A. M. & MORGAN, B. A. 2007. Hydrogen peroxide sensing and signaling. *Mol Cell*, 26, 1-14.
- VEAL, E. A., ROSS, S. J., MALAKASI, P., PEACOCK, E. & MORGAN, B. A. 2003. Ybp1 is required for the hydrogen peroxide-induced oxidation of the Yap1 transcription factor. *J Biol Chem*, 278, 30896-904.
- VENTERS, B. J., WACHI, S., MAVRICH, T. N., ANDERSEN, B. E., JENA, P., SINNAMON, A. J., JAIN, P., ROLLERI, N. S., JIANG, C., HEMERYCK-WALSH, C. & PUGH, B. F. 2011. A comprehensive genomic binding map of gene and chromatin regulatory proteins in *Saccharomyces*. *Mol Cell*, 41, 480-92.
- VERGHESE, J., ABRAMS, J., WANG, Y. & MORANO, K. A. 2012. Biology of the heat shock response and protein chaperones: budding yeast (*Saccharomyces cerevisiae*) as a model system. *Microbiol Mol Biol Rev*, 76, 115-58.
- VIDAL, S., EL MOTIAM, A., SEOANE, R., PREITAKAITE, V., BOUZAHER, Y. H., GÓMEZ-MEDINA, S., SAN MARTÍN, C., RODRÍGUEZ, D., REJAS, M. T., BAZ-MARTÍNEZ, M., BARRIO, R., SUTHERLAND, J. D., RODRÍGUEZ, M. S., MUÑOZ-FONTELA, C. & RIVAS, C. 2019. Regulation of the Ebola Virus VP24 Protein by SUMO. *J Virol*, 94.
- VU, L. D., GEVAERT, K. & DE SMET, I. 2018. Protein Language: Post-Translational Modifications Talking to Each Other. *Trends Plant Sci*, 23, 1068-1080.
- VYSE, K., PAGTER, M., ZUTHER, E. & HINCHA, D. K. 2019. Deacclimation after cold acclimation—a crucial, but widely neglected part of plant winter survival. *J Exp Bot*, 70, 4595-4604.
- WAN, J., SUBRAMONIAN, D. & ZHANG, X. D. 2012. SUMOylation in control of accurate chromosome segregation during mitosis. *Curr Protein Pept Sci*, 13, 467-81.
- WANG, C. M., LIU, R., WANG, L., NASCIMENTO, L., BRENNAN, V. C. & YANG, W. H. 2014a. SUMOylation of FOXM1B alters its transcriptional activity on regulation of MiR-200 family and JNK1 in MCF7 human breast cancer cells. *Int J Mol Sci*, 15, 10233-51.
- WANG, L., WANSLEEBEN, C., ZHAO, S., MIAO, P., PASCHEN, W. & YANG, W. 2014b. SUMO2 is essential while SUMO3 is dispensable for mouse embryonic development. *EMBO Rep*, 15, 878-85.
- WANG, W., WYCKOFF, J. B., FROHLICH, V. C., OLEJNIKOV, Y., HÜTTELMAIER, S., ZAVADIL, J., CERMAK, L., BOTTINGER, E. P., SINGER, R. H., WHITE, J. G., SEGALL, J. E. & CONDEELIS, J. S. 2002. Single cell behavior in metastatic primary mammary tumors correlated with gene expression patterns revealed by molecular profiling. *Cancer Res*, 62, 6278-88.
- WANG, Y., SHANKAR, S. R., KHER, D., LING, B. M. & TANEJA, R. 2013. Sumoylation of the basic helix-loop-helix transcription factor sharp-1 regulates recruitment of the histone methyltransferase G9a and function in myogenesis. *J Biol Chem*, 288, 17654-62.
- WELCH, M. D., IWAMATSU, A. & MITCHISON, T. J. 1997. Actin polymerization is induced by Arp2/3 protein complex at the surface of *Listeria monocytogenes*. *Nature*, 385, 265-9.
- WEN, D., XU, Z., XIA, L., LIU, X., TU, Y., LEI, H., WANG, W., WANG, T., SONG, L., MA, C., XU, H., ZHU, W., CHEN, G. & WU, Y. 2014. Important role of SUMOylation of Spliceosome factors in prostate cancer cells. *J Proteome Res*, 13, 3571-82.
- WESTERBECK, J. W., PASUPALA, N., GUILLOTTE, M., SZYMANSKI, E., MATSON, B. C., ESTEBAN, C. & KERSCHER, O. 2014. A SUMO-targeted ubiquitin ligase is involved in the degradation of the nuclear pool of the SUMO E3 ligase Siz1. *Mol Biol Cell*, 25, 1-16.

- WIMMER, P., SCHREINER, S. & DOBNER, T. 2012. Human pathogens and the host cell SUMOylation system. *J Virol*, 86, 642-54.
- WOHLSCHLEGEL, J. A., JOHNSON, E. S., REED, S. I. & YATES, J. R., 3RD 2004. Global analysis of protein sumoylation in *Saccharomyces cerevisiae*. *J Biol Chem*, 279, 45662-8.
- WOOD, E. J. 1983. Molecular cloning. A laboratory manual by T Maniatis, E F Fritsch and J Sambrook. pp 545. Cold Spring Harbor Laboratory, New York. 1982. \$48 ISBN 0-87969-136-0. *Biochemical Education*, 11, 82-82.
- WU, S. Y. & CHIANG, C. M. 2009. Crosstalk between sumoylation and acetylation regulates p53-dependent chromatin transcription and DNA binding. *Embo j*, 28, 1246-59.
- WU, Z., HUANG, R. & YUAN, L. 2019. Crosstalk of intracellular post-translational modifications in cancer. *Arch Biochem Biophys*, 676, 108138.
- XILOURI, M., BREKK, O. R. & STEFANIS, L. 2016. Autophagy and Alpha-Synuclein: Relevance to Parkinson's Disease and Related Synucleopathies. *Mov Disord*, 31, 178-92.
- XU, G., PAIGE, J. S. & JAFFREY, S. R. 2010. Global analysis of lysine ubiquitination by ubiquitin remnant immunoaffinity profiling. *Nat Biotechnol*, 28, 868-73.
- XU, Z., LAM, L. S., LAM, L. H., CHAU, S. F., NG, T. B. & AU, S. W. 2008. Molecular basis of the redox regulation of SUMO proteases: a protective mechanism of intermolecular disulfide linkage against irreversible sulfhydryl oxidation. *FASEB J*, 22, 127-37.
- YANG, F., HU, L., CHEN, C., YU, J., O'CONNELL, C. B., KHODJAKOV, A., PAGANO, M. & DAI, W. 2012a. BubR1 is modified by sumoylation during mitotic progression. *J Biol Chem*, 287, 4875-82.
- YANG, F., HUANG, Y. & DAI, W. 2012b. Sumoylated BubR1 plays an important role in chromosome segregation and mitotic timing. *Cell Cycle*, 11, 797-806.
- YANG, S. H., GALANIS, A., WITTY, J. & SHARROCKS, A. D. 2006. An extended consensus motif enhances the specificity of substrate modification by SUMO. *Embo j*, 25, 5083-93.
- YOO, Y., WU, X. & GUAN, J. L. 2007. A novel role of the actin-nucleating Arp2/3 complex in the regulation of RNA polymerase II-dependent transcription. *J Biol Chem*, 282, 7616-23.
- YOUNG, P., DEVERAUX, Q., BEAL, R. E., PICKART, C. M. & RECHSTEINER, M. 1998. Characterization of two polyubiquitin binding sites in the 26 S protease subunit 5a. *J Biol Chem*, 273, 5461-7.
- YU, F., SHI, G., CHENG, S., CHEN, J., WU, S. Y., WANG, Z., XIA, N., ZHAI, Y., WANG, Z., PENG, Y., WANG, D., DU, J. X., LIAO, L., DUAN, S. Z., SHI, T., CHENG, J., CHIANG, C. M., LI, J. & WONG, J. 2018. SUMO suppresses and MYC amplifies transcription globally by regulating CDK9 sumoylation. *Cell Res*, 28, 670-685.
- YUNUS, A. A. & LIMA, C. D. 2009a. Purification of SUMO conjugating enzymes and kinetic analysis of substrate conjugation. *Methods Mol Biol*, 497, 167-86.
- YUNUS, A. A. & LIMA, C. D. 2009b. Structure of the Siz/PIAS SUMO E3 ligase Siz1 and determinants required for SUMO modification of PCNA. *Mol Cell*, 35, 669-82.
- ZHANG, F. P., MIKKONEN, L., TOPPARI, J., PALVIMO, J. J., THESLEFF, I. & JÄNNE, O. A. 2008a. Sumo-1 function is dispensable in normal mouse development. *Mol Cell Biol*, 28, 5381-90.
- ZHANG, H., KUAI, X., JI, Z., LI, Z. & SHI, R. 2013. Over-expression of small ubiquitin-related modifier-1 and sumoylated p53 in colon cancer. *Cell Biochem Biophys*, 67, 1081-7.
- ZHANG, J., YUAN, C., WU, J., ELSAYED, Z. & FU, Z. 2015. Polo-like kinase 1-mediated phosphorylation of Forkhead box protein M1b antagonizes its SUMOylation and facilitates its mitotic function. *J Biol Chem*, 290, 3708-19.

- ZHANG, X. D., GOERES, J., ZHANG, H., YEN, T. J., PORTER, A. C. & MATUNIS, M. J. 2008b. SUMO-2/3 modification and binding regulate the association of CENP-E with kinetochores and progression through mitosis. *Mol Cell*, 29, 729-41.
- ZHAO, K., WANG, D., ZHAO, X., WANG, C., GAO, Y., LIU, K., WANG, F., WU, X., WANG, X., SUN, L., ZANG, J. & MEI, Y. 2020. WDR63 inhibits Arp2/3-dependent actin polymerization and mediates the function of p53 in suppressing metastasis. *EMBO Rep*, 21, e49269.
- ZHAO, Q., XIE, Y., ZHENG, Y., JIANG, S., LIU, W., MU, W., LIU, Z., ZHAO, Y., XUE, Y. & REN, J. 2014. GPS-SUMO: a tool for the prediction of sumoylation sites and SUMO-interaction motifs. *Nucleic Acids Res*, 42, W325-30.
- ZHAO, X. & BLOBEL, G. 2005. A SUMO ligase is part of a nuclear multiprotein complex that affects DNA repair and chromosomal organization. *Proceedings of the National Academy of Sciences of the United States of America*, 102, 4777-4782.
- ZHENG, N. & SHABEK, N. 2017. Ubiquitin Ligases: Structure, Function, and Regulation. *Annu Rev Biochem*, 86, 129-157.
- ZHENG, N., WANG, P., JEFFREY, P. D. & PAVLETICH, N. P. 2000. Structure of a c-Cbl-UbcH7 complex: RING domain function in ubiquitin-protein ligases. *Cell*, 102, 533-9.
- ZHOU, W., RYAN, J. J. & ZHOU, H. 2004. Global analyses of sumoylated proteins in *Saccharomyces cerevisiae*. Induction of protein sumoylation by cellular stresses. *J Biol Chem*, 279, 32262-8.
- ZILIO, N., EIFLER-OLIVI, K. & ULRICH, H. D. 2017. Functions of SUMO in the Maintenance of Genome Stability. *Adv Exp Med Biol*, 963, 51-87.